Silicification in Biological Systems

A thesis submitted in partial fulfilment of the requirements for the Degree of Doctor of Philosophy in the University of Oxford.

by Carole Celia Perry.

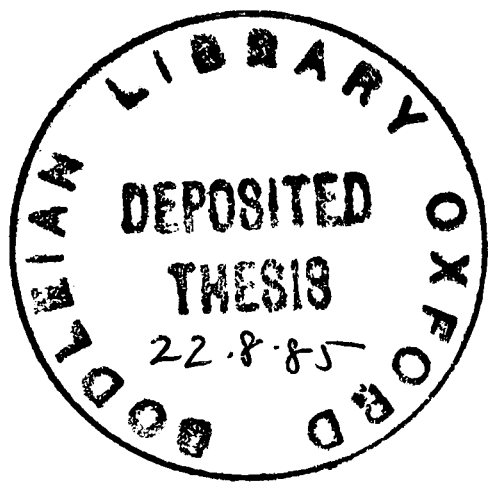

Somerville College
Oxford

Hilary Term
1985

Abstract

Silicification in Biological Systems

Thesis submitted for the Degree of Doctor of Philosophy
by Carole Celia Perry
Hilary Term 1985
Somerville College

This thesis is concerned with the formation and structure of silicified deposits in biology. The major system studied is silicified macrohairs from the lemma of the grass Phalaris canariensis L.. The macrohairs consist of silica and polysaccharides.

Chemical and structural studies on the mineral phase utilised electron microscopy (transmission (TEM), scanning (SEM) and ultra high resolution (HRTEM)), energy dispersive X-ray analysis (EDXA), solid state nuclear magnetic resonance (^{29}Si nmr), infrared spectroscopy, birefringence and nitrogen adsorption experiments. Results showed that the silica is chemically `pure', hydrated, amorphous at a resolution of 10Å and a variety of structural morphologies were observed which are related to the maturity of the macrohair.

Analytical studies at different times after emergence of the inflorescence utilising EDXA and scanning proton microprobe analysis (SPM) showed that the inorganic elements Si, K, P, S and Cl are spatially organised within the macrohairs during silicification. It is proposed that the macrohairs are silicified under strict cellular control.

The organic matrix in the mature macrohairs was investigated by acid hydrolysis and chromatography. The changing emphasis of polysaccharide synthesis in the macrohairs as mineralisation occurs was followed by *in vivo* radioactive labelling of inflorescences at different stages using ^{14}C glucose and ^{3}H arabinose. Analysis of polysaccharides synthesised involved acid hydrolysis and enzymic digestions (Amylase and Driselase), followed by paper and thin layer chromatography with scintillation counting of the products. Results showed that at the early stages of mineralisation, arabinoxylans and cellulose are the major polymers synthesised but as the macrohair matures, largely non-cellulosic glucans (as yet unidentified) are synthesised. It is proposed that the change in emphasis of polysaccharide synthesis during wall development is related to the size and ultrastructural arrangements of silica particles observed. The organic matrix was also observed to give additional order to the system, the resulting material being totally impervious.

A second system, chosen for comparison, is mineralised teeth from the radula of the common limpet Patella vulgata. The mature teeth contain silica, iron oxide (goethite) and an organic matrix.

Investigations on the silicified phase utilising electron microscopy revealed morphological structural variations. Analytical studies involving EDXA and SPM analysis showed that there are complex temporal and spatial variations in the inorganic composition (P, S, Ca, Fe, Si, Cu) in all regions of the teeth. It is proposed that these changes can be correlated with changes in composition of the organic matrix. A comparison is made of the silica from the two systems.

to my parents and to Nick without whom
nothing would be possible.

Acknowledgments

I would like to thank my supervisor Professor R.J.P.Williams for encouragement, enthusiasm and advice freely given at all stages of this enjoyable research project.

I also thank Dr. S.Mann (Bath University) for an introduction to the art of electron microscopy, for practical help at all times and for enjoyable scientific debate.

I thank Drs. F.Watt and G.W.Grime (Nuclear physics laboratory) for assistance with scanning proton microprobe experiments. I wish to also thank Barbara Luke (Zoology department) for assistance with the scanning electron microscope studies.

I wish to thank Dr. C.H.O'Neill (Imperial Cancer Research, London) for drawing our attention to the silicified plant hairs and for providing one of the samples used for this study. I would like to thank Drs. D.W.Parry and M.J.Hodson (Bangor) for the profitable and enjoyable collaboration we have pursued in the course of this work.

Many thanks are due to Dr. S.C.Fry (Edinburgh University) for his valuable help in the chemical studies performed on the organic fraction of the macrohairs. I would also like to thank those many people in the Botany department who helped to make my visits to the department both profitable and enjoyable.

In a similar manner I would like to thank Dr. J.Webb (Murdoch University, Australia) for introducing us to the delights of limpet teeth and for his patience in extracting the radulae for investigation.

Thanks are also due to the many people who have used their skills on my behalf, in particular; Mrs A.Stoker and Dr A.J.Skarnulis for watching over the electron microscope, K.Waters for photography, Mrs C.Palmer for diagrams and Mrs J.Edwards and Mrs S.Compton for typing my tables and

reference lists.

I would also like to thank all members of RJPW's research group (past and present) who through their friendship have enabled a sharing of ideas.

Finally I would like to thank Nick for bearing with me as I produced this thesis and the Medical Research Council for providing me with financial support throughout the course of this work.

Contents

Chapter 1: Introduction

This thesis is concerned with the formation and structure of silicified mineral deposits in biology. Silicification is one aspect of the much wider field of biological mineralisation which is concerned with the formation, structure and function of inorganic solids in living systems. The minerals deposited may be either crystalline or amorphous. Examples of the former include calcium carbonate (calcite, vaterite and aragonite) in shells, hydroxyapatite in bones and teeth and iron oxides (magnetite, goethite and lepidocrocite) in magnetic bacteria and molluscan teeth. The major amorphous mineral is silica which is found in a variety of marine creatures and higher plants. For a more complete list of minerals found in biology see table 1 and reference 1 (Lowenstam,1981). Functions include strength and support, sensory devices and the removal of toxic levels of an element from a system.

Much previous research performed on crystalline materials has involved studies on hydroxyapatite, since incorrect mineralisation can result in weakness and deformation of teeth and bones (Carlisle,1978). It has been shown for such materials that precise mineralisation occurs on a three dimensional protein or glyco protein template (Miller,1984; Glimcher,1984).

Techniques normally applied to the study of inorganic biominerals include high resolution (TEM) and ultra high resolution (HRTEM) transmission electron microscopy. For crystalline materials, such as hydroxyapatite, magnetite and calcium carbonate, much detailed structural information on the mineralising phase and on the modes (mechanisms) of mineralisation can be gained from the use of these microscopical techniques (Mann,1982; Mann et al.,1983).

KINGDOM	MONERA	PROTOCTISTA													FUNGI		ANIMALIA											PLANTAE	
Phylum		Dinoflagellata	Haptophyta	Bacillariophyta	Phaeophyta	Rhodophyta	Chlorophyta	Zygnematophyta	Rhizopodea	Siphonophyta	Charophyta	Heliozoata	Radiolariata	Foraminifera	Mixomycota	Ciliophora	Basidiomycota	Deuteromycota	Porifera	Coelenterata	Platyhelminthes	Ectoprocta	Brachiopoda	Annelida	Mollusca	Arthropoda	Sipuncula	Echinodermata	Chordata	Bryophyta	Trachaephyta
Carbonates:																														
Calcite	✓	✓	✓			✓			✓		✓			✓	✓				✓	✓	✓	✓	✓	✓	✓	✓	✓	✓	✓	✓
Aragonite	✓		?		✓	✓	✓		✓					✓					✓	✓		✓	✓		✓	✓		✓		✓
Vaterite						✓																		✓	✓			✓		✓
Monohydrocalcite	✓																							✓				✓		
Amorph. Hydr. Carb.															✓					✓				✓	✓			✓		
Phosphates:																														
Dahllite	✓														✓			✓										✓		?
Francolite																						✓		✓				✓		
$Ca_3Mg_3(PO_4)_4$																							✓							
Brushite																								✓						
Amorph. Dahllite Precursor																					✓			✓	✓			✓		
Amorph. Brushite Precursor																								✓						
Amorph. Whitlockite Precursor																					✓			✓						
Amorph. Hydr. Ferric Phosphate																					✓			✓			✓			
Halides:																														
Fluorite																								✓	✓		✓			
Amorph. Fluorite Precursor																								✓				✓		
Oxalates:																														
Whewellite							?	✓	✓								✓	?							✓				✓	✓
Weddelite																	✓	?						✓			✓	✓		
Sulfates:																														
Gypsum																				✓									?	✓
Celestite													✓																	
Barite									✓		✓																			
Silica:																														
Opal				✓					?			✓	✓	✓					✓					✓	✓	✓		✓		✓
Fe-Oxides:																														
Magnetite	✓																								✓	✓		✓		
Maghemite	?																													
Goethite																								✓						
Lepidocrocite																			✓					✓						
Ferrihydrite	✓																✓	✓						✓	✓			✓	✓	✓
Amorph. Ferrihydrates														✓										✓				✓		
Mn-Oxides:																														
"Todorokite"	✓																													
Fe-Sulfides:																														
Pyrite	✓																													
Hydrothroilite	✓																													

Table I

Diversity and phylum distribution of biomineralisation products in extant organisms. From an article by Lowenstam (1981).

Amorphous materials such as biological silica, however, have not generally been studied in such depth as conventional (TEM) and (HRTEM) electron microscope techniques give little information on the pattern and structural mechanism of deposition. Previously, it was difficult to obtain silicon free growth conditions necessary both to ascertain the degree of biochemical regulation over silicification and the essentiality of silicon to the correct functioning of a given species. However, through the development of silicon-free laboratory facilities, it has been shown that silicon is an essential element for the functioning of routine processes in diatoms, vertebrates and some higher plants. In diatoms, silicon is required for a number of metabolic processes other than wall formation including synthesis of nuclear DNA polymerases and the metabolism of cyclic nucleotides,(Darley and Volcani,1969; Volcani,1978). The transport of silicon as silicic acid into the cell is biochemically controlled, energy dependent and related to sodium ion gradients across the membrane (Bhattacharyya and Volcani,1980). In vertebrates, silicon is essential for growth and bone development and for collagen and glucosaminoglycan syntheses (Carlisle,1981). In higher plants, silicon is considered essential for the normal growth and development of scouring rushes and grasses (Chen and Lewin,1969). In general, it provides strength and makes the plants less prone to fungal attack (Jones and Handreck,1967). In particular, the presence of silicon increases grain yields from rice (Takashaki,1974).

The degree of biochemical regulation over silicification varies from an apparent lack of control for some plant deposits to total control for frustule formation in diatoms, spicule formation in sponges and basket formation in choanoflagellates (Mann et al.,1982).

Deposition of the polymerised silicic acid may occur in two distinct

biochemical locations. It may occur extracellularly in for example cell walls (higher plants) or intracellularly in specialised cytoplasmic, membrane bounded vesicles, termed the silica deposition vesicle (SDV) and the membrane is known as the the silicalemma. This form of deposition is favoured by all groups other than higher plants where deposition occurs in cell walls, in the cuticular layer and in intercellular spaces (Sangster and Parry,1981), see chapter 3.

The structural forms of silica found as a result of mineralisation are varied and may be used for identification and taxonomic purposes (Parry and Smithson,1966). The morphology of the initially formed deposits is thought to be determined by the spatial constraints of the cellular compartment (often the silica deposition vesicle) in which deposition occurs. Although primary silica particles of 30-40nm in diameter are observed in diatoms (Volcani,1984), sponges (Perry,1984) and higher plants, nothing is known concerning their organisation or the biochemical control exerted over morphological structure adoption.

Data is being accumulated, however, which indicates the involvement of organic matrices with silicification. It is possible that organic matrices occur in association with the mineralising phase promoting nucleation or that they are the template upon which polymerisation occurs (Williams,1984; Mann,1983a). There is much evidence which points to the involvement of organic matrices with mineralisation. For sponges there is a prominent, crystalline, hexagonal, proteinaceous filament in sponge spicules around which silica is deposited. (Garrone,1969; Shore,1972). In diatoms, the siliceous cell wall, the frustule, is encased in a complex organic coat of unusual chemical composition (Hecky et al.,1973) and in testaceous amebae, crysophytes (McGrory and Leadbeater,1981) and

choanoflagellates (Mann,et al.,1982) a fibrillar matrix occurs in the silica deposition vesicles. In higher plants, silica deposition frequently occurs in association with cell wall components which are largely polysaccharidic in origin. It seems likely that organic polymers are in some way involved in determining the deposition pattern though as yet there is no evidence for the formation of a three dimensional template for polymerisation as is the case for materials such as hydroxyapatite.

The material presented in this thesis is concerned with both the structural and mechanistic aspects of silica deposition. The principal system examined has been silicified macrohairs (trichomes) from the lemma of the grass Phalaris canariensis L. This occurs as a contaminant of wheat in certain regions of the world and has been implicated in the aetiology of oesophageal cancer (O'Neill et al.,1980). The fine siliceous macrohairs consist of an inorganic phase of silica and an organic phase of polysaccharide. Physical and chemical studies on the inorganic phase have been undertaken to define precisely the structural components and the chemical and physical nature of the siliceous phase. A range of physical techniques including electron microscopy, solid state nuclear magnetic resonance and infra red spectroscopy were employed. For this system it was important to define whether mineralisation occured as a result of active or passive biochemical processes. Analytical studies on macrohairs at different stages of development using energy dispersive x-ray analysis (EDXA) and proton induced x-ray emission (PIXE) have enabled us to put forward new ideas on silicification in higher plants (particularly trichomes). See chapter 7. The possible role of the organic matrix as an underlying three dimensional template has also been investigated for this system and information concerning changes in cell

wall composition as silicification occurs are presented.

A system chosen for comparison was teeth from the radula of the common limpet Patella vulgata. The radula is used for grazing to provide the limpet with food from the rocks on which it is found. The teeth are hard and will scratch glass. They consist of a crystalline iron oxide (goethite) phase (Lowenstam,1962), an amorphous hydrated silica phase (Sollas,1907), and an organic phase (Runham,1961). The structural and chemical nature of the siliceous phase has been investigated in a similar manner to that described above for the macrohairs. An analytical study employing EDXA and PIXE was undertaken to provide information on the spatial and temporal pattern of elemental deposition within this system. No information concerning the nature of the organic phase was obtained in this study as the chemical composition is known.

Due to the diversity of techniques employed in the study of these two main samples, more detailed introductions are provided in relevant chapters.

1.1 References

1. Bhattacharyya, P. & Volcani, B.E. (1980) Proc. Natl. Acad. Sci. (USA) 77, 6386-6390.

2. Carlisle, E.H. (1978) in Biochemistry of Silicon and Related Problems, ed. Bendz, G. & Lindqvist, I, Plenum Publ. pp. 231-253.

3. Carlisle, E.H. (1981) in Silicon and Siliceous Structures in Biological Systems, ed. Simpson, T.L. & Volcani, B.E. Springer Verlag Publ. pp.69-94.

4. Chen, C.H. & Lewin, J. (1969) Can. J. Bot. 47, 125-131.

5. Darley, W.M. & Volcani, B.E. (1969) Exp. Cell. Res., 58, 334-342.

6. Garrone, R. (1969) J. Microscopie, 8, 581-598.

7. Glimcher, M.J. (1984) Phil. Trans R. Soc. Lond. B 304, 479-508.

8. Hecky, R.E., Mopper, K., Kilham, P., Degens, E.T. (1973) Mar. Biol. 19, 323-331.

9. Jones, L.P.H., Hardreck, K.A. (1967) Adv. Agron. 19, 107-149.

10. Li, C-W., Volcani, B.E. (1984) Phil. Trans. R. Soc. Lond. B 304, 519-528.

11. Lowenstam, H.A. (1981) Science, 211, 1126-1131.

12. Lowenstam, H.A. (1962) Science, 137, 279-280.

13. Mann, S., Williams, R.J.P. (1982) Proc. R. Soc. Lond.B 216, 137-146.

14. Mann, S., Parker, S.B., Ross, M., Skarnulis, J., Williams, R.J.P. (1983) Proc. R. Soc. Lond. B 218, 415-424.

15. Mann, S. (1983a), Structure & Bonding 54, 125-174.

16. McGory, C.B. & Leadbeater, B.S.C. (1981) in Silicon & Siliceous Structures in Biological Systems, ed. Simpson, T.L. & Volcani, B.E., Springer Verlag Publ., pp. 201-230.

17. Miller, A. (1984) Phil. Trans. R. Soc. Lond. B 304, 455-477.

18. O'Neill, C.H., Hodges, G.M., Riddle, P.N., Jordan, P.W., Newman, R.H. & Toulson, E.C. (1980) Int. J. Cancer, 26, 617-628.

19. Parry, D.W. & Smithson, F. (1966) Ann. Bot. (London) 30, 525-538.

20. Perry, C.C. & Williams, R.J.P. (1984) unpublished results.

21. Runham, N.W. (1961) Q. J. Micros. Sci., 102, 371-380.

22. Sangster, A.G., Parry, D.W. (1981) in Silicon and Siliceous Structures in Biological Systems, ed. Simpson, T.L. & Volcani, B.E., Springer Verlag Publ. pp. 383-407.

23. Shore, R.E. (1972) Biol. Bull. 143, 689-698.

24. Sollas, I.B.J. (1907) Quart. J. Microsc. Sci. 51, 115-136.

25. Takahashi, E. (1974) Comparative Plant Nutrition, Yokendo Publishers, Tokyo, Japan.

26. Volcani, B.E. (1978) in Biochemistry of Silicon and Related Problems, ed. Bendz, G & Lindqvist, I., Plenum Publ. pp. 177-204.

27. Williams, R.J.P. (1984) Phil. Trans. R. Soc. Lond. B 304, 411-24.

Chapter 2:Instrumental Techniques

The study on the biological materials presented in this thesis has been performed using a variety of physical techniques. These include electron microscopy (transmission (TEM), scanning (SEM) and ultrahigh resolution transmission (HRTEM)), energy dispersive X-ray analysis (EDXA), proton induced X-ray emission coupled to the scanning proton microprobe (SPM), solid state ^{29}Si and ^{13}C nuclear magnetic resonance, infrared spectroscopy and polarised light microscopy. The organic phase of the macrohairs from the lemma of the grass Phalaris canariensis L. has been studied using solid state ^{13}C nuclear magnetic resonance. A study on polysaccharide synthesis at different stages of silicification has been performed by in vivo radioactive labelling with ^{3}H arabinose and ^{14}C glucose. The results of this latter group of experiments were obtained using biochemical and chromatographic techniques which will be described in detail in chapter 5.

The major physical techniques utilised will now be described.

2.1 Electron Microscopy

For routine study a JEOL 100CX electron microscope was used at an accelerating voltage of 100 KeV. Three viewing modes were possible: transmission (magnification range 330X-250,000X) and with the ASID-4D attachment, scanning (magnification range 10X-200,000X) and scanning transmission (magnification range 300X-300,000X) modes. The system incorporated a KEVEX lithium drifted silicon (Si(Li)) X-ray detector with an energy resolution of 150 eV and a LINK SYSTEMS NOVA 290 computer for X-ray microanalysis in the SEM and STEM modes. X-ray spectra were

visualised on a 625 line video monitor and could be plotted on a 30,000X-Y recorder (Bryans Southern Instruments Ltd.). Integrated peaks were obtained from a 390 printer terminal (Data Dynamics).

In the electron microscope a beam of electrons is produced by thermionic emission from a tungsten hair pin filament cathode. It is accelerated by the potential of the anode (0-100 KeV) and is focused by electromagnetic lenses. Figure 1 shows a diagrammatic representation of the electron microscope. The consequences of the interaction of an electron beam with a sample are shown in figure 2.

The choice of operating mode is dependent upon the information required and the nature of the sample. In TEM and STEM modes, magnification involves a series of magnetic lenses and the image is formed by collection of scattered electrons on a fluorescent screen. In TEM, image contrast is produced by the creation of an intensity deficit in regions of large scattering where electrons produced by elastic and inelastic scattering events are intercepted by the objective aperture. The number of electrons scattered is proportional to both the atomic number and the thickness of the sample and in practice, only samples less than 0.1 microns thick may be viewed in this mode. In STEM, the electron detector is placed below the specimen and electrons transmitted through the sample from the rastering beam are collected. These electrical impulses control the intensity of the cathode ray tube raster. In SEM, the image is built up as the fine beam of electrons is scanned across the specimen by deflector coils, the electron detector counting the number of low energy secondary electrons emitted from each point on the surface. Simultaneously, the spot of a cathode ray tube is scanned across the screen. The secondary electrons are converted into a current which is amplified and used to control the brightness of the cathode ray tube

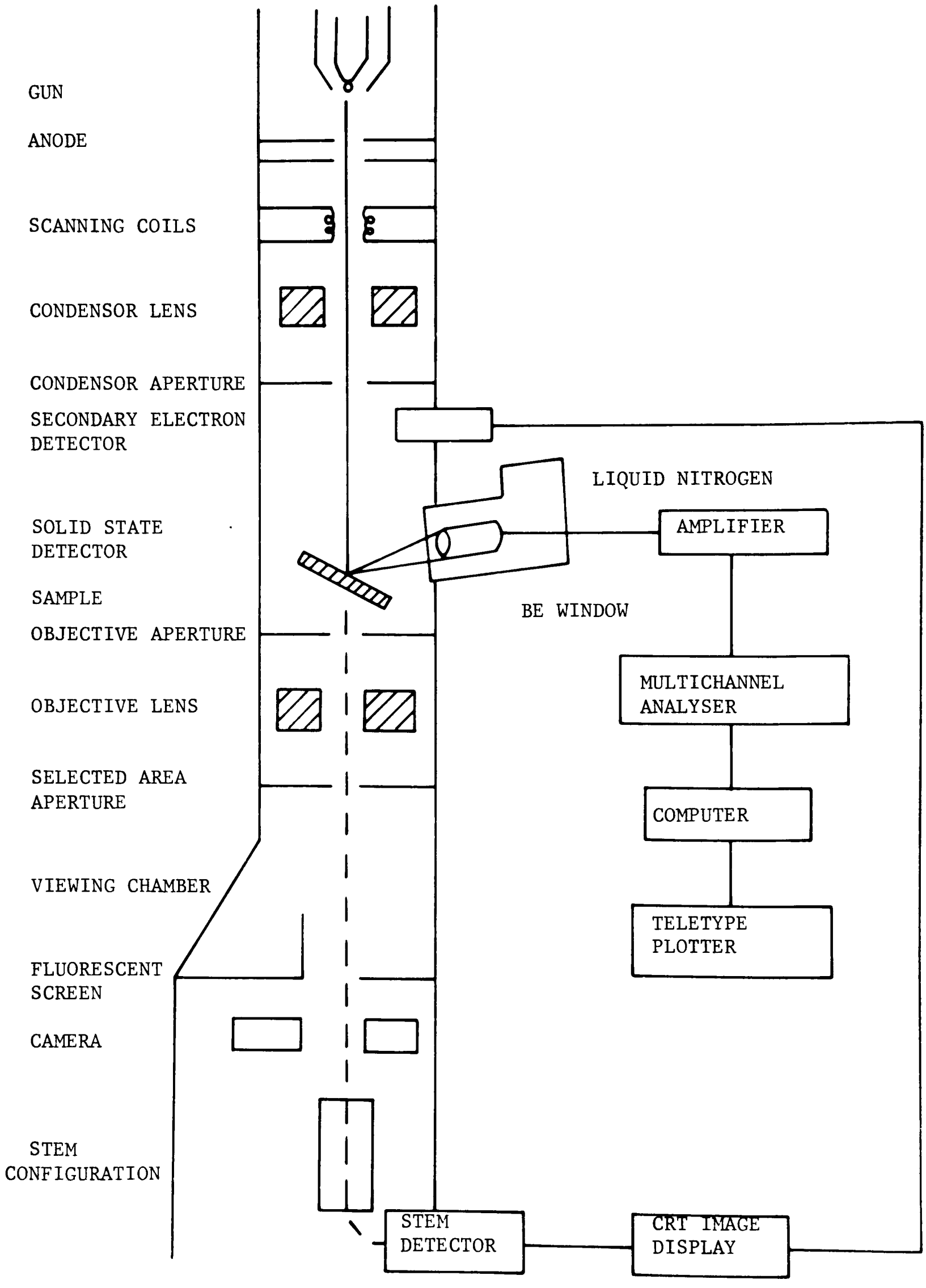

Figure 1

A diagrammatic representation of an electron microscope

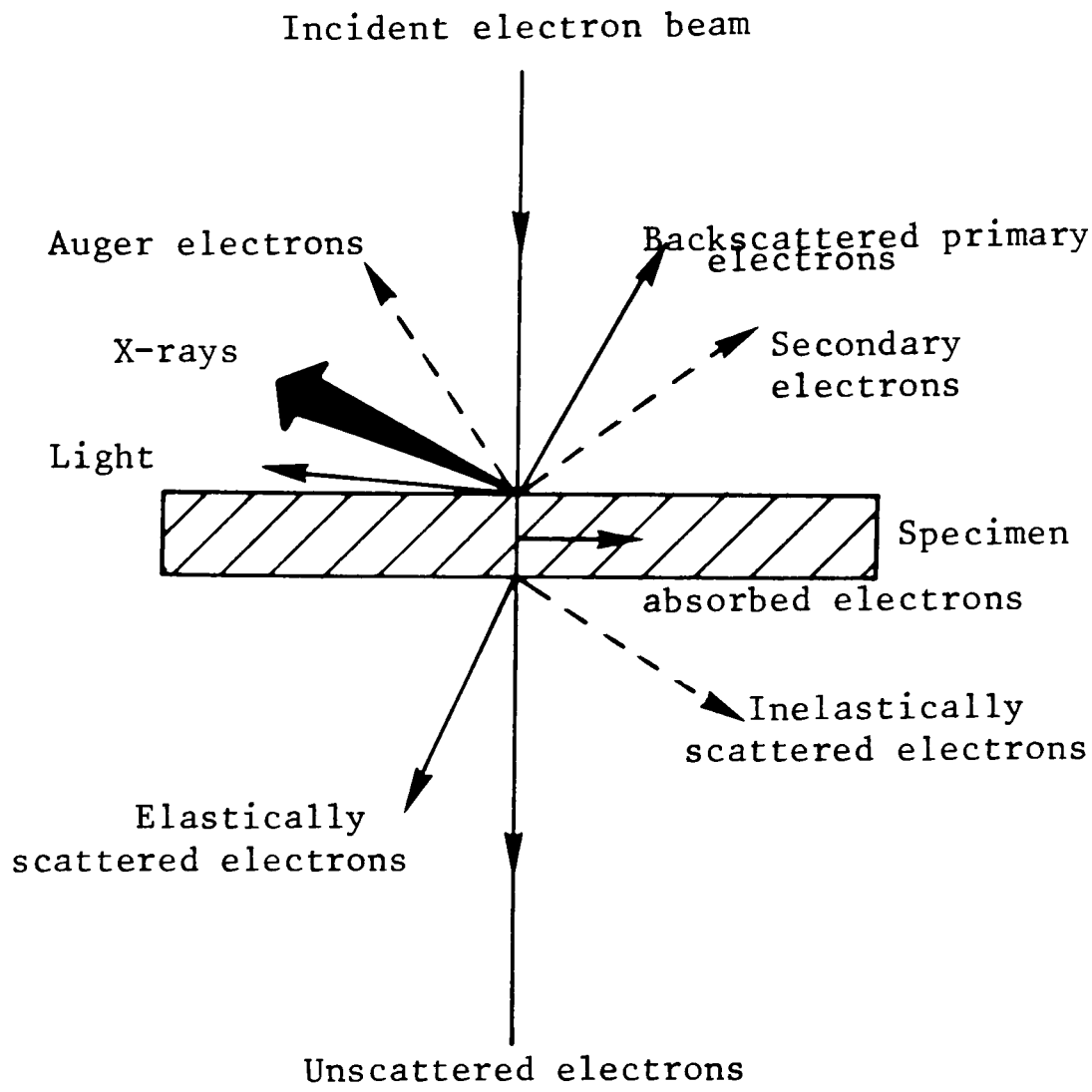

Figure 2

The various consequences of the interaction of the electron beam with the specimen. Light is emitted as visible fluorescence. Elastically scattered electrons suffer no energy loss. Inelastically scattered electrons lose some energy and secondary electrons are of much lower energy than the primary backscattered electrons.

image. Magnification is achieved without the use of lenses and is given as the ratio of the side length of the CRT raster to the side length of the raster on the specimen. Resolution is determined by the diameter of the beam of electrons (5-10 nm) and is less than for TEM. There are no lens abberations as lenses are not used for magnification and the increase in the depth of field which can be utilised means that this is the mode used for the study of bulk samples.

Before use, the electon microscope must be aligned, loaded with film (if required) and the cold trap filled with liquid nitrogen to minimise contamination. For operation at 100 KeV the stable current from a saturated filament was 90 - 100 μA, which was achieved by optimising filament emission and gun bias controls. The alignment procedure involved centralising the beam. In TEM, the alignment translates were used at the smallest spot size and the gun translates at the largest spot size. Alignment of the ASID unit (SEM and STEM), involved centralising the beam as a caustic spot with the ASID alignment tilt controls and as a normal beam with the ASID translate controls. The chosen condensor aperture was then centred by ensuring that the beam image remained symmetrical when the condensors were opened and closed through focus. The condensor astigmatism was corrected to obtain the clearest unsaturated filament image, and the gun tilts adjusted so that the filament image was evenly illuminated.

Samples were prepared by airdrying specimens onto 3 mm formvar coated copper electron microscope grids previously sputtered with a thin film of carbon. When the sample had been introduced by a side entry mechanism into the electron microscope and optimum imaging conditions gained by use of the condensors and focus controls, the voltage and

current centres were aligned. For low magnification work (<100,000X) the current centre was aligned. This was achieved by adjusting the beam alignment tilts over a large range of objective lens focal lengths so that the image under consideration remained centred over a large change in focus conditions. For high magnification work (>100,000X) the voltage centre was aligned by focusing on a hole in the carbon film, turning on the high voltage wobbler and adjusting the beam tilts until the beam pulsated symmetrically about its centre.

A condensor spotsize of 2 was used throughout and increased contrast in the image was produced by switching to the selected area diffraction mode and introducing an objective aperture which was then centred. The final procedure was to check the objective astigmatism. This was performed at a magnification of 250,000X and was corrected to ensure that there was no preferential direction in the image of a blank area of the supporting carbon film. The objective astigmatism was always checked prior to taking micrographs.

Diffraction patterns could be obtained by switching to "selected area magnification" mode (range of magnification 3,300X-66,000X), adjusting the magnification focus then introducing a selected area aperture centred on the area of interest. Switching to the selected area diffraction mode and adjustment of the condensors and focus to give optimum imaging conditions yielded the diffraction pattern. To obtain a full difraction pattern the objective aperture must be removed. In this study, no single crystal or powder diffraction patterns were obtained, since the materials studied were amorphous.

Photography was performed in the TEM mode using the camera at the base of the column fitted with Ilford em FT 155 film. The micrographs were developed using Kodak D19 developer. Routine prints were obtained

from K.Waters (ICL).

For SEM and STEM imaging the sample was introduced as before. The condensor spotsize was set at 4 and the objective aperture removed. The filament emission was then increased to 90-100μA and the SEM or STEM mode selected. An image was produced on the cathode ray tube (CRT) screen by balance of contrast, intensity and brightness controls. Again, focus and astigmatism were checked at all levels of magnification. The image could be viewed at 4 different scan speeds, the slower speeds giving better signal to noise ratios. In principle, the resolution obtainable in the SEM mode was 30Å and in the STEM mode 15Å but this was rarely obtained and, in general, the scanning facilities of the instrument were only used for analysis. No photography was performed in the scanning mode on this instrument.

2.1.1 Ultra-high resolution electron microscopy

The JEOL 200CX electron microscope was used to determine the extent of ordering of the SiO_4 tetrahedra in the sample of macrohairs. The microscope utilised a high brightness LaB_6 filament. The maximum magnification possible was 1,000,000X and a point to point resolution of 2.46Å. Samples were prepared on 2.3mm carbon coated copper grids and entry to the microscope was by way of a top entry stage. This gave greater stability to the system and enhanced resolution. Great care was taken with astigmatism correction prior to taking micrographs which were then taken under different focus conditions.

2.1.2 Scanning electron microscopy

Images presented in this thesis were obtained from a Phillips 500 PSEM electron microscope operating at 40KeV. A resolution of 50Å was possible and the magnification range was 12X-50,000X. Samples were critically point dried if necessary, sputtered with gold and mounted on aluminium stubs. The microscope incorporated a tilt/rotation system which was used to bring samples into the required position for viewing. Photography was performed using a Polaroid land camera attachment and Kodak instamatic film.

I wish to thank Mrs. B. Luke for assistance in obtaining the micrographs presented in this thesis.

2.1.3 Image artefacts

Great care was taken with the analysis of micrographs because of the possibility of image artefacts due to either beam irradiation or electron beam heating. The former may, for amorphous material result in the coalescence of molecules, particularly if they have a high water content; and the later may lead to the disruption of structures adopted because of sample heating.

The samples studied, however, were fairly stable under the electron beam for most conditions and few artefacts occurred.

2.2 Energy dispersive X-ray analysis

In the electron microscope, when the electron beam interacts with a sample X-rays are emitted whenever the critical excitation potential E_c (the energy required to remove an orbital electron from its shell) is exceeded. X-rays, characteristic of the element involved are released as the excited state of the ionised atom returns to its ground state by electron transition from higher to lower energy state. For heavy atoms, several transitions may occur leading to several X-ray emission frequencies, the most intense lines being for transitions to the K(1s) shell (known as K lines). The solid state detector attached to the JEOL 100CX generally detects energies in the range 2-20KeV and for most elements of biological significance the K lines are recorded. However, for heavy atoms, eg. Ag, the critical excitation potential for the K lines lies beyond this region and L lines are used for element characterisation. The detector cannot distinguish elements with atomic number < 10, for two reasons; 1) the X-ray fluorescent yield is low, and 2) the X-rays produced are absorbed by the Be window of the detector. The pulse collected at the solid state detector is integrated, amplified and fed to a multichannel analyser which separates the pulses according to amplitude. The resulting energy spectrum can be displayed on the CRT screen, plotted on paper or the integrated peaks recorded by teletype.

X-rays, characteristic of each element present, are not the only ones to be emitted from the sample and recorded by the solid state detector. The incident electron may be involved in elastic collisions where no energy is lost but the direction of travel is changed or, in inelastic scattering interactions where the electron is deflected and slowed in the electrostatic field of an atomic nucleus. Here, the energy of the X-ray photons emitted are not characteristic of the elements

present but of the geometry of the encounter between electron and nucleus. This is known as continuum or Bremsstrahlung radiation and is proportional to the matrix atomic number and to the square of the accelerating voltage used, and appears as the background of the spectrum (Reed,1975). Background subtraction may be performed on peaks of interest using suitable computer software, or by analysing an adjacent area to the sample and comparing peak height. The presence of Bremsstrahlung or continuum radiation means that theoretical detection limits are never reached. Analytical sensitivity is of the order of 0.1-0.01% for an element embedded in a matrix of another element. In absolute terms, the smallest quantity of an element which may be detected is 100ppm. Tha spatial resolution is dependent upon sample thickness because multiple scattering events of the beam on passing through a sample cause a spreading of the volume from which X-rays are produced and hence detected. For thin sections the maximum resolution obtainable is 1/2 the thickness of the specimen but for bulk analysis this increases to several microns. Inhomogeneities within samples may cause problems with the comprehension of data obtained but this may be overcome by analysing small areas of sample rather than individual points. All EDXA data presented in this thesis has been obtained in this fashion.

Using this system, X-ray microanalysis was performed in the SEM mode with the specimen stage tilted at an angle of 40° towards the detector (unless otherwise stated) and the objective aperture removed. X-rays were collected for 100 seconds. The peaks of interest in the spectrum were then `windowed´, background subtraction performed and the number of counts from the integrated peaks plotted out at the teletype. The spectra were also plotted by the plotter for graphical reference.

X-ray microanalysis is a qualitative technique but may be used semi-quantitatively by utilisation of one of the two following approaches.

The first technique is normally performed by computer as the approach involves iterative calculation. The concentration is proportional to the X-ray intensity for the element divided by correction factors C_z, C_A and C_F for the atomic number, absorption and fluorescent effects respectively. These factors all affect X-ray excitation and hence the observed X-ray intensity.

The concentration of an element C_X may be given as

$$C_X = k.I_X / C_Z.C_A.C_F$$

where I_X is the intensity of the emission line of the element X in the energy spectrum and k is a constant (Reed,1975).

C_Z is the atomic number effect which allows for the fact that X-ray generation varies with matrix composition and incident electron energy. C_A is an absorption correction, necessary because the absorption of the generated X-rays is controlled by their depth distribution and by the absorption coefficients of each of the elements present in the matrix. C_F is the fluorescence correction; necessary to allow for production of additional X-rays from some of the elements present by the primary generated X-rays.

This method of quantisation is only used on thick samples. It was not utilised in this study as suitable software was unavailable.

Another method of quantifying data is to use the simple ratio method of Cheetham and Skarnulis (1981), where the intensity of one peak may be directly compared with another.

For two elements within the same sample analysis area, the equation is,

$$C_X/C_Y = K_{XY} \cdot I_X/I_Y$$

where K_{XY} is a constant for the elements X and Y for a particular microscope. The assumption is that the continuum background is identical for both elements.

C_X = concentration of element X in the sample

C_Y = concentration of element Y in the sample

I_X = X-ray intensity of peak X

I_Y = X-ray peak intensity of peak Y

This procedure is accurate only for thin crystals, where corrections for atomic number effects, absorption and fluorescence are negligible. The biological samples largely studied by X-ray analytical techniques in this thesis have been macrohairs at different stages of development from the lemma of the grass Phalaris canariensis L.. The overall dimensions of these macrohairs do not change from emergence to maturity and it was felt therefore that comparison of X-ray intensities from different elements within the same sample could justifiably be made (chapter 4). It also seemed reasonable, after a very large series of analyses at different stages of maturation had been performed, to compare numerical data obtained for an element, eg. silicon, from different samples. The results presented, however, are not really quantitative. Considerable increases in intensities measured merely indicate an `increase' in the amount of a particular element within a given sample or set of samples. General trends in the changes in the nature of the elemental composition of the samples are, however, presented.

2.3 Scanning proton microprobe analysis

The scanning proton microprobe may, in many ways be considered similar to electron X-ray microprobe facilities as both systems are concerned with the generation and detection of characteristic X-rays produced by interaction of the beam with the sample. However, in order to excite efficiently X-ray production, a high energy (1-4 MeV) proton beam is required rather than the 40-100KeV of the conventional electron beam. The proton beam has a higher inertia than the electron beam and the likelihood of inelastic collisions occurring between beam particles and atomic nuclei is much reduced. This leads to a significantly lower level of continuum or bremsstrahlung radiation and hence increased sensitivity for elemental detection.

All elements with characteristic X-rays of sufficient energy to pass through a beryllium detector window may be detected (atomic number > 11(Na)). The minimum detectable concentration depends upon several factors such as beam energy, the element being detected and the composition of the sample matrix. Some elements (eg. Ag) whose K shell X-rays are too high in energy to be detected efficiently using a Lithium drifted silicon detector are identified by their L and M shell X-rays. The analytical sensitivity of this technique is currently of the order of 10ppm for thin samples and 1ppm for bulk material although theoretical calculations by Folkmann(1978) have shown that 0.1ppm sensitivity is feasible for most elements in the periodic table. This is a considerable improvement on the analytical sensitivity routinely available from the electron microprobe, particularly for bulk samples.

Spatial resolution is determined by the dimensions of the incident

proton beam. There are considerable problems associated with focusing high energy protons and a series of three strong focusing magnetic quadrupole lenses have been used with the Oxford scanning proton microprobe to produce a 1μm diameter beam suitable for analytical work.(Watt et al., 1981,1982) Figure 3 shows the experimental set up employed. For thin samples there is a reduction in resolution compared to the electron microprobe but for bulk samples resolution may be improved. Calculations have shown that a 2MeV proton beam focused down to 1μm diameter deviates by 0.2μm on passing through a 10μm thick sample of carbon (Horowitz and Grovzins, 1975). For a comparable electron microprobe analysis, the beam would be spread by 5μm. There is considerable improvement in resolution obtained if the proton microprobe is used for the analysis of bulk samples.

To obtain spatial and analytical information the beam is scanned across a sample up to 4mm in diameter, data is colected at each point which is recorded and may later be reprocessed in one of several ways. The beam is scanned fast in the vertical direction, pre-quadrupole fast scan coils being used for deflection , and slowly in the horizontal direction, deflection being caused by an induced dipole in the last quadrupole lens. This experimental setup for scanning has been utilised by the scanning proton microprobe in Oxford as lengthy calculations (Grime et al., 1983) have shown that this experimental setup minimises image abberations caused by the quadrupole lenses. The slow scan driver, the fast scan driver and the Si(Li) detector are all connected via analogue to digital converters to a computer.

The PDP11 computer in use in the nuclear physics laboratory in conjunction with the Oxford scanning proton microprobe utilises a multiparameter data handling facility and simultaneously reads the X-ray

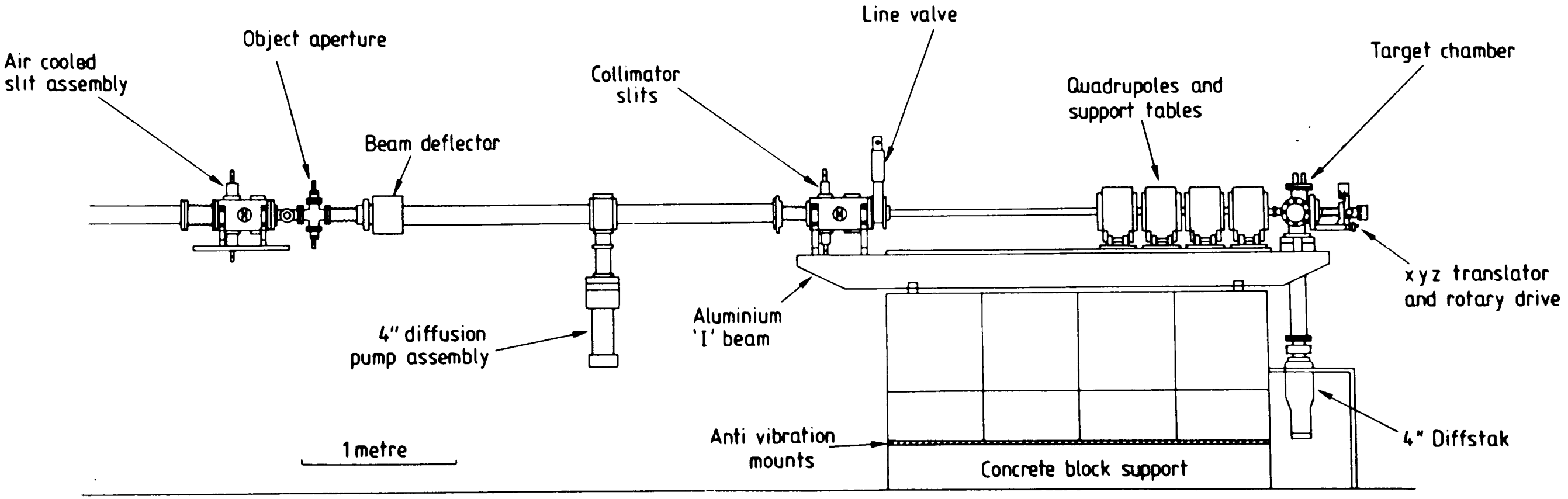

The Oxford microprobe beam line

Figure 3 Schematic diagram of the Oxford Scanning Proton Microprobe showing the object aperture, collimator slits, quadrupole triplet focusing system and target region. The air cooled slit assembly before the object aperture serves to collimate most of the proton beam coming from the accelerator and therefore reduces problems caused by beam heating of the object slits. The focusing system and target region are mounted on concrete blocks to reduce vibration.

pulse height and the X and Y scan voltages. These three numbers represent the elemental source of the X-ray and its location within the sample. They are stored on magnetic tape as a single event. In this way a permanent record of the experiment is taken, which can be replayed in a fraction of the experiment time.

The recorded data is reprocessed in one of several ways. To build up elemental maps, the tape is replayed using suitable computer software to select X-ray events with energies characteristic of the required element. The maps are reconstructed into a display matrix of 256x256 points (pixels) to represent the scanned area, with the elemental concentrations either colour coded or directly correlated with display intensity (monochrome). Colour coding of elemental concentrations means that small changes in local concentration may be clearly observed. The data may also be reprocessed to give X-ray spectra of the whole region under study, or of selected areas within the scanned region. A schematic diagram of microprobe operation is given in figure 4.

The total charge passed through the sample for a given experiment is known for thin samples, and semiquantitative calculations of elemental concentrations may be easily made. There are problems with strict quantitative calculations because of loss of beam energy through the sample and absorption of X-rays produced from deep within the sample. However, for most biological applications involving a heavy element in an organic matrix (eg. plant hairs) this is not a major problem and an accuracy of $\cong$5% is possible for absolute elemental concentrations without the need for internal standards (Johansson and Johansson,1976). I would like to thank Drs. F.Watt and G. Grime for watching over the microprobe for me and for their assistance with the art of computer graphics.

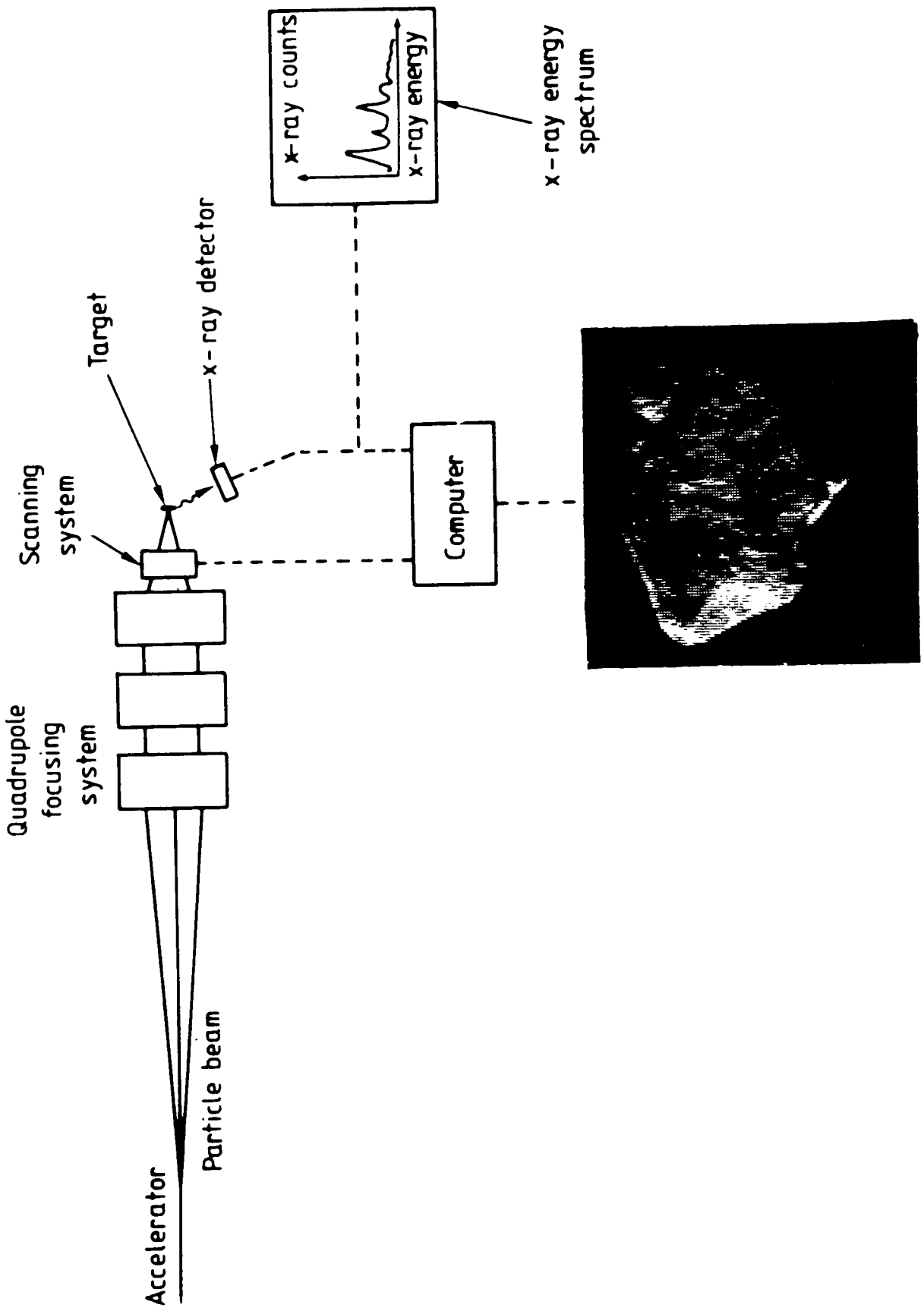

FIGURE 4 Schematic diagram of microprobe operation

2.4 Solid state nuclear magnetic resonance

Investigation of samples in the solid state may be performed by solid state nuclear magnetic resonance in the absence of intramolecular exchange. Solid state nmr provides a means of studying samples in their normal environment and results obtained should provide a bridge between X-ray crystallographic data and results obtained by conventional nmr techniques (Wasylishen and Fyfe, 1982).

In order to obtain high resolution solid state spectra, dipolar interactions and chemical shift anisotropy must be removed or averaged to zero. These problems are not encountered in solution nmr as the nuclear spin interactions are to a large extent averaged by rapid molecular motion.

Dipolar interactions may be homonuclear or heteronuclear in origin. Both can be removed by spinning the sample at the magic angle provided that the rate of sample spinning is large compared with the dipolar interaction. In practice, heteronuclear interactions involving ^{1}H nuclei are removed more efficiently using high power decoupling.

There are problems associated with the accumulation of solid state spectra from dilute spin systems due to the lack of sensitivity and extremely long relaxation times. There are methods of circumventing these problems and a technique utilised involves enhancement of the sensitivity of a dilute spin eg. ^{29}Si or ^{13}C by the transfer of magnetisation from an abundant spin, normally protons. This is termed cross polarisation. This is achieved by applying strong radiofrequency fields to both the abundant and dilute spins. When the Hartman-Hahn condition is satisfied (Hartmann and Hahn, 1962), magnetisation is transferred from the abundant spin

component to the dilute spin component, the resulting signal of the dilute spin component being enhanced. One difficulty of this method is that selective enhancement of certain resonances in the spectrum may occur because a dilute spin in close proximity to an abundant spin will crosspolarise more rapidly than for distant dilute spins. This may be examined by varying the time for which the Hartman-Hahn condition is met. Another advantage of this procedure is that the recycle time between collecting free induction decays (FID's) is determined by the proton spin relaxation time rather than by the dilute spin. In general, the proton spin relaxation time is shorter than for the dilute spin and thus more FID's may be collected in a given time.

A combination of magic angle spinning and crosspolarisation leads to relatively narrow resonances,ca. 50-200Hz and a selective enhancement of certain peaks.

The averaging of the chemical shift anisotropy by magic angle spinning results in a loss of information concerning the chemical shift tensor. This information can be recovered using: 1) slow magic angle spinning (SMASS), 2) off magic angle spinning (OMASS) and 3) rotation synchronized pulse techniques. These are not discussed here as only magic angle spinning (MAS) and crosspolarisation coupled to magic angle spinning (CPMAS) techniques were utilised in obtaining the data presented in this thesis.

The spectrometer used was a Bruker CXP200 operating at 39.73KHz for ^{29}Si and at 50.32KHz for ^{13}C. Spectra were collected as free induction decays (FID's) on disc before Fourier transformation. A simple mathematical manipulation involving an exponential term (exp t/TC) was also applied to improve the signal to noise ratio at the expense of broadening lines by a few Hz. For all ^{29}Si experiments conditions were

determined by running a sample of Q_8M_8 (a siloxane polymer) and optimising operating conditions for this sample. All chemical shifts are quoted as upfield from the resonance of Q_8M_8 set at 11.5ppm. The reference used for ^{13}C experiments was adamantane and the procedure was as described above. All chemical shifts are quoted as downfield from the resonance of adamantane set at 28.7ppm.

I would like to thank Dr. N. Clayden for his help in obtaining the spectra presented in this thesis.

2.5 Infrared spectroscopy

Infrared radiation is absorbed when the oscillating dipole moment due to molecular vibrations interacts with the oscillating electric vector of the infrared beam. Selection rules state that for an interaction to occur the dipole moment at one extreme of a vibration must be different from the dipole moment at the other extreme of the vibration. Functional groups have characteristic vibration frequencies in the range $4000cm^{-1}$ to $625cm^{-1}$ and the greater the strength of the bond between two atoms, the higher the frequency of the vibration. Stretching and bending vibrations may be observed but bending vibrations are only observed below $1500cm^{-1}$. All spectra were recorded on a Pye Unicam SP2000 operating between $4000cm^{-1}$ and $400cm^{-1}$. Samples were prepared by crushing a small amount of material in an agate mortar with a drop of liquid hydrocarbon (nujol). The mull was then pressed between flat plates of sodium chloride and the spectrum recorded at room temperature.

All other techniques used such as birefringence and nitrogen adsorption studies were only used to a small extent and will be described in the relevant sections of chapter 3.

2.6 References

1. Cheetham, A.K. & Skarnulis, A.J. (1981) Analyt. Chem. 53, 1060-1064.

2. Folkmann, F. (1978) in Material Characterisation Using Ion Beam Techniques, ed. Thomas, J.P. & Cachard, A. Plenum Publ. pp.239-281.

3. Grime, G.W. & Watt, F. (1983) "Beam Optics of Quadrupole Probe Forming Systems", Adam Hilger.

4. Hartmann, S.R. & Hahn, E.L. (1962) Phys. Rev. 128, 2042-2053.

5. Horowitz, P. & Grovzins, L. (1975) Science, 189, 795-797

6. Johansson, S.A.E. & Johansson, T.B. (1976) Nucl. Instr. & Meth. 137, 473-516.

7. Reed, S.J.B. (1975) Electron Microprobe Analysis, Cambridge University Press.

8. Wasylishen, R.E. & Fyfe, C.A. (1982) in Annual Review of NMR Spectrocopy, 12, 1-79.

9. Watt, F., Grime, G.W., Blower, G.D. & Takacs, J. (1981) IEEE Trans. Nucl. Sci. NS28, 1413-1416.

10. Watt, F., Grime, G.W., Blower, G.D., Takacs, J. & Vaux, D.J.T. (1982) Nucl. Instr. Meths. 197, 65-77.

Chapter 3: Chemical, physical and structural studies on macrohairs from the lemma of the grass Phalaris canariensis

3.1 Introduction

Many plants have been shown to contain localised deposits of amorphous silica. The plant families represented include horsetails (Equisetaceae), grasses (Poaceae), sedges (Cyperaceae), the ginger family (Zingiberaceae), spiderworts (Commenlinaceae), nettles (Urticaceae), the elm family (Ulmaceae), the vervain family (Verbenaceae), the hemp family (Cannabaceae) and the pea family (Fabaceae).(Voronkov et al., 1975. Sangster and Parry,1981).

Silica is often found deposited in hairs (trichomes) but may also occur in stomata, ordinary epidermal cells and in the Poaceae (grasses), in specialised `silica cells´. Silica deposits may also be found in the leaves, stems, roots and reproductive structures of these plant families.

In general, the nature of the ´opaline silica´ or `silica gel´ has been studied macroscopically by light microscopy and scanning electron microscopy. Deposition may be extracellular or intracellular and for vascular plants, at least three types of silicified deposit have been distinguished.

a) extracellular deposits:-

(1) in which the silica is associated with cell walls both in the subterranean and in the aerial organs. Examples include endodermal cells of grasses (Jones et al.,1963) and the cells of strengthening tissues such as sclerenchyma cells (Parry and Kelso,1975).

(2) in which the silica is associated with the cuticular layer. Examples include the cuticle of the rice leaf (Yoshida et al.,1962)

b) intracellular deposits:-

(1) these include those that infill the cell lumen such as in root intercellular spaces and stem silica cells (Montgomery et al.,1979)

The chemical environmentsin which these deposits are found are biochemically very different. Cell wall deposits are associated with a polysaccharide matrix, cuticular deposits with fatty acids and lipids and intracellular deposits with proteins.

The function of these silicified deposits may include structural support, defence against predators (including pathogens, fungi, insects and larger animals) and as a means of removing toxic quantities of silicic acid from the plant.

The diversity of gross structural forms which may be found among these deposits, (some of which the morphology is so precise that it may be used for taxonomic purposes (Parry and Smithson,1964)) leads us to enquire into the degree or nature of the control exerted over the deposition process. Various mechanisms of silicification in higher plants have been proposed (Sangster and Parry,1981. Kaufmann et al.,1981). They rely essentially on passive processes, cellular control is not thought to be required for the induction or furtherance of precipitation. Changes in pH, membrane filtration and transpiration have been considered as possible mechanisms for initiating polymerisation and aggregation of silica from supersaturated silicic acid solutions. The morphologies of the deposits formed have been suggested to be determined by the size and shape of the biological compartment in which precipitation occurs and there need then be no specific mechanism for spatial organisation.

Some components of the mineralisation process have previously been studied and reliable experimental data is available relating to the

uptake of silicon as silicic acid into some species (Barber and Shone,1966). The uptake of silicic acid is found to be linked to the metabolic pathway for plants such as barley (Hordeum vulgare L. var Procter) and dwarf beans (Phaseolus vulgaris L.) though for others such as peas, uptake is governed by purely passive processes.

Information relating to the means of silicon transport within plants, including silicon accumulation within horsetail is, however, conflicting (Raven,1983). Some authors believe that silcon is simply transported in the xylem as silicic acid (Peggs and Bowen,1984), whereas others, who have extracted silicon containing complexes from plants believe that silicon is transported in a chelated form (Weiss and Herzog,1978). Other authors have tried to extract the same complexes and have failed. They therefore state that silicon is not transported in a complexed form in disagreement with the above (Peggs and Bowen,1984). These conflicting views need to be resolved and it seems likely that as varied deposits may be found within a single plant species, there may indeed be more than one pathway for silicon transport.

The general aim in this thesis is to elucidate the different processes of silicification, especially in plants.

In this chapter and the next we are concerned with the pattern and nature of silica deposition within the macrohairs of the lemma of the grass Phalaris canariensis L.. A structural electron microscopical study is reported for macrohairs at different stages of development. Investigations into the chemical and physical nature of the silicified phase are also presented as they provide us with information required to understand in some small way the events of silicification within the macrohairs of this plant system.

A study of these macrohairs is important from a medical perspective since they have been implicated in the aetiology of human oesophageal cancer and have been found as contaminants of wheat flour in certain regions of the world (O'Neill et al.,1980. O'Neill et al.,1982). The effect of macrohairs of Phalaris canariensis L. on the development of cancer in mouse fibroblasts has recently been described (O'Neill et al.,1980. Bhatt et al.,1984).

The morphology of the system has been described previously (Hubbard,1954). The inflorescence is made up of spikelets, figure 1, each consisting of two equal outer glumes enclosing three florets. The lower two florets are reduced to small sterile lemmas occurring below the base of the much larger lemma and palea of the fertile floret. The lemma and palea enclose the floral organs, and ultimately, the caryopsis. The bracts (lemma and palea) are densely covered with fine siliceous macrohairs, figure 1.

The data presented in this chapter will detail the chemical and physical nature and structural morphology of the silicified material from the macrohairs taken from the lemma of the grass Phalaris canariensis L..

(a)

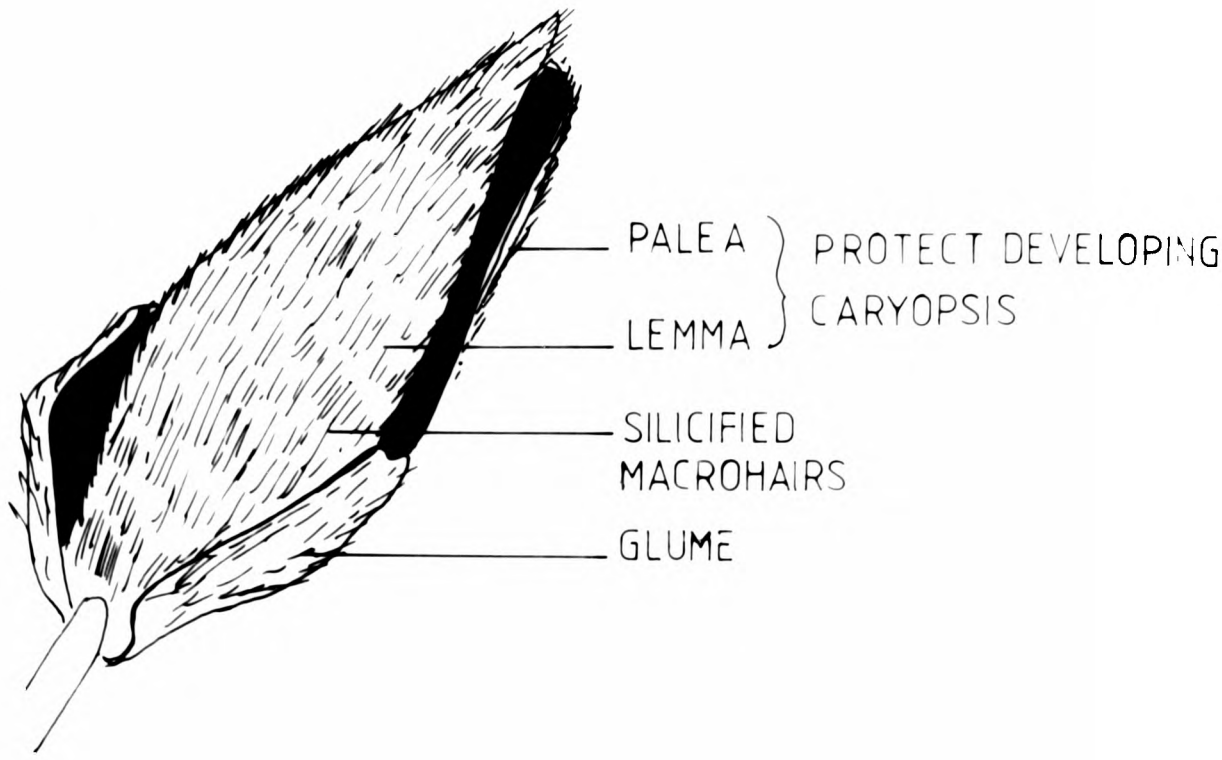

(b)

Figure 1

(a) a diagrammatic representation of the inflorescence of the grass Phalaris canariensis L., showing relevant anatomical features.

(b) SEM of a region of silicified macrohairs. Bar represents 50µm.

3.2 Materials and Methods

3.2.1 Plant culture

Treated mature macrohairs from the lemma of the grass Phalaris canariensis L. of Australian origin were provided by Dr C.H.O'Neill (Imperial Cancer Research, London). These had been prepared by boiling in a mixture of concentrated sulphuric and nitric acids for 24 hours to remove all organic matter. Repeated washings and sedimentation followed by freeze-drying yielded a white powder. This material, as analysed by gas chromatography, contained less than 0.4% organic material.

Untreated macrohairs were collected from a dust extraction room of a grain exporter (Darly Downs Grain Exporters Pty Ltd, Queensland, Australia) and prepared for electron microscopy as described below.

Macrohairs used for the developmental studies were collected from plants grown from seed provided by Dr D.Wyn Parry (University College of North Wales, Bangor). Seeds were grown in moist compost. The plants were watered according to need and on alternate days were given a solution of silicic acid (ca. $100/10^6$), produced by allowing amorphous silica to dissolve in distilled water. When each inflorescence appeared, the date was noted and the inflorescence tagged. Samples for study were removed from midway down each inflorescence. Individual spikelets were removed at the following stages: 1) at emergence, 2) 3 days after emergence, 3) 7 days after emergence, 4)9 days after emergence, 5) 24 days after emergence and 6) 40 days after emergence of the inflorescence. All samples were studied immediately in the electron microscope unless otherwise stated.

3.2.2 Electron microscopy

3.2.2.a Scanning electron microscopy of macrohairs from P.canariensis

Young florets, up to and including the sample taken seven days after emergence were treated before attachment to the electron microscope stub to prevent shrinkage of the specimen. Samples were fixed in 3% glutaraldehyde in sodium cacodylate buffer for 2-3 hours and then rinsed with an identical buffer solution. The samples were dehydrated in acetone and critically point-dried before coating and mounting. Individual florets were attached to aluminium stubs with double-sided tape. Specimens were coated with gold (Nanotech sputterer) and studied and photographed using a Phillips PSEM 500 scanning electron microscope.

Acid treated mature and immature macrohairs and untreated macrohairs were prepared in a similar manner.

3.2.2.b Transmission electron microscopy of macrohairs

Both untreated and acid-treated samples of macrohairs were studied by TEM. Samples were prepared for study in a JEOL 100CX high resolution electron microscope by suspending a small quantity of the powder (sometimes crushed using a pestle and mortar) in distilled water, sonicating and placing a drop on a Formvar-coated 3mm copper grid, previously sputtered with a thin film of carbon to minimise beam damage in the electron microscope, and left to dry on filter paper in the air at room temperature. The silicified material from samples of immature hairs was isolated by acid digestion of organic material from the lemma using a 4:1 mixture of boiling concentrated nitric acid and sulphuric acid. The infertile florets, developing seed and flower organs were removed manually before acid treatment. Samples 9 days after emergence of the inflorescence required 10 minutes of treatment whereas samples at 18 days

required 2 hours to oxidise the organic material present. Repeated washing and centrifugation followed by freeze-drying yielded a fine white powder. Samples for TEM work were prepared as for the mature sample.

Immature samples of untreated hairs were prepared for study by gently rolling the lemma on a copper electron microscope grid, which resulted in several hairs becoming attached to the copper grid.

3.2.2.c Ultra-high resolution transmission electron microscopy of macrohairs

Acid treated fragments from samples of mature macrohairs were studied by HRTEM. Samples were prepared for study in a JEOL 200CX ultra-high resolution electron microscope by suspending a small quantity of the powder (sometimes crushed using a pestle and mortar) in distilled water, sonicating and placing a small drop on a Formvar-coated 2.3mm diameter copper grid, previously sputtered with a thin film of carbon to minimise beam damage in the electron microscope, and left to dry on filter paper in the air at room temperature.

3.2.3 Solid state nuclear magnetic resonance of macrohairs

Both untreated and acid treated samples of mature macrohairs were studied by ^{29}Si nmr. An untreated sample of macrohairs was also studied by ^{13}C nmr to observe the general characteristics of the associated organic polymer.

Samples were studied by magic angle spinning (MAS) and magic angle spinning coupled to cross polarisation (CPMAS) techniques.

3.2.4 Infra-red specroscopy of macrohairs

Both untreated and acid treated samples of mature macrohairs were studied by infra-red spectroscopy. Samples were prepared for study in an Pye Unicam SP2000 by grinding a small amount of the sample using a pestle and mortar with a drop of hydrocarbon (nujol). Reference samples of an industrial amorphous precipitated silica and finely ground quartz were also run under identical experimental conditions.

3.2.5 Birefringence of macrohairs

Untreated mature samples and acid treated 9-day, 24-day and mature samples were studied using a polarising microscope.

3.2.6 Nitrogen absorption measurements

The experimental procedures were performed by Dr J.D.F.Ramsay of AERE Harwell utilising standard techniques as described in an article by Ramsay and Booth (1983).

3.3 Results

3.3.1 Structural studies of macrohairs

3.3.1.a Structural studies of mature macrohairs

The structural components and microarchitecture of treated and untreated mature macrohairs of Phalaris canariensis L. were investigated by electron microscopy. SEM showed intact macrohairs with smooth surfaces often with lengths greater than 100μm. An accurate determination of length was impossible because many hairs had fractured near the base. The maximum diameter was 8μm to 12μm which decreased gradually to a sharply pointed tip. Untreated macrohairs viewed parallel to the hair axis showed internal structure. Several concentric cylinders of silicified material were observed with a central axial channel, figure 4.c. Acid-treated macrohairs showed similar internal structure but the concentric cylinders of silica were more clearly differentiated, often showing a marked separation of adjacent zones, figure 4.d.

The microarchitecture of finely crushed samples of the macrohairs was investigated by TEM. Acid-treated macrohairs were very readily crushed but untreated samples only revealed large, essentially intact fragments of the macrohairs. Three different microstructural forms of silica were observed; fibrous, globular, and sheet-like. These were distinguished by differences in morphology, size, and the organisation of the particles on a microscopic scale. The different arrangements of silica particles were observed to vary in their stability in the electron beam. No single crystal or powder electron diffraction patterns could be obtained for any of the samples studied in the TEM mode and the different microstructural arrangements within the particles can all be classified as amorphous (Mann et al 1983). Figure 2 shows the three different

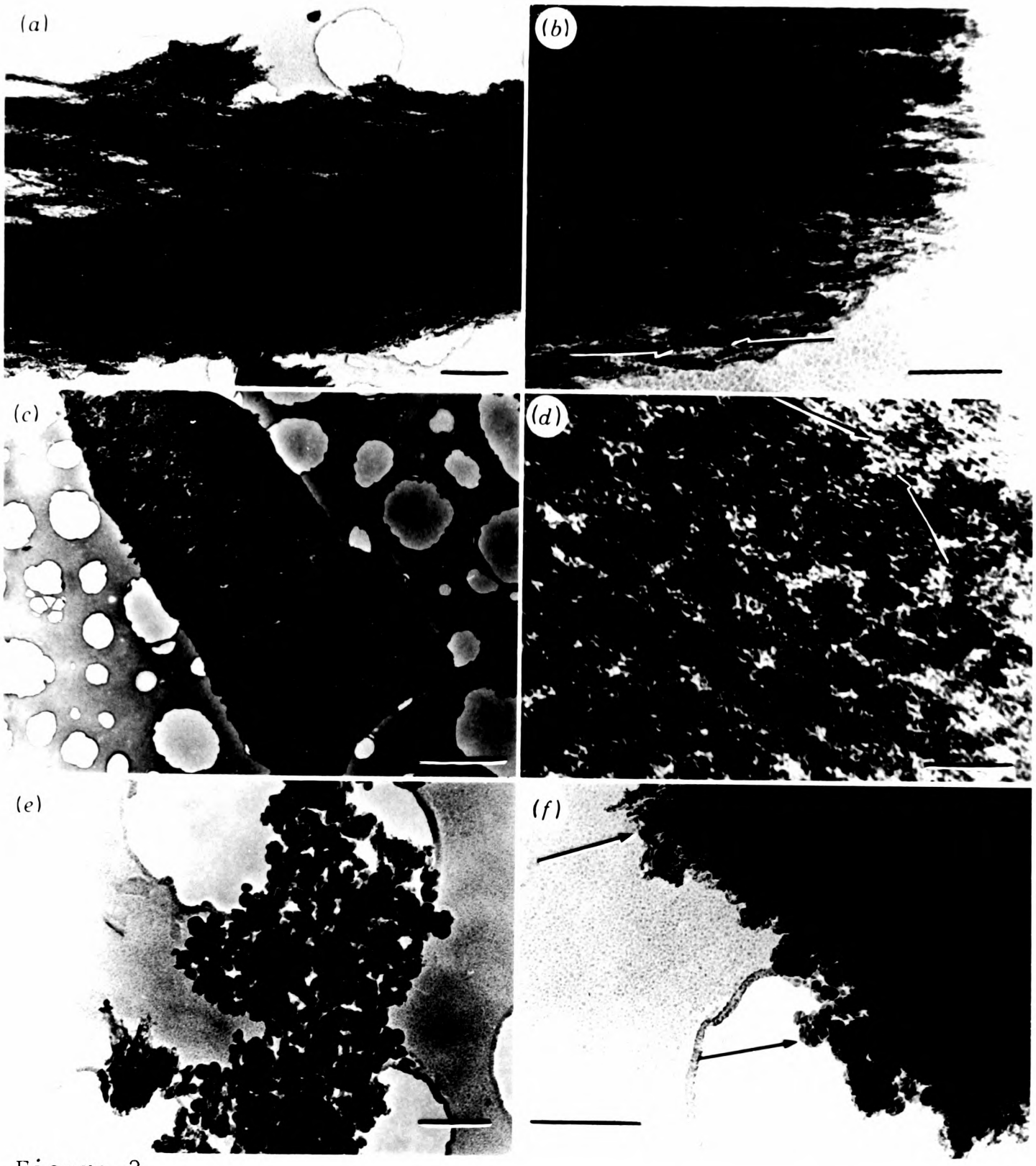

Figure 2

TEM of acid-treated silicified fragments of macrohairs. (a) Fibrous material. Bar represents 0.5µm. (b) High magnification image of fibrous material showing that the continuous strands of silica are formed by the ordered aggregation of microparticles (arrows). Bar represents 0.1µm. (c) Sheet-like material. Bar represents 1µm. (d) High magnification image of sheet-like material showing close packing of silica aggregates within the thin layer. Some directional preference for aggregation can be seen (arrows). Bar represents 0.1µm. (e) Globular material. Bar represents 0.25µm. (f) Fragment showing both globular and fibrous material in close association (arrows). Bar represents 0.25µm.

structural types. The fibrous material seen in figure 2a,b exhibits a clear linear direction. Particles are ca. 5nm in length and 2-3nm in diameter. Particles are joined end-on (see regions between arrows) to give continuous strands that suffered beam damage resulting in the coalescing of the discrete particles to give areas of undefined structure and direction.

Globular and sheet structural types were composed of silica spheres of 5-8nm in diameter. They differ in the packing arrangements of the particles and by their response to bombardment by the electron beam. In the sheet-like material, figures 2c and 2d, thin layers of particles were found. The distribution of particles appears fairly random, though at higher magnification a slight directional preference was observed. Chains of particles, as indicated by arrows in figure 2d, can be observed among the more random arrangement of the other particles. The particles are closely packed and suffered little beam damage.

The globular substructure, figures 2e and 2f, was composed of irregular spheres of varying diameter (40-120nm diameter) packed together in a random manner. At higher magnification these large particles appeared to comprise smaller silica particles of 6-8nm diameter. The globular substructure was beam-sensitive and on prolonged exposure coalesced to give regions of undefined structure. Such structures were often found in close proximity to the fibrillar material (arrows on figure 2f).

To determine the spatial location of the substructure types, images were recorded of fractured ends of intact untreated macrohairs, figure 3a. Sheetlike material was observed at the outer edge at which specific thickening of the outer wall was often observed, figure 3b. No more detailed information could be gained, however, on the nature of this

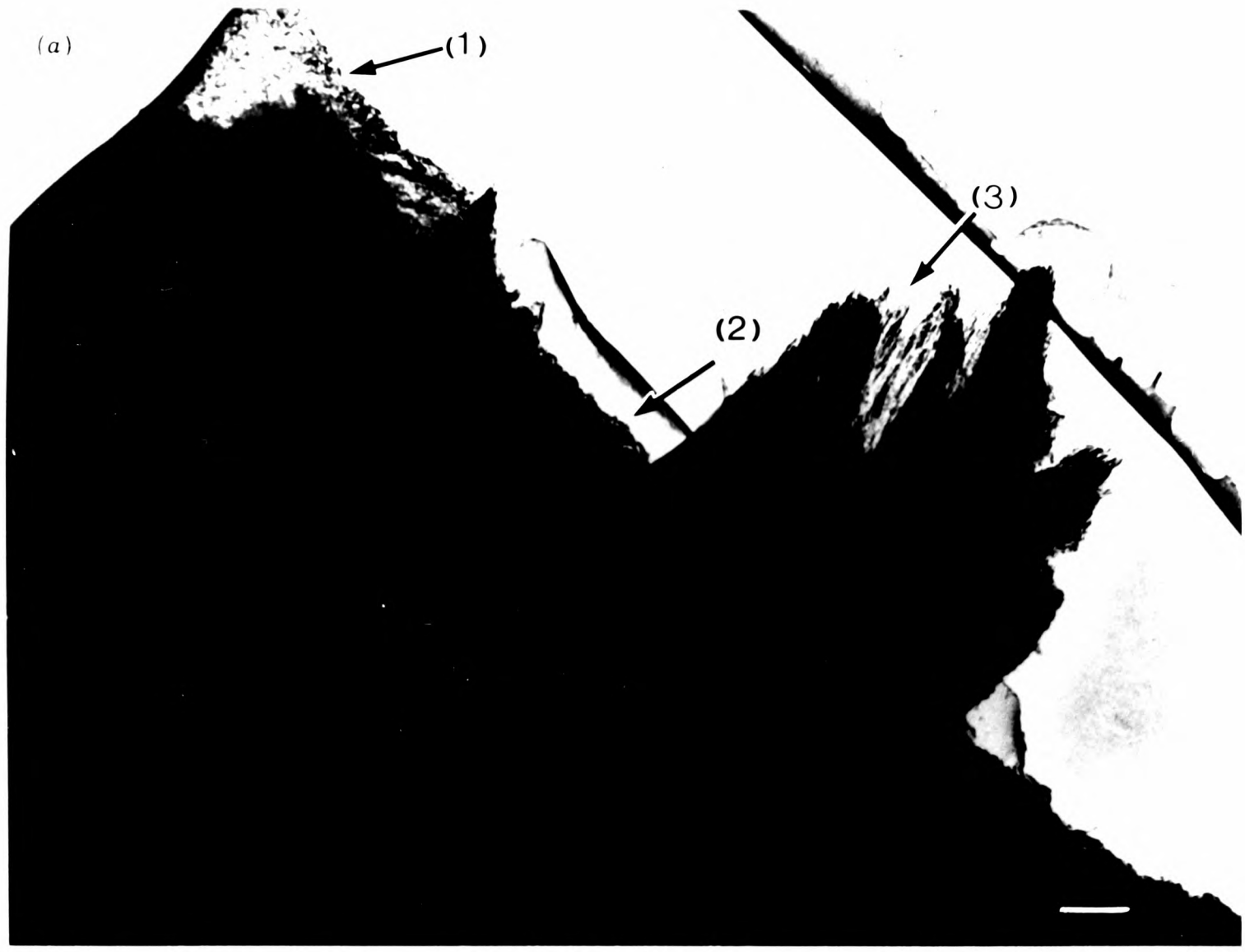

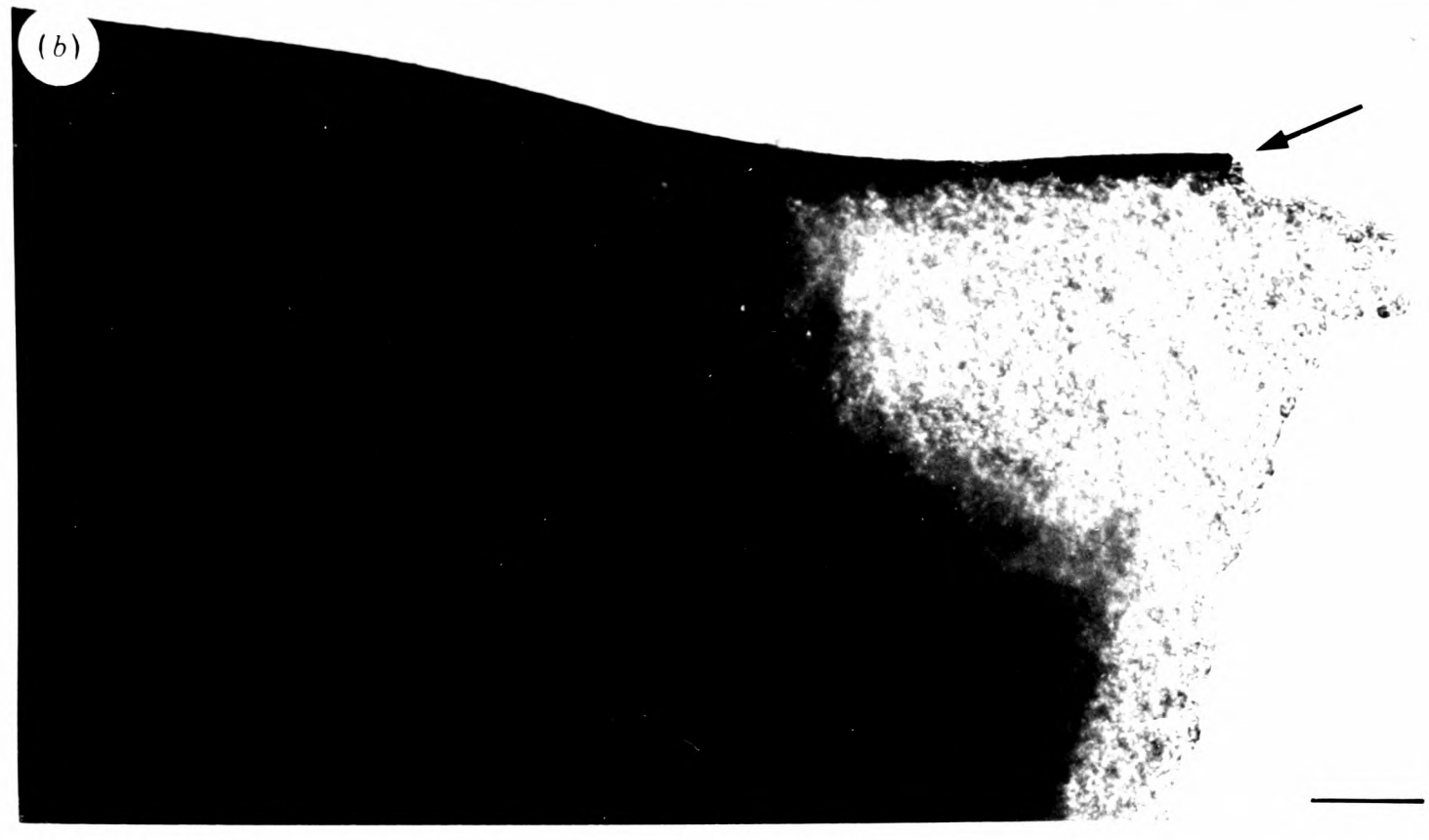

Figure 3

(a) Transverse view of a fractured end of a macrohair, showing sheet-like (arrow 1), globular (arrow 2) and fibrillar (arrow 3) material. Bar represents 0.5µm. (b) High magnification image showing the presence of sheet-like material at a thin edge. Note the specific thickening of the outer wall. Bar represents 0.2µm.

thickening. Fibrous material was observed as an extension from the central region of the macrohair and was oriented parallel to the central axis of the macrohair. Globular particles were observed at a small distance from the central region of the macrohair. However, it is difficult to discern the three-dimensional arrangement of these structural types from the two-dimensional projections recorded in the electron microscope. A developmental study was therefore undertaken to elucidate in more detail the temporal and spatial organisation of the silicified structures.

3.3.1.b Structural studies of developing macrohairs

Immature acid-treated samples were studied by TEM and SEM. Scanning electron micrographs taken of fractured ends of macrohairs showed that nine days after emergence of the inflorescence there was a thin rim of silica of uniform thickness (ca. 0.5μm) on the outer surfaces of the macrohair, figure 4a. Small localised deposits could be observed on the smooth inner surface of the silica. Considerable thickening of this layer had occurred at 24 and 40 days, figures 4b and 4c. At 24 days the inner surfaces were crenulated and at 40 days there were distinct boundaries between silicified zones that were totally absent in the 9 day sample.

Corresponding TEM investigations showed that at nine days largely sheet-like material was found, figures 5a and 5b, but that at 24 days both sheet-like and globular material were observed, figures 5c and 5d. At 40 days after emergence, globular material was mainly observed and there was evidence for the presence of the fibrillar material, figures 5e and 5f.

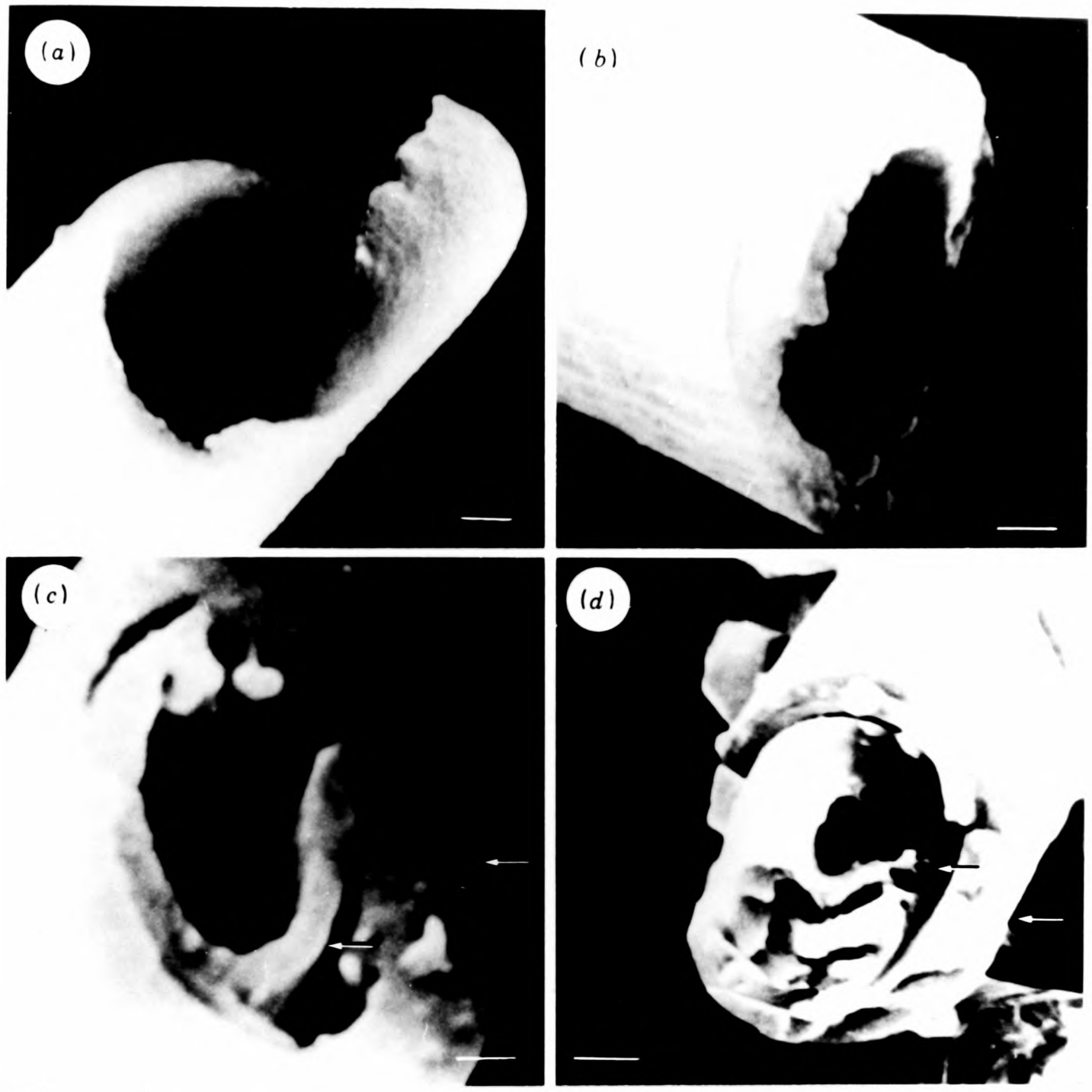

Figure 4

SEM of fractured ends of macrohairs. (a) Acid treated 9 day sample. A thin rim of silica of equal thickness can be seen on the inner surface of the silicified material. Bar represents 1µm. (b) Acid treated 24 day sample. Bar represents 1µm. (c) Acid treated 40 day sample showing a marked separation of adjacent zones (arrowed) and a central axial cylinder. Bar represents 1µm. (d) Untreated mature sample showing concentric cylinders of silicified material and central axial channel.

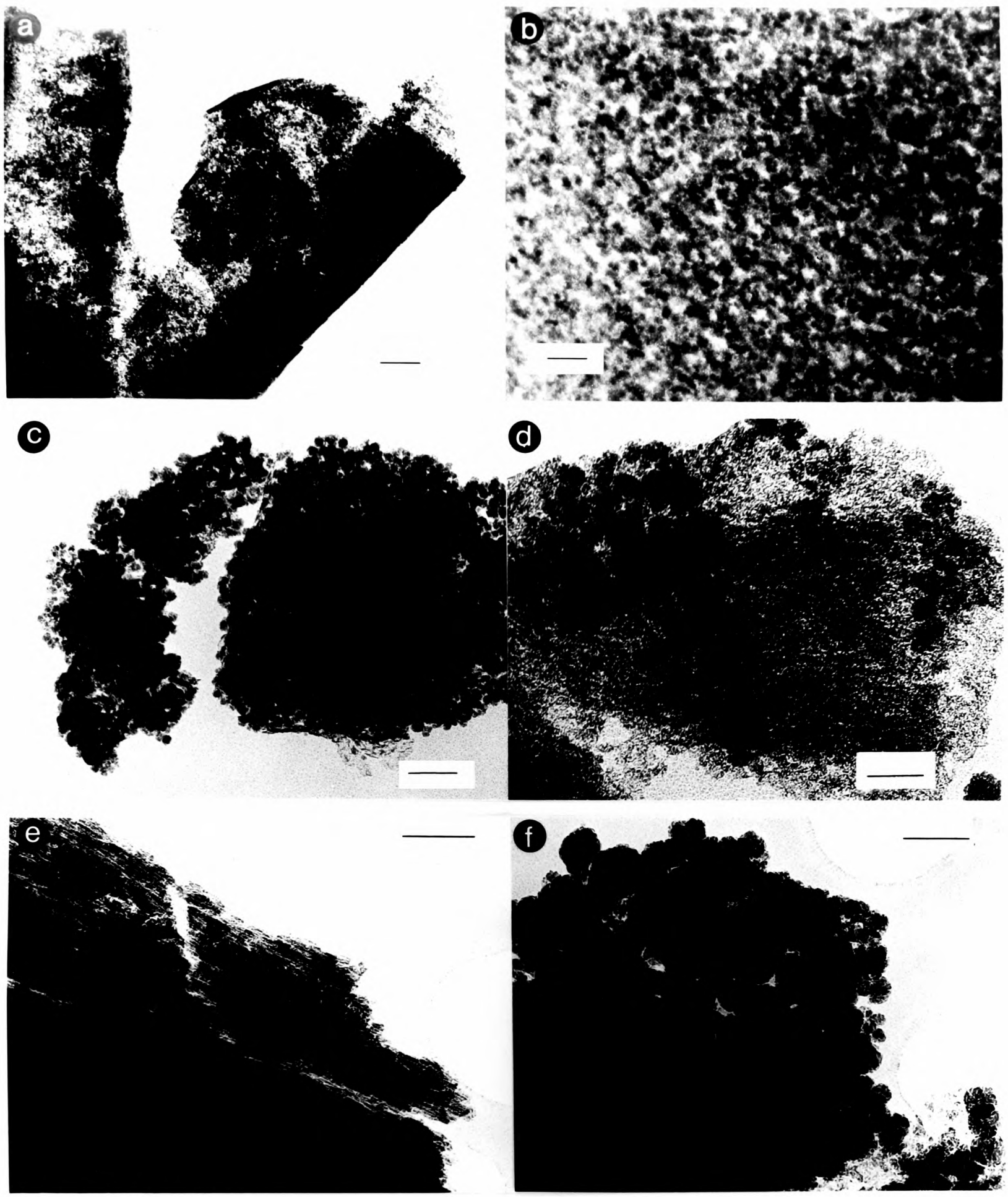

Figure 5

TEM of acid treated fragments from macrohairs at different stages of development.

(a) 9 day sample. Sheet-like material. Bar represents 200nm.

(b) High magnification image of sheet-like material with some globular material superimposed. Bar represents 100nm.

(c) 24 day sample. Globular material. Bar represents 200nm.

(d) 24 day sample. Globular and sheet-like material. Bar represents 200nm.

(e) 40 day sample. Fibrillar material showing a marked directional preference for aggregation. This material was not found in earlier samples. Bar represents 200nm.

(f) 40 day sample. Globular material. Bar represents 200nm.

3.3.2 Chemical and Physical studies of mature macrohairs

3.3.2.a X-ray microanalysis

Untreated and acid-treated samples were analysed by EDXA and in both cases, only silicon was detected. A representative analysis is shown in figure 6.

3.3.2.b Ultra high resolution transmission electron microscopy

Thin fragments of acid-treated samples were studied by HRTEM. A typical image is shown in figure 7. The opaline bodies have no order down to a level of 10Å. The material may therefore be classed as totally amorphous.

3.3.2.c Solid state nuclear magnetic resonance

Both untreated and acid-treated samples of macrohairs were studied by solid state ^{29}Si nmr. The untreated sample was also studied by ^{13}C nmr. Figure 8 shows the spectra obtained by MAS and CPMAS on the acid-treated materials. Peaks are assigned as indicated. A substantial number of silicon atoms (≏50%)have hydroxyl groups attached. To remove any ambiguity attached to the peak assignment at -101.8 ppm (which could possibly have arisen from Si(1 Al, 3 OSi≡) as well as $Si(OSi\equiv)_3(OH)$) a ^{27}Al nmr spectrum was attempted. No aluminium was detected and as Si/Al ratios in excess of 2000:1 can be measured by this technique, the absence of aluminium from the sample is confirmed.

The absorption resonances obtained are broad (6-8.8 ppm) as compared to the ^{29}Si absorptions of quartz, stishovite and dealuminated zeolites where the narrowness of the absorption reflects the crystallinity of the sample. The broadness of the peaks is similar to that observed for synthetic silica gels and indicates the non-crystalline nature of this

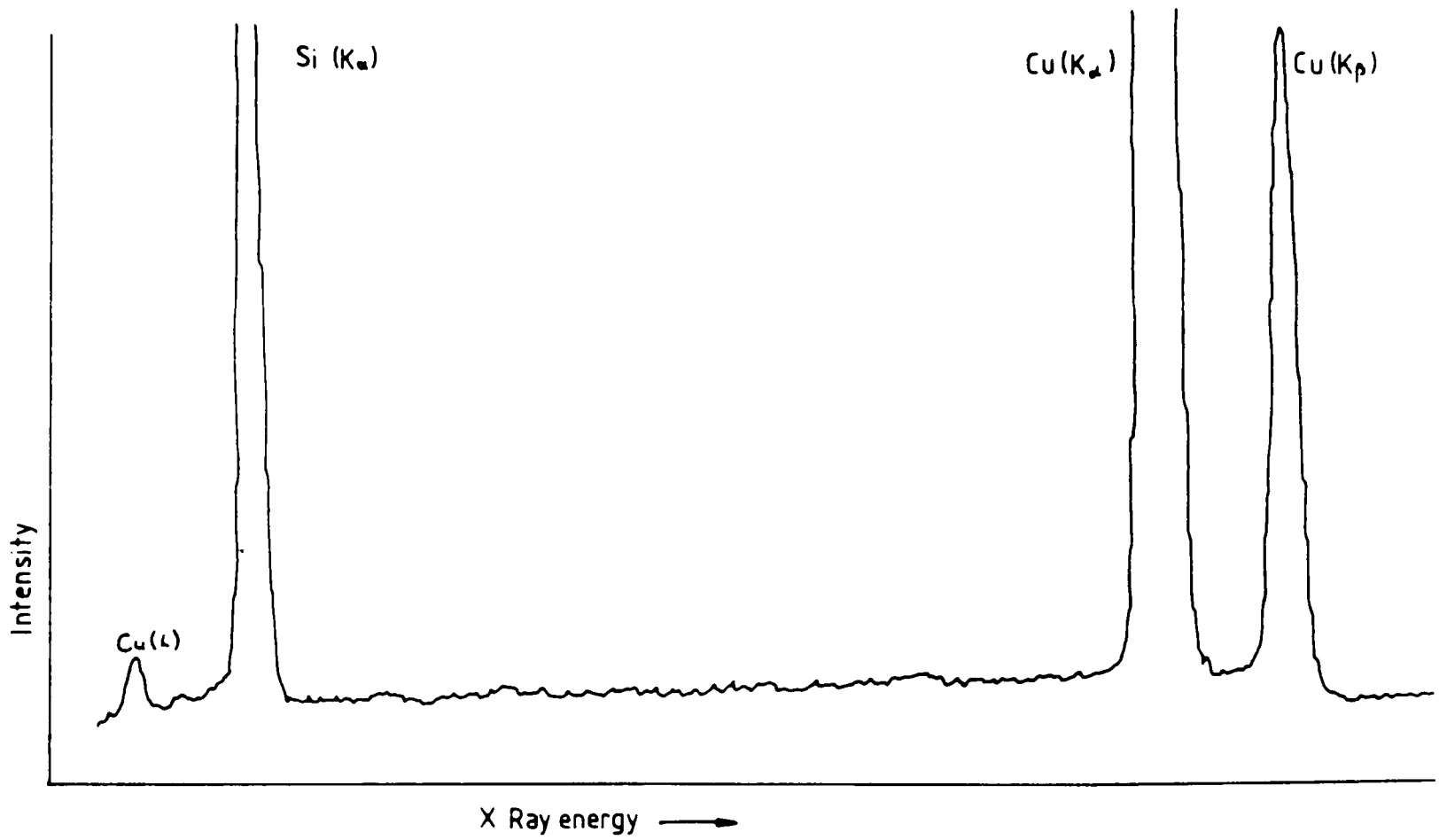

Figure 6

EDXA analysis of a mature macrohair from the lemma of the grass Phalaris canariensis L.. Si is the only element detected.

The Cu peaks arise from X-rays produced by the copper grid during analysis.

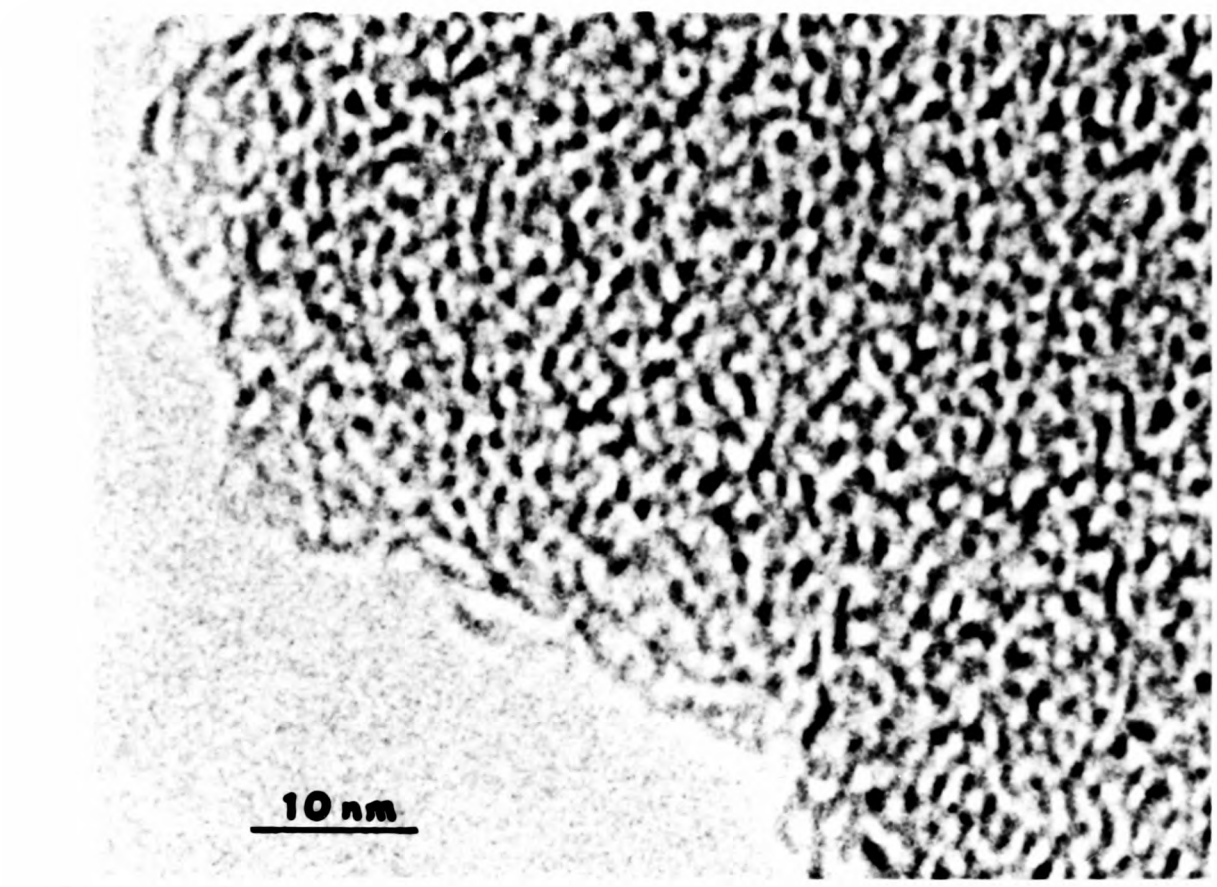

Figure 7

Ultra high resolution transmission electron micrograph of a fragment of silicified macrohair. Bar represents 10nm.

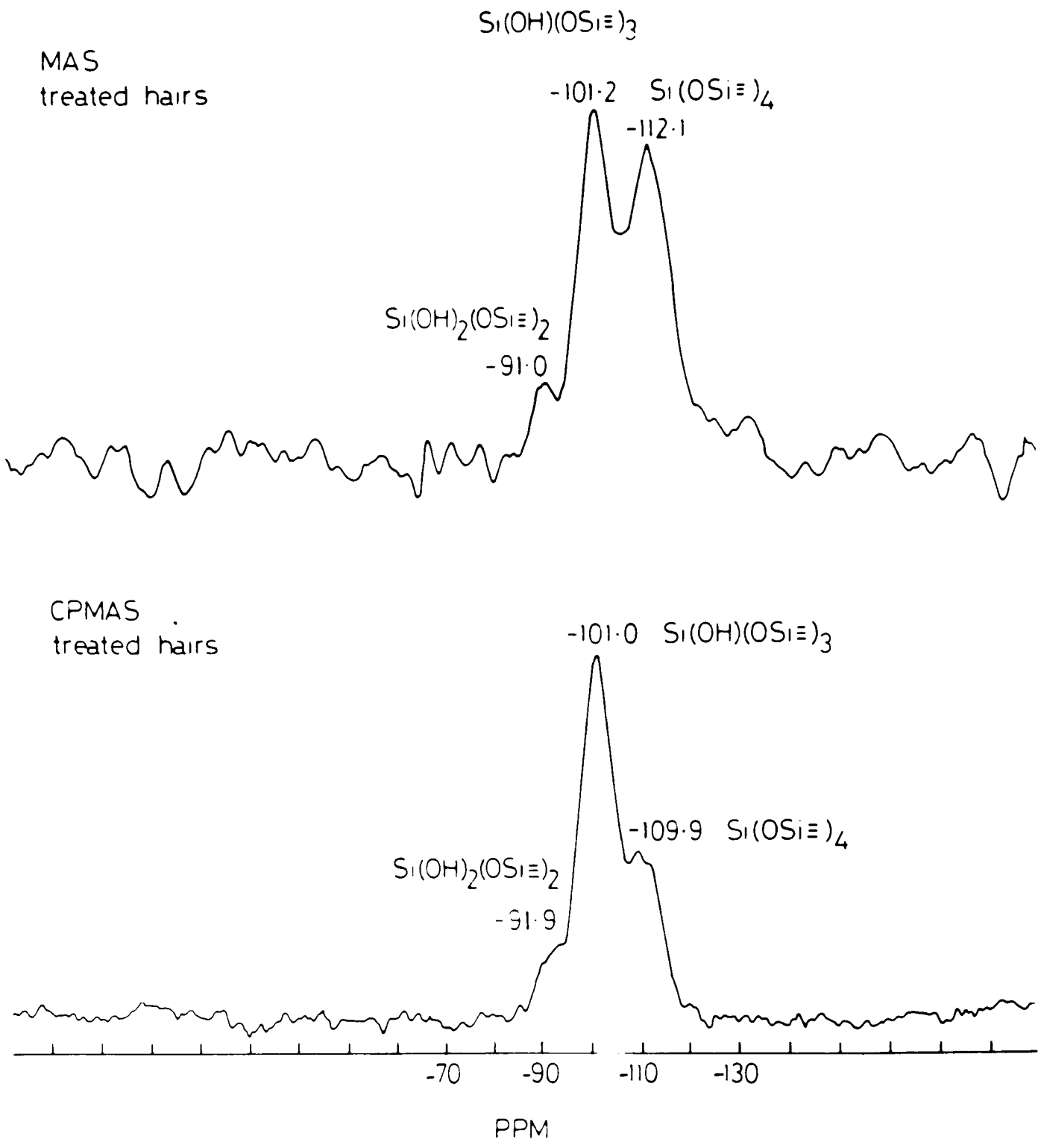

Figure 8

^{29}Silicon MAS and CPMAS spectra of samples of macrohairs from Phalaris canariensis L.. Peak assignments are as indicated.

biological material (Maciel and Sindorf,1980).

Confirmation of the presence of hydroxyl groups was obtained by performing CPMAS experiments on the samples. Using this technique, silicon atoms attached via oxygen to hydrogen atoms will relax faster due to the irradiation pulse than silicon atoms with no hydroxyl groups attached and the absorptions corresponding to $(OH)Si(OSi\equiv)_3$ and $(OH)_2Si(OSi\equiv)_2$ will be selectively enhanced. This is indeed the case, figure 8.

Analysis of the untreated sample by ^{29}Si nmr using MAS and CPMAS experiments yielded similar spectra to those obtained for the treated sample, figure 9. However, better resolution was obtained from a much smaller sample (volume for volume).

The spectrum obtained by ^{13}C MAS on the untreated sample is given in figure 10. The spectrum indicates the presence of a polysaccharidic matrix associated in some way with the silica. A spectrum obtained from the hemicellulosic extract is also presented for comparison. The spectral lines are less well resolved although a greater volume of sample was used for the experiment.

3.3.2.d Infrared spectral studies on mature macrohairs

Both untreated and acid-treated samples of macrohairs were studied by infrared spectroscopy. Two reference samples of finely crushed quartz and an industrial amorphous silica were also studied. The references were used to relate the physical characteristics of the system under investigation to known silicas. Results are presented as spectra, figure 11. The spectrum of quartz shows absorptions at 1172(s), 1082, 790(s), and 460(m) cm^{-1} but virtually no absorption in the hydroxyl region around 3300 and 1600 cm^{-1}. The second reference, silicic acid, has broader

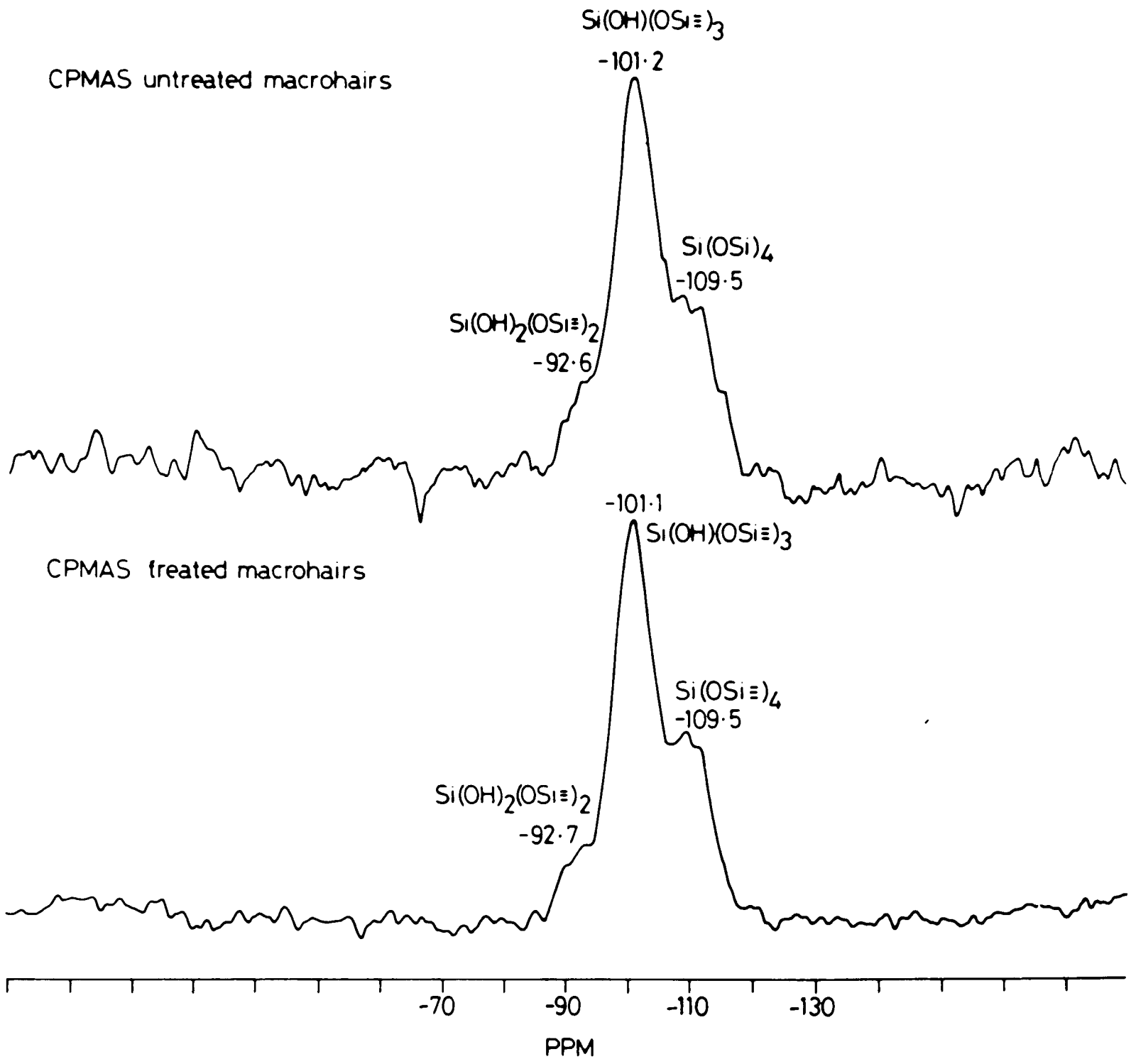

Figure 9

A comparison of the ^{29}Si CPMAS spectra from untreated and treated samples of macrohairs from the grass Phalaris canariensis L.. There was a decrease in the time required for data accumulation for the untreated sample.

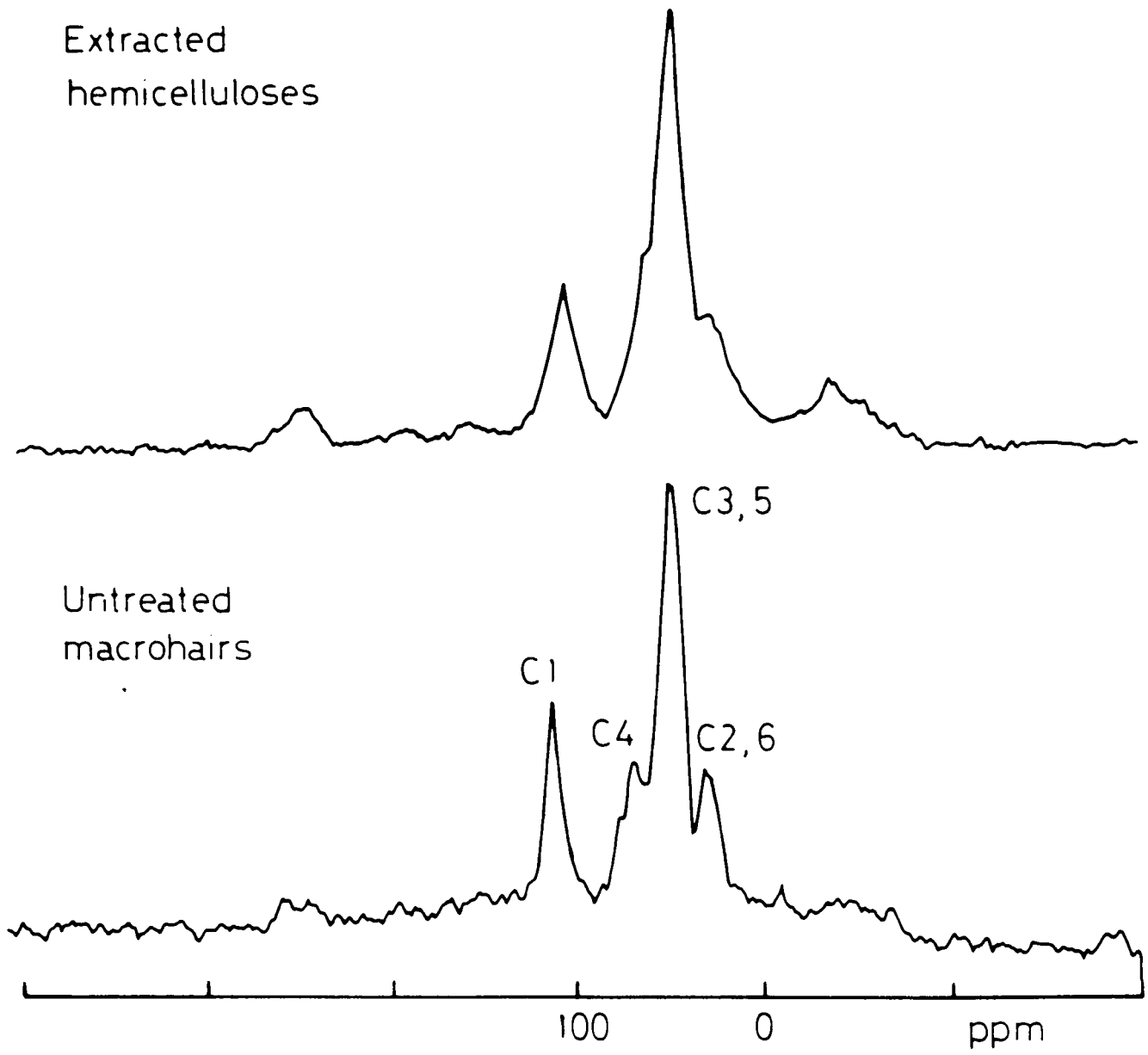

Figure 10

^{13}C MAS spectra obtained from the untreated macrohair sample and from a sample of extracted polysaccharide. Peak assignments are shown for the untreated macrohair sample. Assignments were made by comparison with data in the literature.

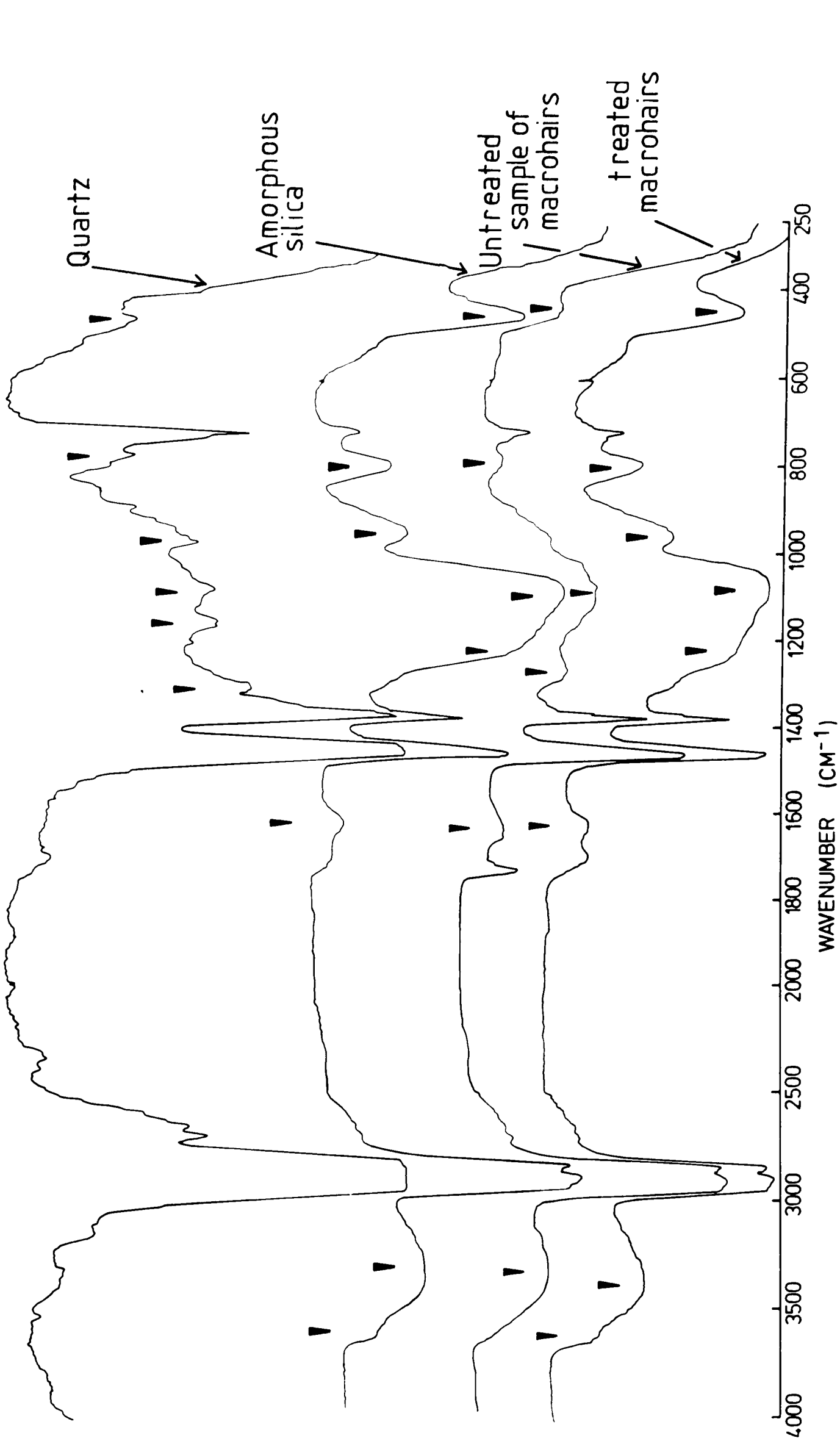

Figure 11

Infrared spectra obtained from quartz, amorphous silica and treated and untreated samples of plant macrohairs.

absorption peaks at 1210, 1090(s),800(w) and 470(m) cm^{-1} as well as peaks at 966(m) cm^{-1} and a broad region of absorption from 3220 to 3640 cm^{-1} with minor peaks. The new peaks arise from Si-OH and OH stretching and bending modes. The macrohairs from the lemma of the Phalaris seeds give spectra very similar to those of silicic acid and similar to other forms of opaline amorphous silica. The Si-OH peaks are quite distinct from those of bound water at 3435 and 1600 cm^{-1}. Similar results have been obtained for silica from diatoms (Katani,1971). A notable feature of the spectrum produced from the untreated macrohair sample is the similarity to the quartz spectrum in the 700-1400cm^{-1} region.

Prolonged acid treatment to remove organic matter from the macrohairs gives a sample of which the resulting silica infrared spectrum closely resembles that of industrial amorphous silicas which still contain $Si(OH)(OSi\equiv)_3$ units.

3.3.2.e Birefringence studies

Untreated and acid-treated 9 day, 24 day and mature samples were studied using a polarising microscope. Birefringence was only observed for the mature untreated and acid-treated samples which contained fibrillar packing arrangements of the silica particles. In the immature samples, where fibrillar material is not found, no birefringence was observed though it was appreciated that the nature of the organic component which had been removed from these samples may have a role to play in determining the degree of optical activity observed within the sample. O'Neill et al (1980) have previously shown that the mature acid-treated macrohairs are birefringent but stated that the material was crystalline. This, however, with the evidence presented here is seen not to be the case.

3.3.2.f Nitrogen adsorption

Nitrogen adsorption experiments were performed on untreated and acid-treated samples. Nitrogen adsorption isotherms, measured at 77K were recorded by Dr. J.Ramsay (AERE, Harwell) on both samples. From these isotherms it was possible to derive the specific surface area S_{BET} and the mean pore size r_p for each sample. The treated material had a high specific surface area ($241 m^2 g^{-1}$) and a mean pore size of 36Å. (N.B. the distribution of sizes was large). Similar experiments performed on the untreated material gave no measurable surface area or porosity which suggests that the silica and the polysaccharide are intimately associated.

3.4 Discussion

The results presented in this chapter indicate that silicification in macrohairs of the lemma of Phalaris canariensis L. commences as the inflorescence emerges. The different structural morphologies of silica located within the macrohairs appear to be initiated at precise time intervals during development. At less than seven days after emergence of the inflorescence only thin sheets of silica particles are formed. By 24 days after emergence of the inflorescence both sheet-like and globular material are present but fibrillar material is only present as the macrohairs approach maturity. At maturity there appears to be a zoning of the silicified material within the macrohairs, figure 4d which was not observed for macrohairs studied at 24 days after emergence of the inflorescence. The occurrence of morphological variations in the silicified material suggests precise changes with time of the local environment within the macrohair where polymerisation and deposition of

the different forms of silica takes place.

In each substructural arrangement the silica particles are chemically `pure´ and crystallographically amorphous(Mann et al.,1983) but may, as in the case of the fibrillar component, be arranged in ordered microscopic arrays of rod-shaped particles. Previous workers (O´Neill et al., 1980) have shown that the macrohairs are birefringent and therefore inferred that the material was crystalline and optically anisotropic. However, a body consisting of parallel rod-shaped particles composed of isotropic material (such as amorphous silica), which are embedded in an isotropic medium of different refractive index, will show double refraction provided that the rods are narrower than the wavelength of light (Hartshorne and Stuart, 1970). We have observed birefringence only in mature macrohairs (acid-treated and untreated), which is consistent with the relatively late deposition of the fibrillar substructure that is presumably embedded in a thickened cell wall matrix (Hodson et al., 1984).

The chemical and physical characterisation of the silica utilising infrared spectroscopy and solid state nuclear magnetic resonance has shown that the nature of the untreated material is similar to that of synthetic silica gels and to silica extracted from diatoms (Katani,1971) as it contains $Si(\equiv OSi)_3(OH)$ and $Si(\equiv OSi)_2(OH)_2$ units as well as many $Si(\equiv OSi)_4$ units. The treated material contains fewer hydroxyl groups within its structure and is more similar in nature to industrial amorphous silicas. The hydroxyl groups are found both on the surface and on the interior of the macrohairs (Mann et al.,1983). From a comparison of the behaviour of the different ultrastructural types in the electron beam it appears that the globular material has more hydroxyl groups associated with it than the two other particulate arrangements. The

untreated material is closely associated with an organic matrix of polysaccharides which appears to give additional order to the system since, although less silica (weight for weight) was present in the untreated sample, sharper, better resolved ^{29}Si nmr spectra were more readily obtained. The organic matrix thickens as silicification occurs as evidenced by the increased time required to remove the organic material from the macrohairs by acid treatment. Further evidence for a close association of the organic matrix with the silica was obtained from nitrogen absorption experiments. The treated material was porous, the voids being of sizes expected from the TEM ultrastructural evidence. The untreated sample, however, was not porous indicating that the organic and inorganic phases are intimately associated with one another.

Clearly, the mode of aggregation of microscopic silica particles from a supersaturated silicic acid solution could be affected by the close proximity of the organic matrix. Another factor which may affect aggregation is the presence of any inorganic constituents within the macrohair volume. Both these factors may produce changes in the surface charge of the primary particles which ultimately leads to different ultrastructural forms of silica being adopted (Iler, 1979). Alternatively, changes in the rate and form of aggregation may be influenced by the level of supersaturation and pH of the cellular fluid. Thus the cellularly controlled process of wall deposition may result in the organisation and differentiation of deposited silica particles. It seems unlikely that passive transpirational processes could result in such precise spatial and temporal biomineralised structures.

The time dependent involvement of inorganic components in the mineralisation process is presented in chapter 4 and the characterisation of the organic matrix intimately associated with the silica of these macrohairs is presented in chapter 5. Only then will we be able to define the importance of the various factors in determining the precise adoption of variable structural forms during biomineralisation.

3.5 References

1. Barber, D.A., Shone, M.G.T. (1966) J. Exp. Bot., 17, 569-578.

2. Bhatt, T., Coombes, M. & O'Neill, C.H. (1984) Int. J. Cancer, 34, 519-528.

3. Engelnhardt, G., Lohse, U., Samoson, A., Magi, M., Tarmak, M. & Lippmaa, E. (1982) Zeolites, 2, 59-62.

4. Fyfe, C.A., Gobbi, G.C., Klinowski, J., Thomas, J.M. & Ramdas, S. (1982) Nature, 29, 530-536.

5. Hartshorne, N.H. & Stuart, A. (1970) Crystals and the Polarising Microscope, London: Edward Arnold.

6. Hodson, M.J., Sangster, A.G. & Parry, D.W. (1984) Proc. R. Soc.Lond. B 222, 413-425.

7. Hubbard, C.E. (1954) Grasses. Harmondsworth: Penguin.

8. Iler, R.K. (1979) The Chemistry of Silica. John Wiley & Sons, New York, p.174.

9. Jones, L.P.H., Milne, A.A. & Wadham, S.M. (1963) Plant and Soil, 18, 358-371.

10. Katami, A., (1971) Mar. Biol. 8, 89-95.

11. Kaufman, P.B., Dayanandan, P., Takeoka, Y., Bigelow, W.C., Jones, J.D. & Iler, R.K. (1981) in Silicon and Siliceous Structures in Biological Systems, ed. Simpson, T.L. & Volcani, B.E., Springer Verlag, pp.409-449.

12. Maciel, G.E. & Sindorf, D.W. (1980) J. Am. Chem. Soc. 102, 7606-7607.

13. Mann, S., Perry, C.C., Williams, R.J.P., Fyfe, C.A., Gobbi, G.C. & Kennedy, G.J. (1983) J. Chem. Soc. Chem. Commun., pp.168-170.

14. Montgomery, D.J. & Parry, D.W. (1979) Ann. Bot. (Lond) 44, 79-84.

15. O'Neill, C.H., Hodges, G.M., Riddle, P.N., Jordan, P.W., Newman, R.H. & Flood, R.J. (1980) Int. J. Cancer 26, 617-628.

16. O'Neill, C.H., Pan Qiong-Qing, Clarke, C., Liu Fu-Sheng, Hodges, G., Ge Ming, Jordan, P., Chang Yu-Ming, Newman, R.H. & Toulson, E. (1982) Lancet 1, 1202-1206.

17. Parry, D.W. & Kelso, M. (1975) Ann. Bot. (Lond) 39, 995-1001.

18. Parry, D.W. & Smithson, F. (1964) Ann. Bot. (Lond.) 28, 169-185.

19. Peggs, A. & Bowen, H. (1984) Phytochem. 23, 1788-1789.

20. Ramsay, J.D.F. & Booth, B.O. (1983) J. Chem. Soc., Faraday Trans. 1, 79, 173-184.

21. Raven, J.A. (1983) Biol. Rev. 58, 179-207.

22. Sangster, A.G. & Parry, D.W. (1981) in Silicon and Siliceous Structures in Biological Systems, ed. Simpson, T.L. & Volcani, B.E., Springer Verlag, pp. 383-407.

23. Voronkov, M.G., Zelchan, G.I. & Lukevitz, E. (1975) Silizium und Leben, Akademie-Verlag, Berlin.

24. Weiss, A. & Herzog, A. (1978) in Biochemistry of Silicon and Related Problems, ed. Bendz, G. & Lindqvist, I., Plenum publ. p.109.

25. Yoshida, S., Ohnishi, Y. & Kitagishi, K. (1962) Soil. Sci. Pl. Nutr. Tokyo, 8, 1-5.

Chapter 4: Analytical Studies on silicified macrohairs from the lemma of the grass Phalaris canariensis L.

4.1 Introduction

In the previous chapter, information concerning temporal variations in the ultrastructure of silica aggregates in mineralised macrohairs was discussed. The variations in ultrastructure lead us to question the nature of the local environment within the macrohairs as silicification takes place. The environment in which precipitation occurs can be altered by changes in local ionic atmosphere or by the presence of organic molecules/ macromolecules.

In this chapter, mineralisation is discussed on the basis of an analytical study of macrohairs as silicification occurs.

Two methods of analysis were used in this analytical study: Energy dispersive X-ray analysis (EDXA) and proton induced X-ray emission (PIXE) coupled to a scanning proton microprobe (SPM). EDXA, as described previously (chapter 2) has an optimal resolution of half the specimen thickness for thin samples and a detection capability of 10^{-17}g or 100ppm. However, for thick samples, as is the case of analysis of the macrohairs, resolution is limited to a couple of microns and the limits of detection are of the order of 100-1000ppm. EDXA is therefore used to indicate the general changes in inorganic content within a macrohair or to indicate general differences between samples at different stages of development. The SPM has an optimal resolution of 1 micron and a detection capability of < 1ppm. The resolution obtainable varies little with sample thickness and this method was used to provide more detailed information on silicified samples taken at two different time points during mineralisation.

4.2 Materials and Methods

4.2.1 Samples

Macrohairs for analytical studies were obtained from plants grown from seed as described previously (chapter 3). The growing plants were watered with a solution containing dissolved silica on alternate days during the growth period. When each inflorescence appeared, the date was noted and the inflorescence tagged. Samples for study were removed from midway down each inflorescence. For the electron microprobe study, individual spikelets were removed at the following stages: (1) 2 days before the inflorescence emerged, (2) as the inflorescence appeared (emergence), (3) 1.5 days after emergence, (4) 3 days after emergence, (5) 5 days after emergence, (6) 6 days after emergence, (7) 7 days after emergence, (8) 9 days after emergence, (9) 18 days after emergence and (10) 40 days after emergence of the inflorescence. Samples for proton microprobe studies were taken at 4 days and 40 days after emergence of the inflorescence. All samples were studied immediately in either the electron microprobe or the proton microprobe unless otherwise stated.

4.2.2 Energy dispersive X-ray analysis of macrohairs

A Jeol 100CX Temscan analytical electron microscope, fitted with a Kevex Li-drifted Si detector, and operating at 100KeV was used for analysis of samples which were prepared for study by gently rolling the lemma on a copper electron microscope grid. The samples were set at an angle of 40° to the detector and were analysed for 100s in the SEM mode. An area ca. 2μm x 2μm at the centre of the hair was analysed and the distance of the analysis area from the tip or base of the hair noted. The

analytical data is presented graphically but a selection of the numbers obtained is given in appendix 1.

4.2.3 Proton induced X-ray analysis of macrohairs

Macrohairs 4 days after emergence of the inflorescence were rolled onto 2μm thick mylar film supported by an aluminium holder. The 40 day sample was mounted in an identical manner using 1μm thick polypropylene film as a target backing.

The two samples were scanned by a 4MeV proton beam focused down to a spot size of less than 2μm in diameter with a transmitted beam current of 100pA. Elemental maps were constructed as described previously (chapter 2). Point analyses were also performed and the position of analysis noted. These analyses give better statistics than the elemental maps. The absence of inhomogeneity was checked by reference to the elemental maps. The point analytical data are presented graphically in the form of X-ray spectra and tabulated as concentrations in micrograms per square centimetre. The data produced from scanning the proton beam over an area of sample are represented as two dimensional elemental maps which are colour coded for elemental concentration. Both samples were studied by SEM after analysis. SPM sample holders were affixed to aluminium stubs with double-sided adhesive tape and coated with gold prior to viewing in the Phillips PSEM 500 scanning electron microscope.

4.3 Results

4.3.1 Elemental distribution in developing macrohairs

4.3.1a Silicon

EDXA analysis of macrohairs from Phalaris canariensis showed that before emergence the hairs contained no silicon (figure 1a). At emergence, there was an insignificant level of silicon above background in the hairs. At two days after emergence, silicon was present within the hairs, largely at the tip (figure 1b). The levels of silicon were found to be much reduced when analyses were carried out at small distances from the tip (figures 1c,d). By seven days after emergence of the inflorescence the entire length of the hair was silicified to some extent though there still appeared to be more silica towards the tip of the hairs. At later stages in development, for example, at 9,18 and 40 days, the levels of silicon further back from the macrohair tip steadily increased (figures 2 and 3).

SEM micrographs of the inflorescence bracts surrounding the caryopsis showed that the macrohairs were fully formed but were very delicate distortable structures before emergence (figure 4a). At three and seven days the macrohairs towards the tip of the caryopsis were more rigid, presumably silicified, while macrohairs towards the base were still flexible and presumably unsilicified (figure 4b and 4c). By twentyfour days all the macrohairs appear straight and are presumably silicified (figure 4d).

Figure 5 shows the increase in the average amount of silicon within each macrohair with age, recorded at the tip and 0.16mm from the tip. For each day there is a spread of points that may be attributed to the inhomogeneity of the samples of macrohairs studied at each stage. The

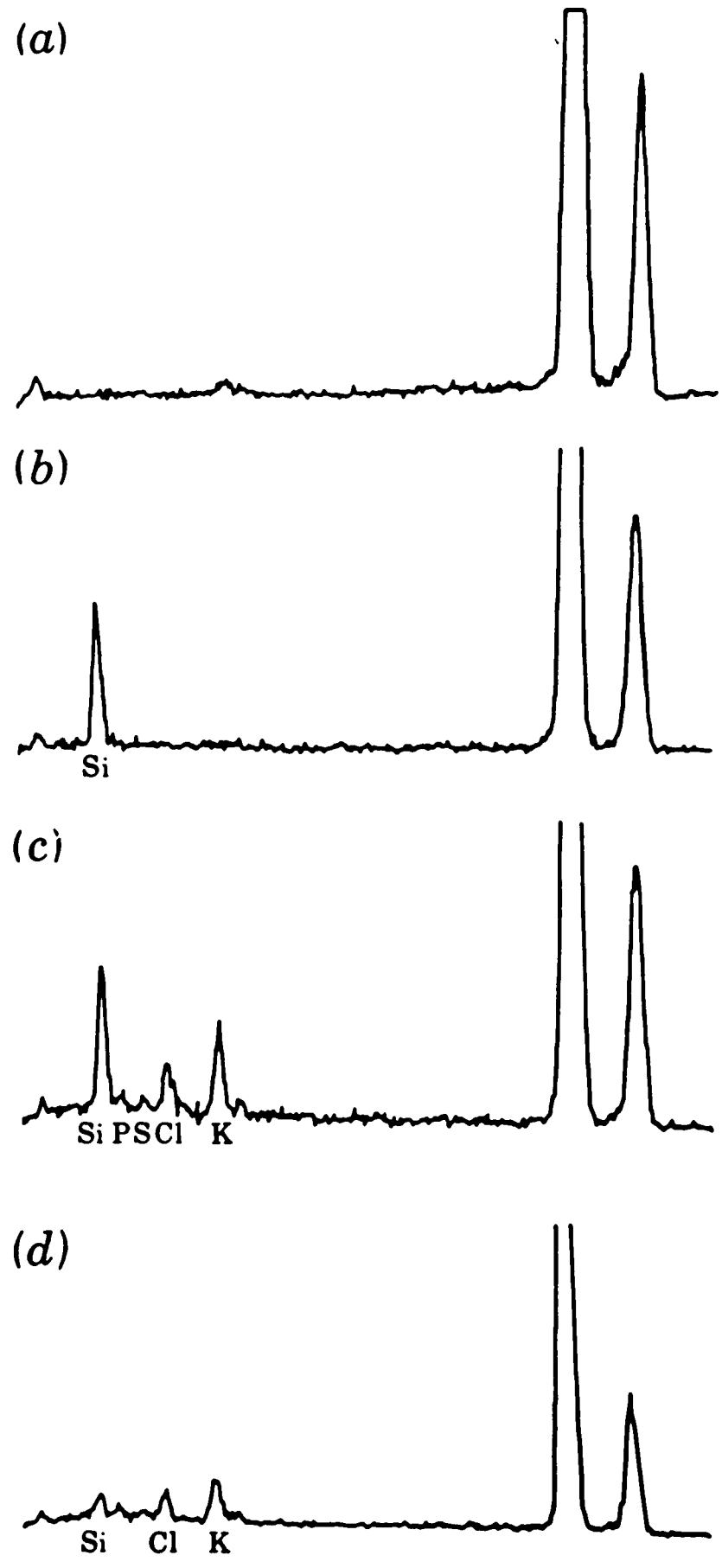

Figure 1

(a) EDXA of macrohair immediately prior to emergence. The large peaks arise from the copper EM grid. (b) EDXA of the tip of a macrohair two days after emergence. Only silicon was detected. (c) EDXA of macrohair two days after emergence, 0.007mm from the tip, Si, P, S, Cl and K were detected. (d) EDXA of macrohair two days after emergence, 0.023mm from tip. Much lower levels of Si, P, S, Cl and K were detected.

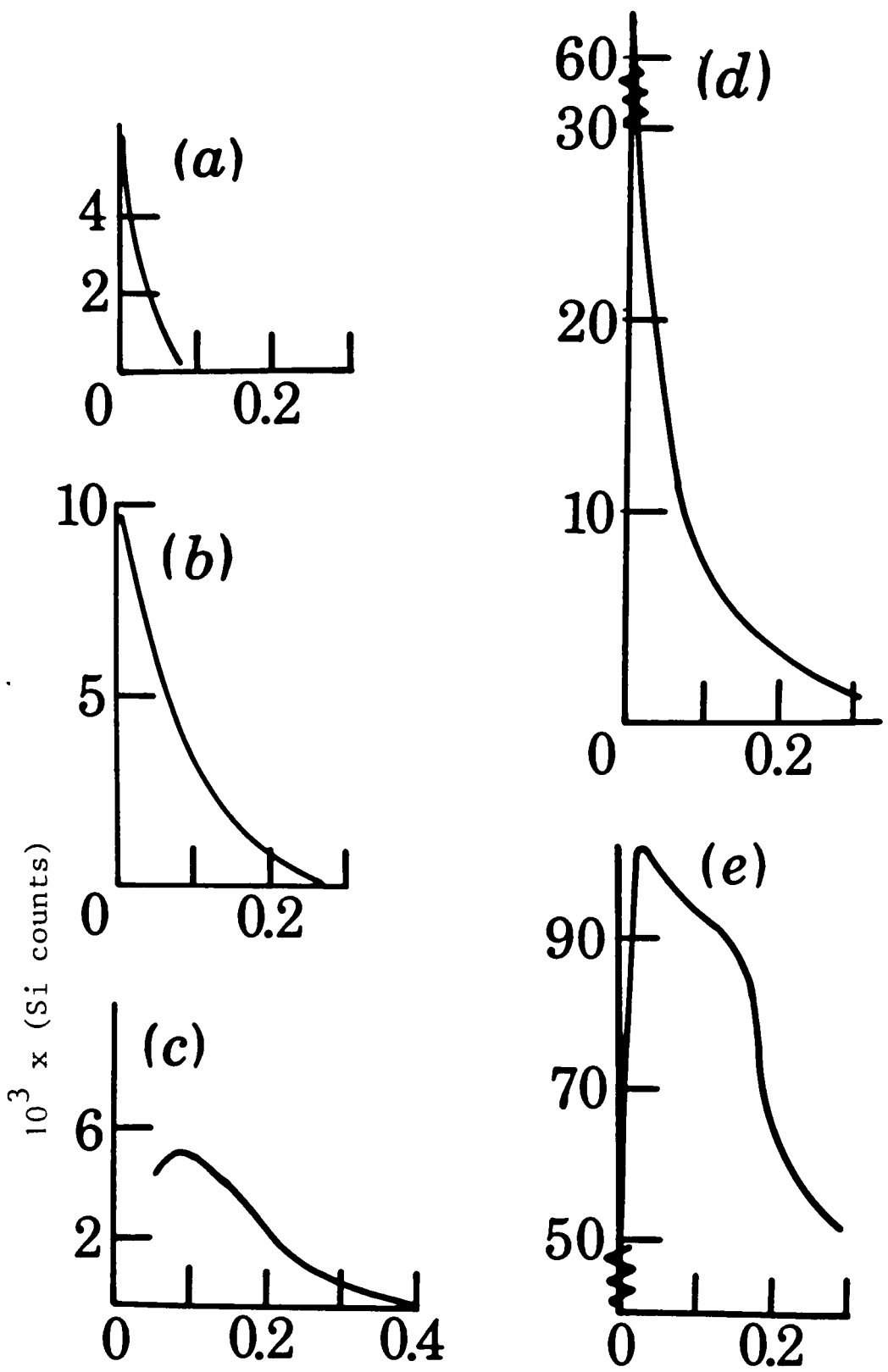

Figure 2

Levels of silicon compared with distance of analysis point from the tip of the macrohair at: (a) 1.5 days; (b) three days; (c) five days; (d) nine days; (e) 40 days after emergence of the inflorescence.

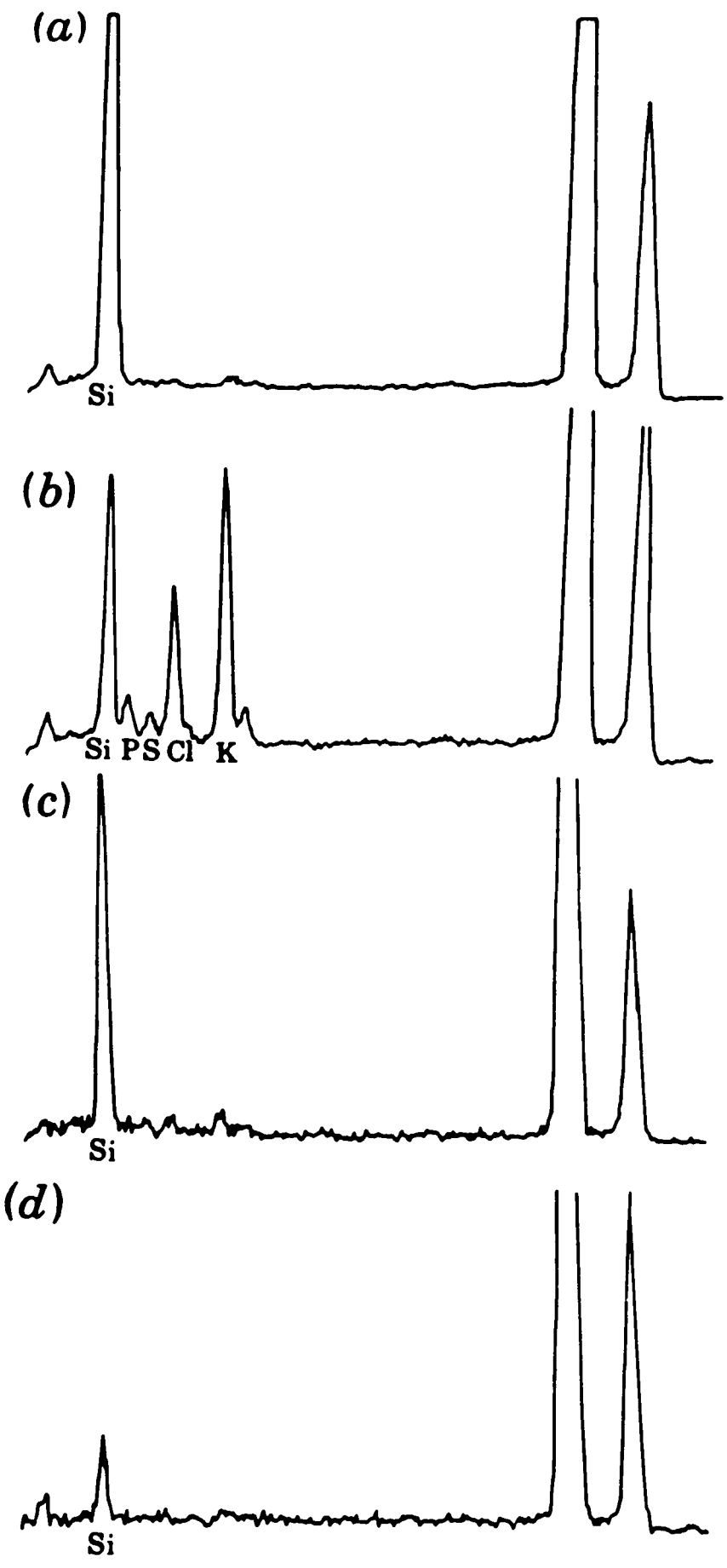

Figure 3

A series of EDXA analyses along the length of a macrohair at five days after emergence of the inflorescence.
(a) Tip of macrohair; (b) 0.06mm from tip of macrohair; (c) 0.2mm from tip of macrohair; (d) base, 0.3mm from tip of macrohair.

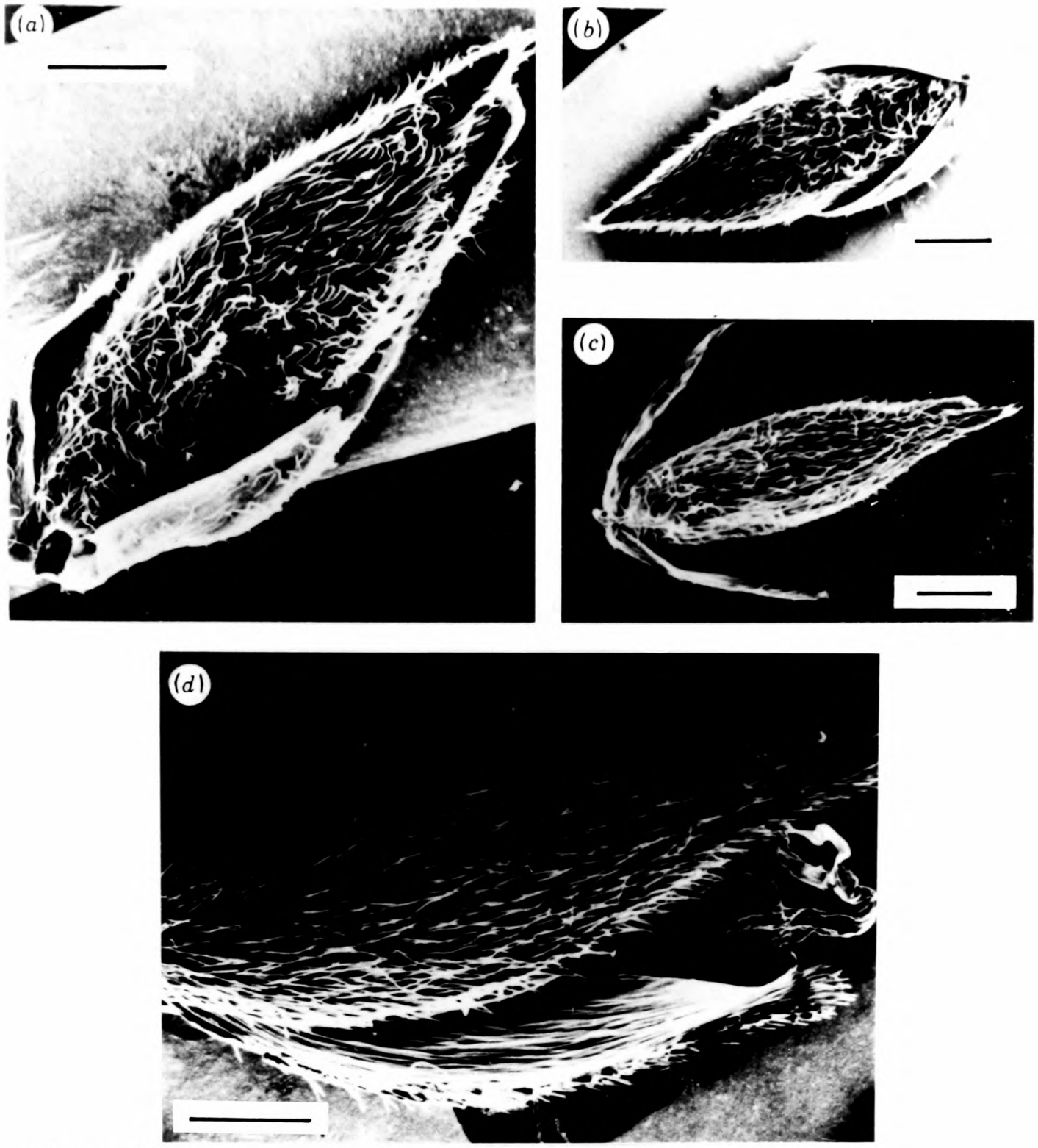

Figure 4

SEM of inflorescence bracts at different stages of development. (a) before emergence of the inflorescence. The hairs are fully formed but very flexible. Bar represents 5µm. (b) three days after emergence of the inflorescence. Bar represents 10µm. (c) seven days after emergence of the inflorescence. Bar represents 10µm. (d) twenty-four days after emergence of the inflorescence. Bar represents 5µm.

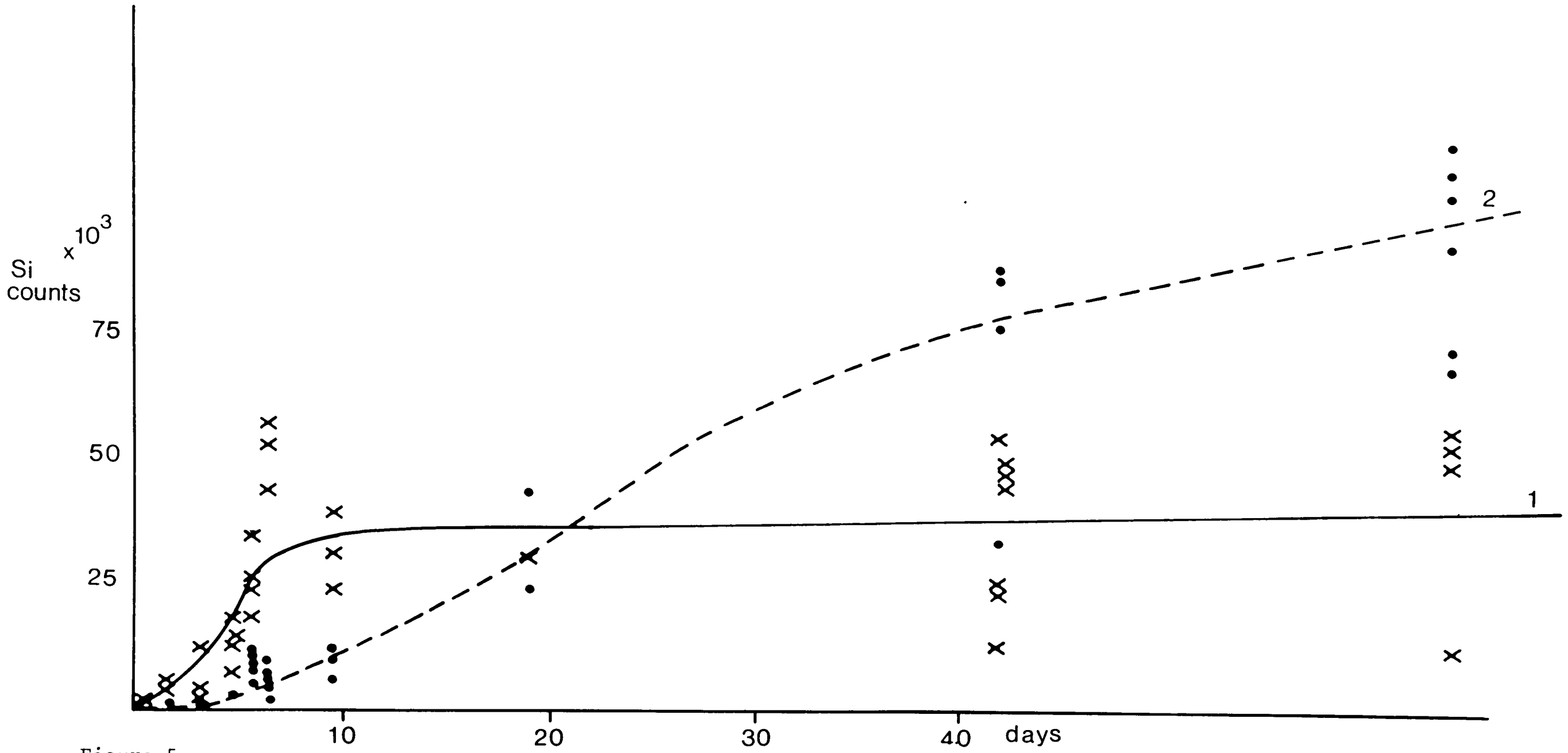

Figure 5

Levels of silicon within the macrohairs plotted against the number of days after emergence. (1) Tip of macrohair, (2) 0.16mm from tip of macrohair. Silicon levels in the tip rise rapidly at about 5 days after emergence and remain constant thereafter. Silicon levels 0.16mm from the tip rise gradually and by 40 days are much greater than at the tip.

number of days after emergence used as a reference date for each sample is only generally applicable since it refers to the stage of development of the inflorescence itself and not to individual macrohairs on the lemma. For all samples taken there is a distribution of levels of silica within the macrohairs.

For each of the different days, analysis was carried out at different points along the length of many macrohairs and the average silicon distribution was plotted against distance of the analysis point from the tip of the hair. Figure 2 shows the pattern of silica distribution within the macrohair during development. Initially, silica occurs only at the tip but with time, levels at a distance from the tip increase. After day 4 there is often a localised maxima of silica close to the tip. This may be a real phenomenum due to topographical changes in the macrohair or it may be an artefact arising because of our analysis technique. However, for nearly all samples studied this local maximum was apparent (figure 6).

4.3.1b Other elements

Analysis of mature untreated hairs along their length showed only small amounts of K, S and Cl. Levels were of the order of 1% total inorganic content or lower and an even distribution throughout the length of the macrohair was found (figure 8a).

Sequential analysis carried out along the length of the untreated hairs at different levels of maturity showed that: (1) before emergence of the inflorescence bracts there were no readily detectable elements within the macrohairs; and (2) at 2-18 days after emergence detectable quantities of K,S,Cl and P were present which vary along the length of the macrohair with age. Figure 3 shows a representative series of

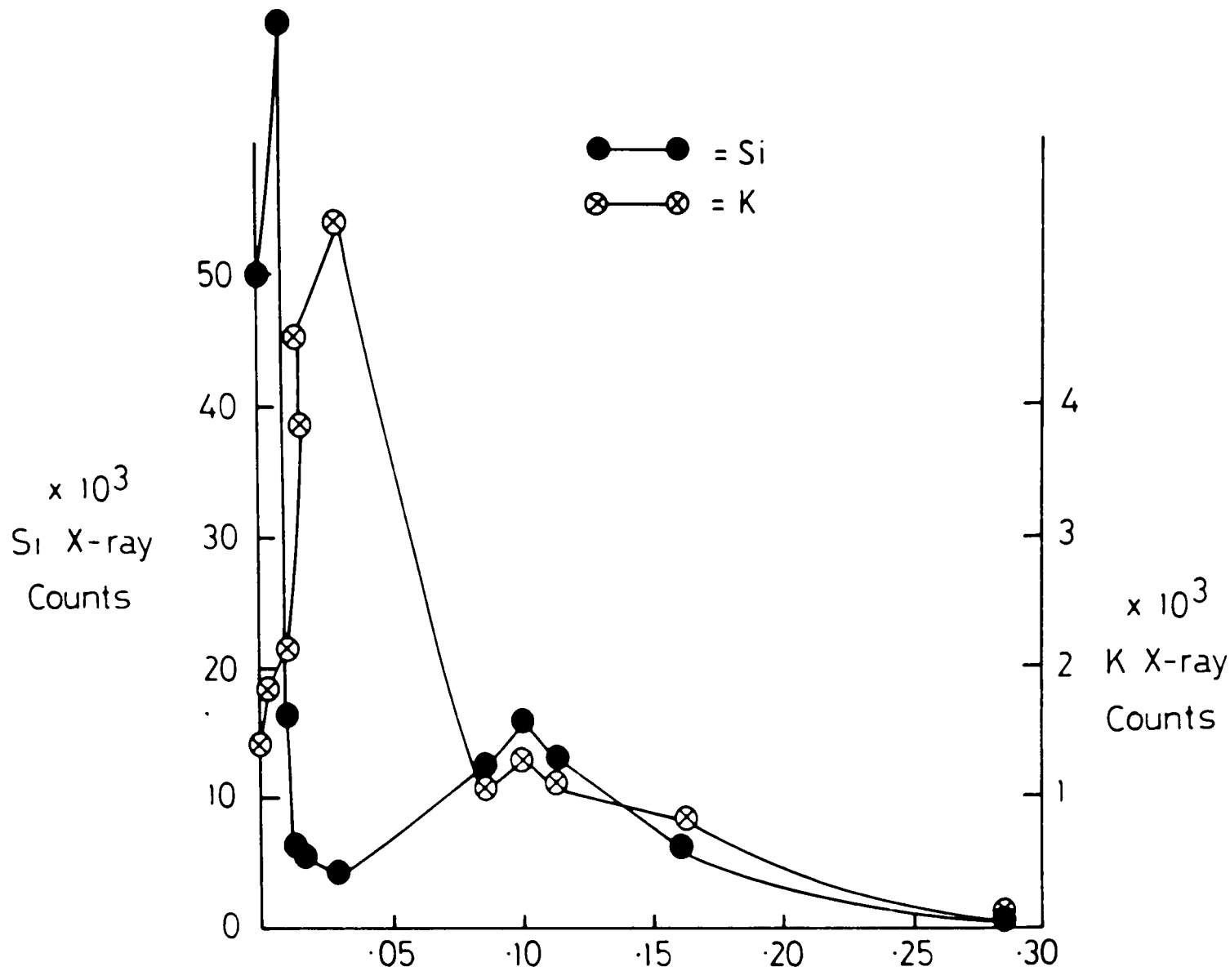

Figure 6

Levels of silicon and potassium detected compared with the distance of analysis point from the tip of a macrohair at five days after emergence of the inflorescence. Different vertical scales are used to draw attention to the local maximae present.

analyses taken along the length of a macrohair at 5 days. (see also figure 2b-d for analyses at 2 days). At both these stages of macrohair development there is a zone some distance back from the tip that is high in K, Cl, P and S and at further distances towards the base the levels of these elements decrease. This is represented graphically in figure 6 where different vertical scales are used to draw attention to local maximae present. In some of the samples analysed at this stage a second maximum of silicon was observed at a further distance from the tip.

Another indication of the spatial and temporal changes in the levels of other elements other than silicon within the macrohair can be gained by comparing K/Si levels at various points along the length of the macrohair for different days (figure 7a). By 18 days after emergence of the inflorescence, levels of inorganic elements other than silicon were low within the macrohair and the levels approach those of the mature macrohair. The maximae of all other elements other than Si change in a similar fashion along the length of the macrohair with time, K_{max} receding towards the base as mineralisation progresses (figure 7b). Little information could be obtained on the location patterns of the phosphorus and sulphur, however, as the detected count rates were barely above background.

An indication of the degree of mobility of the different elements or ions present within the macrohairs was provided by studying a sample previously left to stand in distilled water for four days. Figures 8b and 8c show that in comparison with an untreated macrohair, the water-treated sample had lost most of its inorganic content, particularly K, Cl, P and S, implying that these elements are mobile within the macrohairs and are largely not incorporated into the silicified structure. Acid treatment

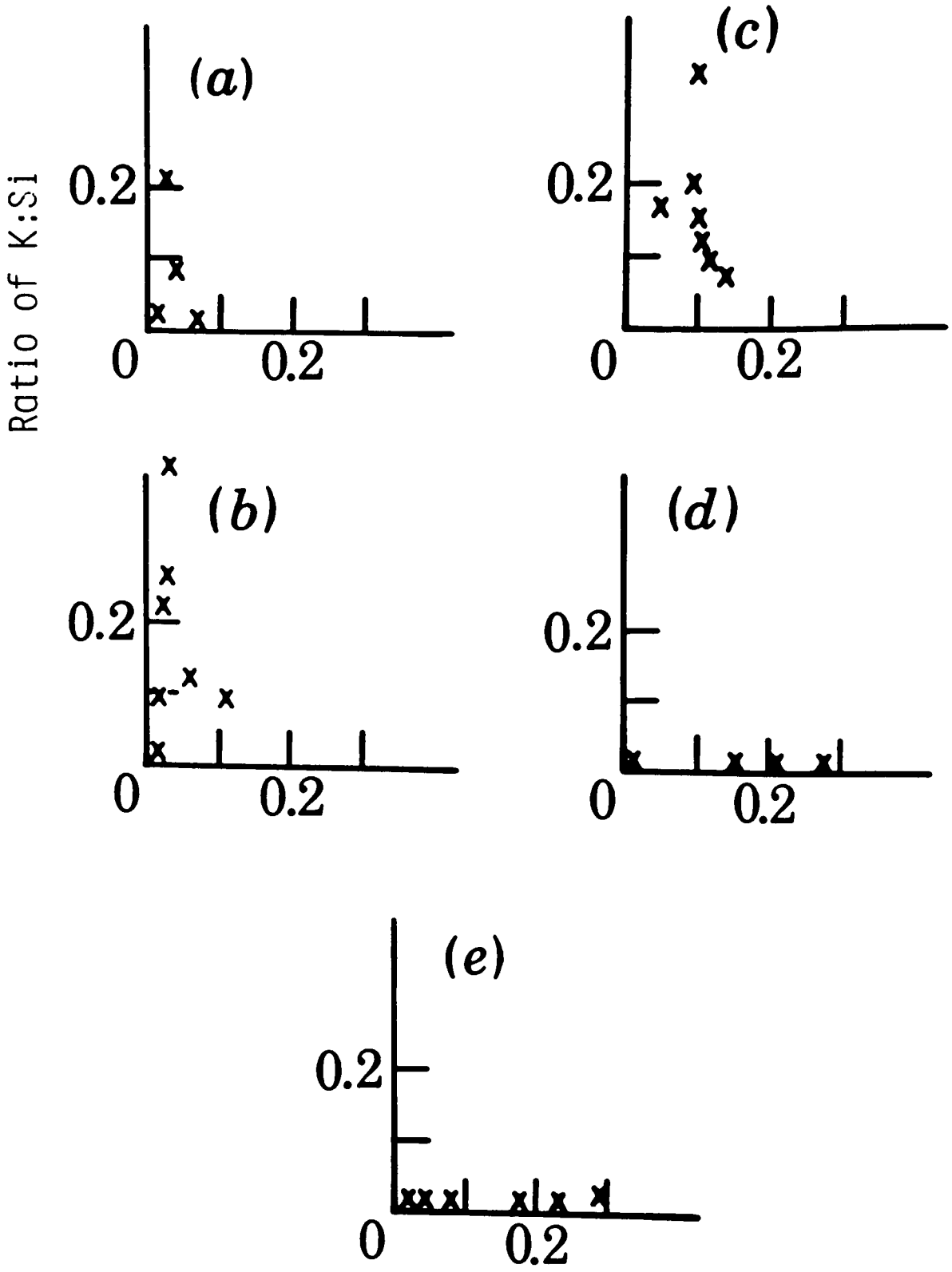

Figure 7[a]

K:Si ratios compared with distance from tip of macrohair at different stages after emergence. For days 1½(a), 5(b) and 9(c) there is a peaking of the K:Si ratio at varying distances back from the tip. At 18(d) and 40(e) days the K:Si ratio is low and constant along the length of the macrohair.

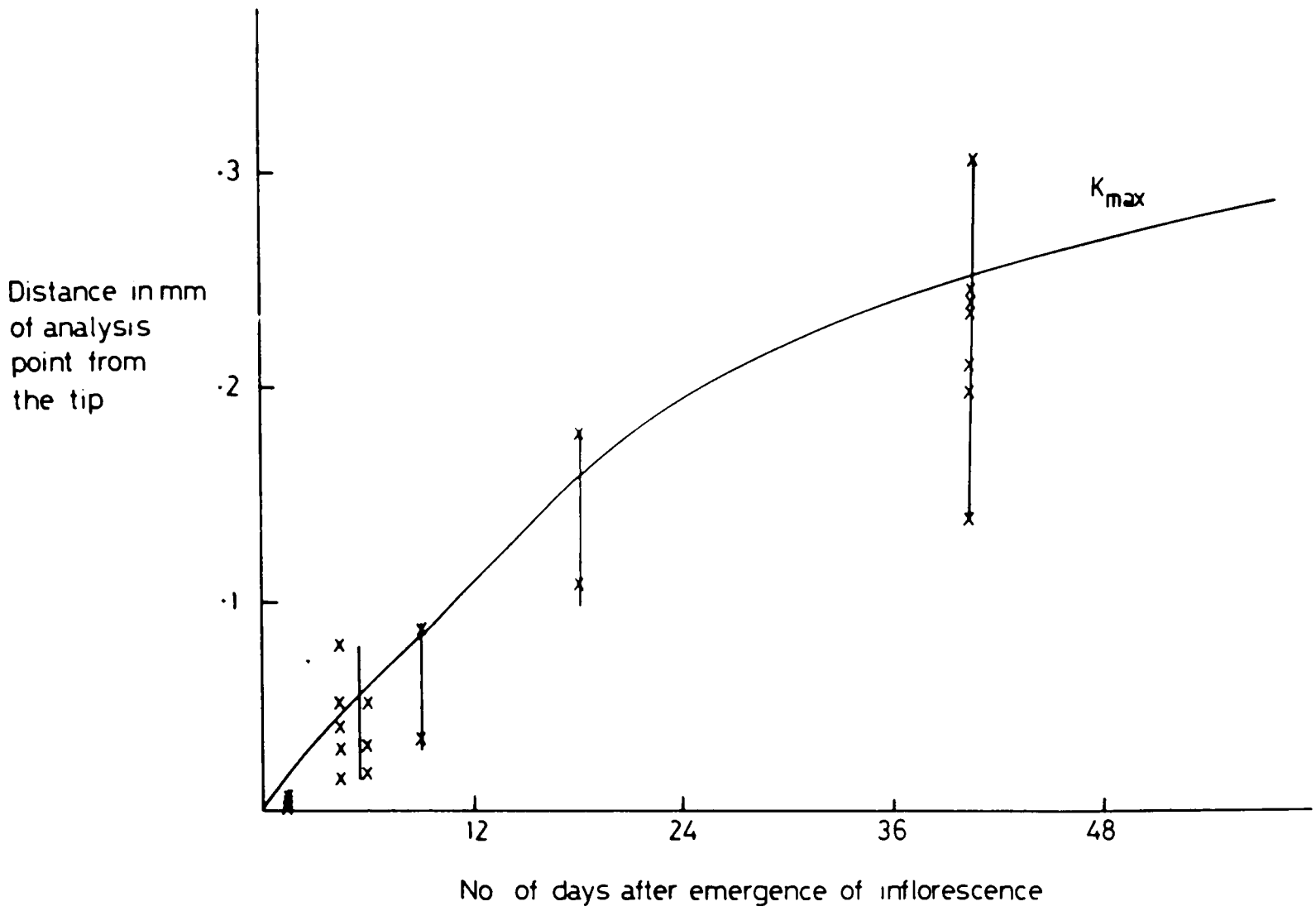

Figure 7b

K_{max} within the macrohair is plotted against the number of days after emergence of the inflorescence. The wide scatter of points for each stage indicates that the individual macrohairs are at different stages of development. K_{max} retreats towards the base as the macrohairs mature.

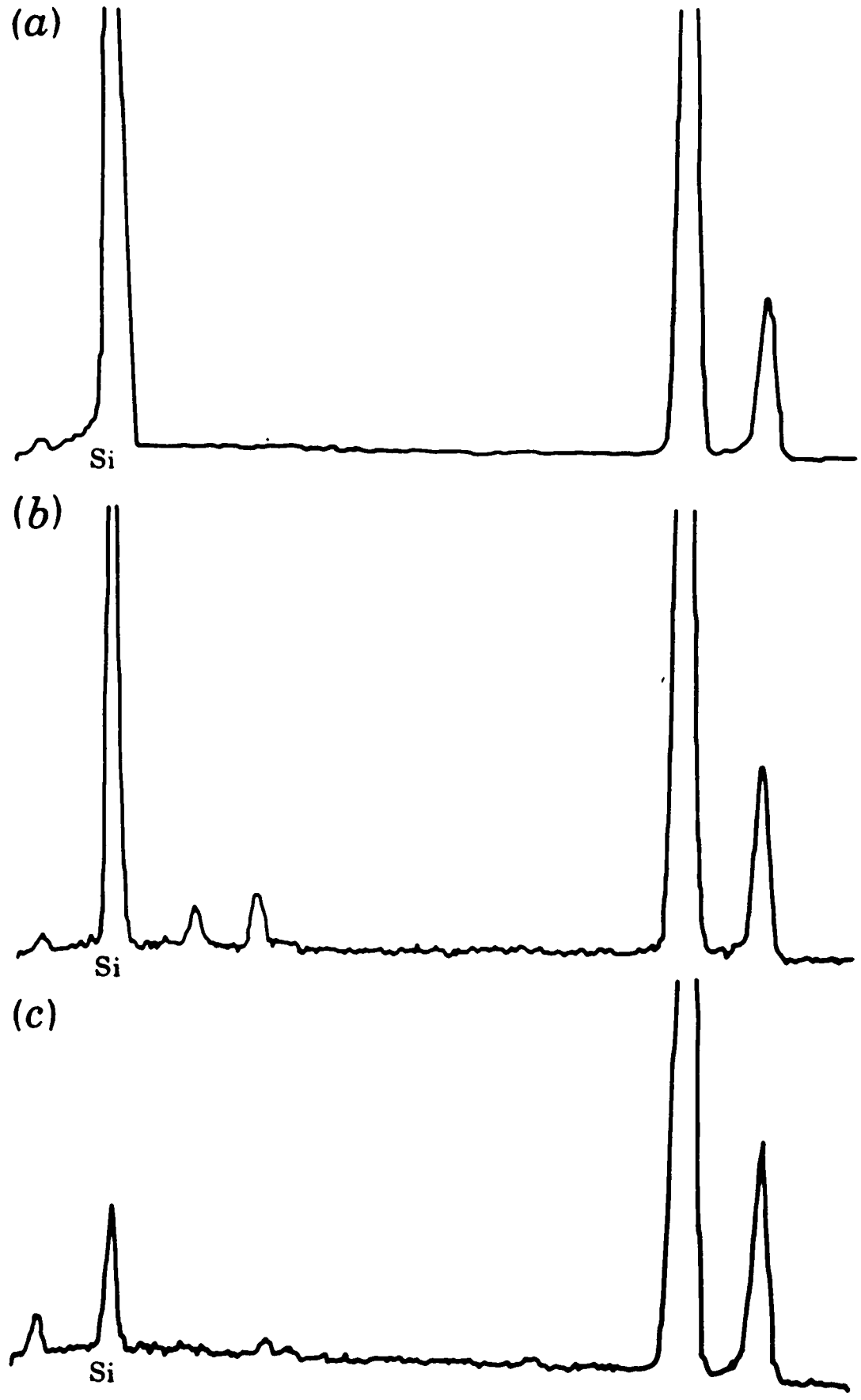

Figure 8

EDXA analyses of: (a) mature untreated macrohair. The K, S, Cl levels are insignificant above background for all positions analysed on the macrohair. (b) Seven day sample at 0.03mm from tip; (c) seven day sample at 0.03mm from the tip: analysis performed after keeping sample in water for four days before mounting and showed loss of K, P, Cl, S.

similarly removes virtually all inorganic material other than silica from samples of macrohairs.

4.3.2 Scanning proton microprobe analysis of macrohairs

Experiments on macrohairs were carried out using the Oxford SPM to confirm results obtained by EDXA (see previous section) and to provide additional information about the distribution of the elements, especially those such as phosphorus and sulphur which are lowest in concentration.

A representative series of X-ray spectra resulting from SPM point analyses carried out along the length of a macrohair is presented for a sample at four days after emergence of the inflorescence, (figure 9). The distance of the analysis point from the tip of the macrohair is noted for each sample. Silicon is largely found at the tip of the macrohair (figure 9a). At small distances from the tip the amounts of inorganic elements such as P, S, Cl and K increase (figure 9b). Analysis carried out at points further along the length of the macrohair showed that there is a second peak in the silicon concentration at about 170μm from the tip of the macrohair but there is no second maximum of the other elements present (figure 9c). There is also no silicon at the base of the macrohair (figure 9d). At 40 days after emergence of the inflorescence, the level of silicon along the entire length of the macrohair is much higher (figure 9e and 9f). The levels of K, Cl, P and S are much lower in the region near the tip (table 1). Near the base, the levels of K and Cl are similar to those found in immature macrohairs (figure 9f). There is no specific localisation of any of the inorganic elements within the macrohairs and the level of silicon is approximately constant. This information is presented graphically in figure 10.

A comparison of all the analytical data obtained from the PIXE

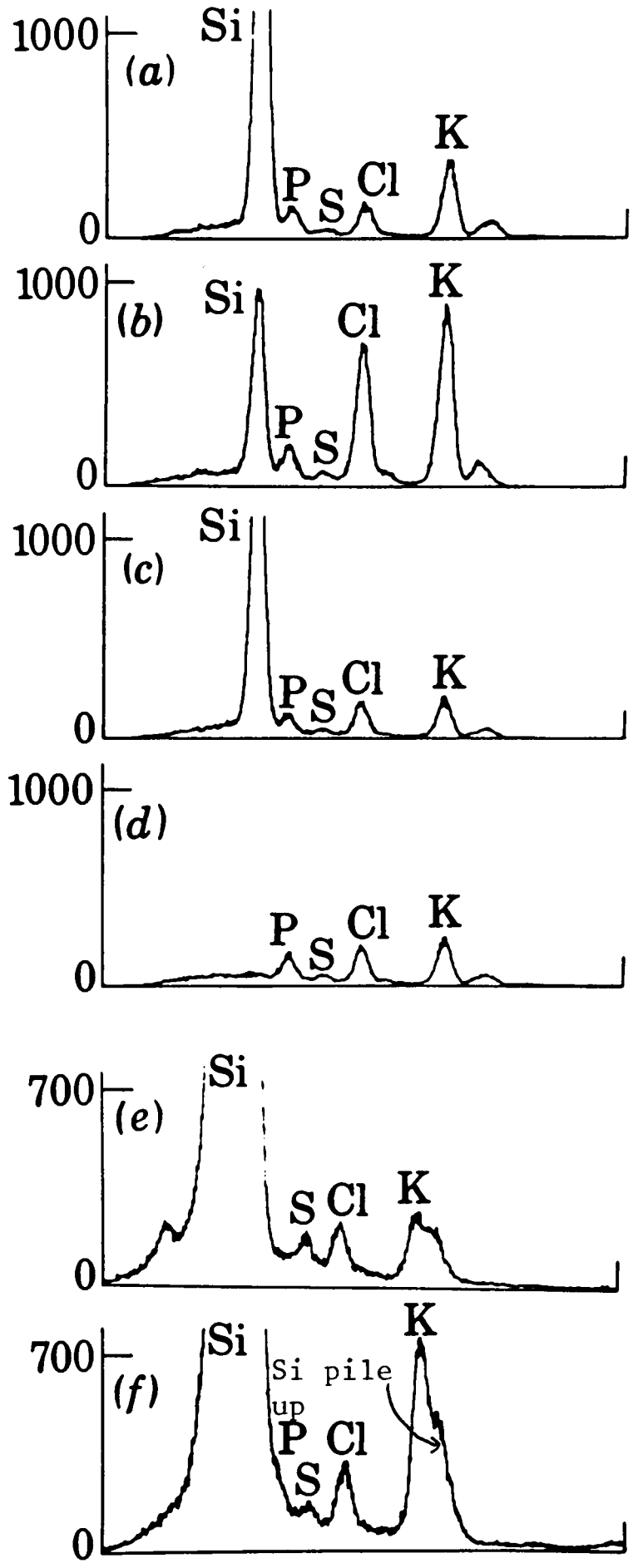

Figure 9

X-ray spectra produced from point analyses carried out by SPM at different positions along the length of a macrohair. For point analyses a, b, c and d, the total proton beam charge (Q) passing through the sample is 0.55μC. For point analyses e and f, the total proton beam charge (Q) passing through the sample is 0.05μC.

(a) Immature sample (four days) tip. High levels of Si but low levels of all other elements.
(b) Immature macrohair (four days), 65μm from the tip. Much reduced levels of Si with associated increases in the levels of the other elements.
(c) Immature sample (four days), 166μm from the tip. Second Si maximum. Low levels of all other elements.
(d) Immature sample (four days), 426μm from the tip (base). No Si. Low levels of all other elements.
(e) Mature macrohair (40 days), tip. Very high levels of Si. Low levels of all other elements.
(f) Mature macrohair (40 days), 604μm from the tip (base). Very high levels of Si. Slightly increased levels of the other elements. Si pile up.

Table 1

Analytical data extracted from analyses performed at different points along the length of a macrohair at 4 days and 40 days after emergence of the inflorescence

	concentration $g\ cm^{-2}$ (NB.allowances for varying detector efficiency included)				
4-day macrohairs	Si	P	S	Cl	K
tip	12.21	0.53	0.14	1.00	3.37
5 m from tip	19.79	0.83	0.25	2.09	5.70
27 m from tip	2.20	0.89	0.25	30.40	34.10
65 m from tip	4.50	0.69	0.17	4.43	8.13
166 m from tip	9.07	0.30	0.14	1.06	1.72
426 m from tip (base)	0.07	0.58	0.16	1.11	2.08
mature macrohairs					
tip	61.0	-	0.09	0.28	0.70
65 m from tip	52.8	-	-	0.26	1.00
161 m from tip	47.0	-	0.02	0.30	0.76
342 m from tip	58.0	0.06	0.08	0.26	1.95
484 m from tip	46.0	0.04	0.07	0.25	1.51
626 m from tip (base)	59.0	0.08	0.01	0.41	2.08

No absorption effects are included

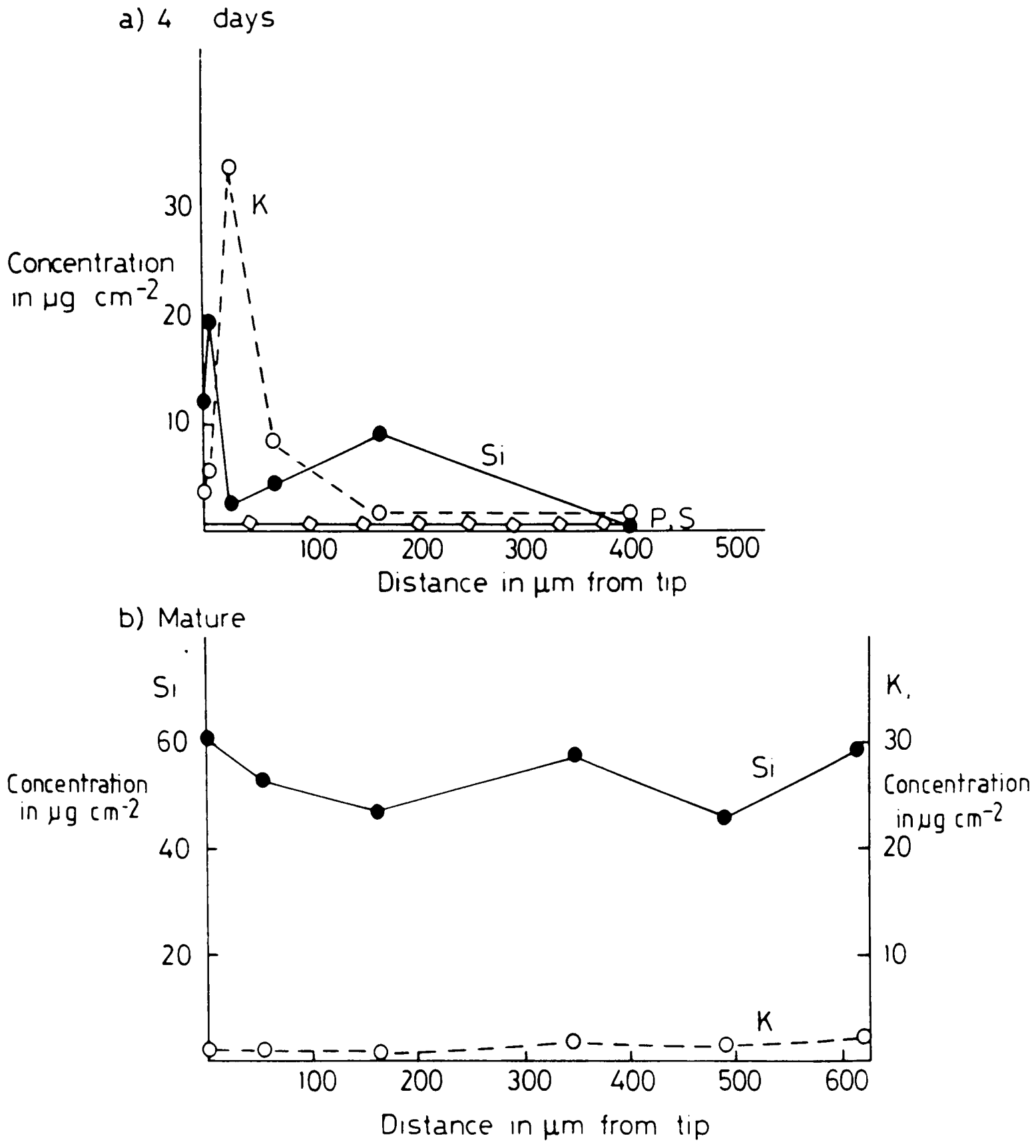

Figure 10

Levels of silicon,potassium and phosphorus and sulphur compared with distance of analysis point from the tip of the macrohair at a) 4 days and b) 40 days after emergence of the inflorescence. In the immature sample two peaks of silicon are observed. One peak of potassium is observed which occurs behind the initial silicon deposit at the tip. The levels of phosphorus and sulphur are much lower but vary little with distance of the analysis point from the tip of the macrohair. At maturity, the level of silicon is virtually constant throughout the entire length of the macrohair. The levels of potassium present are much lower and consistent along the length of the macrohair. Phosphorus can only be detected towards the base but the level of sulphur detected is similar to that in the immature sample

experiments for the 4-day and the 40-day sample (table 1) showed that, in general, for the 4-day macrohairs: (1) the level of P is 5-10 times higher; (2) the level of S is two times higher; (3) the levels of K and Cl are 10-30 times higher in the tip region and two times higher in the basal region; (4) the level of Si is 3-5 times lower in the tip region and up to 20 times lower in the rest of the macrohair.

To appreciate the distribution of each of the several elements within the whole of a macrohair two-dimensional elemental maps were reconstructed from the recorded X-ray data collected for each sample. The elemental maps of the macrohairs four days after emergence of the inflorescence are presented in figure 11 (left side). Maps of the tip region are given in figure 11 (right side). Maps for a similar sample of macrohairs 40 days after emergence of the inflorescence are presented in figure 12 (left side) with maps of the tip region shown in figure 12 (right side). As a rough visual guide, low elemental concentrations are represented by light blue, with increasing concentrations represented by the colours mid and dark blue, red, orange and yellow. The elemental concentration colour coding is shown in table 2. It is worth noting that for each map the colour coding represents different absolute elemental concentrations. The maps clearly show the localisation of inorganic elements within the macrohair at the early stages of silicification and confirm the results obtained from the point analyses presented previously. A SEM micrograph of both samples (figure 13) shows that the macrohairs are not noticeably damaged by this treatment.

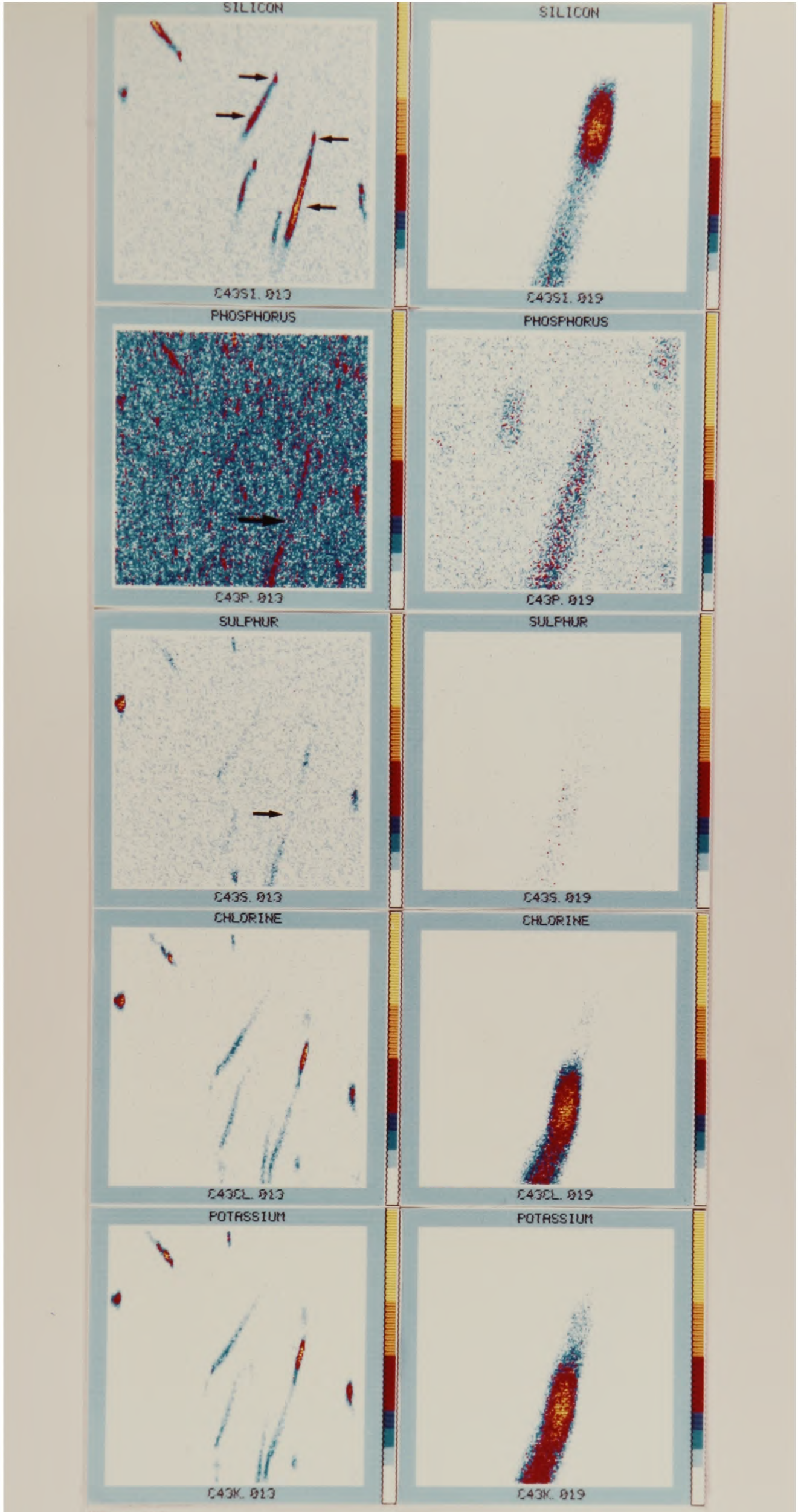

Figure 11

Elemental maps of macrohairs 4 days after emergence of the inflorescence A 4 MeV proton beam was used with a 250µm Be X-ray filter. Spatial resolution, less than 2µm x 2µm. LHS area is 800µm x 800µm. RHS area is 60µm x 60µm. Light blue is the lowest concentration. Increases in concentration are denoted by mid blue, dark blue, red, orange and yellow. For a more exact correlation between colour and concentration see table 2. Arrows on the Si map show the presence of two maxima in the deposition pattern. Arrows on the P and S maps show that minimal quantities are found when the silican concentration is high. The K and Cl maps correspond closely to one another and show a local maximum behind the initial silica deposit at the tip of the macrohair.

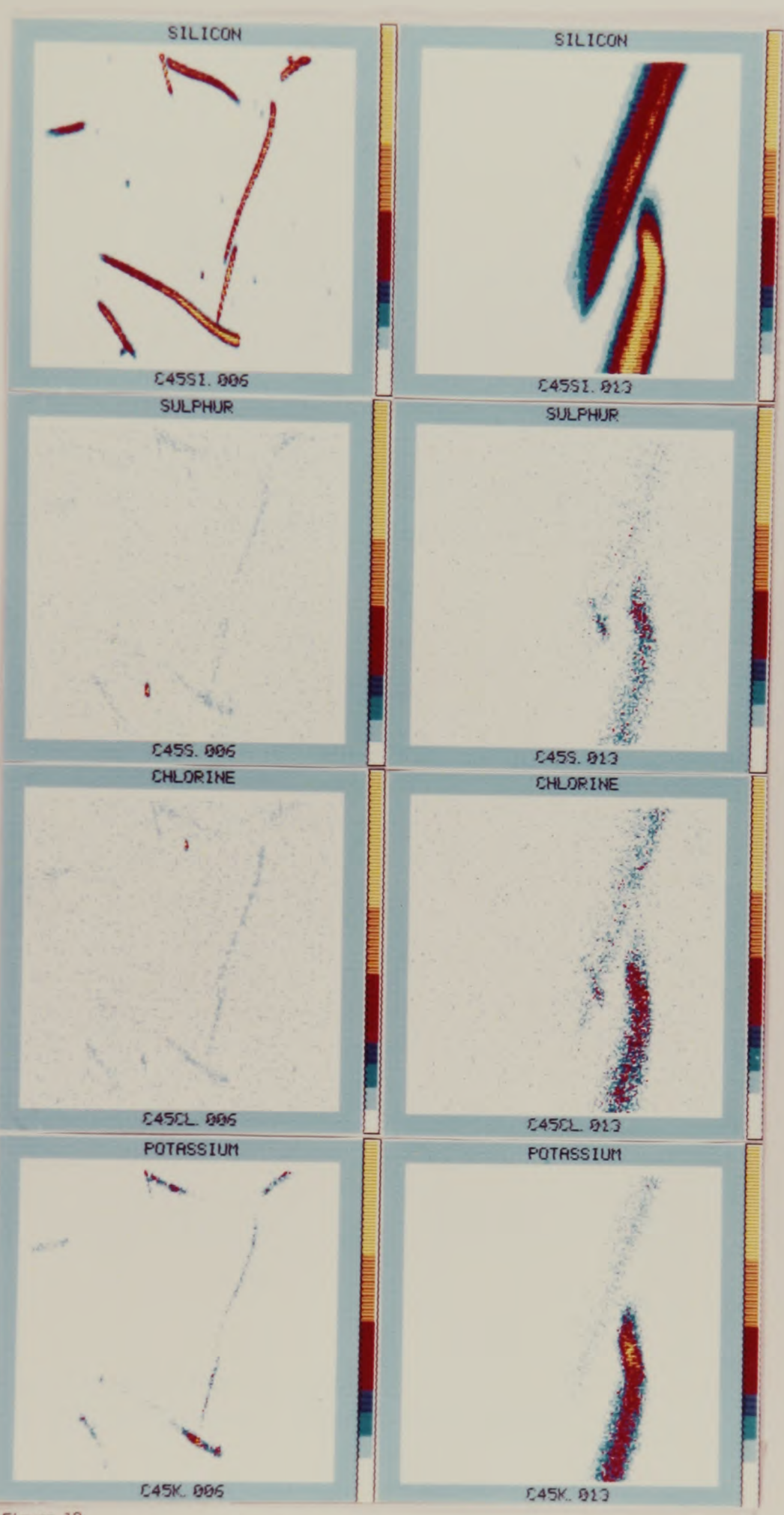

Figure 12

Elemental maps of macrohairs 40 days after emergence of the inflorescence. A 4 MeV proton beam was used with a 250μm Be X-ray filter. Spatial resolution, less than 2μm by less than 2μm. Left hand side area is 1000μm x 1000μm. Right hand side area is 120μm x 120μm. Light blue is lowest concentration: increases in concentration are denoted by mid blue, dark blue, red, orange and yellow. For a more exact correlation between colour and concentration see table 2. There is no specific localisation of any of the inorganic elements within the macrohairs though the levels of K, Cl and S do increase towards the base of the macrohairs. The levels of P were so low that a two-dimensional colour map could not be constructed.

Table 2

Macrohair colour photograph key

	light blue	mid blue	dark blue	red	orange	yellow
immature macrohairs figure 11, left side						
Si	0	7.7	15.4	23.0	30.7	41.0
P	0	4.0	7.0	10.1	13.1	16.1
S	0	2.5	6.3	10.1	13.9	20.2
Cl	0	5.9	14.7	23.6	32.5	47.2
K	0	7.8	19.4	31.1	42.8	62.2
immature macrohairs tip only figure 11, right side						
Si	0	5.8	11.7	17.5	23.4	31.2
P	0	2.5	6.25	10.0	-	-
S	0	2.0	5.1	8.1	-	-
Cl	0	6.2	15.6	25.0	34.3	49.9
K	0	7.1	17.7	28.3	38.9	56.6
mature macrohairs figure 12, left side						
Si	0	9.5	23.6	37.8	52.0	75.6
S	0	0.8	2.0	3.4	4.7	4.7
Cl	0	1.0	2.4	3.9	5.4	5.4
K	0	1.8	4.6	7.4	10.2	14.8
mature macrohairs tip only figure 12, right side						
Si	0	17.4	34.8	52.3	69.7	92.9
S	0	0.4	1.0	1.7	2.3	-
Cl	0	0.4	1.1	1.7	2.3	3.4
K	0	1.1	2.7	4.4	6.1	8.0

No absorption effects are included
All units are micrograms per square centimetre

Figure 13

SEM micrographs of the macrohair samples after analysis by SPM. The macrohairs are not visibly altered by the treatment a) 4 day sample. Bar represents 150μm. b) 40 day sample. The arrowed macrohair is broken and slightly tilted such that in the SPM a greater depth of sample is analysed which accounts for the local maximae observed in all the images.Bar represents 100μm.

4.4 Discussion

Information about the nature of the chemical and biological environment within the macrohairs has been provided by both EDXA and SPM studies on developing macrohairs and by work carried out by Hodson et al. (1984). Analysis has shown that the chemical environment changes significantly during the development of the silicified macrohair. The two analytical techniques utilised have yielded complimentary information. EDXA gave information on the overall changes in inorganic content which occur during mineralisation. PIXE and SPM results gave more detailed information on the major components at selected stages of mineralisation and also gave reliable data on the minor inorganic components of this silicifying system. EDXA has shown that at emergence of the inflorescence, little silica is associated with the macrohairs. They are essentially organic fibres, the composition of which, after drying, is typical of cell wall material. At this very early stage the macrohairs are probably a simple flexible cell structure and transverse sections show internal structures and organelles typical of a cell surrounded by a thick wall. PIXE has not been used on these samples.

Both EDXA and PIXE results showed that silicification has commenced after about one day after emergence of the inflorescence and then largely only at the tip of the macrohair. EDXA results show that at emergence of the inflorescence there are insignificant levels of inorganic ions within the macrohairs but for macrohairs studied up to 18 days after emergence there is a high localised inorganic content within the macrohairs. This localised region occurs at a small distance from the tip and recedes towards the base as the amount of silica deposited increases. Often, during the early stages of silicification there may be comparable

quantities of potassium ions and silicon within the macrohair.

PIXE results show that potassium and chlorine are concentrated behind the initial deposit of silica, and are also present at lower levels throughout the entire macrohair. Low levels of phosphorus and sulphur are also present along the entire length of the macrohair and there is no specific localisation of these elements.

At the four-day stage of development after emergence of the inflorescence, two maxima in the silica profile along the length of the macrohair were frequently observed. The SPM studies show that the silicon maximum in the central region of the macrohairs corresponds to minima in the amounts of potassium, chlorine, sulphur and phosphorous (figure 11). No clear explanation for these phenomena can be given but they may result from direct cellular involvement with precipitation. A possibility is that two cells are involved and that the second silicon maximum occurs in the region between them.

As the macrohairs approach maturity, both methods of analysis have shown that the levels of deposited silicon are significantly higher throughout the macrohair, extending considerable distances from the tip. The levels of potassium and chlorine as revealed by PIXE are much lower than those found in the immature macrohairs and there is no loger any specific localisation of silicon, potassium or chlorine within the macrohair. Virtually no phosphorous is detected within the mature macrohair (extraction of numbers from point analyses only) but the level of sulphur within the macrohair is only slightly less (twofold) than that found within the immature macrohair.

The presence of considerable quantities of potassium, chlorine, phosphorous and sulphur within the immature macrohair indicates that the

cell contents are present within the macrohair. The absence of phosphorous or lowered amounts of the elements sulphur, chlorine and potassium at maturity indicates that cell contents are absent within the mature macrohairs. These observations agree with the findings of Hodson et al. (1984) who used staining methods. There would appear to be cell contnts within the macrohairs only at the early stages of silica deposition. The deposition pattern varies with age as at first the silica is only deposited at the very tip of the macrohairs. Subsequently, two heightened zones of silica are observed and finally, at maturity, the level of silica throughout the entire length of the macrohair is approximately constant. The change in the quantity of detected silicon present within the macrohairs and the change in its localisation together with the changes in cell associated elements suggest strongly that the process of silicification is connected with cellular activity.

The maintained levels of sulphur within the mature macrohair compared with the decrease in phosphorous levels indicates that the cell wall (or other membranous structure), which remains even when the cell contents are withdrawn from the macrohairs, contains sulphur.

The information obtained from the analytical study on macrohairs from the lemma of the grass Phalaris canariensis L. may be correlated with the findings of the structural study as follows:

(1) In macrohairs from emergence up to 18 days after emergence of the inflorescence, silicification occurs in the thickening cell wall of the macrohair in the form of sheet-like and globular particulate arrangements. Significant levels of inorganic ions are found within the system and cellular components are present within the macrohair. The cellular activity leading to the thickened cell wall occurs interactively with silica deposition, both processes occurring simultaneously.

(2) In macrohairs 18 days after emergence up to maturity, silicification continues in the cell wall in the form of globular and, later, fibrillar arrangements of particles. There is apparently little further cell wall thickening and levels of inorganic ions within the macrohair are lower and not localised. Thus there is no evidence for the presence of cellular components within the macrohair during this stage. There is a large increase in silica found within the macrohairs during this stage of development and only at maturity are distinctive concentric rings of material found within the macrohair.

Previous mechanisms put forward to explain the silicification process in plants have largely concentrated on physical processes such as transpiration or a change in pH, or both, to bring about the deposition of silica. A high degree of chemical control or specific chemical control is not thought to be required since the silica adopts the shape of the container in which it is found. The work presented here points strongly to the opposite conclusion, that is, that the silicification process in these plant macrohairs is governed by changes in cellular processes and indeed, it seems unlikely that passive transpiration processes could result in such precise spatial and temporal biomineralised structures.

4.5 References

1. Hodson, M.J., Sangster, A.G. & Parry, D.W. (1984) Proc. R. Soc. Lond. B 222, 413-425.

Chapter 5: The organic component of the macrohairs from the lemma of the grass Phalaris canariensis

5.1 Introduction

Every living cell is surrounded by a membrane which is based upon a complex assembly of lipids and proteins. For almost all plant cells, the membrane, known as the plasmalemma deposits on its outer surface a layer of material known as the cell wall. The primary cell wall that is laid down while the cell is enlarging is largely composed of polysaccharides, though non-saccharide components such as lignin and protein may be incorporated to give a rigid structure. When growth of the primary cell wall is complete a secondary wall layer may be deposited within the primary cell wall, the thickness and chemical composition of which is dependent upon cell type. The secondary cell wall which surrounds the lumen is complicated in structure and can vary from the apparently simple and homogeneous to a complex of several concentric lamellae alternating either in chemical composition or in physical constitution or both (Preston,1974).

In the macrohairs from the lemma of the grass Phalaris canariensis L., the primary cell wall is laid down prior to emergence of the inflorescence (Hodson et al., 1984). After emergence of the inflorescence, secondary wall synthesis commences, deposition of polysaccharide being in advance of silica deposition (Hodson et al.,1984). This is also true for silica deposition in the rice hull (Dayanandan, 1983). The silica is deposited within the defined matrix of the secondary cell wall.

The following studies were undertaken in order to identify the chemical composition of the secondary cell wall in which silica is

chemical composition of the secondary cell wall in which silica is deposited and to investigate any time dependent variations in cell wall composition which may in turn be related to the different ultrastructural forms of silica observed.

Experiments were performed on samples of mature macrohairs and on samples at different stages of wall development of macrohairs from inflorescences which had been fed with ^{14}C labelled glucose or ^{3}H arabinose at different stages of wall development. The stages chosen were : 1) emergence of the inflorescence, 2) 4 days after emergence, 3) 14 days after emergence, 4) 24 days after emergence and 5) 35 days after emergence of the inflorescence.

The inflorescences were fed with a solution of the labelled sugar (see materials and methods), which were partially incorporated into polysaccharides synthesised at the above times, any unincorporated material being removed by sequential washings prior to analysis. Detection of radioactive products was by scintillation counting and autoradiography, after chromatography of the samples. The advantages of employing a radioactive label in structure determination are many. Very small quantities of sugars may be detected ($10^{-9}g$)(Fry,1983) and problems with contamination from autolysis of enzymes used in the analyses, or from other polysaccharides present are minimised because only molecules containing the radioactive label are detected. We can, therefore, obtain information on polysaccharides synthesised at a particular time point during cell wall development.

Procedures available for structural analysis of polysaccharides may be of chemical, enzymic or physical nature. Only chemical and enzymic procedures have been employed in these studies but physical techniques such as electrophoresis, gas or liquid chromatography coupled to mass

spectrometry on derivatised polysaccharide samples and fast atom bombardment mass spectrometry and nuclear magnetic resonance, on underivatised samples may be profitably used in primary structure determination (McNeil et al., 1984). A brief description of chemical and enzymic techniques, most of which are used here for structural analysis, is now presented. Indications of the information which may be gained from each method are also given.

5.1.1. Complete acid hydrolysis

Complete acid hydrolysis is used to determine the monosaccharide composition of the polysaccharide/s being studied. The technique relies upon reagents cleaving glycosidic bonds but leaving monosaccharides untouched. Strong acid, 2M trifluoroacetic acid (TFA) at 120°C or 72 % H_2SO_4 at room temperature followed by 3% H_2SO_4 at high temperature (100° C), is used to effect cleavage of the glycosidic bonds within the polysaccharide. 2M trifluoroacetic acid does not cleave glycosidic bonds in crystalline cellulose but use of H_2SO_4 does effect cleavage of the glycosidic bonds involved. Problems do arise because of differences in the ease of cleavage of the glycosidic bond for different sugars and in the concomitant degredation of the monosaccharides which may occur. Furanose, pentose and 6-deoxy hexose sugars are hydrolysed faster than hexoses which in turn are hydrolysed faster than uronic acids or 2-deoxy 2-amino sugars. If the two hydrolyses detailed above are run in parallel then information will be gained on the nature of the hemicellulose / pectic fraction and then on the trifluoroacetic acid resistant cellulose fraction.

5.1.2 Mild acid hydrolysis

Mild acid hydrolysis is used to obtain information on the chemical composition of short side chains in polysaccharides. It utilises variations in the rate of hydrolysis of the glycosidic bond for different monosaccharides. Usually, 0.1M trifluoroacetic acid or 1M oxalic acid are used at 100 °C. This method may be used in conjunction with other techniques, such as periodate oxidation, as removal of side chains will make available more hydroxyl groups for oxidation and the reaction products will therefore be different. This will give information on the linkage position of side chains within the polysaccharide/s eg. whether a sugar is linked via c-3 or c-6.

When the chemical composition of the polysaccharide / s is known, information on the linkage and sequence of the monosaccharides can be obtained. Detailed information on linkage can be obtained by using one, or, more frequently, a combination of the following techniques.

5.1.3 Methylation analysis

Methylation analysis is widely used to determine the position of linkages between component monosaccharide residues in polysaccharides. This is often achieved by treating the carbohydrate with methyl sulphinyl carbanion to form polyalkoxide ions, followed by methylation with methyl iodide, (Hakomori, 1964 and Sandford et al.,1971). The methylated carbohydrates are then hydrolysed and the partially methylated monosaccharides reduced and acetylated. The resulting alditol acetates of methylated sugars are separated by gas chromatography and identified by their retention times and mass spectra (Lindberg, 1981). Problems include undermethylation, incomplete hydrolysis and degradation. This method has

not been utilised in this study because of problems in adapting it to radioactive samples.

5.1.4 Periodate Oxidation/Smith degradation

This is widely used to determine the position of linkages between component monosaccharide residues in polysaccharides and to determine the degree of branching, hence identifying the structural nature of the polysaccharide itself. The method relies upon the ease of oxidation of 1,2 diols in monosaccharide units to dialdehydes by the use of periodate at pH 3-5 (Bobbitt, 1956). The resulting dialdehydes are unstable in water and are reduced with sodium borohydride. Acid hydrolysis is performed to cleave remaining glycosidic linkages. The resulting material is chromatographed and yields a mixture of monosaccharides, produced from periodate unreactive material, alcohols such as glycerol and erythritol, glycollaldehyde and formic acid. The reaction may be followed by measurement of the amount of periodate consumed, or the amount of formic acid liberated but in practice, when very small quantities of material are used, detection of products after separation by chromatography is the only feasible method and gives more information.

The reaction products obtained are dependent upon the monosaccharide composition of the polysaccharide, the positions of glycosidic linkages and the degree and nature of any branching present. Examples of polysaccharides and their reaction products are:

cellulose ⟶ erythritol and glycollaldehyde
(β1→4 linked glucose)

amylose ⟶ erythritol and glycollaldehyde
(α1→4 linked glucose)

callose ⟶ glucose (periodate unreactive)
(β1→3 linked glucose)

homoxylan ⟶ glycerol and glycollaldehyde

(β1→4 linked xylose)

arabinoxylan ⟶ xylose, glycollaldehyde
(β1→4 linked xylose with α1→3
linked arabinose on each residue)
xyloglucan ⟶ erythritol, glycerol and glycollaldehyde
(β1→4 linked glucose,
xylose substituted α1→6)

This procedure has not been successfully used on these samples.

5.1.5 Enzymic hydrolysis

Hydrolysis by enzymes provides an alternative method for the controlled hydrolysis of polysaccharides. The information obtained is not limited as in acid hydrolyses, because enzyme activity is specific for a particular type of monosaccharide and /or linkage. Information may be gained from both enzyme resistant structures, partially hydrolysed structures and the monosaccharides produced. Enzymes which hydrolyse polysaccharides may be divided into two groups, endo- and exo-polysaccharide hydrolases. Endo-polysaccharide hydrolases are specific for linkage and monosaccharide residue, and cause random fragmentation of homopolysaccharides to give a homologous series of oligosaccharides, eg α-amylase which gives a random series of D-glucose α(1→4)-oligomers on reaction with amylose. Exo-polysaccharide hydrolases are specific for monosaccharide unit and stereochemistry at C-1 but do not usually differentiate between the residues attached glycosidically at C-1. They cleave polysaccharides by sequential removal of residues from one end of the molecule, usually the non reducing end, eg β-amylase which removes maltose units sequentially from amylose, producing an almost quantitative amount of maltose if the reaction is allowed to proceed to completion.

Hydrolysis of glycosidic linkages by enzymes is accomplished by the breaking of the glycosyl-oxygen bond.

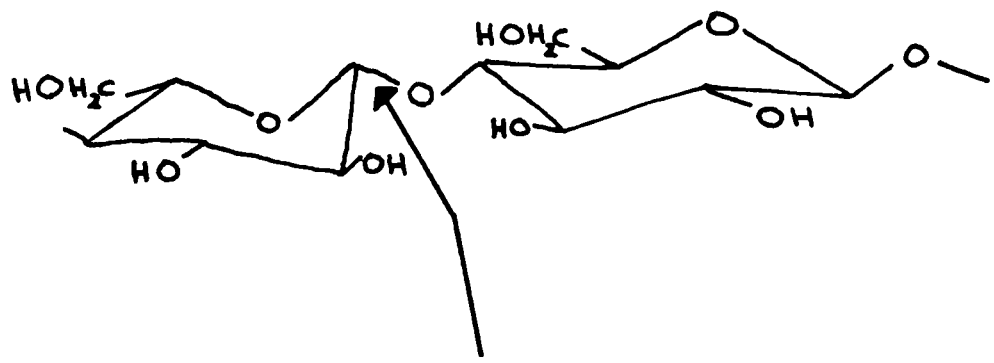

glycoside and polysaccharide hydrolases attack here

Enzymes may also be used in a pure form for the determination of monosaccharide sequences within a given polysaccharide. These enzymes remove specific monosaccharide units linked by specific linkages from the nonreducing end of a polysaccharide, eg β-D-galactosidase removes D-galactosyl residues linked β-glycosidically to the polysaccharide. The use of sequential enzyme hydrolyses is a well established technique for the analysis of the carbohydrate portion of macromolecules (Li, 1976).

Two enzyme mixtures were utilised in this study. A mixture of α-and β- amylase was used to confirm that starch was synthesised at some time points during cell wall maturation. The driselase enzyme mixture, containing a mixture of fungal exo- and endo- hydrolases including cellulase, pectinase, β-xylanase and β-mannanase but lacking α-xylosidase and feruloyl esterase activity, was used in the generation of oligosaccharides containing driselase resistant linkages within the polysaccharides (eg xyloglucan) and to investigate whether ferulic acid and feruloyl esters were present within the cell wall matrix. This again gives information on the structure of the hemi-cellulosic fraction and on crosslinking agents present within the cell wall.

The experimental results presented in this chapter yield information on the organic fraction of the macrohair cell walls, including information on the types of polysaccharide synthesised, monosaccharide composition, linkages between monosaccharides and the nature of potential cross-linking agents present within the cell wall.

5.2 Materials and methods

5.2.1 Plant culture and sample preparation

Untreated macrohairs were collected from a dust extraction room of a grain exporter (Darly Downs Grain Exporters Pty. Ltd., Queensland, Australia). They were washed and sieved through a 100 μm sieve to remove extraneous matter.

Samples of macrohairs for developmental studies were collected from plants grown from seed (wild type) provided by the botanical gardens, Oxford. Seeds were grown in moist compost in a greenhouse. The plants were watered according to need and twice a week were given a solution of silicic acid (ca. $100/10^6$), produced by allowing amorphous silica to dissolve in distilled water. When each inflorescence appeared, the date was noted and the inflorescence tagged. Samples for study were removed by cutting the stem two inches below the inflorescence. Two samples were removed at each of the following stages: (1) at emergence of the inflorescence, (2) 4 days after emergence of the inflorescence, (3) 14 days after emergence of the inflorescence, (4) 24 days after emergence of the inflorescence and (5) 35 days after emergence of the inflorescence. The inflorescences were carefully transferred to narrow centrifuge tubes to which had been added 0.1 ml of a solution containing either 100 μCi of D-(U-^{14}C) glucose, specific activity 330 mCi/mmol or 4mCi of L-(1-^{3}H) arabinose, specific activity 2.5 Ci/mmol. The tops of the tubes were covered with parafilm to prevent evaporation and samples were left overnight under conditions of constant temperature (25°C) and light. When the sugar solution had been absorbed, about 8 hours after the addition, distilled water was added and the inflorescences allowed to transpire for

a further 24 hours. Samples of hairs for study were prepared after disection of the lemma from the inflorescence. Using a light microscope, macrohairs were removed by gently rolling the lemma on sellotape. All spikelets from each inflorescence were treated in an identical manner, care being taken to prevent contamination from other cellular material. The `selotape samples´ were cleaned as follows:

For days 0, 14, 24 and 35, samples were left standing in methyl cyclohexane which dissolves the adhesive, for 1 week. The selotape backing was removed and the suspension of hairs was transferred to a stoppered centrifuge tube and spun. The supernatant was rejected and the pellet was washed sequentially in;

1) Methylcyclohexane (twice)

2) Ethyl acetate

3) Phenol/acetic acid/water, 2:1:1

4) The sample was left standing in the above for 3 days at 25 °C to remove all cellular/cytoplasmic material.

5) Phenol/acetic acid/water, 2:1:1

6) Distilled water (three times)

7) Methanol

The pellet was resuspended in 5ml methanol and kept for analysis. The 4 day sample was cleaned as follows. The sample was left overnight in phenol/acetic acid/water (2:1:1). The selotape backing was removed and the sample filtered using a glass fibre filter. This was washed sequentially in;

1) Chloroform (three times)

2) Methylcyclohexane (three times)

3) Phenol/acetic acid/water, 2:1:1 (three times)

4) Distilled water (three times)

6) Chloroform/methanol/water 10:10:3

7) Chloroform/methanol 1:1 (three times)

8) Chloroform (three times)

9) Methylcyclohexane (three times)

The filters with macrohairs attached were dried and kept for analysis. This sample was the first sample cleaned before we realised that phenol and selotape backing reacted to give a sticky mass which was only removed with great difficulty. For enzyme digestion experiments, the resulting filters were ground using a pestle and mortar and the resulting fine powder mixed to a slurry with methanol.

5.2.2 Estimation of radioactivity

Samples produced by ^{14}C and ^{3}H incorporation at days 0, 14, 24 and 35 were estimated by taking 0.5 ml of the hair suspension, mixing with 5 ml triton containing scintillation fluid (containing 0.33% PPO and 0.033% POPOP in toluene:triton (2:1)) and counting. Counting efficiency for ^{3}H was 3% (approx). Counting efficiency for ^{14}C was 20%(approx).

Samples from day 4 were estimated by submerging a piece of filter paper in 5 ml non-triton scintillant (containing 0.5% PPO and 0.05% POPOP in toluene) and counting. Efficiency as above.

For analysis of samples after paper chromatography, strips 4cm long and 1cm wide were cut from the chromatogram, non-triton containing scintillation fluid added and the sample counted as before.

5.2.3 Experimental and Preparative Procedures for Non radioactive samples

5.2.3.1 Isolation of polysaccharides from macrohairs

0.1g of macrohairs were treated with 5ml 1% potassium oxalate at pH 4.6 and at 120°C for 1 hour. After cooling the supernatant was removed and the sample delignified by treatment with a 5% solution of sodium hypochlorite at room temperture for 1 hour. The supernatant was removed after centrifugation and 5ml of 20% potassium hydroxide added to the pellet. The resulting mixture was left stirring overnight. The resulting suspension was centrifuged and the supernatant dialysed against distilled water for 48 hours and finally freeze dried.

5.2.3.2 Quantitative analysis of sugars

This was performed on standard sugar solutions, untreated macrohairs and on the sample described previously.

a)Hexoses (Glc , Gal , Man)

To 5-50 μg hexose in 0.5 ml H_2O (solution or suspension), 1 ml of 0.2 % anthrone in concentrated H_2SO_4 was added. The sample was mixed and heated at 100 °C for 5 minutes. After cooling absorption at 620nm (A_{620}) was read using a colorimeter.

1μg Glc $\rightarrow A_{620} \sim$ 0.02

b)Uronic acids (GlcA, GalA, 4-O-Me-GlcA, GalAMe-ester)

To 1-10μg uronic acid in 0.2 ml H_2O (solution or suspension) 1.2 ml of ice cold concentrated H_2SO_4 containing 12.5 mM $Na_2B_4O_7.10H_2O$ was added. The sample was mixed and heated at 100°C for 5 minutes. After cooling , 20 μl of 0.15% m-hydroxybiphenyl in 0.5% NaOH was added. This was mixed and left at room temperature for 5 minutes, After cooling absorption at 520nm (A_{520}) was read using a colorimeter.

1μg GalA $\rightarrow A_{520} \sim$ 0.06

c)Pentoses (Ara, Xyl)

To 1-10 μg pentose in 0.5 ml H_2O (solution or suspension) 0.5 ml of concentrated HCl containing 0.1% $FeCl_3.6H_2O$ and 0.1% orcinol (freshly prepared) was added. The sample was mixed and heated at 100 °C for 20 minutes. After cooling, absorption at 670nm (A_{670}) was read using a colorimeter.

1μg Ara $\longrightarrow$ $A_{670} \sim$ 0.01

5.2.3.3 Acid Hydrolysis

This was used for macrohairs and the extracted material (not for cellulose and only qualitatively for uronic acid containing polysaccharides). The polysaccharide or macrohairs was suspended at 10mg/ml (1%) in 2M trifluoroacetic acid (TFA) in a pyrex tube. It was sealed and heated or autoclaved at 120 °C for 1 hour. The samples were cooled prior to chromatography.

5.2.3.4 Chromatography

Paper chromatography was generally performed on Whatman no. 1 paper by the descending method. Thin layer chromatography was performed on cellulose thin layers (Merck Art. 5552). Solvent systems used for paper chromatography were ethylacetate:pyridine:water (EPW) (8:2:1 by volume), EPW (10:4:3 by volume), butan-1-ol:acetic acid:water (BAW) (12:3:5 by volume) and for thin layer chromatography, BAW (3:1:1 by volume) followed by EPW (10:4:3 by volume) in the same dimension. Samples were run with appropriate marker mixtures according to experiment. Sugars were stained on paper and on thin plates using aniline hydrogen phthalate or silver nitrate.

5.2.4 Experimental Procedures for Radioactive Samples

5.2.4.1 Acid hydrolysis

a)Mild acid hydrolysis

0.5 ml of radioactive (^{14}C or ^{3}H) hair suspension (or the equivalent of) from days 4, 14, 24 and 35 was dried on a Savant speed vac. concentrator. 0.25 ml of 0.1 M trifluoroacetic acid (TFA) was added and the suspension heated at 100 °C for 1 hour. After spinning, the supernatant was removed for paper chromatography. Paper chromatography was performed on Whatman no.1. Samples were run in ethylacetate:pyridine:water (EPW) (8:2:1) for 16 hours with xylose, arabinose, glucose and galactose as markers. Strips were cut and subjected to scintillation counting.

b)Complete acid hydrolysis

0.5ml of radioactive (^{14}C) hair suspension (or the equivalent of in crushed filter) from days 0, 4, 14, 24 and 35 was dried on a speed vac concentrator. Samples were hyrolysed in 72% H_2SO_4 as a 5% solution at 20° C and shaken for 1 hour. The solution or suspension was then added to 20 volumes of distilled water, (3% H_2SO_4) autoclaved or heated at 120°C for 1 hour and then cooled. 1 drop of 0.1% bromophenol blue indicator solution per ml of sample was then added. Barium carbonate powder was added to neutralise the remaining acid. The sample was frozen, thawed and centrifuged and the supernatant kept for chromatography. This method does not produce quantitative results as some of the material is lost in the solid barium carbonate.

c)2M Trifluoroacetic acid hydrolysis

0.5 ml of radioactive, (^{14}C or ^{3}H) hair suspension (or the equivalent of in crushed filter) from days 0, 4, 14, 24,and 35 was dried on a speed vac. concentrator. Samples were hydrolysed in 2M trifluoroacetic acid (TFA) at 120°C for 1 hour. The ^{3}H samples were thoroughly mixed and the suspension applied to Whatman no. 3 and run for 16 hours in ethylacetate:pyridine:water (EPW) (8:2:1) with markers of GalA, Glc, Gal, Man, Xyl, Ara, Rha and MeXyl. The marker strips were stained and the sample runs cut up into strips and subjected to scintillation counting. Samples from days 4 and 14 were rerun, the supernatant only being used for chromatography. The ^{14}C samples were used for paper chromatography and thin layer chromatography on cellulose plates. The paper chromatography was run as above. For thin layer chromatography the samples were run in butanol:acetic acid:water (BAW) (3:1:1) and then in ethylacetate:pyridine:water (EPW) (10:4:3) in the same dimension with a similar marker mixture. After staining, the tlc plate was exposed to an x-ray plate for 1.5 months. After exposure, the thin layer chromatography plate and x-ray plate were photographed and the tlc plate cut into strips and scintillation counted.

5.2.4.2 Dimethylsulphoxide (DMSO) extraction

A DMSO extraction to remove starch was performed on ^{14}C samples from days 4, 14, 24 and 35. 0.5ml of hair suspension, or the equivalent of, was dried using a speed vac concentrator, 2.5ml of 90% dmso (10% water) was added and mixed well to give a complete resuspension of hairs/filter and transferred to a screw-top tube. The procedure was repeated on any remaining hairs to give 5ml total suspension. Samples were pooled, sealed and left shaking for two days.

The samples were centrifuged, and 2.0ml of the supernatant recentrifuged in a clean tube. 1.5ml of the clear supernatant was added to 15ml triton containing scintillant, shaken and scintillation counted. The hairs were resuspended in 5ml 90% DMSO and shaken overnight. The sample was spun, the supernatant rejected and the residue washed in DMSO and MeOH. The pellet was resuspended in MeOH and dried on a speed vac. concentrator. 0.1ml of 90% DMSO and 1.0ml of triton containing scintillant were added and the samples scintillation counted. NB the presence of DMSO did not affect counting efficiency.

5.2.4.3 Enzymic hydrolysis

5.2.4.3.a Driselase digestion

Driselase (Sigma Chem. Co.) (a commercial mixture of fungal exo- and endo-hydrolases including cellulase, pectinase, β-xylanase and β-mannanase but lacking α-xylosidase and feruloyl-esterase activity) was used for cell wall digestion. Driselase digestions were performed on ^{3}H samples from day 4, 14, 24 and 35. A 0.5 ml sample of hair suspension in MeOH was dried using the speed vac. concentrator, 30μl of 5% driselase in acetate buffer (pH 4.8) and a trace of toluene added, the reaction vessel sealed and the samples incubated at 37°C overnight. The reaction was stopped by drying the supernatant on Whatman no. 1 chromatography paper and running with a marker mixture in ethylacetate:pyridine:water (EPW) (8:2:1) for 30 hours. The paper was dried, the marker mixture stained with aniline hydrogen phthalate and the remainder cut up into strips and subjected to scintillation counting.

A further driselase digestion on samples from days 14, 24 and 35 was performed on radioactive material eluted with water from strips 3, 4 and

5 (the disaccharide region) of the chromatogram. The strips were washed in toluene to remove the scintillation fluid from the paper and then in methylcyclohexane and left to dry. The samples were eluted with distilled water using a small syringe and concentrated. The digestion was performed as before. The supernatant and markers were run on Whatman no. 1 paper in butanol:acetic acid:water (BAW) (12:3:5) overnight. The marker strip was stained and the sample strips cut and counted as before. The main peak disaccharide was eluted as before and rerun in ethyl acetate:pyridine:water(EPW) (10:4:3). The three main zones of ^{3}H radioactivity were detected by autoradiography and were eluted as before. These regions X, Y and Z were concentrated and subjected to acid hydrolysis using 2M trifluoroacetic acid. The supernatant was chromatographed on Whatman no. 1 paper in ethylacetate:pyridine:water (EPW) (8:2:1) overnight followed by staining of the marker strips and scintillation counting of strips cut from the chromatogram.

The paper chromatogram from the second driselase digestion was subjected to autoradiography and was studied in uv light, ammonia fumes being used to identify phenolic compounds.

5.2.4.3.b<u>Amylase digestion</u>

Amylase (Sigma) was prepared by mixing 2mg of αamylase and 2mg of βamylase in 5 ml of 10 mM phosphate buffer at pH 7.0. Amylase digestions were performed on ^{14}C samples of days 4, 14, 24 and 35. 0.5 ml of hair suspension was dried using a speed vac. concentrator, 30μl of amylase solution and a trace of toluene was added, the reaction vessel sealed and the samples incubated at 37 $^{\circ}C$ overnight. The reaction was stopped by drying onto Whatman no.1 paper. Samples and marker mixtures were run in ethyl acetate:pyridine:water (EPW) (8:2:1) overnight. After drying, the

marker strip was stained and the remainder cut up into strips and subjected to scintillation counting.

Material from the second strip (disaccharide zone) of samples 14 and 24 was taken and eluted as previously described. They were concentrated and rerun on Whatman no.1 paper in ethyl acetate:pyridine:water (EPW) (10:4:3) for two sessions of 22 hours with drying inbetween. Non radioactive markers of several disaccharides and trisaccharides each with glucose added were also run under identical conditions. Marker strips were stained and the radioactive strips subjected to scintillation counting. These strips were later stained with $AgNO_3$ to locate the nonradioactive markers.

5.2.4.4 Identification of Hydroxycinnamic acids

Hydroxycinnamic acids fluoresce under long wavelength ultra violet light. They were located by observing the fluorescence exhibited under long wavelength uv light (with and without NH_3). On paper, free ferulic acid fluoresces blue, turning bright blue with ammonia, feruloyl esters fluoresce blue, turning intensely blue-green with ammonia and P-Coumaric acid is invisible before treatment with ammonia but fluoresces violet in its presence. P-Coumaroyl esters are also invisible without ammonia but fluoresce blue in its presence.

5.3 Results and Discussion

5.3.1 Non-radioactive samples

5.3.1.1 Composition of macrohairs and polysaccharide extract

The composition of the mature macrohairs from the lemma of the grass Phalaris canariensis was ascertained by complete acid hydrolysis of a sample followed by chromatography and a series of quantitative monosaccharide assays. The composition of an extract produced by 20% potassium hydroxide treatment was similarly determined.

The data obtained from thin layer chromatography of the hydrolysate produced by 2M trifluoroacetic acid treatment is given in figure 1. The macrohairs are largely composed of xylose and arabinose with smaller quantities of glucose and galactose and traces of uronic acids and mannose. (NB. this method does not hydrolyse cellulose). The relative proportions of the various monosaccharides present were obtained by comparison of the intensity of the sample spots obtained with those produced by the marker mixture, see Table 1.

The extract produced by treatment with 20% potassium hydroxide (as above) was composed of xylose and arabinose.No other monosaccharides could be detected by TLC but paper chromatography (results not shown) detected traces of both glucose and galactose. The relative proportions of the monosaccharides visibly present on the TLC plate were obtained by comparison with spots produced from the marker mixture. See figure 1 and Table 1.

Quantitative analysis of hexoses, pentoses and uronic acids was performed on a sample of untreated macrohairs and on material extracted by 20% alkali treatment. A set of standard glucose, arabinose and glucuronic acid solutions was used for each set of experiments. Data for

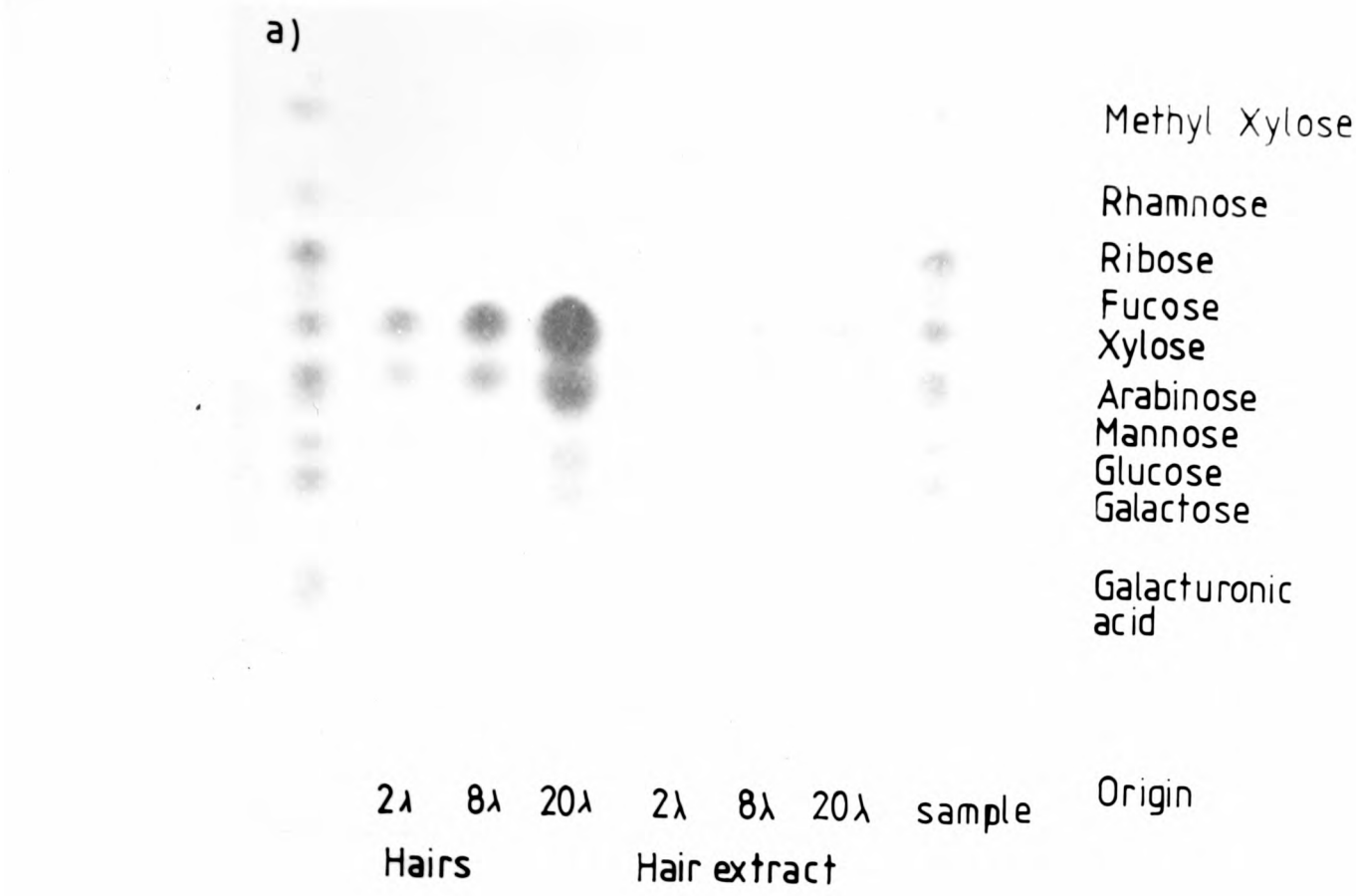

Figure 1

(a) TLC of non-radioactive, 2M TFA hydrolysed samples. TLC using BAW (3:1:1) followed by EPW (10:4:3) in the same dimension.
(b) TLC of ^{14}C glucose labelled, 2M TFA hydrolysed samples. Similar TLC conditions to the above. Nb. Stained spots represent the total amount of a particular monosaccharide within a sample at a given time point.
(c) X-ray plate taken from TLC plate (b). This shows the monosaccharide composition of the labelled polysaccharides (excluding cellulose) for a sample at a given time point. Data is not presented for day 0 as no blackening of the X-ray plate was observed. The changes in emphasis of the polysaccharides synthesised is given in the main text.

Table 1

The composition of mature macrohairs from the lemma of the grass Phalaris canariensis and the composition of a polysaccharide extract from a macrohair sample

Composition of mature non-radioacive macrohairs

(1) Results obtained from 2M TFA hydrolysis.

	(a)	Ratio/glc	µg sugar/mg hairs (c)
Xyl	0.5	5.7	153
Ara	0.313	3.6	97
Glc (b)	0.0875	1.0	27
Gal	0.05	0.6	16

The results were obtained by 2M trifluoroacetic acid hydrolysis and TLC of the supernatant. The dilutions were quantified with respect to standards.

(a) numbers were obtained from a calculation of 1/µl of hydrolysate required to give equivalent colour to 10µg of sugar as in the marker spots.

(b) non-cellulosic glucose (callose, mixed link glucan, starch etc.)

(c) from (2) using known total pentose content of mature macrohairs)

(2) Results obtained from quantitative assays
(see section 5.2.3.b)

Hexose (anthrone)	300µg/mg hairs
Pentose (orcinol)	250µg/mg hairs
Uronic acids (m-OH-biphenyl)	negligible
Silica (estimated by GLC)	420µg/mg
Water (thermogravimetric analysis)	40µg/mg

(3)Results obtained from GLC of untreated macrohairs

C	N	H
25.56%	0.77%	3.78%

Other elements present are silicon and oxygen only. The percentage of protein present is probably less than 4.0% (calculated from the nitrogen figure). The percentage of silica present assuming the remainder to be amorphous silica and polysaccharide is 42%.

Composition of non-radioactive alkali extract of mature macrohairs

(4) Results obtained from 2M trifluoroacetic acid hydrolysis.

Xyl/Ara ratio of 2:1
Glc and Gal not detected by TLC

The results were obtained by 2M trifluoroacetic acid hydrolysis and TLC of the supernatant. Sugars were stained with Wilson's dip and quantified with respect to standards.

(5) Results obtained from Quantitative assays
(see section 5.2.3.b)

Hexose (anthrone)	90μg/ml
Pentose (orcinol)	500μg/ml
Uronic acids (m-OH-biphenyl)	negligible

ratio of Pentose : Hexose is 5.6:1

the standard solutions is presented graphically in figure 2. Absorbance at a given wavelength (hexose A_{620}, pentose A_{670} and uronic acids$_{520}$) is plotted against mass of monosaccharide present in each sample. The data for the samples of unknown composition is presented graphically in figure 3. Absorbance at a given wavelength is plotted against volume of the sample (solution or suspension) used. Comparison of the standard graphs with the data obtained from the two samples of unknown composition yields information on the relative quantities of hexose, pentose and uronic acid present within these samples . See Table 1.

The quantitative composition of the macrohairs is given below:

Hexose (including cellulose)	300µg/mg hairs
Pentose	250µg/mg hairs
Uronic acids	negligible
Silica	420µg/mg hairs

As the total quantity of pentose sugars present within the macrohairs is known the absolute amounts of all the different monosaccharides present within the macrohairs were also calculated. See table 1.

The quantitative composition of the alkali extract is given below.

Hexose (non-cellulosic)	90µg/ml
Pentose	500µg/ml
Uronic acids	negligible

See table 1.

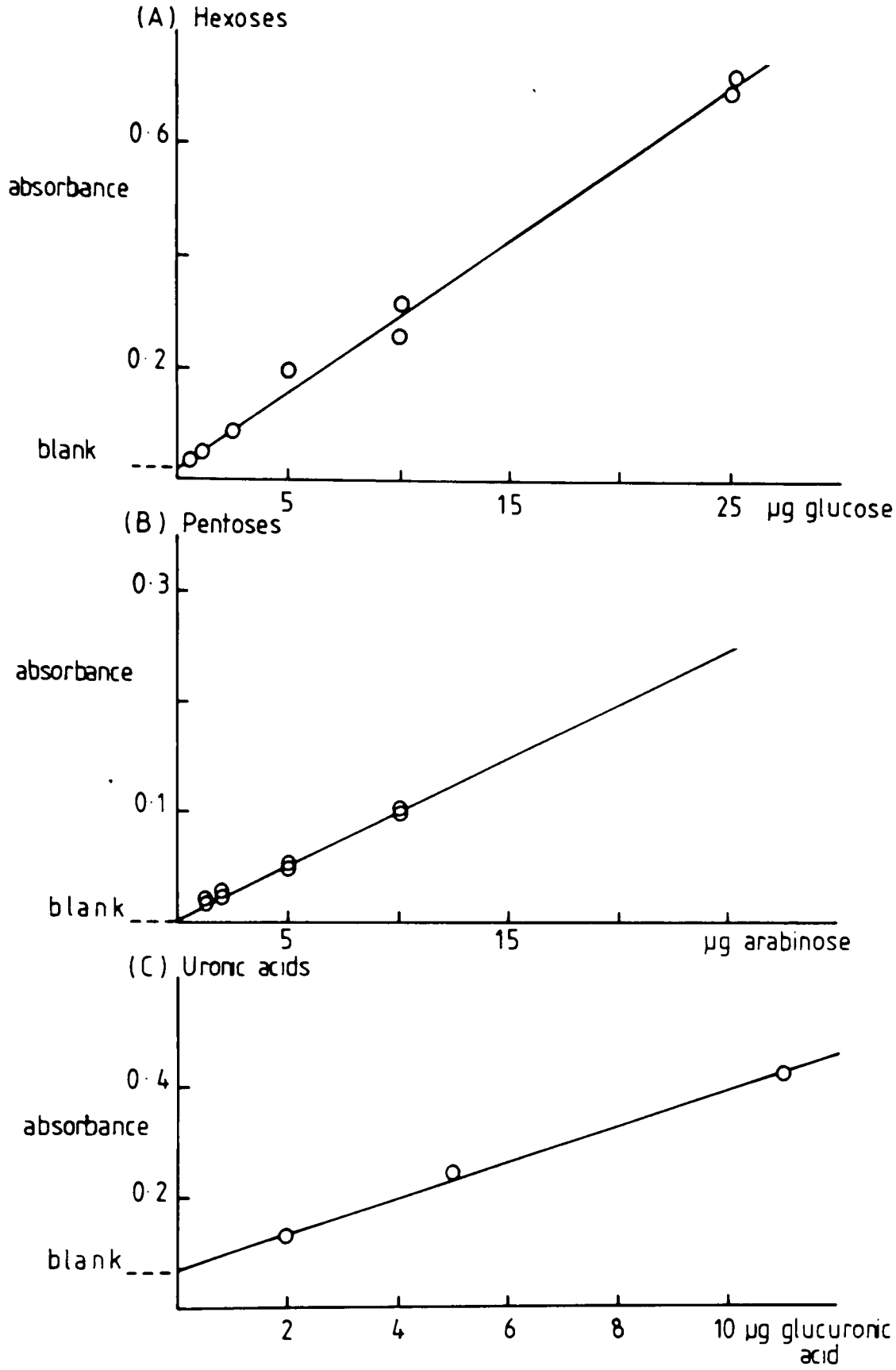

Figure 2

Standard curves for quantitative analysis of monosaccharides

a) Hexoses read A_{620}

b) Pentoses read A_{670}

c) Uronic acids read A_{520}

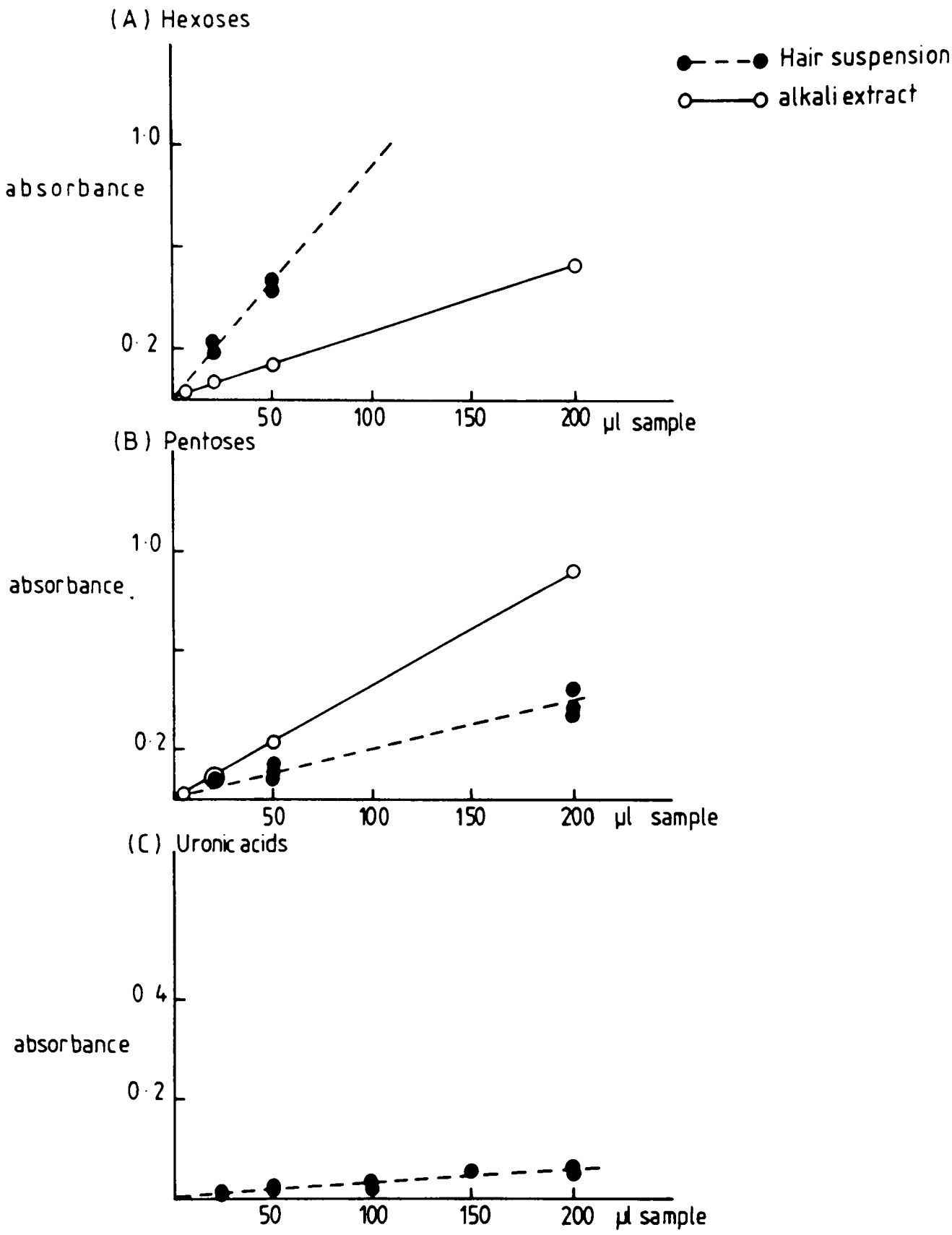

Figure 3

Quantitative analysis of a suspension of macrohairs in water and of polysaccharides extracted from the macrohairs using 20% alkali

a) Hexoses read A_{620}

b) Pentoses read A_{670}

c) Uronic acids read A_{520}

The ratio of pentose:hexose is 5.6:1 which is comparable to the ratio of 5.8:1 obtained from the 2M trifluoroacetic acid hydrolysis of the sample of macrohairs.

It seems reasonable, therefore, that the alkali treatment described, removes virtually all non-cellulosic polymers from the cell wall. These polymers are largely based upon xylose and arabinose but the levels of glucose and galactose present cannot be ignored as the polymers they result from may be important components of the thickened cell wall.

The results of a GLC analysis on the mature macrohairs are also presented in Table 1. The silica content of the macrohairs has been calculated from these figures, assuming 4.0% protein and that all other material is either polysaccharide or amorphous silica.

5.3.2 ^{14}C labelled samples

5.3.2.1 Degree of incorporation of the label

The degree of incorporation of the radioactive label into the macrohairs was estimated by scintillation counting on samples of macrohairs produced by the isolation technique described in section 5.2.1. The results are presented in Table 2.

The maximum rate of incorporation of the ^{14}C labelled glucose into polysaccharides synthesised within the macrohair was at day 14. The rate of incorporation at days 4 and 24 was of a similar order of magnitude. The rate of synthesis of polysaccharide incorporating radioactive label at day 0 (emergence) is approaching zero and the rate of synthesis at day 35 (approaching maturity) is an order of magnitude lower than for incorporation and synthesis at days 4, 14 and 24.

Table 2

The rate of incorporation of radioactivity into the cell wall of macrohairs at different stages of development.

Days post emergence of the inflorescence	Total cpm see section 5.2.2	% of supplied (a)
0	220	0.00022%
4 (b)	105000	0.105%
14	137000	0.137%
24	104000	0.104%
35	12000	0.012%

(a) assuming a counting efficiency of 20%, 1 μCi = 10^6 cpm.

(b) Approximate, because filter method for cleaning was used.

Each of the following experiments was performed on 1/10 of the total hair preparation.

5.3.2.2 Acid hydrolysis

This was performed on all samples to ascertain changes in monosaccharide composition of the polysaccharides being synthesised as mineralisation progressed. All numerical data is presented in Table 3 and gives rates of incorporation at given stages of development.

`Weak´ acid (W) hydrolysis was performed on hair samples from 4, 14, 24 and 35 days after emergence of the inflorescence using 0.1M trifluoroacetic acid (TFA) at 100°C for 1 hour followed by paper chromatography of the supernatant. Data is presented numerically in Table 3 and graphically in figure 4.

`Moderate´(M) acid hydrolysis was performed on samples labelled as 0, 4, 14, 24 and 35 days after emergence of the inflorescence using 2M trifluoroacetic acid at 120°C for 1 hour. This was followed by paper chromatography and thin layer chromatography of the supernatant. The TLC plate was subsequently exposed to an X-ray film for 1.5 months to obtain a high resolution image of the location of the ^{14}C. The spots from the plate were cut out and scintillation counted. Numerical data is presented in Table 3 and figure 1, 5, 6, 7 and 8.

`Strong´(S) or complete acid hydrolysis was performed on samples labelled as 0, 4, 14, 24 and 35 days after emergence of the inflorescence using 72% sulphuric acid at room temperature for 3 hours followed by 3% sulphuric acid at 120°C for 1 hour. Followed by paper chromatography of the supernatant. Numerical data is presented in Table 3 and figures 5, 7 and 8.

Table 3

Numerical data for the ^{14}C glucose labelled samples:

		DAYS				
		0	4	14	24	35
^{14}C started with		22	10500?	13700	10400	1200
^{14}C recovered	W	not done	736	3208	4270	508
in soluble	M	7	1007	3940	4468	750
material	S*	19	1379	2417	2899	433
	M(TLC)	29	1069	1341	1344	204
"Polymer"	W	-	479	2218	3855	403
	M					
	S	-	-	-	-	
"Disacch"	W		43	298	337	51
	M					
	S	-	-	-	-	
	M(TLC)	5	42	138	100	21
Galactose	W	-	(0)	(0)	(0)	(0)
	M					
	S	-	-	-	-	-
	M(TLC)	3	47	75	179	19
Glucose	W	-	(0)	(0)	(0)	(0)
	M	7	118	1867	4988	586
	S	19	797	1762	2698	359
	M(TLC)	5	87	478	690	103
Mannose	W	-	(0)	(0)	(0)	(0)
	M	0	24 (1.2)	42 (0.7)	155(11.2)	25(6.1)
	S	0	19 (1.5)	24 (1.3)	82(11.2)	15(5.9)
Arabinose	W	-	182	417	46	35
	M	0	288(14.5)	562 (9.7)	77(5.6)	47(12.5)
	S	0	200(15.4)	204(11.2)	55(7.5)	16(9.5)
	M(TLC) (incl. man)	5	297	207	87	19
Xylose	W	-	33	275	32	19
	M	0	577(29.0)	1469(25.3)	148(10.7)	92(24)
	S	0	363(27.9)	427(23.4)	64 (8.8)	43(25)
	M(TLC)	8	562	306	54	31
Uronic acid #	M(TLC)	2	34	92	90	2
Methylxylose@	M(TLC)			45	56	10
non-cellulosic	M	7	118	1867	4088	586
Glc	S		77	589	2169	264
Cellulosic	M		1104	3722	1003	210
Glc	S		720	1173	531	95

		0	4	14	24	35
Total cpm including cellulose & non-cellulosic Glc	M		2111	7662	5471	960
	S		1379	2417	2899	433
Total cpm excluding non-cellulosic Glc	M		1993	5795	1383	374
	S		1302	1828	730	169
$\frac{\text{Ara}}{\text{Ara+xyl}} \times 100\%$	W		84.7%	60.3	59.0	64.8
	M		33.3%	27.7	34.2	33.3
	S		35.5%	32.3	46.2	27.1
$\frac{\text{non cell Glc}}{\text{non cell Glc+Ara+xyl}} \times 100\%$		M	12.0%	47.9	94.8	80.8
		S	12.0%	48.2	94.8	81.7
DMSO-soluble fraction as % of total polysacch			33.9%	11.7	49.5	74.5
non cellulosic Glc as % of total cpm	M		5.6%	24.4	74.7	61.0
	S		5.6%	24.4	74.8	61.0
Cellulosic Glc as % of total cpm	M		52.2%	48.6	18.3	21.9
	S		52.2%	48.5	18.3	21.9
Mannose as % of total cpm	M		1.1%	0.5	2.8	2.6
	S		1.3%	1.0	2.8	3.5
Arabinose as % of total cpm	M		13.6%	7.3	1.4	4.9
	S		14.5%	8.4	1.9	3.7
Xylose as % of total cpm	M		27.3%	19.2	2.7	9.6
	S		26.3%	17.7	2.2	9.9

Table 3

Numerical data for the ^{14}C glucose labelled samples:

acid hydrolysis experiments + DMSO extraction data for days 0, 4, 14, 24, & 35

numbers presented as counts per minute corrected for background levels of radiation.

Each experiment was performed as 1/10 total sample.

W = 0.1M TFA hydrolysis

M = 2M TFA hydrolysis samples chromatographed by paper chromatography

S = H_2SO_4 hydrolysis

M(TLC) = 2M TFA hydrolysis with TLC.

\# = upper limit

\- = not measured

* = ^{14}C lost in $BaCO_3$!

@ Tentative identification

(0) extrapolated from ^{3}H results

excluding polymers

numbers in brackets represent cpm (counts per minute) as a % of the total ^{14}C excluding non-cellulosic glucose.

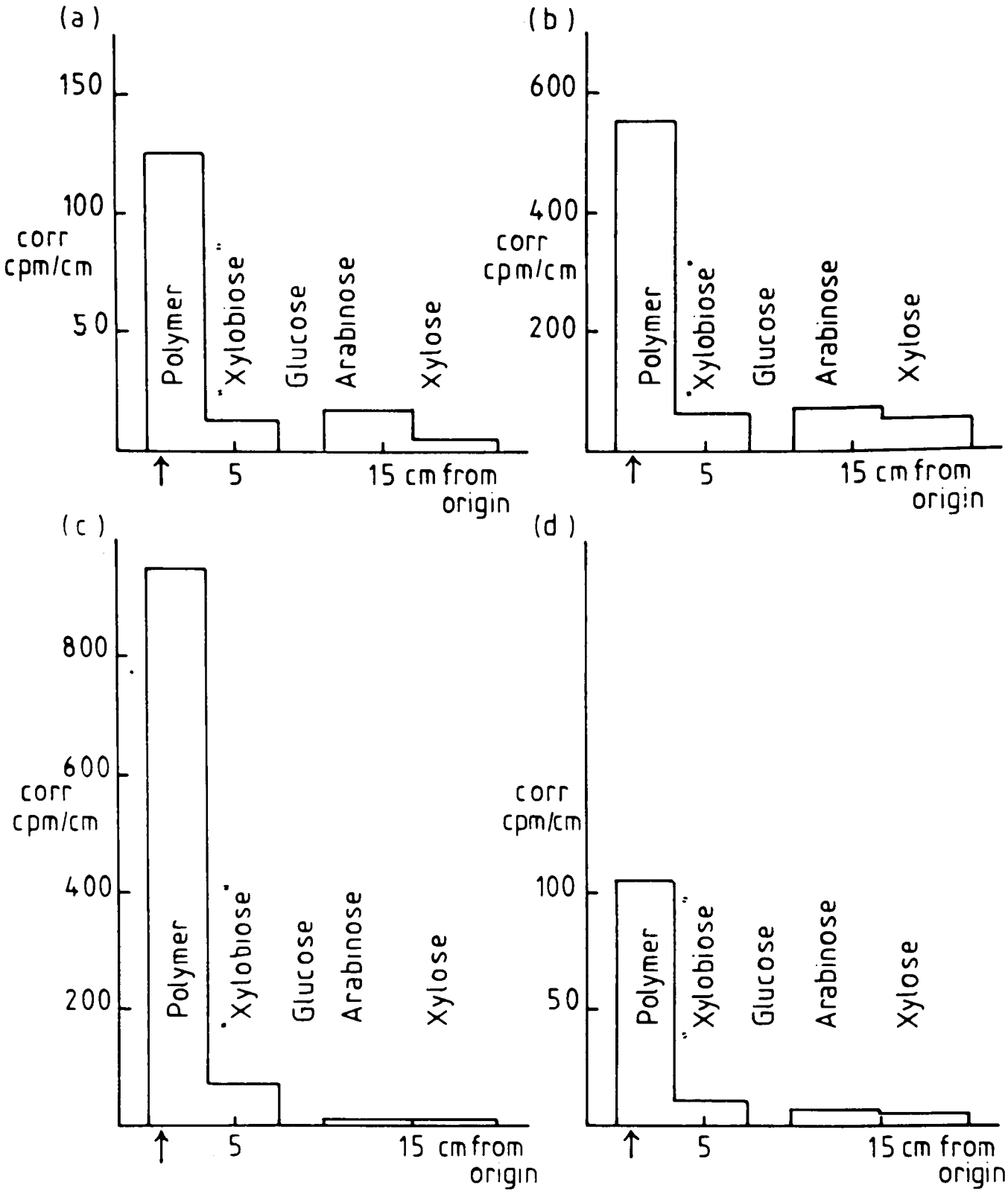

Figure 4

Mild acid hydrolysis of ^{14}C labelled samples.

Extract analysed by PC in EPW (8:2:1) for 16 hours

a) 4 day sample

b) 14 day sample

c) 24 day sample

d) 35 day sample

a) 4 day sample

b) 14 day sample

c) 24 day sample

d) 35 day sample

e) 0 day sample

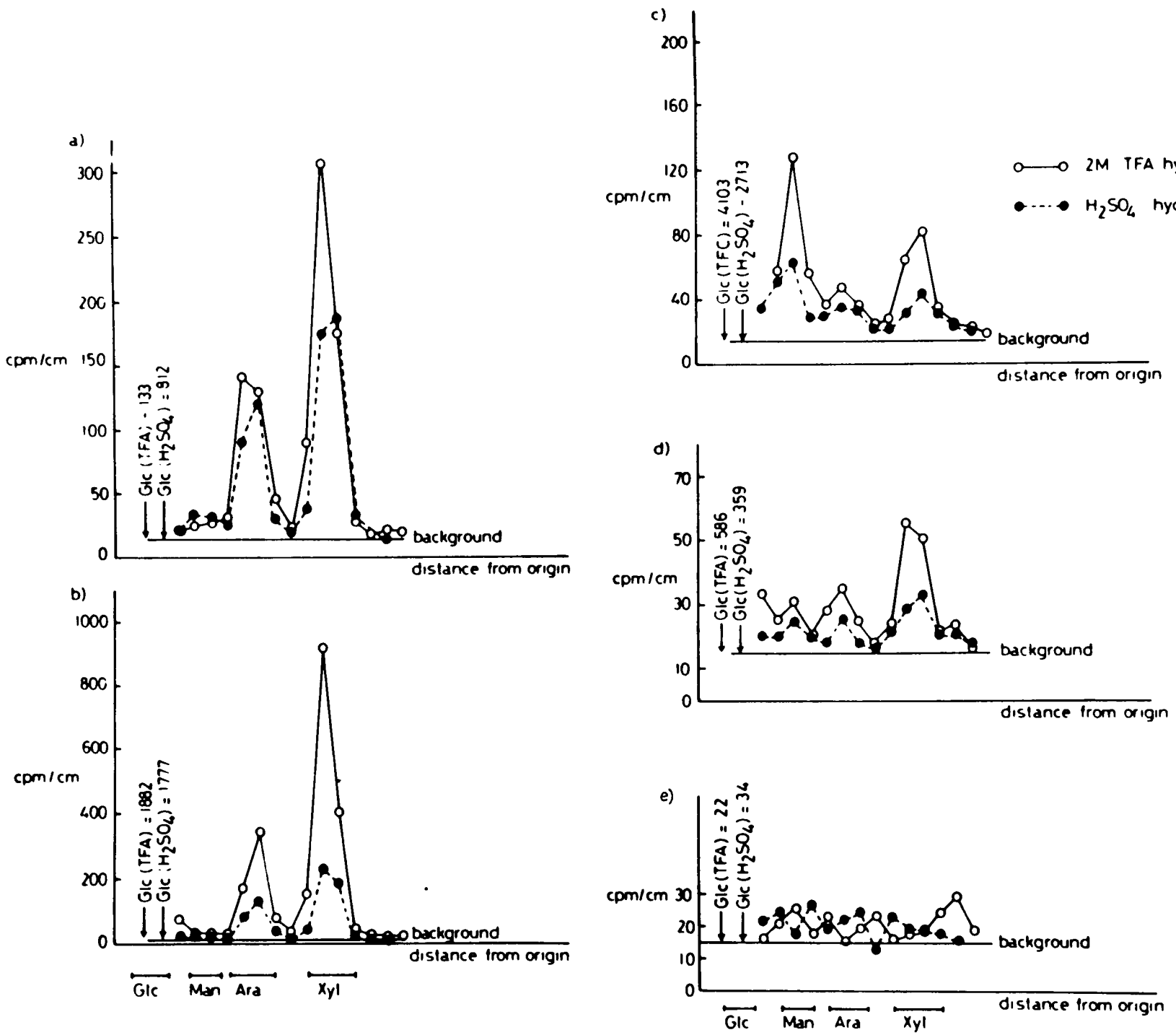

Figure 5

2M TFA and complete acid hydrolysis of ^{14}C labelled samples of macrohairs.

Samples were analysed by PC in EPW (8:2:1) for 16 hours.

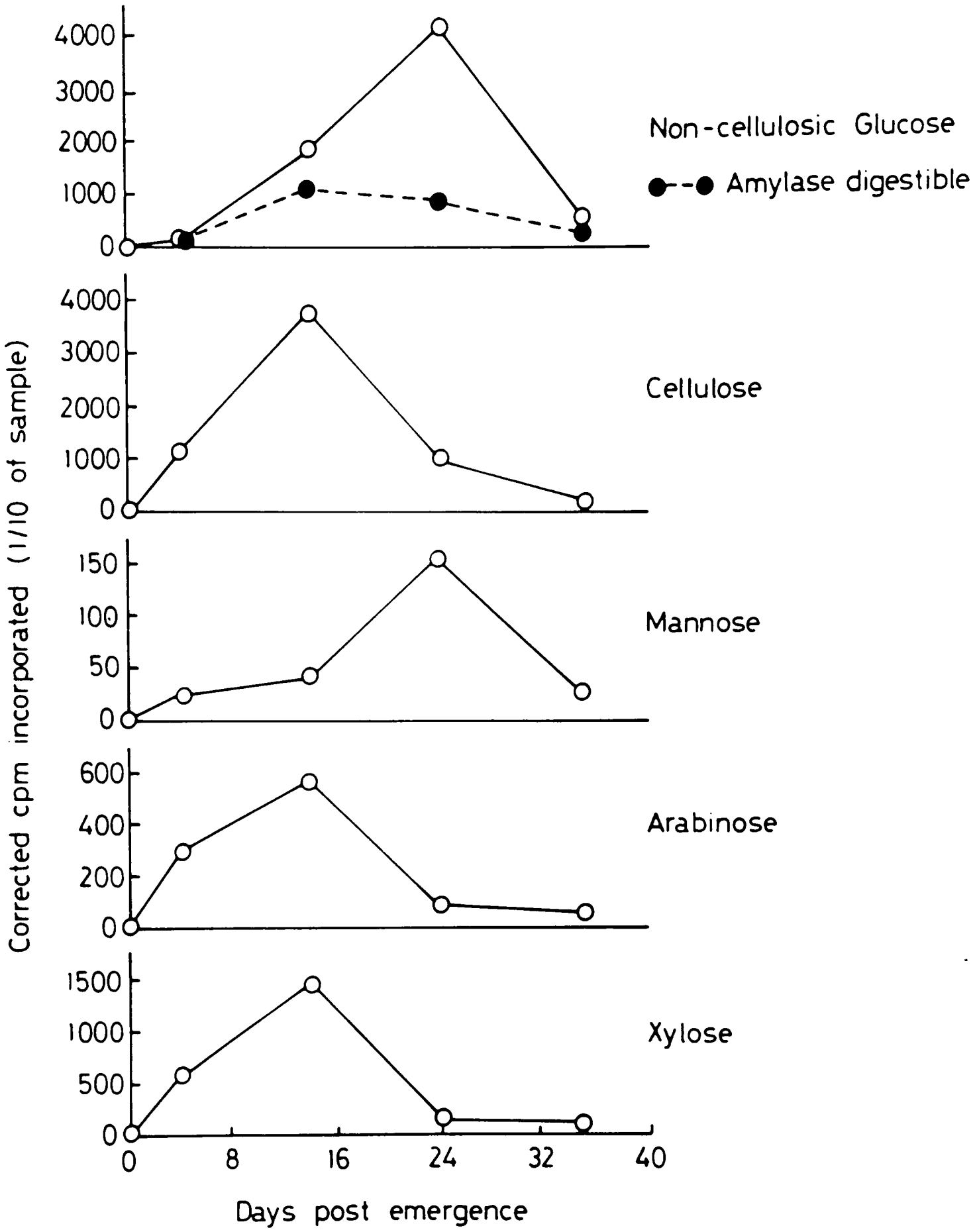

Figure 6

2M TFA hydrolysis of ^{14}C labelled material at different stages of development of the macrohair sample to show the ^{14}C absolute counts per minute incorporated into the different polysaccharides.

Samples were analysed by PCin EPW (8:2:1) for 16 hours.

a) non-cellulosic glucose (amylase digestible material (starch) is also indicated)

b) cellulose

c) mannose

d) arabinose

e) xylose

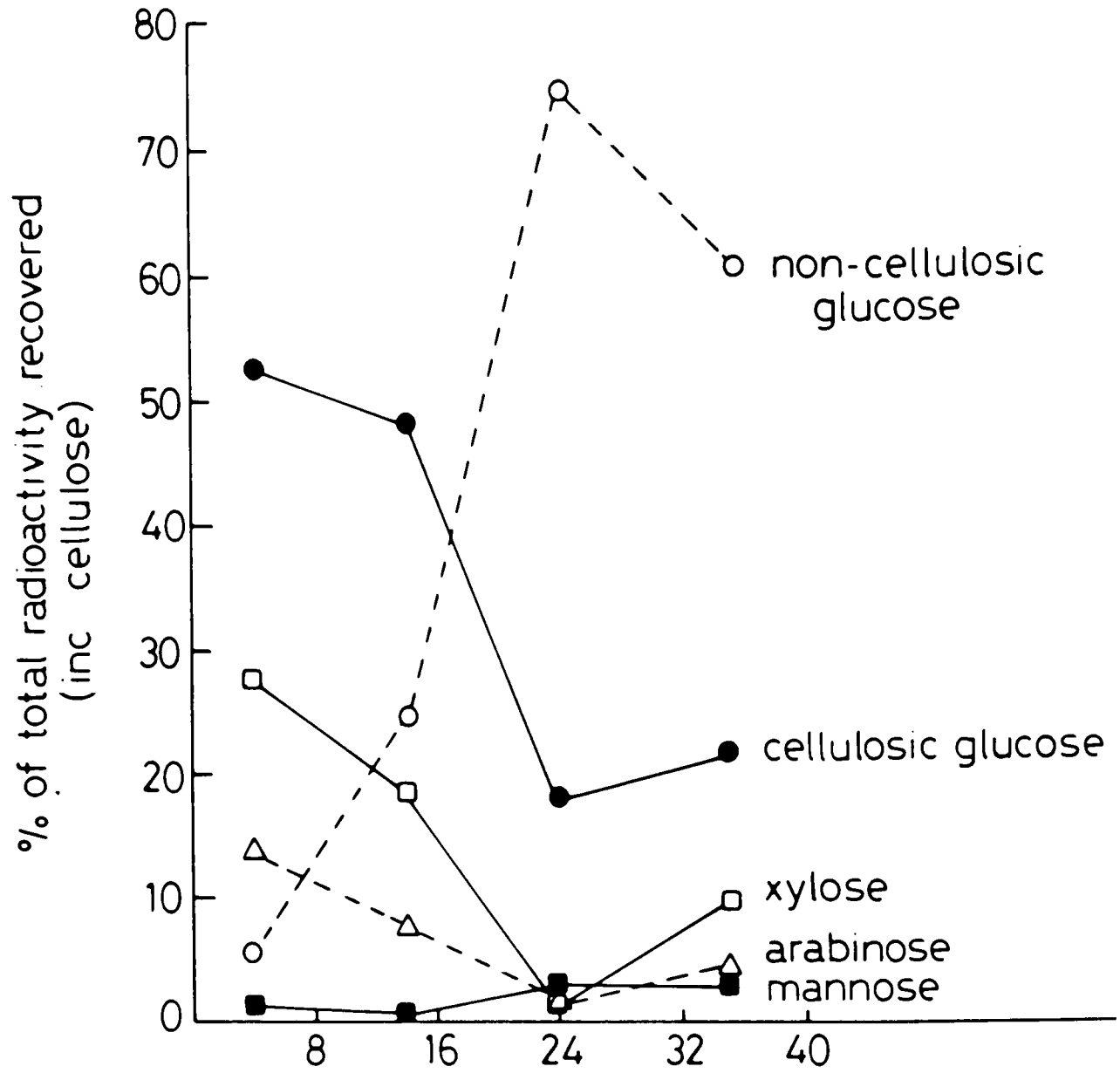

Figure 7

2M TFA and 'complete' acid hydrolysis of ^{14}C labelled 4, 14, 24 and 35 day samples of macrohairs. For numerical data see Table 3. Changes in emphasis of polysaccharide synthesis with maturation are plotted as percentages of the total radioactivity recovered.

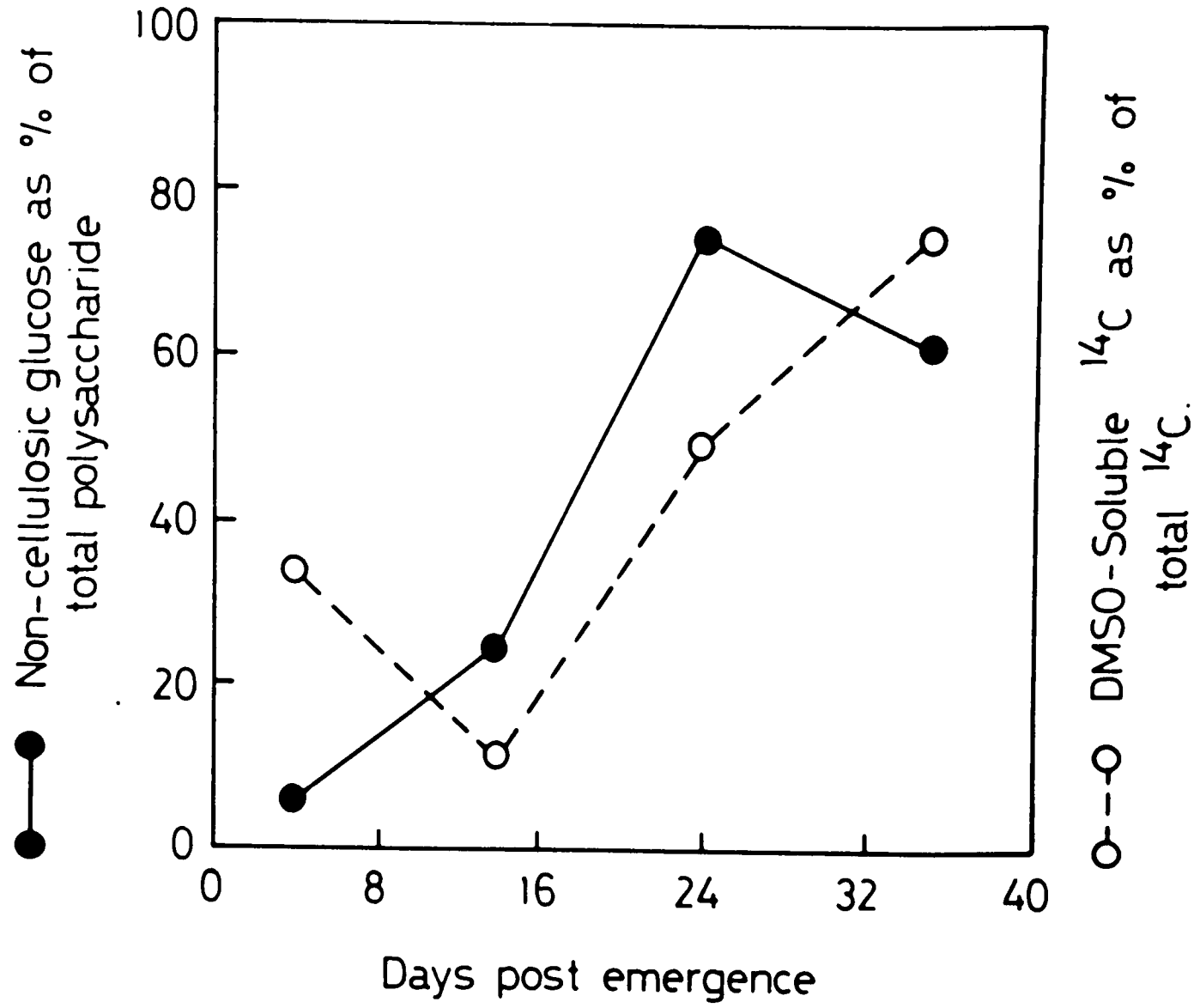

Figure 8

^{14}C starch/ non-cellulosic glucan analysis.

At each sampling point, non-cellulosic glucose and DMSO soluble radioactivity is plotted as a percentage of the total ^{14}C recovered.

A dimethylsulphoxide (DMSO) extraction was performed on samples labelled as 4, 14, 24 and 35 days after emergence of the inflorescence using 90% DMSO with shaking followed by washing. The DMSO soluble fraction and the residue were scintillation counted and the residue kept for further experiments. Numerical data is presented in Table 3 and figure 8.

The results obtained from the acid hydrolysis involving concentrated sulphuric acid give an indication of the total composition of the polysaccharides being synthesised at any one given time, as all polysaccharides, including cellulose, are hydrolysed by this treatment.

However, this method of hydrolysis does not give any indication of the rate of incorporation of radioactive glucose into cellulosic and non-cellulosic polymers during cell-wall maturation. This information is obtained from analysis of data obtained after acid hydrolysis of macrohair samples using 2M trifluoroacetic acid. The method gives the rate of incorporation of non-cellulosic glucose into polymer as cellulose is not hydrolysed under the conditions of the experiment. Paper and thin layer chromatography were performed on the supernatant. A photograph of both the tlc plate and X-ray film image, figure 1, show pictorially both the total polysaccharide composition (all monosaccharides produced by acid hydrolysis are stained using Wilson's dip)(figure 1b) and changes in emphasis of polysaccharide synthesis at the different time points (figure 1c). The TLC plate shows that on hydrolysis of all the samples largely xylose, glucose and arabinose are produced. The overall quantitative pattern of the monosaccharides is xylose > glucose > arabinose >> any other monosaccharide.

The X-ray film image shows pronounced shifts in emphasis of polysaccharide synthesis at the different sampling points.

Day 0 : little can be seen

Day 4 : ara = xyl > glc > others

Day 14: xyl = glc > ara > others

Day 24: glc > gal > man/ara* > xyl > others

Day 35: glc > xyl > ara > gal > others

* Not resolved by TLC.

Trace levels of other monosaccharides synthesised include uronic acids and a monosaccharide which co-chromatographed with methylxylose but was not identified as such by ^{3}H labelling experiments.

The results obtained by paper chromatography give virtually identical data. The numbers obtained were prefered for comparison with numerical data produced by `complete´ acid hydrolysis as statistical counting errors on the analysis of a larger, more radioactive sample were greatly reduced. Comparative graphical data for the two hydrolysis procedures is given in figure 5. The 2M trifluoroacetic acid hydrolysis data gives tha rate of incorporation of non-cellulosic glucose into polymer as well as the rate of incorporation of xylose and arabinose into polymers. The rate of incorporation of cellulosic glucose can be calculated by comparison with results obtained after `complete´ acid hydrolysis of samples using sulphuric acid.

Numerical calculations of % composition for both sets of data (including allowances for cellulosic glucose) show remarkable agreement, Table 3 and figure 7. The percentage composition of material synthesised changes dramatically with time. At day 4 , the rates of polymer synthesis incorporating cellulosic glucose, xylose and arabinose are high, whereas

rates of polymer synthesis incorporating non-cellulosic glucose is low. At day 24, the situation is reversed and the rate of polymer synthesis incorporating non-cellulosic glucose is much higher than for the synthesis of other polymers. This is very clearly seen in figure 6, where for a given sample, the absolute incorporation of radioactive label is plotted against sampling point for each monosaccharide. The change in emphasis of polysaccharide synthesis is clear. Polysaccharides incorporating xylose, arabinose and cellulosic glucose are synthesised during the early stages of wall thickening and polymers incorporating non-cellulosic glucose and mannose are synthesised to a greater extent during the later stages of development. Little or no polysaccharide is synthesised as the inflorescence emerges (day 0) and again, at the sampling point approaching maturity (day 35), the rate of incorporation of radioactive label and, therefore, the level of synthesis of polysaccharide, is much reduced.

A comparison of the arabinose:(xylose+arabinose) ratios for all three hydrolysis procedures (Table 3 and figure 13) shows that, under mild acid conditions, arabinose is released preferentially to xylose from the polysaccharide. The increased acid lability of the arabinose indicates that it is furanosyl-linked within the polysaccharide. The removal of some xylose indicates that the hydrolysis conditions were a little severe as under ideal conditions virtually all arabinose, furanosyl-linked, would be removed leaving essentially all xylose and arabinose pyranosyl-linked untouched. At all stages of development, the hydrolysis procedures except the mild acid treatment show that the arabinose:(xylose+arabinose) ratio varies little and may indicate that a single polysaccharide (a heavily substituted arabinoxylan) is synthesised during the course of secondary wall development.

The DMSO extraction was performed to remove starch from the cell wall preparations. Data is presented numerically in Table 3 and graphically in figure 8. "Cell wall" synthesis relative to "starch" synthesis peaks on day 14. A comparison of the percentage DMSO soluble material with non-cellulosic glucose is given in figure 8b. The data for the DMSO extractable material for day 4 seems abnormally high but may be explained if acetylated xylans and glucomannans are present as these also would be partially removed by this procedure (Bouveng and Lindberg,1965). At day 24, there is a high proportion of non-cellulosic glucose which is not DMSO extractable (not starch). This material is likely to be either a mixed $\beta 1 \rightarrow 3$, $\beta 1 \rightarrow 4$ linked glucan or a $\beta 1 \rightarrow 3$ linked glucan (callose) or a mixture of the two. At present the identity of the polysaccharide is unknown.

5.3.2.3 Amylase digestion

This was performed on samples of macrohairs from 4, 14, 24 and 35 days after emergence of the inflorescence to identify the presence of starch within the macrohair samples. A mixture of $\alpha$and βamylases was used and the hydrolysate paper chromatographed. The results are presented numerically in Table 4 and graphically in figures 9, 10 and 11. In all samples, a disaccharide and glucose were the only mobile hydrolysis products, figure 9. The identity of the disaccharide was confirmed by rerunning relevant samples eluted from chromatogram strips (as indicated in figure 9) in a different solvent system more specific for the chromatographic separation of disaccharides, figure 10. Maltose, an enzymic hydrolysis product of starch was identified using a non-radioactive internal marker which was subsequently stained with silver

Table 4

Amylase digestion products at different stages of wall development

	Day				
	0	4	14	24	35
					Cpm
mobile (Glc and Maltose)		165(16.6)	1066(42.0)	860(34.2)	280(43.1)
Immobile (and insoluble)		826	1470	1654	369
Total recovered (? on inclusion of insoluble material)		991	2536	2514	649

( ) = % of total as derived from starch. All other glucans are not affected by this treatment.

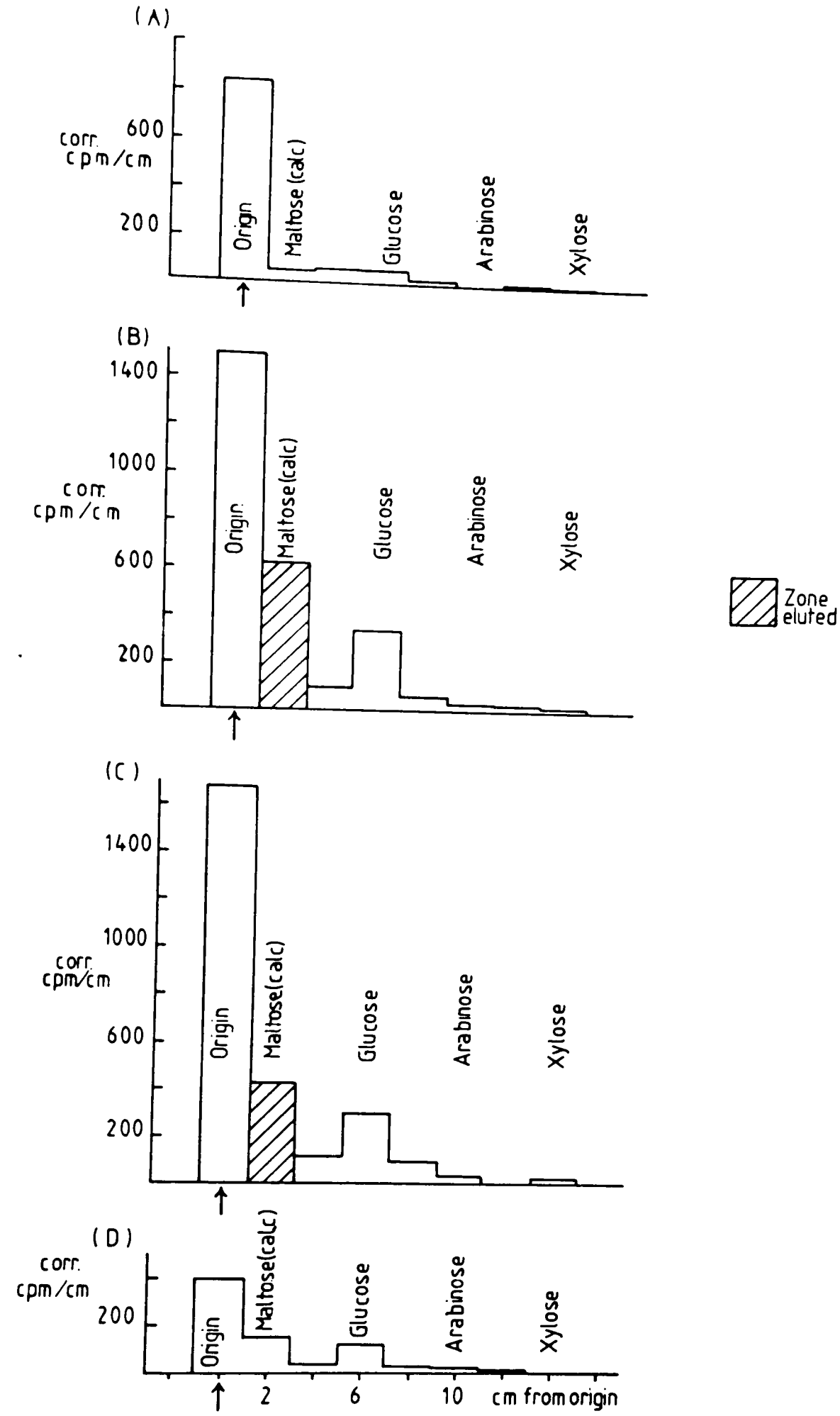

Figure 9

Amylase digestion on ^{14}C labelled samples.

Samples analysed by PC in EPW (8:2:1) for 16 hours.

a) 4 day sample

b) 14 day sample

c) 24 day sample

d) 35 day sample

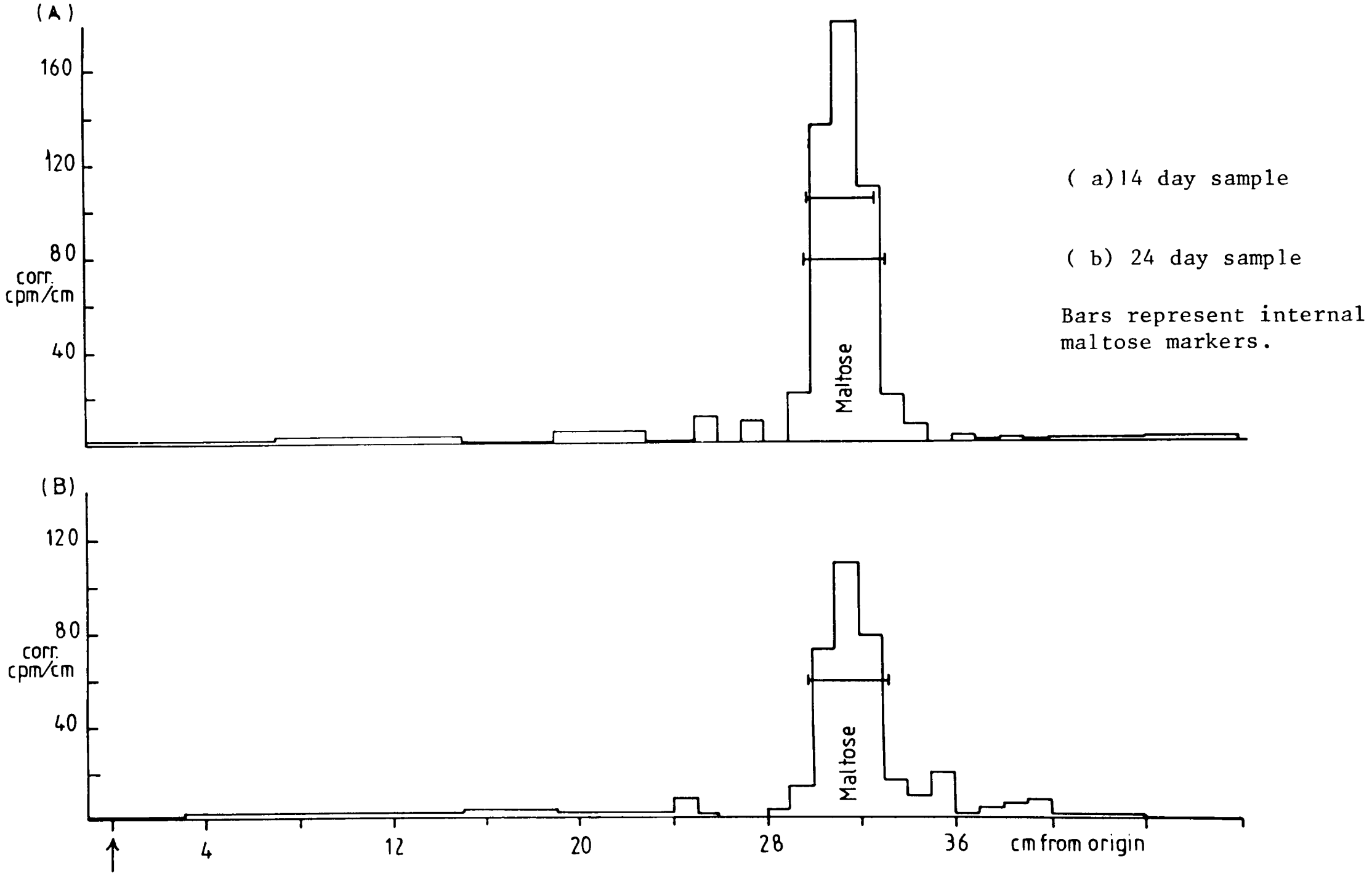

(a) 14 day sample

(b) 24 day sample

Bars represent internal maltose markers.

Figure 10 Analysis for starch using amylase digestion. Samples were analysed by PC in EPW (10:4:3) for 2X16 hours with drying in between. Confirmation for the presence of maltose.

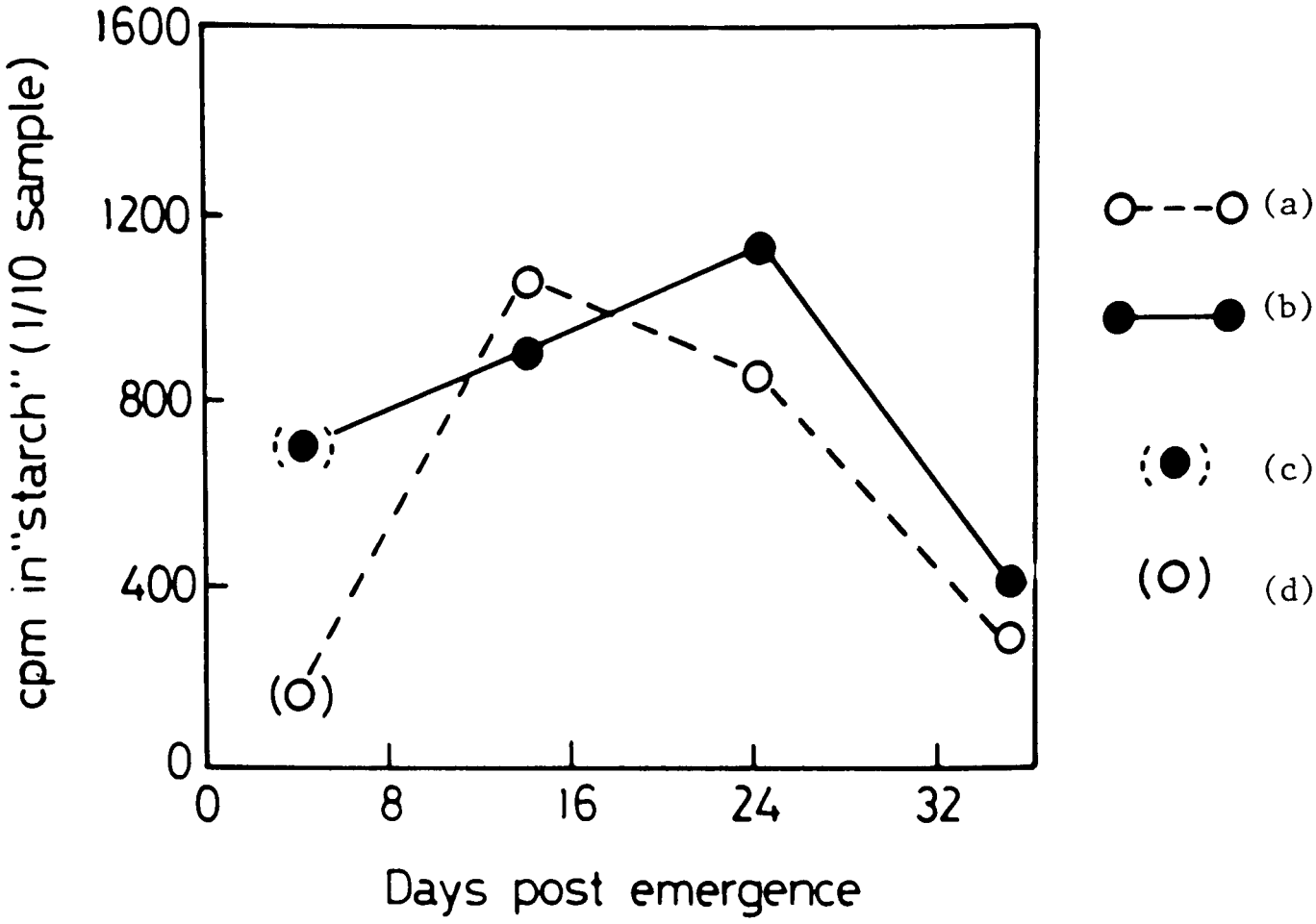

Figure 11

A comparison of the amount of ^{14}C labelled glucose/maltose present in starch as detected by amylase digestion and DMSO soluble material.

(a) Glucose and maltose released by amylases

(b) DMSO-soluble

(c) clearly not all glucose

(d) filter method; dilute amylase

nitrate. The results of enzymic degradation indicate that starch synthesis peaks on day 14. The data is consistent with that obtained from the DMSO extraction procedure and is presented in figure 11. The rates of synthesis of starch are much lower than the overall figures obtained for non-cellulosic glucose produced by 2M trifluoroacetic acid hydrolysis and there is additional evidence that starch is not the only non-cellulosic glucan synthesised particularly at day 24 during cell wall development. Other polymers which may be present include a $\beta 1\rightarrow 3$ linked glucan (callose), or a mixed link, $\beta 1\rightarrow 3$, $\beta 1\rightarrow 4$ linked glucan or possibly a xyloglucan although this seems unlikely as the synthesis of xylose and arabinose is very low at day 24. The identity of the polysaccharide/s remains to be determined.

5.3.3 ^{3}H arabinose labelled samples

5.3.3.1 Rate of incorporation of radioactivity

The rate of incorporation of the radioactivity into the macrohairs was estimated by scintillation counting samples of macrohairs produced by the isolation technique described previously in section 5.2.1. The results are presented in Table 5.

The maximum rate of incorporation of the ^{3}H labelled arabinose into polysaccharides synthesised within the macrohair was at day 14. The samples, however, appeared to be synthesising detectable levels of polysaccharide both at emergence of the inflorescence and as the inflorescence approached maturity. If the % incorporation figures are compared for both the ^{3}H and the ^{14}C labelling similar rates of incorporation are observed except at day 0 where for the ^{3}H arabinose

Table 5

The rate of incorporation of radioactive ^{3}H label into the cell wall of macrohairs at different stages of development

Days post emergence of the inflorescence	Total cpm see section 5.2.2	% of supplied (a)
0	11,600	0.0045
4 (b)	125,000	0.048
14	775,000	0.298
24	177,000	0.068
35	96,000	0.037

(a) assuming a counting efficiency of 3%, $1\mu Ci = 6.6 \times 10^{4}$ cpm

(b) approximate because filter method of cleaning was used.

labelled sample there was a 10 fold increase in incorporation into polysaccharide synthesised within the macrohair sample.

Each of the following experiments was performed on 1/10 of the total hair preparation.

5.3.3.2 Acid hydrolysis

This was performed on all samples to ascertain changes in monosaccharide composition of the polysaccharides being synthesised at a given stage of mineralisation as mineralisation progressed. All numerical data is presented in table 6.

`Weak´ acid hydrolysis (W) was performed on samples from 4, 14, 24 and 35 days after emergence of the inflorescence using 0.1M trifluoroacetic acid at 100°C for 1 hour followed by paper chromatography of the supernatant. Data is presented numerically in Table 6 and graphically in figures 12 and 13.

`Moderate´ acid hydrolysis (M) was performed on samples from 0, 4, 14, 24 and 35 days after emergence of the inflorescence using 2M trifluoroacetic acid at 120°C for a hour followed by paper chromatography of all material produced. This procedure was repeated for days 4 and 14 and only the supernatant was loaded. Numerical data is presented in Table 6 and graphical data in figures 13, 14a, 14b and 15.

The complete acid hydrolysis (excluding cellulosic glucose) using 2M trifluoroacetic acid gives the monosaccharide composition of polysaccharides synthesised during cell wall development after labelling with radioactive arabinose. The monosaccharides detected were varying amounts of xylose, arabinose and glucose, figure 14a. The material which remains at the origin consists of labelled cellulose and any radioactive

Table 6

Numerical data for the ^{3}H arabinose labelled samples:

		Days				
		0	4	14	24	35
^{3}H started with		1160	12500?	77500	17700	9600
Total ^{3}H recovered	W		253	21371	6611	3055
	M	290	6300	47900	15000	7200
Total excluding polymer & insol.	W		133	10528	2497	804
	M	218	5135	37458	12615	6026
	M_R		5081	21002		
Disaccharide	W		45	1863	673	315
	M	0	0	0	0	0
	M_R		0	0		
Glucose (non-cellulosic)	W	0	0	0	0	0
	M	33(15.1)	95(1.85)	3114(8.3)	1950(15.5)	195(32)
	M_R		75(1.48)	1696(8.1)		
Arabinose	W		54	6881	1270	173
	M	64(29.4)	2841(55.3)	15232(40.7)	4335(34.4)	1440(23)
	M_R		2726(53.7)	8954(42.6)		
Xylose	W		34	1844	555	316
	M	102(46.8)	2041(39.7)	17819(47.6)	5700(45.2)	2261(37)
	M_R		2042(40.2)	10026(47.7)		
MeXyl	W					
	M	0	133(2.6)	48(0.13)	30(0.24)	14(0.23)
	M_R		0			
$\frac{Ara}{Ara+Xyl} \times 100\%$	W		61.4%	78.9%	69.6%	35.4%
	M	38.0%	58.2%	46.0%	43.2%	38.9%
	M_R		57.2%	47.2%		
$\frac{Glc}{Glc+Ara+Xyl} \times 100\%$	M		1.9%	8.6%	16.3%	34.5%
	M_R		1.5%	8.2%		

Table 6

Numerical data for the ^{3}H arabinose labelled samples:

Acid hydrolysis experiments for days 0,4,14,24 & 35

Numbers presented as counts per minutes corrected for background levels of radiation.

Each experiment was performed on 1/10 total sample.

W = 0.1M TFA hydrolysis

M = 2M TFA hydrolysis

M_R = 2M TFA hydrolysis (repeat)

numbers in brackets, are % of the total ^{3}H measured.

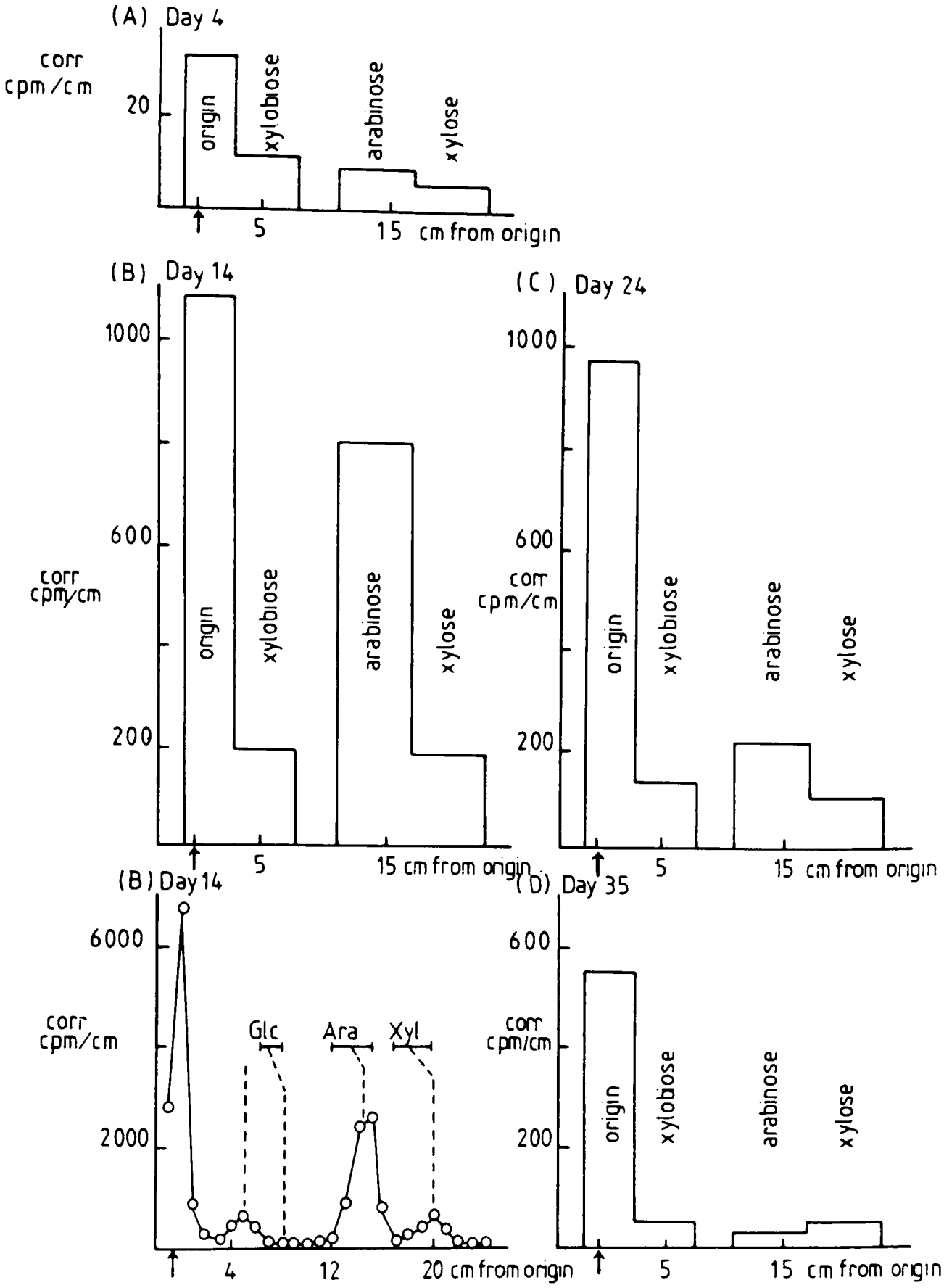

Figure 12

Mild acid hydrolysis of ^{3}H labelled sample.

Samples analysed by PC in EPW (8:2:1) for 16 hours.

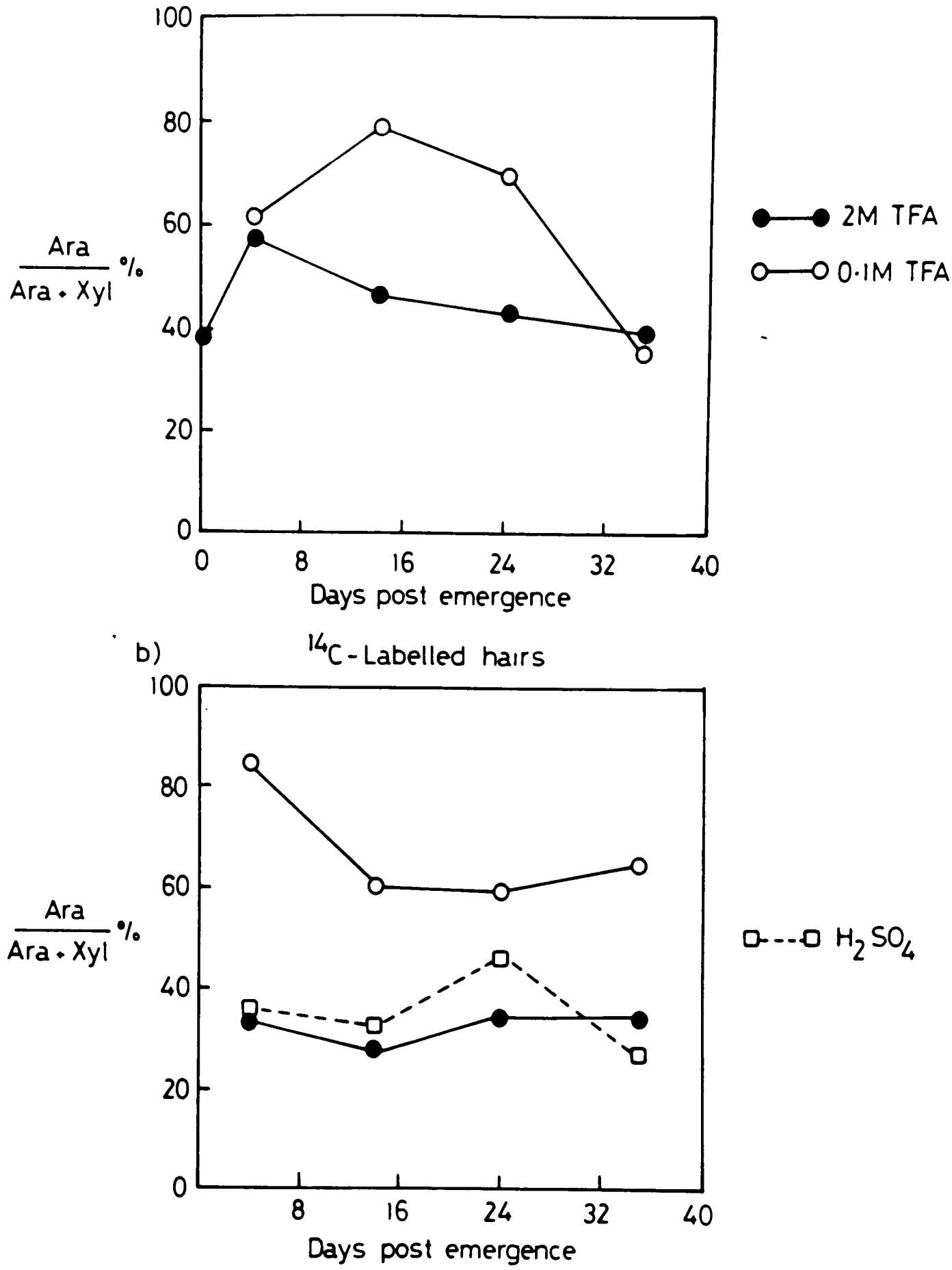

Figure 13

(Ara/Ara+Xyl) percentage ratios for ^{3}H and ^{14}C labelled macrohair samples under different hydrolysis conditions and at different stages of development.

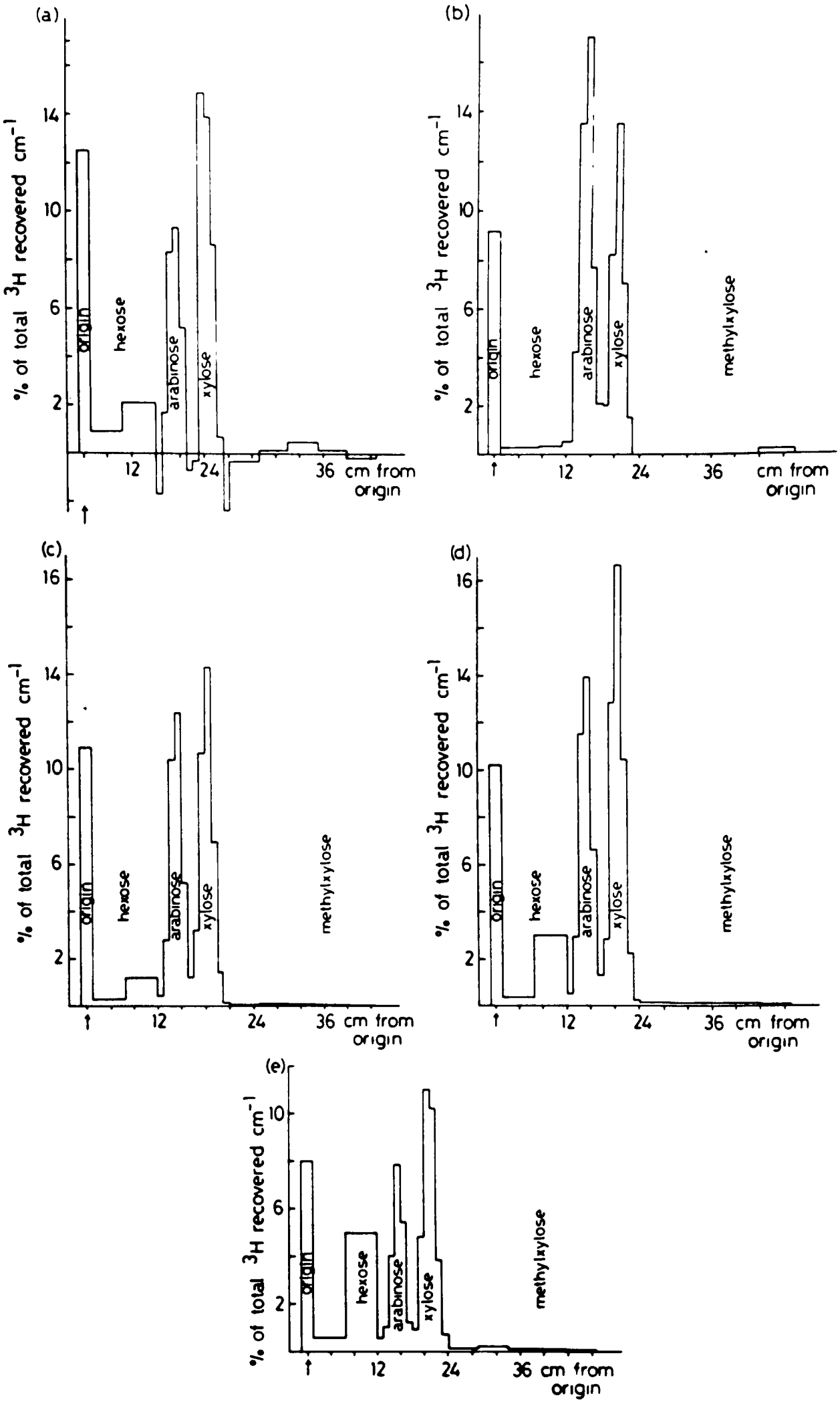

Figure 14a

2M TFA acid hydrolysis on ^{3}H labelled samples of macrohairs at different stages of development.

Samples were analysed by PC in EPW (8:2:1) for 16 hours.

a) 0 day sample

b) 4 day sample

c) 14 day sample

d) 24 day sample

e) 35 day sample

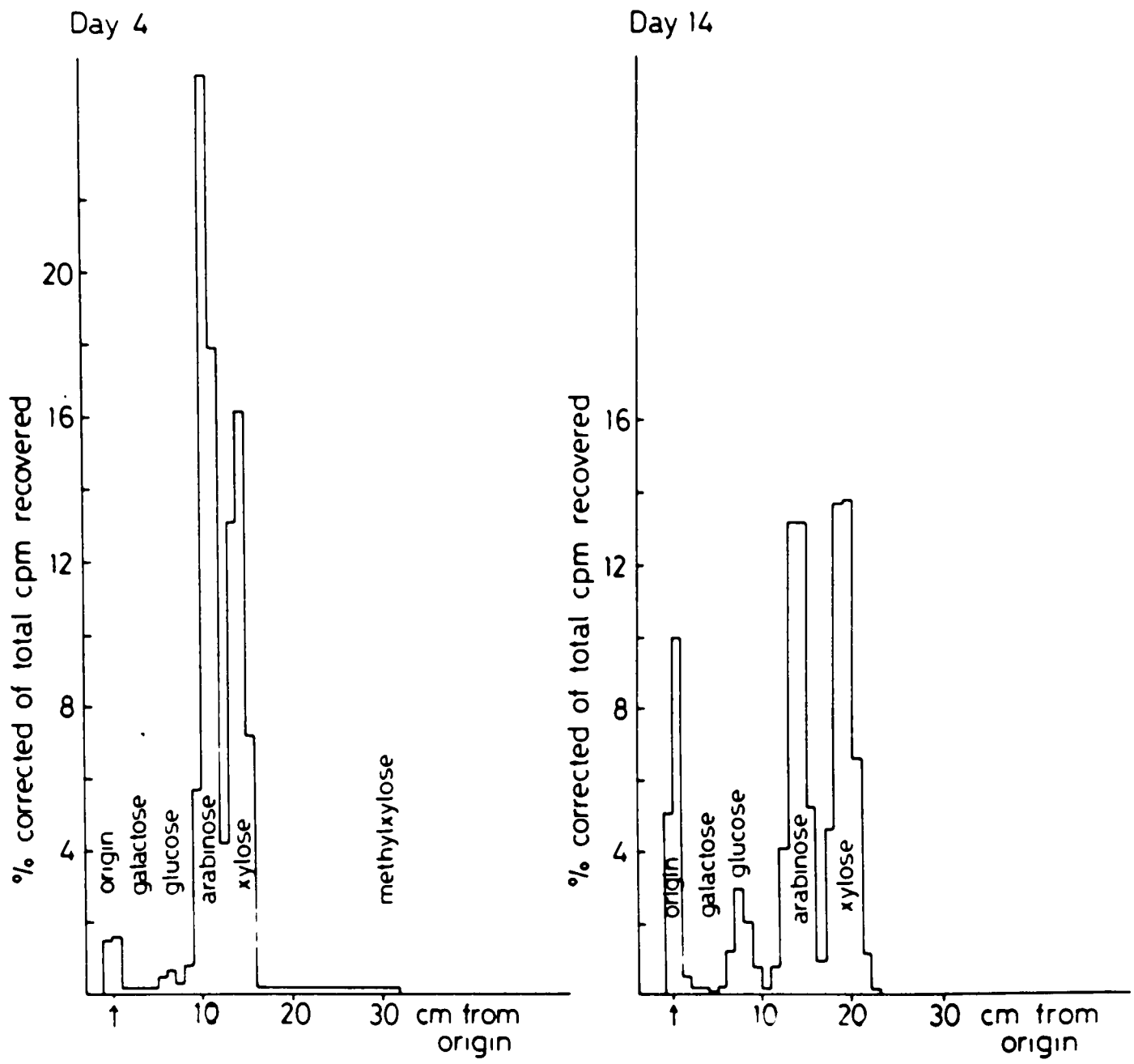

Figure 14b

2M TFA acid hydrolysis on ^{3}H labelled samples.

Samples were analysed by PC in EPW (8:2:1) for 16 hours.

Insoluble material was not loaded onto the chromatogram.

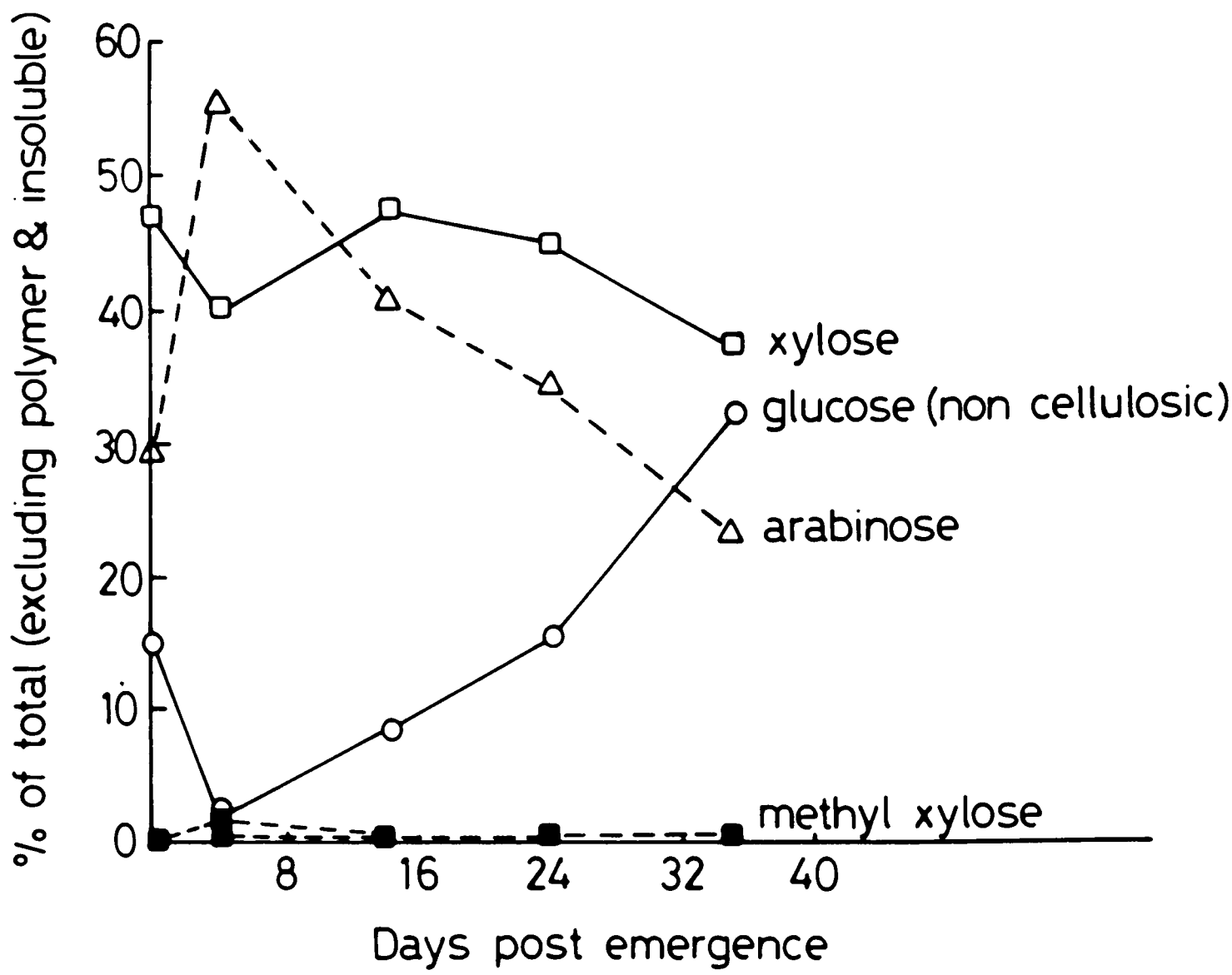

Figure 15

2M TFA acid hydrolysis of ^{3}H labelled 0, 4, 14, 24 and 35 day samples of macrohairs. For numerical data see Table 6. Changes in emphasis of polysaccharide synthesis with maturation are plotted as percentages of the total (excluding polymer and insoluble) radioactivity recovered.

oligomers of glucose, arabinose and xylose which were not degraded by treatment with 2M trifluoroacetic acid. The changes in the relative abundance of the monosaccharides with time is shown in figure 15. Trace levels of methyl xylose were thought to be present but were not conclusively identified by paper chromatography (repeat on day 4, figure 14b).The rate of hexose (non-cellulosic) synthesis increased between days 4 and 35 as the cell wall matured. The hexose was identified as glucose, figure 14b. The significance of the increase was difficult to interpret because the gluconeogenic pathway by which the glucose is produced from pentoses may not be constant. However, the hexoses are consistently ^{3}H labelled with approximately a 1/6th the efficiency of ^{14}C.

The arabinose:(arabinose+xylose) ratio was compared for all developmental stages for both `moderate´ and `weak´ acid hydrolyses. A comparison with the ^{14}C data is shown in figure 13. The ratio is higher for the weak acid hydrolysis indicating that arabinose is preferentially released from the polysaccharide. However, some xylose is also released, figure 12, indicating that hydrolysis conditions were too `strong´. The reasons are as previously explained for the $^{14}C$ data. The ara:(ara+xyl) ratio for the `medium´ acid hydrolysis is higher for the ^{3}H data than for the ^{14}C data. The value is 38-58% as compared to 27-46% for the ^{14}C data.This possibly indicates that the UDP-Xyl-4-epimerase involved in the interconversion of xylose and arabinose is not acting precisely at equilibrium. Figure 16 shows a) how different polysaccharides are synthesised after feeding with ^{3}H arabinose and b) how feeding with either ^{3}H or ^{14}C sugars affects the product polysaccharides formed. The step between UDP-arabinose and UDP-xylose (as starred) may not be at equilibrium.

(a)

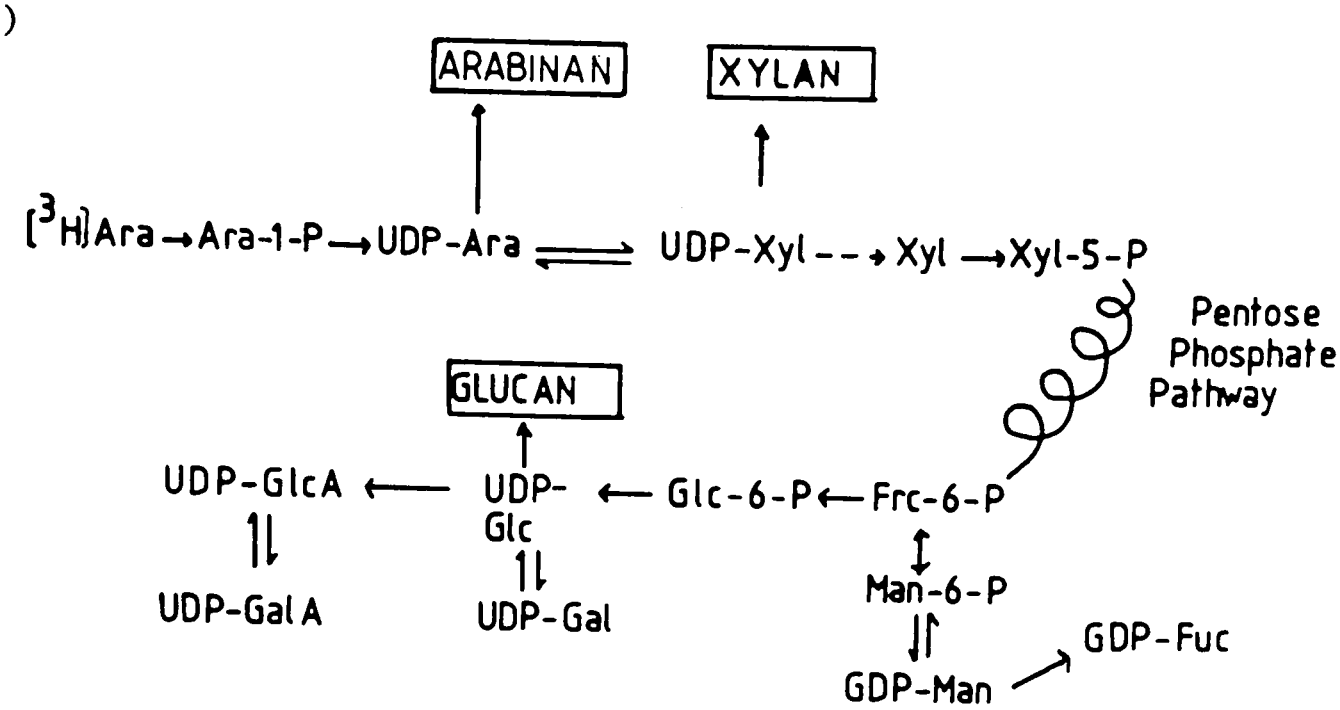

(b)

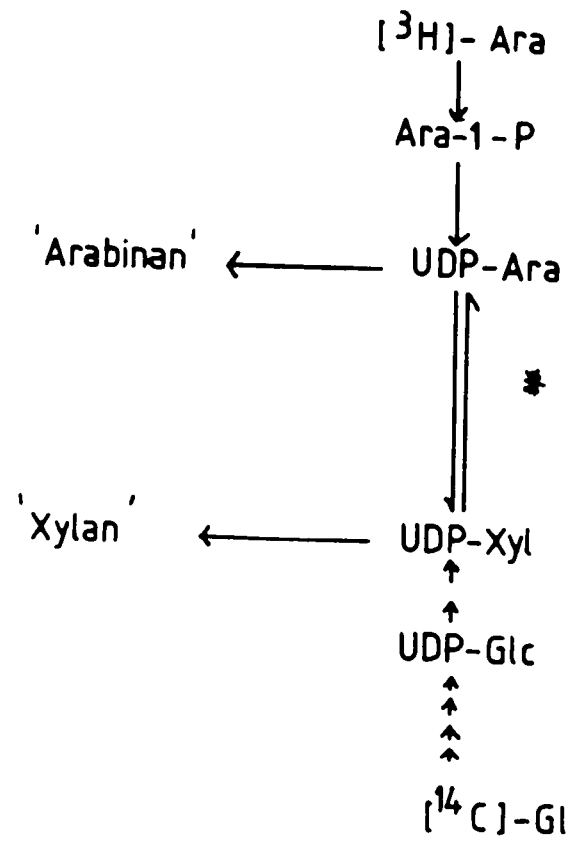

Figure 16

a) To show the possible pathway by which hexoses are synthesised after feeding the inflorescences with labelled pentose sugars.

b) To show pathways by which xylans and arabinans are produced after feeding of the inflorescences with either ^{14}C labelled glucose or ^{3}H labelled arabinose. The conversion between UDP-Ara and UDP-Xyl (starred) may not be at equilibrium.

5.3.3.3 Driselase digestion

Driselase digestion was performed in order to identify whether a xyloglucan was one of the polysaccharides present in the cell wall of the developing macrohairs. This method was utilised as the enzymic mixture should hydrolyse all glycosidic bonds except xylosyl α1→6-glucose and the presence of a disaccharide as a digestion product which subsequently gives xylose and glucose on acid hydrolysis is indicative of the presence of a xyloglucan which is known to occur in small amounts in other grasses.

^{3}H arabinose labelled samples of dried macrohairs at 4, 14, 24 and 35 days after emergence of the inflorescence were subjected to enzymic hydrolysis with Driselase. The hydrolysate was paper chromatographed and relevant strips were scintillation counted. The results are presented graphically in figure 17. The day 4 sample contained little monosaccharide in the hydrolysate although this may in part be due to the fact that dilute enzyme was used for this reaction. Day 14 and 24 samples gave radioactivity in the disaccharide region, glucose, xylose and arabinose. The day 35 sample gave radioactive regions corresponding to a disaccharide and glucose. Comparison of these results with those obtained from the strong acid hydrolysis of similar samples showed that the Driselase digestion removed xylose and arabinose less efficiently than glucose from the macrohairs. Possible explanations are that the polymers are heavily acylated or that the presence of silica prevents the enzyme penetrating the cell wall.

The disaccharide/s fragments produced by Driselase digestion were subjected to a further Driselase digestion under identical conditions. The resulting hydrolysate was paper chromatographed, autoradiographed and

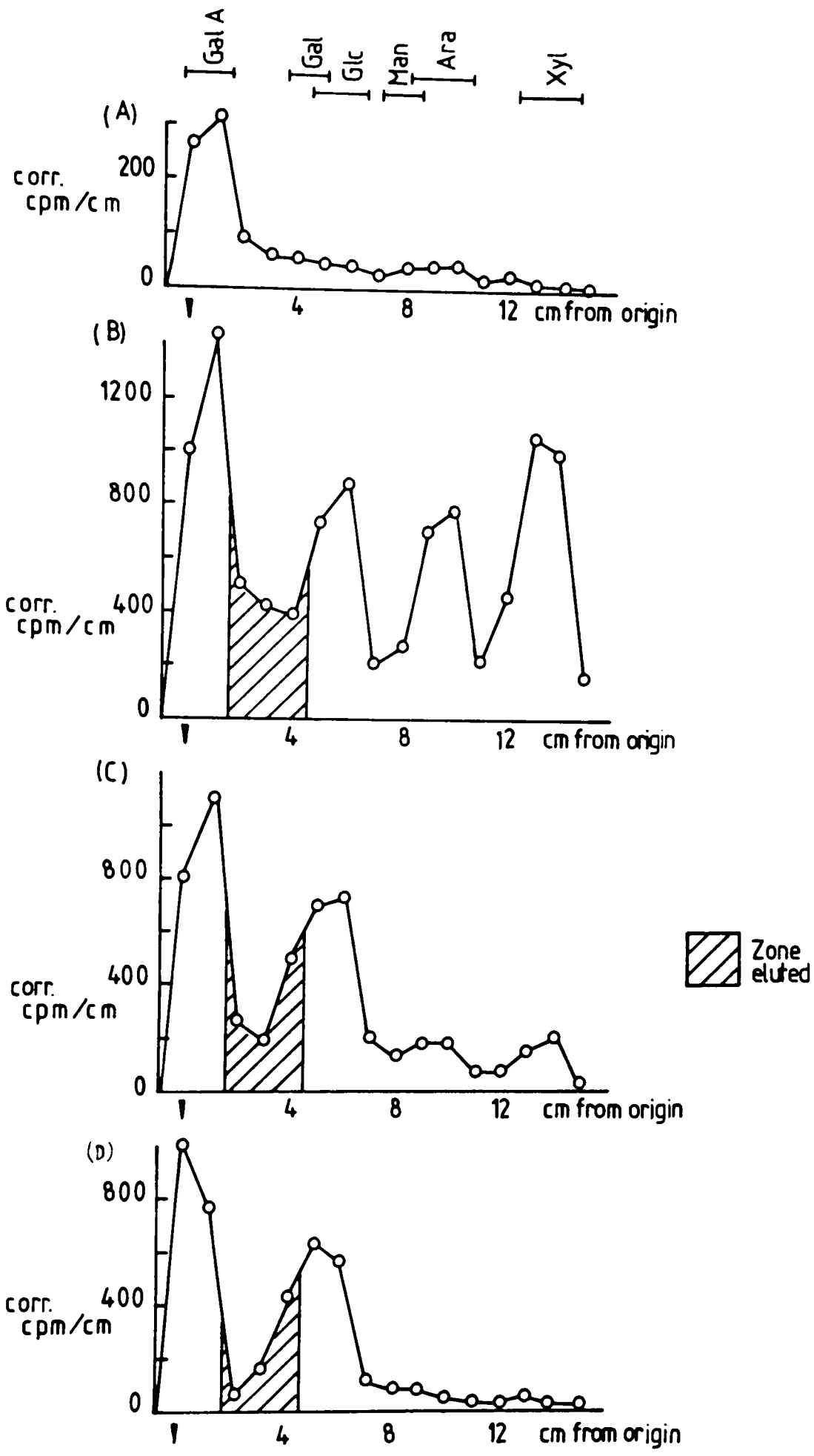

Figure 17

Driselase digestion results from ^{3}H labelled samples.

Samples were analysed by PC in EPW (8:2:1) for 30 hours.

The shaded area represents the disaccharide region which was eluted for further enzymic digestion.

a) 4 day sample (dilute enzyme)

b) 14 day sample

c) 24 day sample

d) 35 day sample

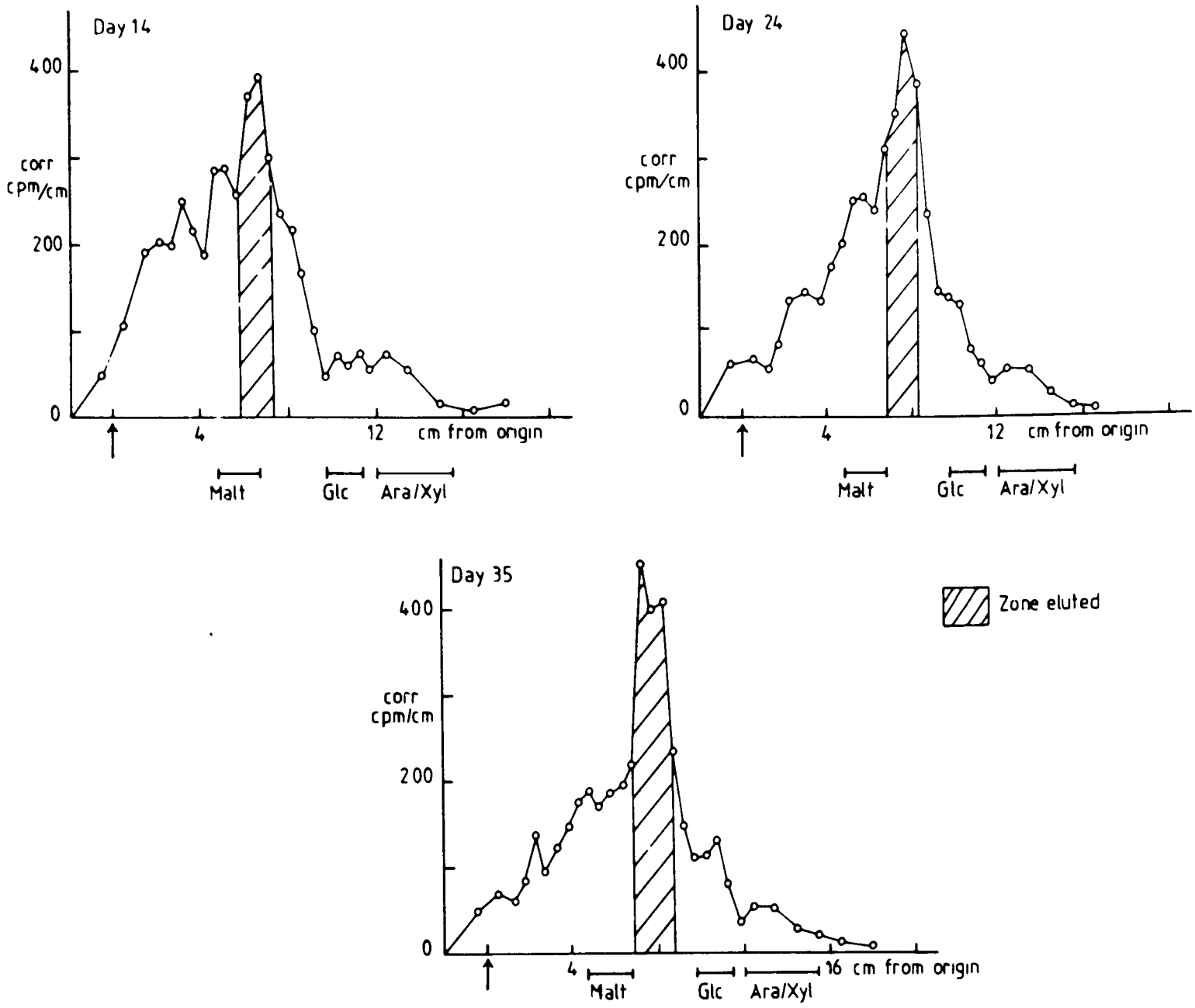

Figure 18

Second driselase digestion on oligosaccharide region.

Samples were analysed by PC in BAW (12:3:5) for 16 hours.

The main disaccharide (shaded area) was eluted for further analysis in each case.

examined under ultra-violet light with and without ammonia. The chromatograms produced by the second Driselase digestion gave areas which fluoresced in ultra-violet light, some of which changed colour in the presence of ammonia fumes, figure 19. Areas corresponding to regions of localised radioactivity in two of the samples, as shown by autoradiography are also highlighted. The fluorescent spots produced after the second Driselase digestion were identified as feruloyl esters and ferulic acid by reference to published data (Fry, 1982).

An extended peak of radioactivity is observed in the disaccharide region which does not correspond to the position of the maltose marker Figure 18. The peak shape is similar for all three samples although there does appear to be another appreciable component in the day 14 sample as evidenced by a large shoulder on the left-hand side of the major peak. Material from the major peak (the shaded areas in figure 18) was identified by further chromatography followed by acid hydrolysis and chromatography. This major peak yielded three different disaccharides in all three samples, figure 20. Strong acid hydrolysis and chromatography gave the monosaccharidic composition of the three disaccharides.

Results show that

X: unknown as acid hydrolysis gave pc immobile material

Y: Galactobiose

Z: Glucobiose

The disaccharides X, Y and Z produced by this procedure obviously contain linkages not recognised by Driselase or are substituted e.g. by acetate, ferulate or silanolate groups which prevent enzymic digestion.

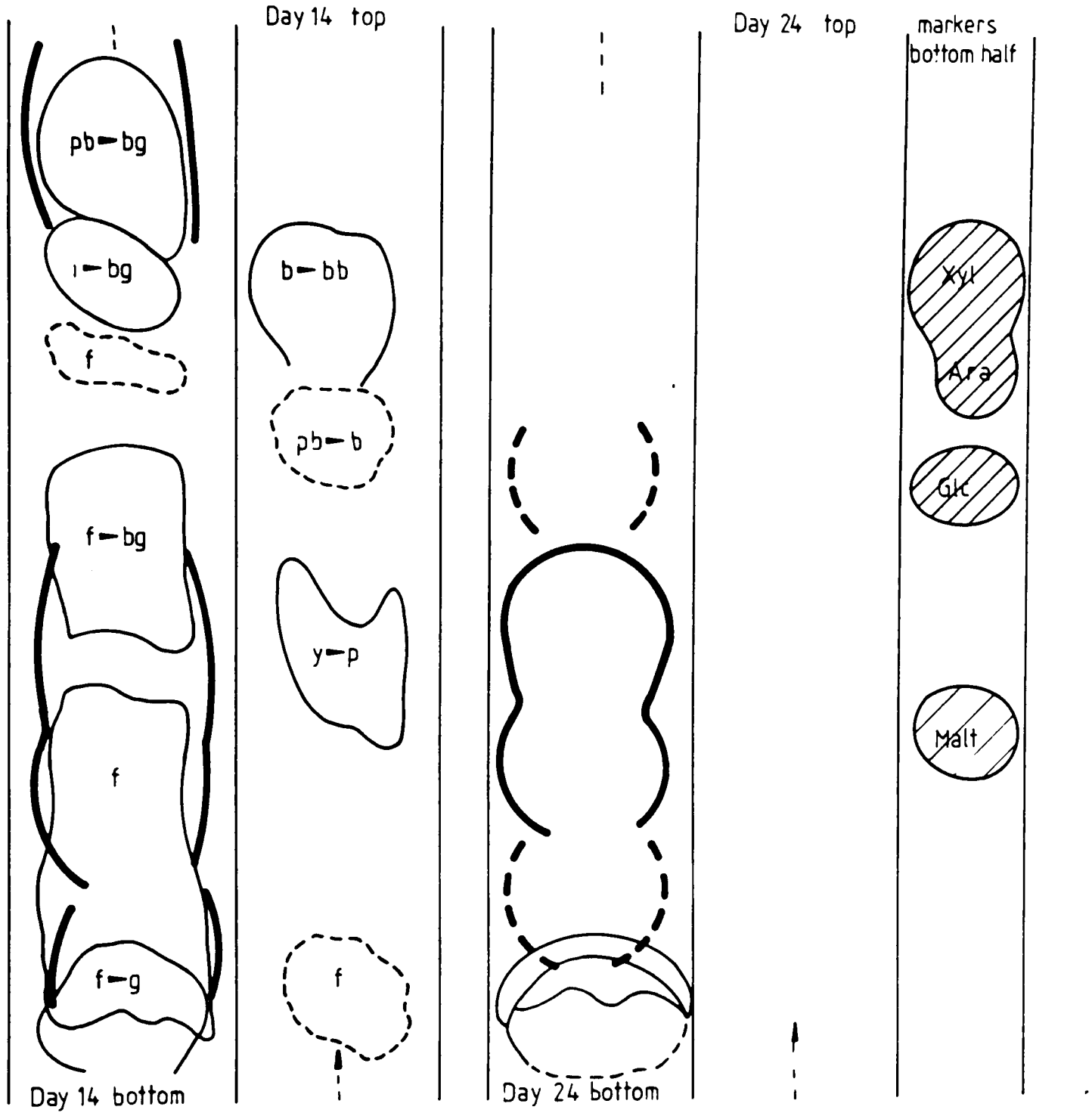

Figure 19

Second driselase digestion of oligosaccharide region produced by first driselase digestion. Samples were analysed by PC in BAW (12:3:5) for 16 hours.

^{3}H spots by spark chamber

uv fluorescent zones (f=faint, g=green, b=blue, i=invisible, p-=pale, b-=bright and y=yellow)

← =shift with ammonia

Samples were run for 14, 24 and 35 day samples. The general trends obtained for all three samples was similar to that observed for day 14 (drisel 1).

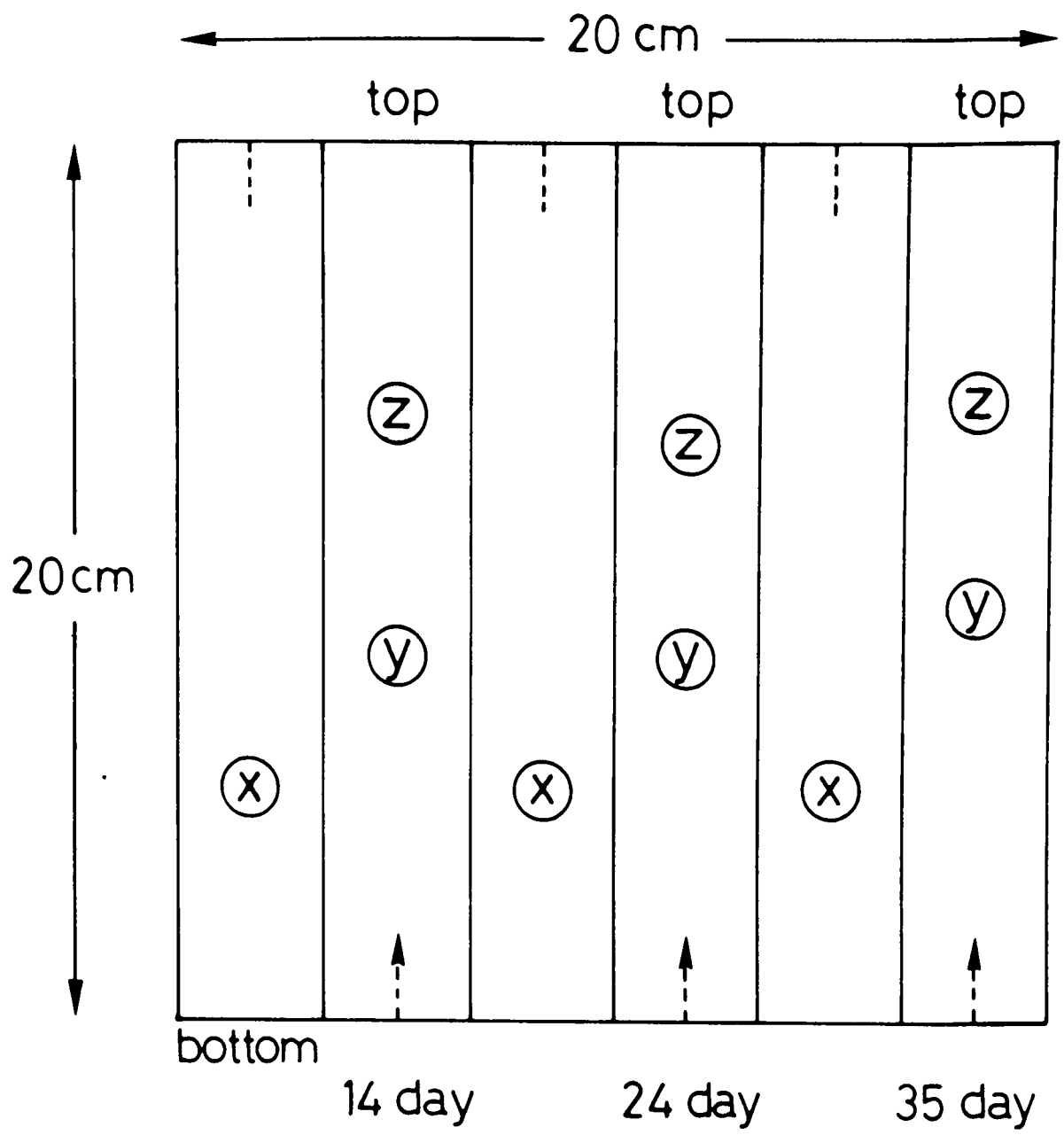

Figure 20

A diagrammatic representation of an autoradiograph produced by rechromatography of the main peak disaccharide from the second driselase digestion.

Samples were analysed by PC in EPW (10:4:3) for 32 hours.

X, Y and Z are three different disaccharides.

5.4 General Discussion and Conclusions

The results presented in this chapter have shown that there are distinct changes in polysaccharide composition as the cell wall matures. The proportions of the major components cellulose, starch, unidentified glucan and arabinoxylan change dramatically as mineralisation takes place within the cell wall. The presence of silica does not appear to greatly affect the results obtained for the various acid hydrolyses or amylase digestions performed but it may have an effect on the data obtained from the Driselase digestion. This procedure, in particular, shows that the samples of macrohairs studied are not simply an admixture of amorphous silica and polysaccharide but rather that there is an intimate association between the different phases present.

Studies on polysaccharide extracted from other silica containing plants such as rice (Maningat et al., 1982) have shown the same principal cell wall monosaccharides, namely, xylose, arabinose and glucose which the present study has found. Their cell wall preparations were often contaminated by silicon but no direct information on the role of the polysaccharide was reported. Other work on rice hull has shown that it contains 37% cellulose, 20% hemicellulose composed mainly of a xylan and silica. This is similar to the information obtained in this work (Section 5.3.1). Various hemicelluloses for these plants have been characterised including arabinoxylans and xyloglucans. The arabinoxylans consist of a backbone of $\beta(1\rightarrow4)$ linked D-xylosyl residues and side chains of a single L-arabinofuranosyl group attached to some of the backbone residues through an $\alpha(1\rightarrow3)$ linkage. The ratio of xylose:arabinose and hence the degree of substitution of the backbone varies from 11:1 for rice hull (Watanabe et al.,1983) to 13:10 for rice endosperm (Shibuya and

Misaki,1978). The xyloglucans found also vary in their structure (Watanabe et al.,1984). These results show that structural heterogeneity among polysaccharides may occur within an individual plant. Structural heterogeneity may arise because in each part of the plant the individual polysaccharides have (slightly) different functions to fulfil within the cell wall.

The Gramineae in general are known to contain "mixed linked" β(1→4, 1→3) linked glucans where the proportion of β(1→3) linked glucosyl residues varies from 30-50% (Nevins et al.,1978). It seems feasible that the unknown glucan from the macrohair samples studied could be a polymer of this type.

On the other hand, trichomes from other silicified plants eg. Urtica dioica (stinging nettle) and (cannabis), consisting of a mineralised phase and a polysaccharide phase, have been found by electron microscopical histochemical techniques to contain a β(1→3) linked glucan (callose), (Waterkeyn, 1982). Although there is little reported biochemical data on callose in the Gramineae, it is feasible that it may be a necessary polymer for silica deposition in specialised cells such as trichomes.

Previous workers have measured changes in polysaccharide composition of plants or parts of plants at different stages of maturity (Reid and Wilkie, 1969) and have shown that the ratio of cellulose:hemicellulose in leaves and stems of many grasses lies within the range of 0.8-1.6:1.0 from youth to maturity (Wilkie,1979). The most marked increase in hemicellulose content in grasses is observed in the growth period before change from a vegetative to a floral morphology occurs (Bailey and Connor,1972). All these studies utilised samples containing cell walls from different cell types and the results obtained, although indicative

of general trends in synthesis, cannot be directly applied to any one given cell type.

In the case of this present study, however, single cell samples only were investigated. The production of trichomes in this system is reproducible season by season and is genetically controlled (Moore,1984). The data obtained is therefore indicative of the changing wall composition for an individual cell type. We may draw certain conclusions for this cell type:-

(1) The total composition of the mature macrohairs is 30% hexose (including cellulose), 25% pentose, 0% uronic acids, a maximum of 4% protein and about 40% silica.

(2) During the early stages of secondary wall synthesis only cellulose and an arabinoxylan are synthesised. At later stages, starch and an unidentified glucan are also synthesised.

(3) Incorporation of exogenous sugars is maximal at day 14 when cellulose and arabinoxylans form the major part of material synthesised.

(4) The high ratio of arabinose:xylose (6:10) suggests the synthesis of a highly substituted arabinoxylan.

(5) Incorporation of sugars into starch is maximal at day 24, although this may be partly due to contaminating pollen. ?

(6) The non-cellulosic glucan synthesised during the later stages of wall development is likely to be either a mixed linked glucan or callose or a mixture of the two.

(7) There are no appreciable levels of xyloglucan within the developing cell wall.

(8) The cell walls are unusually Driselase resistant. This may be for one of several reasons which include a) the monosaccharide residues are

substituted by acetate, ferulate or silanolate groups, or b) the silica forms an impervious network which cannot be penetrated by the enzyme. (9) Feruloyl esters are present within the cell wall (not radioactively labelled) and may be possible cross-linking agents within the cell wall.

These general conclusions show that the cell wall associated with the silicified phase in these macrohairs is complex. The general compositional information is similar to that found for other grasses (Wilkie, 1979). The changes in the emphasis of synthesis of the various polysaccharides may be related to the different structural morphologies which are found at comparable time points during maturation of the trichome and this will be discussed further in chapter 7.

5.5 References

1. Bailey, R.W. & Connor, H.E. (1972) N.Z. J. Bot. 10, 533-544.

2. Bobbitt, J.M. (1956) Adv. Carb. Chem., 11, 1-41.

3. Bouveng, H.O. & Lindberg, B. (1965) Meth. Carb. Chem. 5, 147-150.

4. Dayanandan, P., Kaufman, P.B. & Franklin, C.I. (1983) Am. J. Bot. 70, 1079-1084.

5. Fry, S.C. (1982) Biochem. J., 203, 493-504.

6. Fry, S.C. (1983) Planta, 157, 111-123.

7. Hakomori, S. (1964) J. Biochem. (Tokyo) 55, 205-208.

8. Hodson, M.J., Sangster, A.G. & Parry, D.W. (1984) Proc. R. Soc. Lond. B 222, 413-425.

9. Lindberg, B. (1981) Chem. Soc. Rev. 10, 409-434.

10. Li, Y.T. & Li, S-C., (1976) Methods in Carb. Chem. 7, 221-225.

11. Maningat, C.C. & Juliano, B.O. (1982) Phytochem. 21, 2509-2516.

12. McNeil, M., Darville, A.G., Fry, S.C. & Albershiem, P. (1984) Ann. Rev. Biochem. 53, 625-663.

13 Moore, D. (1984) personal communication.

14. Nevins, D.J., Yamamoto, R. & Huber, D.J. (1978) Phytochem. 17, 1503-1505.

15. Preston, R.D. (1974) "The Physical Biology of the Plant Cell Wall",Chapman & Hall Publ.

16. Reid, J.S.G. & Wilkie, K.C.B. (1969) Phytochem, 8, 2059-2065.

17. Sandford, P.A., Hakomori, S. & Conrad, H.E. (1971) Biochem. 5, 1508-1517

18. Shibuya, N. & Misaki, A. (1978) Agric. Biol. Chem. 2267-2274.

19. Stinard, P.S. & Nevins, D.J. (1980) Phytochem., 19, 1467-1468.

20. Watanabe, T., Shida, M., Furuyama, Y., Tsukamoto, K., Nakajima, T. & Matsuda, K. (1983) Carb. Res. 123, 83-95.

21. Watanabe, T., Shida, M., Murayama, T., Furuyama, Y., Nakajima, T. & Matsuda, K. (1984) Carb. Res. 129, 229-242.

22. Waterkeyn, L., Bienfait, A. & Peeters, A. (1982) La Cellule, 73, 267-287.

23. Wilkie, K.C.B. (1979) Adv. in Carb. Chem. & Biochem. 36, 215-264.

Chapter 6: A Study on Mineralisation in the Teeth of the common limpet Patella vulgata L.

6.1 Introduction

In previous chapters, the mineralisation of silica in a plant system has been discussed in relation to both the inorganic and organic components present. The macrohairs contained only one mineral phase which showed structural variations. It was decided to investigate a silica from another biological system for comparative purposes.

The system chosen for study was mineralised teeth from the radula of the common limpet Patella vulgata. The mature teeth are known to contain both amorphous silica and iron oxide (goethite, αFeOOH) mineral deposits. The radula of the full grown limpet is approximately 7cm long and 2mm wide. It carries approximately 200 rows of transverse teeth. An electron micrograph of a section of a radula is shown in figure 1a. Each row consists of 13 teeth: a vestigal central tooth and on each side, first two single cusped lateral teeth, then a pleuricuspid marginal tooth and, on the outer edge, 3 small single cusped marginal teeth. The central tooth and the lateral teeth are the only teeth which are heavily mineralised. In general, only lateral teeth were studied. A diagrammatic representation of a lateral tooth is given in figure 1b. The various terms which are used to describe the different regions of the tooth are labelled.

Below is a brief account of work reported previously on the structure, composition and formation of the mineral phases in these teeth.

The mineral composition of the limpet radula has been shown to

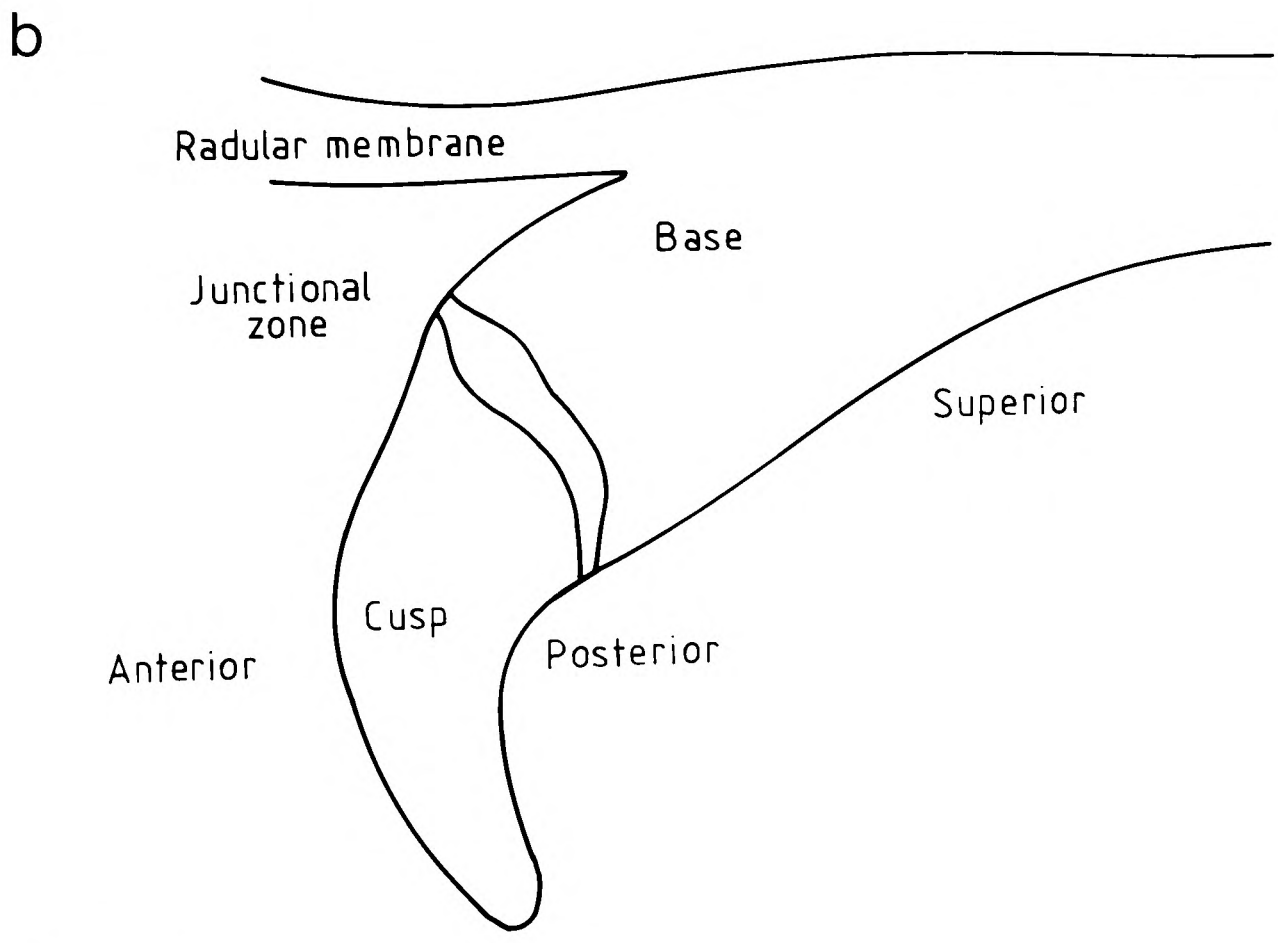

Figure 1

a) SEM of a mature section of a radula from the common limpet Patella vulgata L.. The central tooth[a], lateral teeth,[b] pleuricuspid marginal tooth[c] and the marginal teeth[d] are clearly labelled. The bar represents 250μm.

b) A diagrammatic representation of a longitudinal section through a lateral tooth from the limpet Patella vulgata showing relevant anatomical detail. The superior epithelium surrounds the tooth before emergence. The teeth have the same general form throughout development.

contain 12% ferric oxide and 10% silica by weight (Jones et al,1935). The teeth are fairly hard and scratch glass. The iron oxide is present in the form of goethite (αFeOOH) (Lowenstam et al.,1962) and the silica in the form of `opaline´ amorphous silica containing 9% removable water (Sollas,1907). Mineralisation is thought to commence at row 13 from the proximal end of the radula when iron is secreted into the radula by cells in the superior epithelium (Runham,1961) but the site of silicon secretion into the radula is unknown. A scanning electron microscopical and X-ray analytical study (Runham,1969) has shown that only iron, silicon and a small amount of sulphur could be detected in the radula. The teeth could be subdivided into a cusp, a junctional area where the cusp is joined to the base, and the base which is embedded in the radular membrane. As a result of analytical studies on mature teeth, the cusp could be subdivided into a posterior iron-rich area (44-57% Fe,1-6% Si) and an anterior silicon-rich area (22-30% Fe,27-32% Si). The percentages of the elements present are relative to the analysis of pure element standards in the electron microscope under identical conditions. The junctional zone consisted of a poorly mineralised layer at its border with the cusp and an iron rich layer where it joined the base. The upper part of the base (5% Fe, 16% Si) could be clearly differentiated from the silicon rich anterior and lower parts of the base (3-4% Fe, 28-35% Si). No minerals were detected in the membrane. The analytical procedures used showed that iron was present in the cusps at row 25 and the concentration increased to 28% at row 50 where there was an even distribution of iron throughout the cusp. Silicon was first detected at row 50 and it was after this stage that spatial differentiation of the two phases occurred. Mineralisation was complete by row 120, the teeth then being exposed in

the buccal cavity and available functionally. The SEM study showed that the teeth were covered with a thin "enamel-like" layer and the teeth cusps appeared to consist of fibres grouped into 1μm bundles. It was suggested that the fibres contained the silicon-rich phase and the intervening matrix the iron-rich phase. The orientation of the fibres within the teeth was thought to be related to the direction of movement of the tooth during feeding as it had been shown that the teeth exhibited well defined planes of wear (Runham et al.,1967).

The previous investigations utilising SEM and X-ray microprobe analysis at low voltage have given detailed information on the general pattern of distribution of the major elements within the radular teeth. However, no indication of the microscopic structural nature of the mineral phases has been obtained and no information relating to the spatial involvement of inorganic elements in mineralisation is available.

It is to these issues that the data presented in this chapter address themselves. It describes high resolution transmission electron microscopy, scanning electron microscopy, X-ray microprobe analysis, scanning proton microprobe analysis and solid state nuclear magnetic resonance experiments. Data is presented for the analytical biomineralisation studies and for structural studies on the amorphous silica phase. However, no structural information for the iron oxide phase is presented since this work was performed by Dr. S.Mann (currently at the Dept. of Chemistry, University of Bath).

6.2 Materials and Methods

6.2.1 Samples

Limpets (Patella vulgata L.) were collected from the Gower Peninsula and the radulae dissected on the same day as collection. Dissected radulae were stored in a solution of 90% methanol at 4 C. For electron microscopical and analytical studies the cellular material surrounding the radula was removed by treatment with a 1% solution of sodium hypochlorite for 30 minutes. Samples of teeth for analytical studies were dissected from intact radulae under a light microscope and the row number of the tooth noted. A sample in which only the silica remained `silica only´ sample was produced by treating teeth with concentrated hydrochloric acid until all the iron had been removed. The sample was centrifuged and washed 5 times with distilled water. The resulting material was freeze-dried to yield a white powder. This material was used for SEM and TEM microscopical studies and for solid state nmr experiments.

6.2.2 Electron microscopical studies

6.2.2a SEM of lateral teeth from the common limpet Patella vulgata L.

Radulae, individual teeth and teeth containing silicon only were studied by SEM. Radulae were treated by fixing and critically point drying prior to study to minimise shrinkage of the unmineralised regions of the specimen. Samples were fixed in 3% glutaraldehyde in a sodium cacodylate buffer for 2-3 hours and then rinsed with an identical buffer solution. The samples were dehydrated in acetone and critically point dried before coating and mounting. Intact radulae and intact teeth were mounted on

silver coated aluminium stubs, coated with gold (Nanotech sputterer) and studied using a Phillips PSEM 500 scanning electron microscope.

Individual teeth previously examined using the scanning proton microprobe were also imaged by SEM. The holders used for the scanning proton microprobe experiments were fixed to aluminium stubs using double sided sticky tape, coated with gold and studied in an identical fashion.

6.2.2.b Transmission Electron Microscopy (TEM) of lateral teeth from the radula of the common limpet Patella vulgata L.

Both untreated and acid treated samples of teeth were studied using a JEOL 100CX high resolution electron microscope. Samples were prepared for study by suspending a small quantity of the sample (sometimes crushed by a pestle and mortar) in distilled water, sonicating and placing a drop of the suspension on a formvar-coated copper grid, previously sputtered with a thin film of carbon to minimise beam damage in the electron microscope. They were left to dry on filter paper in the air at room temperature.

6.2.3 Energy Dispersive X-ray Analysis (EDAX) of lateral teeth from the common limpet Patella vulgata L.

A JEOL 100CX Temscan analytical electron microscope, fitted with a Kevex Li-drifted Si detector, operating at 100 Kev was used for analysis. Intact teeth and small fragments of treated and untreated teeth were analysed in the SEM mode. After disection, intact teeth of defined position along the radula were affixed to carbon blocks and analysed at an angle of 35-40° to the detector for 100s. Areas 2μm x 2μm were analysed at different positions for each tooth and the analysis area in

relation to the gross structure was noted. The fragmented samples were set at an angle of 40° to the detector and were analysed for 100s.

6.2.4 Scanning Proton Microprobe Analysis (SPM) of lateral teeth from the common limpet Patella vulgata L.

The Oxford scanning proton microprobe, fitted with a Kevex Li-drifted Si detector, operating at 4MeV was used for analysis. Teeth were disected at specific points along the radula, supported with double-sided adhesive tape on 1 m thick polypropylene film and scanned point by point by the proton beam focussed down to a spot size of less than 2μm x 2μm. X-rays were collected and two dimensional elemental maps constructed where the colour code represents the distribution of a single element within the sample.

6.2.5 Solid State ^{29}Silicon Nuclear Magnetic Resonance experiments on lateral teeth from the common limpet Patella vulgata L.

Silica produced by treatment of intact radulae with concentrated hydrochloric acid was studied by ^{29}Si nmr. The sample was mixed in a 1:3 ratio by weightwith finely powdered sucrose to provide sufficient volume of an homogenous sample to fill the rotor. Magic angle spinning (MAS) experiments were performed.

6.3 Results

6.3.1 SEM of teeth from the radula of the common limpet Patella vulgata L.

Intact teeth and the radula of the common limpet Patella vulgata have previously been studied using SEM (Runham,1969).

The overall morphology and structural composition of acid treated limpet teeth have been investigated by SEM. Representative analyses show that only silicon is detected, figure 2. Many tooth cusps remain intact after acid treatment, but figures 3 and 4 show a representative series of micrographs from large fragments produced by this treatment. All samples break at the base. This region is infilled with `blocks´ of silicified material. Beneath these `blocks´ the teeth appear solid and there are no channels further into the teeth, figure 3.5. The outer surface of the tooth remains smooth after acid extraction of the iron-containing mineral, figures 3.1 and 3.5. Samples with the outermost surface removed also show little structure, figure 4.6. Many teeth break at the tip to give evidence for a central empty channel, see later, figures 3.1, 3.3, 3.6 and 4.1. The anterior side of the tooth may be missing completely, figures 3.2 and 3.6 but the inner surface on the posterior side, although fairly smooth, analyses for silicon, figure 2.4. Material at the edges of the broken tips has directional character, the silica being precipitated in the line of the tooth, figures 3.1, 3.3, 4.2 and 4.3. However, bidirectional material is sometimes found towards the tip region, figures 4.1 and 4.2 and in the central region of the cusp, figure 4.4. In small fragments of the cusp, material incorporating large voids and with no general overall direction is observed, figure 4.5. In all structures where fibrils are observed they are generally observed clumped together,

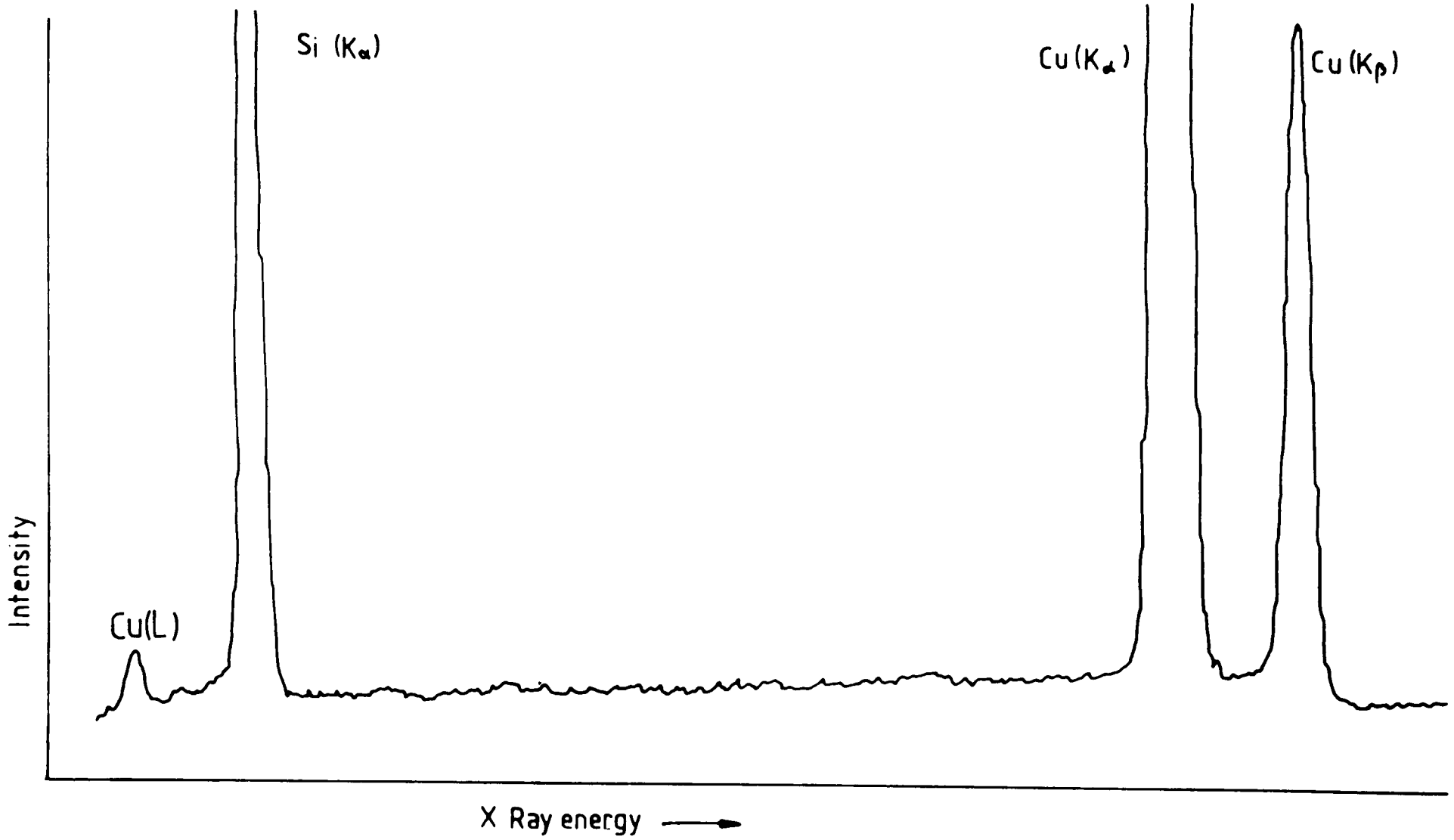

Figure 2

EDXA analysis of a 'silicon only' sample of teeth from the limpet Patella vulgata. Si is the only element detected. The Cu peaks arise from X-rays produced by the copper grid during analysis.

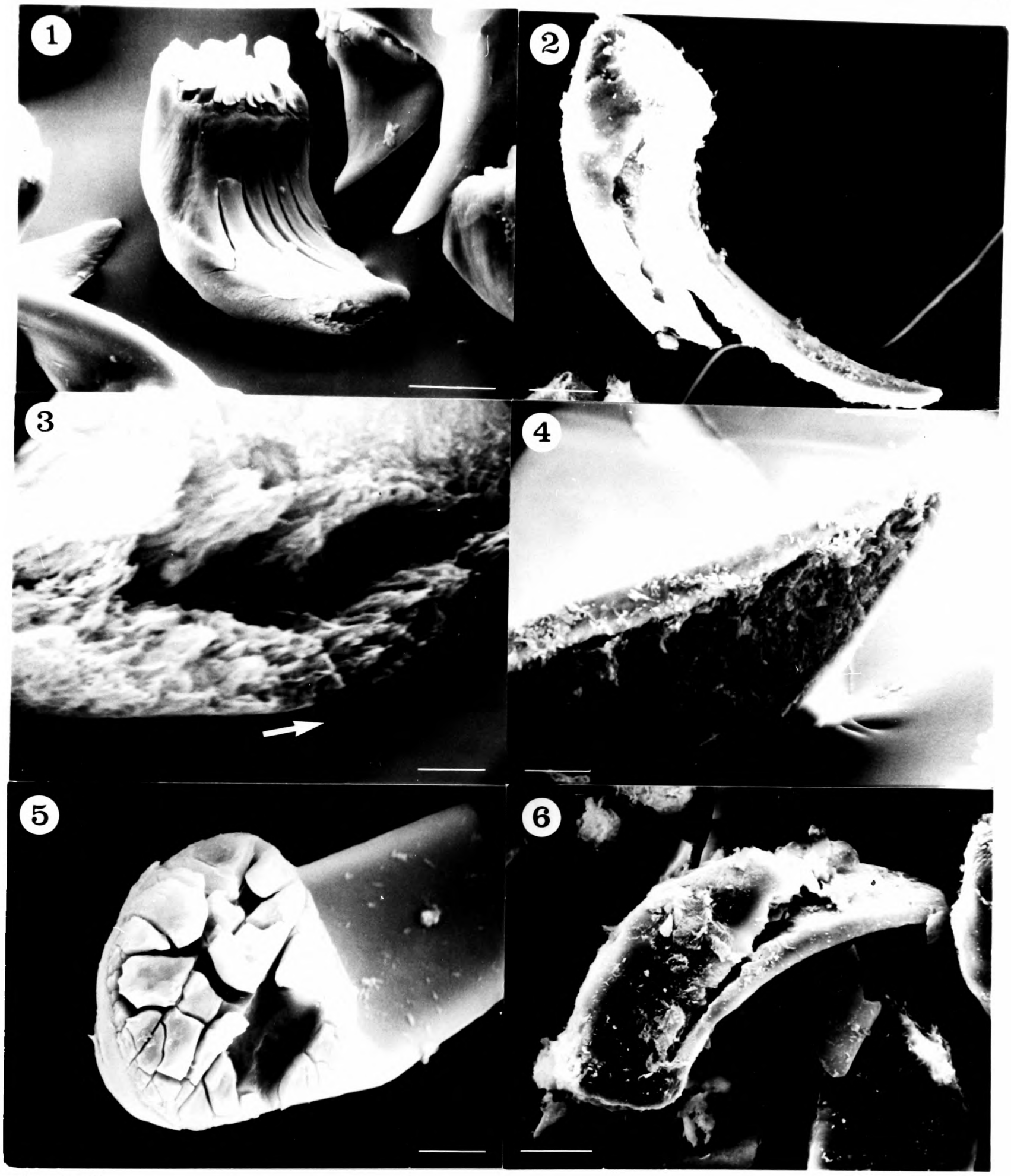

Figure 3

SEM of the 'silica only' sample of limpet teeth.

(1) this shows silicified blocks at the base of the cusp, a broken tip, gashes in the posterior surface of the tooth and an area empty of silica. Bar represents 50μm.
(2) the anterior surface has broken away leaving a central non-silicified area. Bar represents 50μm.
(3) a higher magnification image of (1) showing the central void and the directional character of the fibrous silicified material (arrowed). Bar represents 5μm.
(4) a higher magnification, tilted image of (2) to show the smooth surface and the structure of the silicified material underlying it. Bar represents 20μm.
(5) the small blocks at the basal region analyse for silicon and leave a solid inpenetrable surface when removed. Bar represents 20μm.
(6) another broken cusp showing a clear differentiation between the posterior and anterior regions of the cusp. Bar represents 40μm.

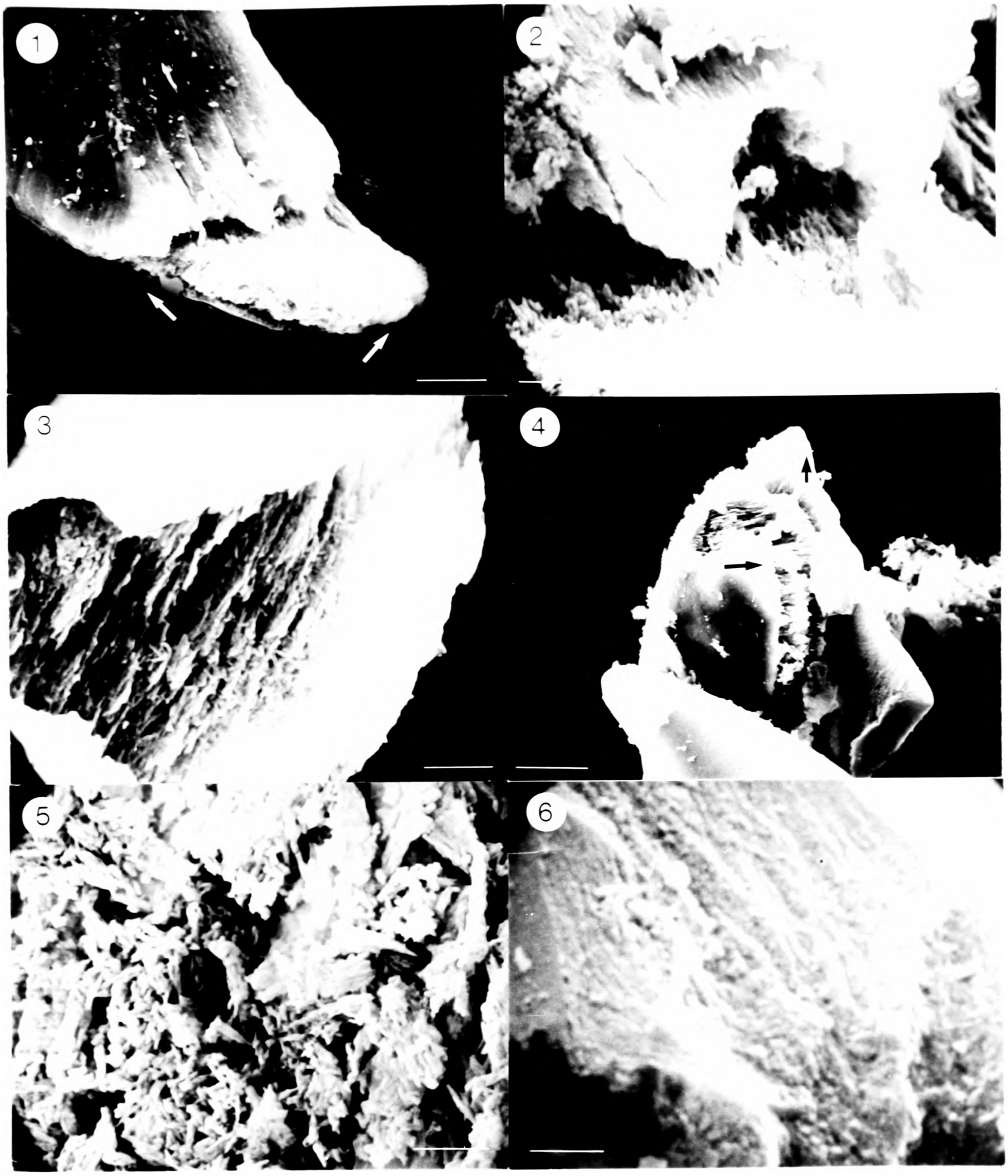

Figure 4

SEM of fragments from the 'silica only' sample of limpet teeth.
(1) a broken cusp showing gashes in the posterior surface, a central void region and fibrous material (arrowed). Bar represents 20µm.
(2) a higher magnification image of (1). Note the bidirectional nature of the silicified material. Bar represents 5µm.
(3) broken area of cusp showing smooth outer surfaces and fibrous material in the line of the cusp. Bar represents 5µm.
(4) a broken area of cusp showing fibrous silicified material running in two directions (arrowed). The inner surface of the outermost layer appears fairly smooth. Bar represents 5µm.
(5) a central region of a broken cusp showing small silicified fibrous elements. Note, there is no directional preference and there are large voids. Bar represents 5µm.
(6) a smooth area of silicified material immediately below the outer (organic) layer. There is very little structural detail and the material appears solid. Bar represents 1.5µm.

figures 4.3 and 4.5. More detailed structural information could not be gained using this technique.

6.3.2 Transmission electron microscopy of fragments from the teeth of the common limpet Patella vulgata

The structural components and microarchitecture of fragments of radular teeth from the common limpet Patella vulgata were investigated using TEM. Energy dispersive X-ray analysis was used to confirm the elemental composition of samples. Studies of fragmented intact teeth yielded areas of iron, mixed iron/silicon and iron/calcium/phosphorus/silicon. Few fragments containing silicon only were observed but they were inadequate for structural analysis. All structural data was obtained for the acid treated sample. A representative X-ray spectrum is shown in figure 2. Figures 5 and 6 show representative examples of the various silicified morphologies which typically are found within the system. All structures are built up from small 5-15nm diameter particles which are largely not affected by the electron beam (see effect of beam on silica extracted from grass macrohairs, chapter 3.3.1). No single crystal or powder diffraction patterns could be obtained for any of the samples studied in TEM and the different microstructural arrangements of particles can be classified as amorphous. The silica particles are often observed to be separated from one another as if on an organic matrix. However, three distinct silicified particulate morphologies were observed, namely globular, sheet-like and tube-like. Within these three categories there appeared to exist further subdivisions according to the amount of silicon present, the size of the particles comprising the structure and the overall directional character of these different structures.

The globular material has no directional character and the 30-50nm diameter particles are built up from small, 5-10nm particles, figures 5.1,6.2 and 6.3. The small `primary´ particles may also aggregate as in figure 5.2.

The sheet-like material divides into two categories, dependent upon whether the edges of the material are thickened or not, figures 5.1, 5.4 and 5.6 show examples of the former and figures 6.1, 6.2 and 6.4 examples of the latter type of sheet-like material. Sheet-like material with smooth thickened edges frequently shows fibrillar arrangements of the fundamental 15nm diameter particles which run parallel to the line of the thickened edges, figures 5.4 and 5.6. No structural information can be obtained from these smooth thickened edges. The pieces of sheet-like material without thickened edges vary in width between 80-180nm but are consistently built up from fundamental particles 10-15nm in diameter. The directional nature of the arrangements of fundamental particles is not as pronounced as in the sheet-like material with thickened edges but some directional preference is observed. Particles may be aligned with the major axis of the fragment or be aligned at an angle of 30° to the major axis, figures 6.1 and 6.4. Often, globular material is associated with this particulate arrangement, figure 6.2.

The tube-like material may also be categorised by the nature of the `tube´ edges. `Thin´ tubes 30-60nm wide have little silicon associated with them and have smooth outer edges, figures 5.3 and 5.5. Circles of material, as in figure 5.6 are probably tubular material viewed end on. Analysis shows that there is a small amount of silicon associated with them and they do not have thickened edges. They have an outer diameter of 240nm but no further structural information relating to these structures

could be obtained. Tubes with thickened edges vary greatly in size with an outer diameter of 50-300nm, with a corresponding variation in edge thickness of 12-100nm. For all these structures, the outer edge shows structure and is built up from 10-15nm diameter silica particles, figures 6.1 and 6.3. The ends of these tubes may be open or closed and the internal region (between the thickened edges) may also contain 10-15nm silica particles, see figures 6.1 and 6.3. No local microscopic directional character is observed for this particulate arrangement. An explanation of the tube-like material is that what we observe as thickened edges, which we define as the edges of the tubes may in fact be strengthening bands for a much larger tube-like structure as in figure 6.3, arrowed, where the majority of the tube is less densely silicified. The outer diameter of this tube is 300nm. It would seem likely that the circles of material as in figure 5.6 are similar structures viewed along their major axis.

6.3.3 Elemental distribution in Lateral limpet teeth using energy dispersive X-ray analysis

Elemental analysis was performed on lateral teeth disected from radulae which have previously been treated with 1% sodium hypochlorite to remove the radular membrane. The two samples studied were a) mature teeth, rows 100-120 and b) immature intact teeth from rows 25-30. Data is presented for analyses at different positions on the tooth for teeth samples taken from row 30 and row 100.

In the immature tooth, figure 7, iron can be detected in both the cusp and the base, although the highest concentrations are observed on the basal side of the junction zone. Chlorine is detected throughout the tooth but silicon, phosphorus and calcium are only detected in the base

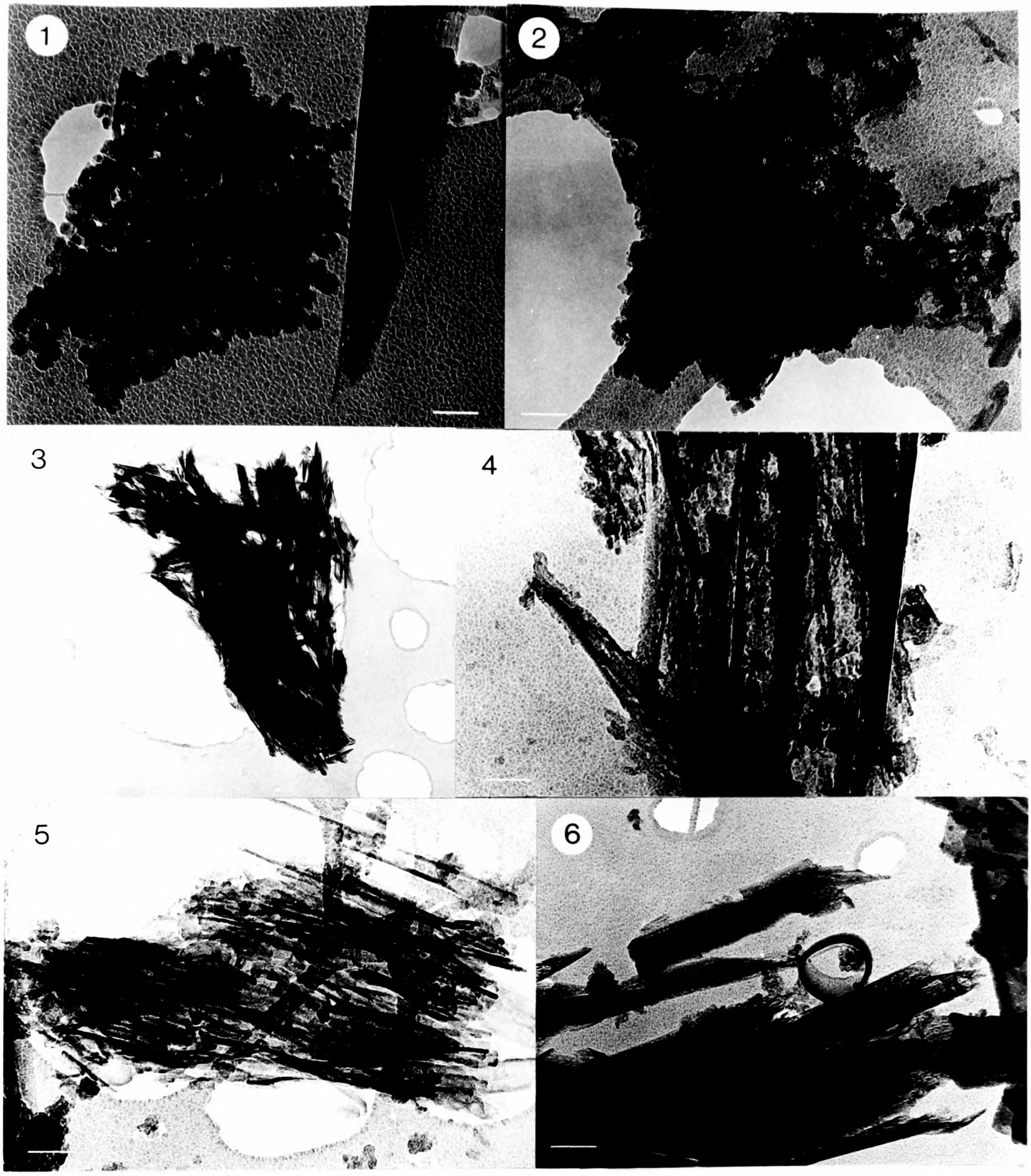

FIGURE 5
TEM of acid-treated silicified fragments of limpets teeth
1) Globular material and an edge of silicified sheet
   Bar represents 66nm.
2) Aggregates of very small silica particles.
   Bar represents 80nm.
3) Flat tube-like material. No thickened edges and not highly silicified.
   Bar represents 0.3um
4) Silicified material with parallel, non-thickened edges. Perhaps this may be considered as sheet-like material, the small silica particles showing marked directional preference (arrowed).
   Bar represents 76nm
5) Flat tubes with thickened edges which show no easily discernible ultrastructure. This material is not heavily silicified.
   Bar represents 80nm
6) Sheet-like material with distinct orientational preference for the silicified aggregates (arrowed). An example of a silicified tube viewed end on.
   Bar represents 166nm.

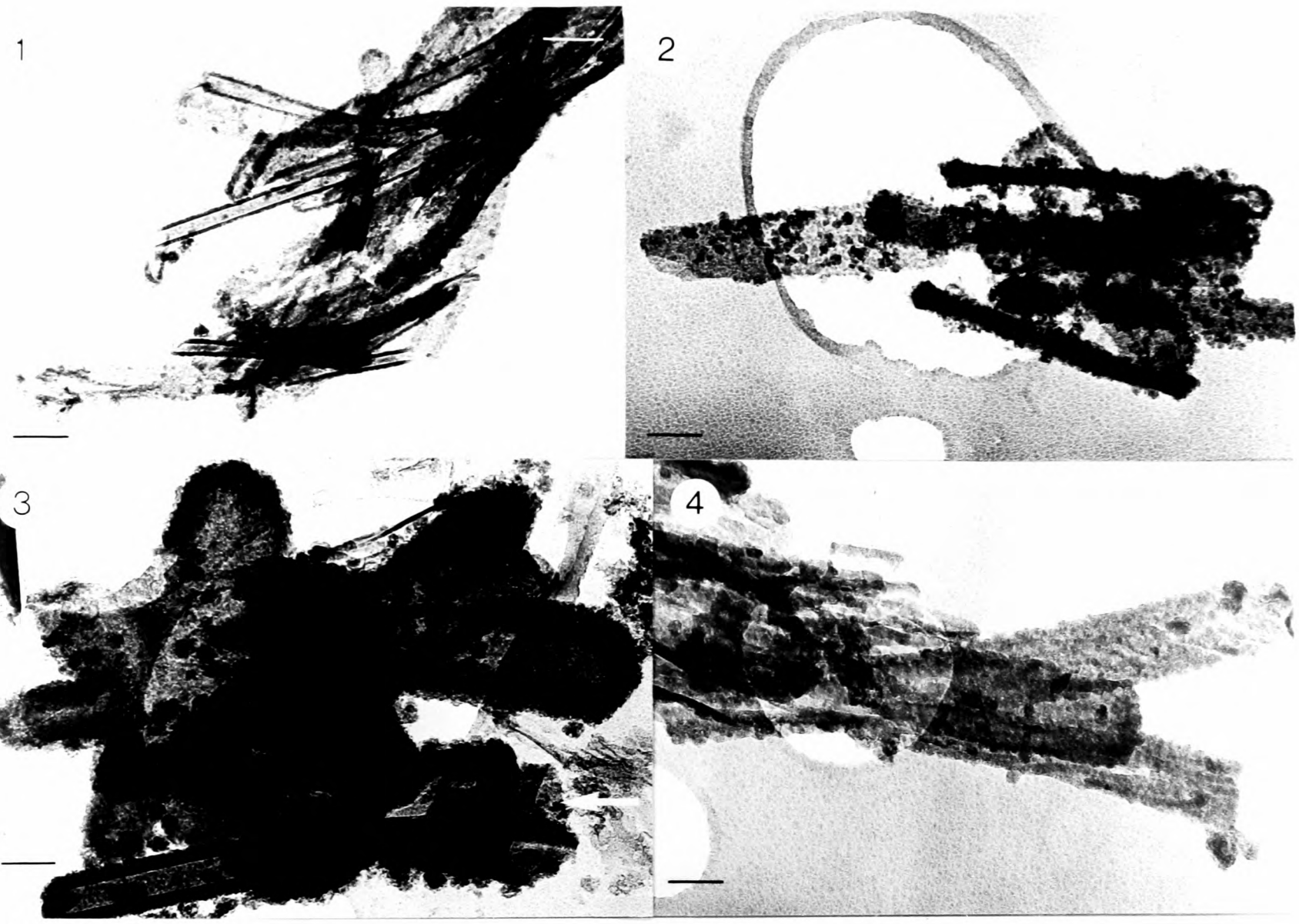

FIGURE 6
TEM of acid-treated silicified fragments of limpet teeth.
1) Tubular-like material with thickened edges showing structural detail. Flat sheets of material showing directional preference for the aggregates (arrowed) and globular material.
Bar represents 166nm.
2) Long straight sheets, some globular material and tube-like structures.
Bar represents 76nm.
3) Open tubes and tubes with enclosed ends. These both have thickened edges which show structural detail. The unthickened areas of the tube-like material are also silicified.
Bar represents 148nm.
4) Flat sheet-like material, note the two different directional preferences for the material (arrowed) and the close association of tube-like material with thickened edges which shows structural detail.
Bar represents 66nm.

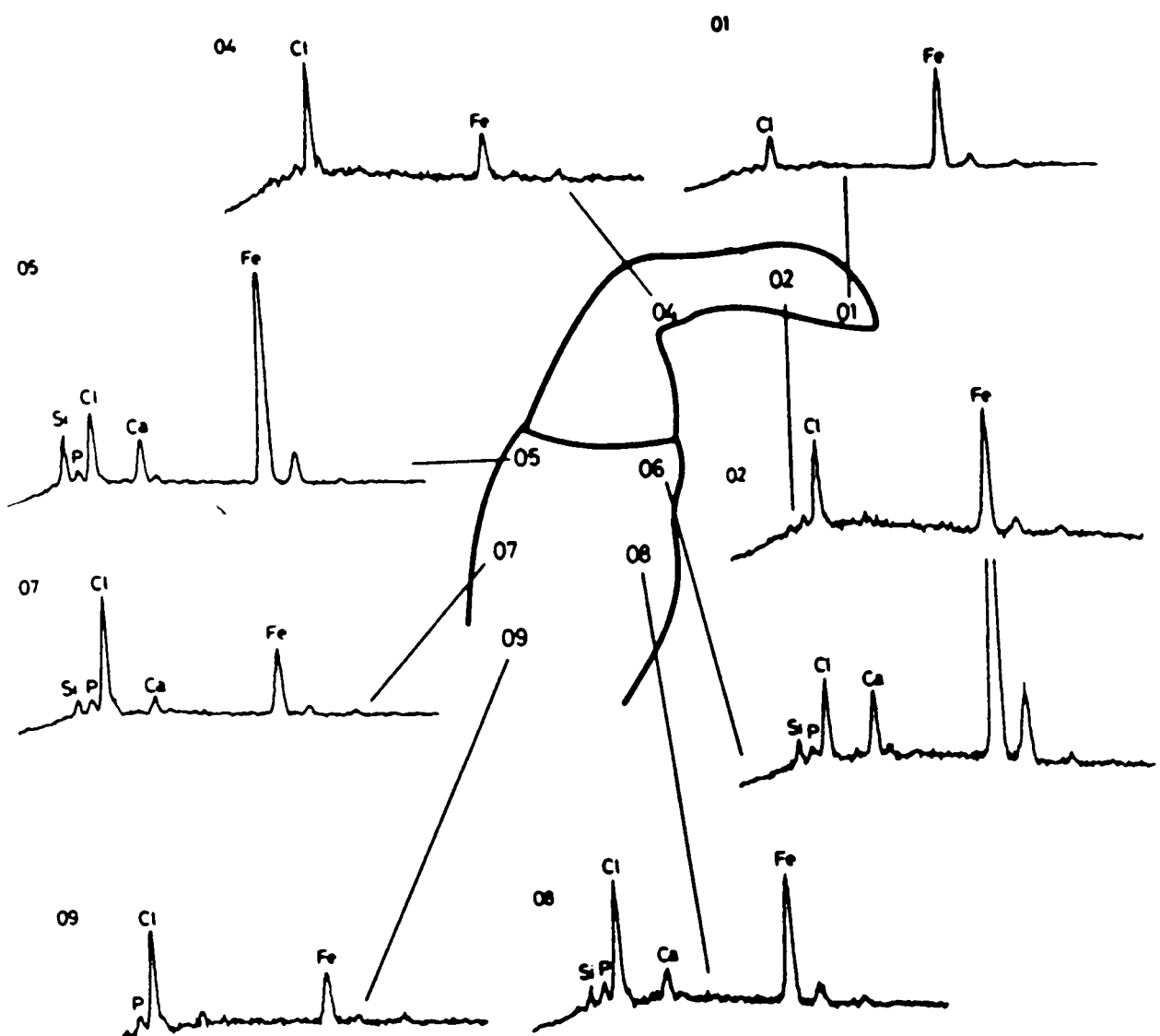

Figure 7

EDXA analyses performed at different positions as indicated for an immature limpet tooth from row 30 of the radula. No silicon or phosphorus could be detected. The chlorine is probably residual from the cleaning procedure. The chemical composition of the tooth changes dramatically at the junction zone.

of the tooth. Little or no sulphur is detected (cf. Runham,1969). Probably the chlorine peak largely arises as a result of the hypochlorite treatment. There may also be an extremely small amount of copper detected within the base but the levels are approaching those obtained from background analyses and must, therefore, be treated with caution. EDXA was not able to define whether the iron present within the cusp was in the posterior or anterior region and silicon and phosphorus could not be detected within the cusp.

In the mature teeth, figure 8, iron, silicon and trace amounts of copper are present within the cusp. Again, no sulphur is detected.The silicon is largely concentrated towards the base of the cusp but the iron content is high throughout the entire cusp. There is a distinct chemical boundary at the junction zone. Behind the junction zone phosphorus, chlorine and calcium are detected in addition to iron and reduced levels of silicon. No silicon, phosphorus and chlorine are detected on the anterior side of the base. It is possible that there is a small amount of chlorine present within the tooth, but again, the amount detected may arise from incomplete washing after hypochlorite treatment.

6.3.4 A developmental study on the mineralisation of lateral Limpet teeth using the Scanning proton microprobe

Elemental analysis was performed on lateral teeth disected from radulae, which had previously been treated with 1% sodium hypochlorite solution to remove the overlying radular membrane. Four samples of intact teeth were studied. The stages chosen were row 10, (early white immature tooth), row 28 (immature tooth with yellow base), row 35 (faintly yellow tooth) and row 120 (fully mineralised tooth). Data is presented

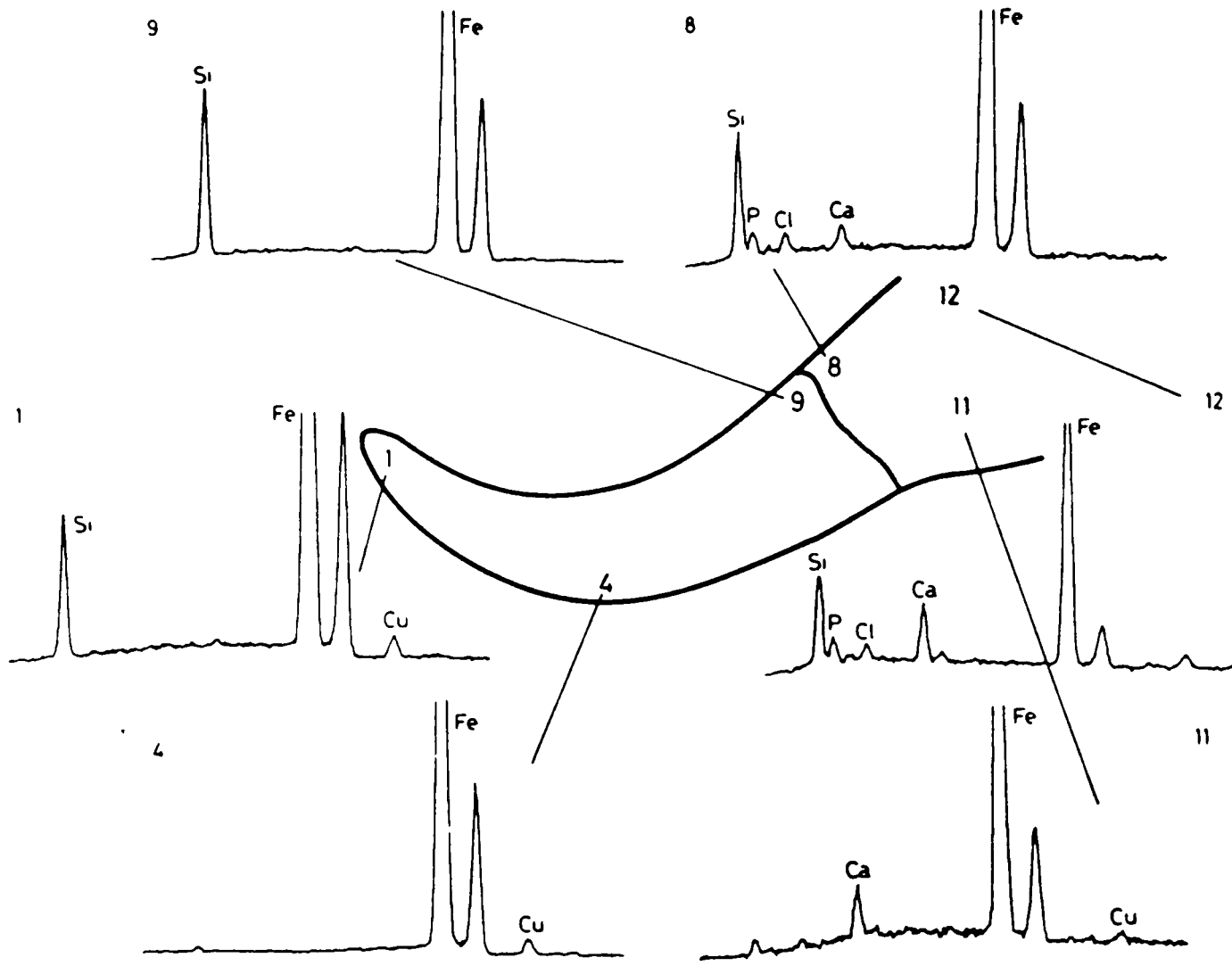

Figure 8

EDXA analyses performed at different positions as indicated for a mature limpet tooth taken from row = 100 of the limpet radula. The chemical composition of the tooth changes dramatically at the junction zone. A small amount of copper is observed in both the cusp and base of the tooth, but interpretation is difficult because of X-rays given off from the copper specimen holder.

pictorially for all stages. No quantitative data could be obtained because of absorption of the low energy Si(Kα), P(Kα) and Ca(Kα) X-rays by the iron matrix within the tooth during mineralisation from row 35 onwards. Electron micrographs are provided for teeth analysed from rows 28, 35 and 120, but a corresponding image could not be obtained from the sample analysed from row 10 as the flexible structure moved before fixation and the resultant electron micrograph bears little resemblance to the image obtained using the scanning proton microprobe. The chlorine map indicates the positions of the teeth.

Analysis of an early white immature tooth (row 10) showed the presence of low levels of iron, silicon, sulphur and chlorine throughout the tooth and radular membrane with higher levels of silicon located towards the tip of the cusp. Most of the sulphur was located in the radular membrane. The teeth were soft and there was little or no evidence of mineralisation, figure 9.

Mineralisation of the teeth was observed at about row 20 where a brown colouration was visible at the base. Analysis of a tooth from row 28 was undertaken, figure 10. A SEM micrograph showed the sample to be well formed in the base, but the poorly mineralised cusp was considerably distorted on drying, figure 11. The base contained iron, silicon, phosphorus, sulphur, calcium and, at a very low level, copper, figure 12. All the elements in the base were, to some degree, preferentially located just below the junctional zone. This differentiation was particularly marked for iron, phosphorus and calcium indicating that there is a distinct locality for the onset of iron mineralisation within the base. While silicon and sulphur were found equally distributed in both the cusp and the base, iron and calcium were much lower in the cusp. Superposition

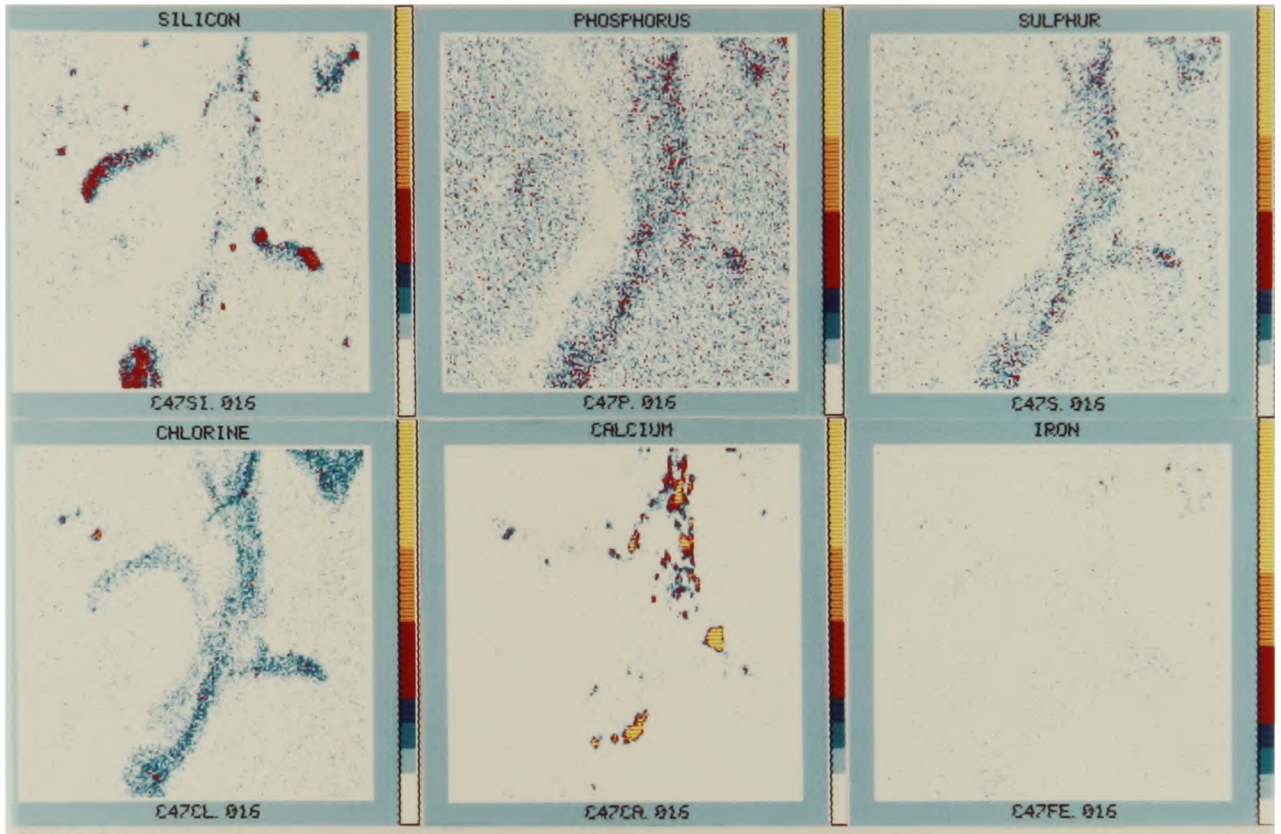

Figure 9

SPM elemental maps of an immature, unmineralised lateral tooth from row 10 of the limpet radula. A 4 MeV proton beam was used with a 250μm Be X-ray filter. Spatial resolution, less than 2μm x 2μm. Each picture represents a total area of800μm x 800μm. The colour code represents the distribution of a single element within the sample. Light blue is the lowest concentration. Increases in concentration are denoted by mid blue, dark blue, red, orange and yellow. The chlorine map gives an indication of the overall tooth shape as a SEM micrograph of the sample could not be obtained.

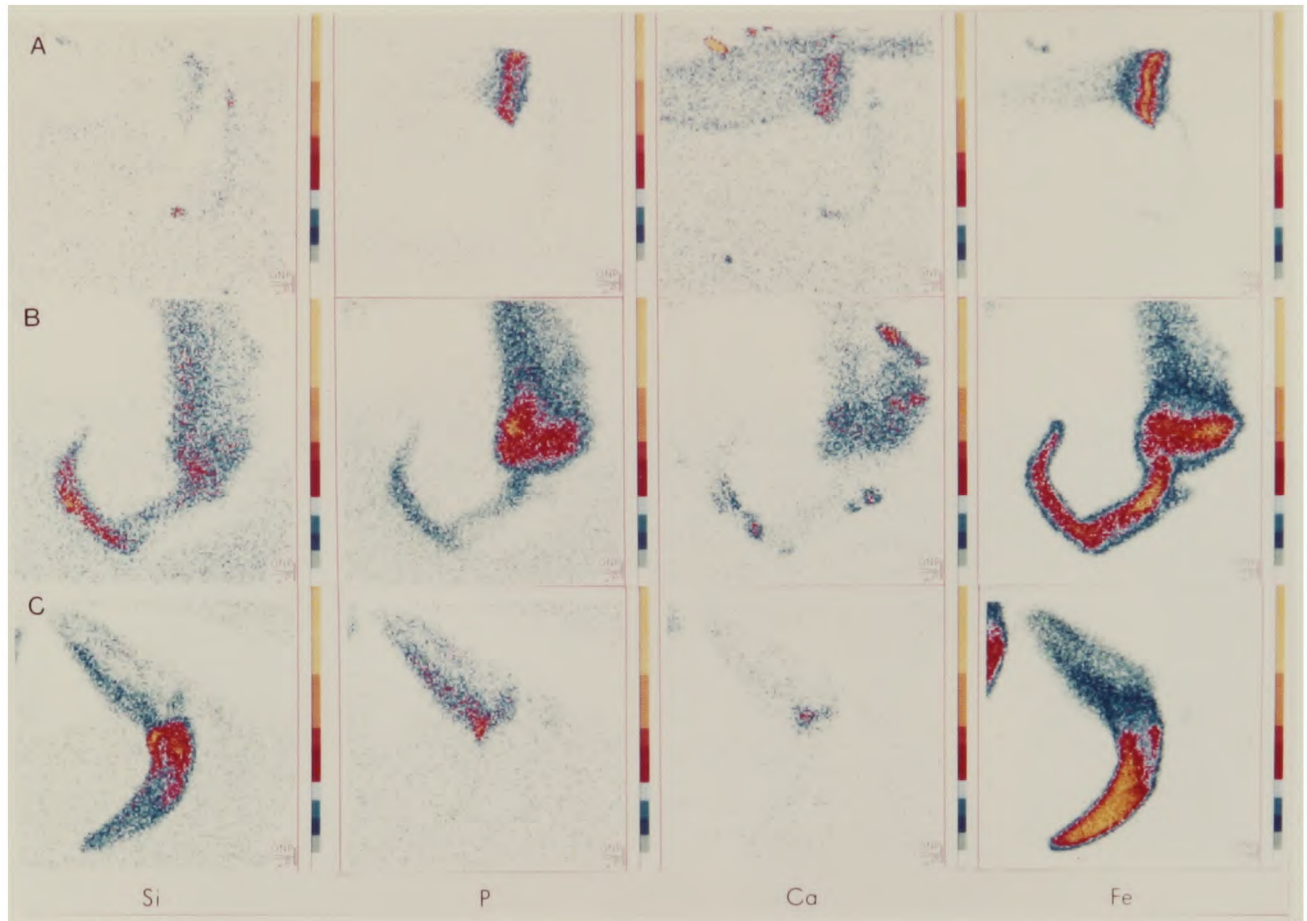

Figure 10

SPM elemental maps of lateral teeth at various stages of mineralisation along the limpet radula. A 4 MeV proton beam was used with a 250µm Be X-ray filter. Spatial resolution, less than 2µm x 2µm. The colour code represents the distribution of a single element within a sample. Light blue is lowest concentration. Increases in concentration are denoted by mid blue, dark blue, red, orange and yellow. Note that the same colour represents different elemental concentrations in different analyses but the colour coded sequence is always the same.

a) tooth from row 28. Each picture represents a total area of 220µm x 220µm.

b) tooth from row 35. Each picture represents a total area of 300µm x 300µm.

c) tooth from row 128. Each picture represents a total area of 500µm x 500µm.

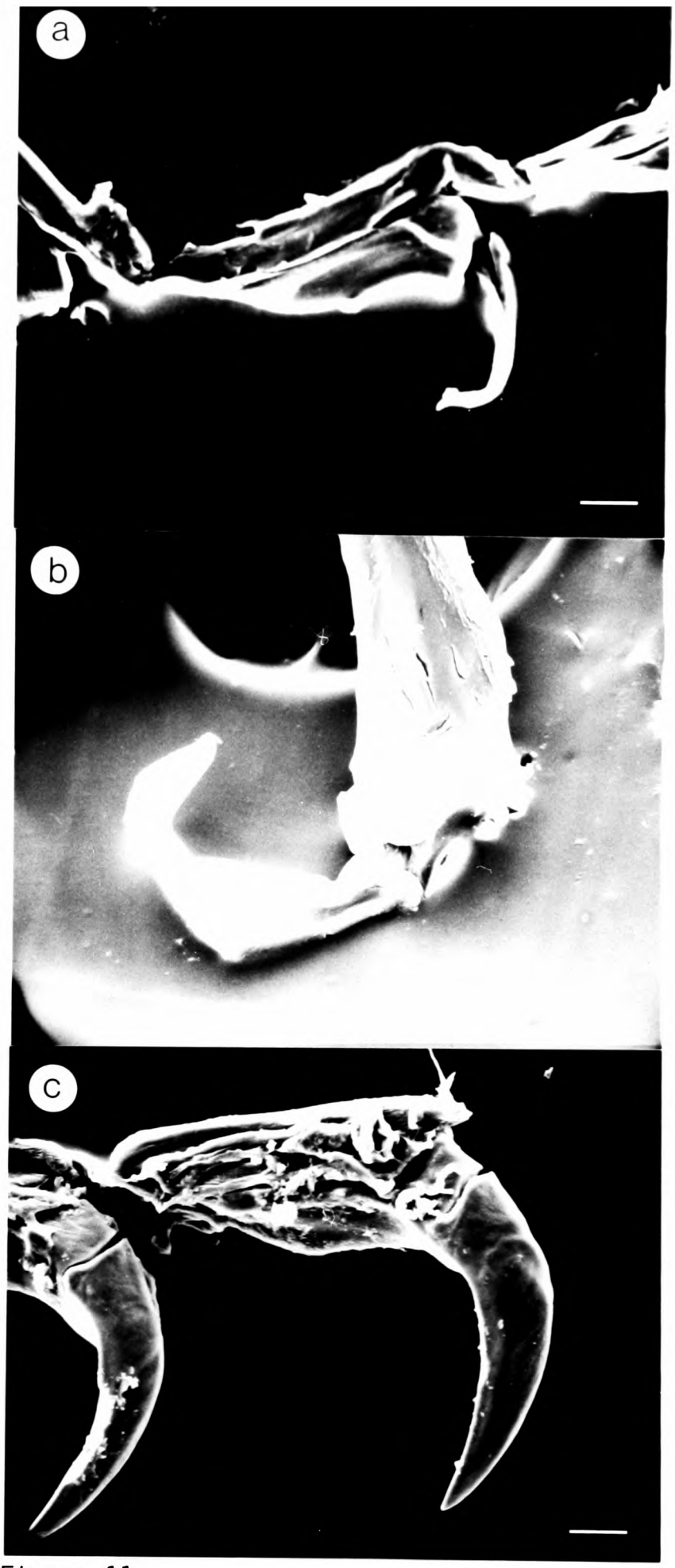

Figure 11

SEM micrographs of teeth from the radula of the common limpet Patella vulgata L. at different stages of mineralisation. After analysis by PIXE, samples were sputter-coated with gold and viewed in a Phillips PSEM 400 electron microscope.

(a) tooth from row 28, bar represents 50µm.

(b) tooth from row 35, bar represents 25µm.

(c) tooth from row 128, bar represents 50µm.

At the early stages of mineralisation the tooth cusp is considerably distorted on drying.

of the iron, calcium and silicon maps showed that there was differentiation of these elements within the cusp, with silicon and calcium concentrated towards the anterior side. There was little detectable phosphorus and copper in the cusp. Calcium and sulphur were both present in the radular membrane.

Substantial iron mineralisation of the cusp occurred between row 28 and row 35. Iron maps showed that the initial impregnation of the cusp occurred above the junctional zone and then extended with considerable development towards the tip of the cusp. The teeth were not yet rigid and the sample, figure 11 was again distorted on drying. A tooth at row 35 showed that high concentrations of iron were present in the base (localised below the junctional region, but with a significant concentration extending back towards the radular membrane) and throughout the cusp, figure 10. Silicon was present in the cusp and base, but was localised more at the anterior side of the cusp and the anatomically superior region of the base. Little silicon was present at the very tip of the cusp. Phosphorus and calcium continued to be localised where the iron concentration was high in the base but were also present in localised regions in the cusp. Sulphur, chlorine and copper (low levels see figure 12) were detected in the cusp and base with greater concentrations observed in the base.

Analysis of a mature mineralised tooth (row 120), which is now a rigid body, showed that iron concentrations were now greater in the cusp than base, figure 11. The posterior region of the cusp showed high levels of iron from the tip to the junctional region, whereas the anterior side had higher levels of silicon towards the tip of the cusp. There appeared to be no preferential localisation of iron in the base as in the earlier teeth. There was a gradation of iron concentration within the base with

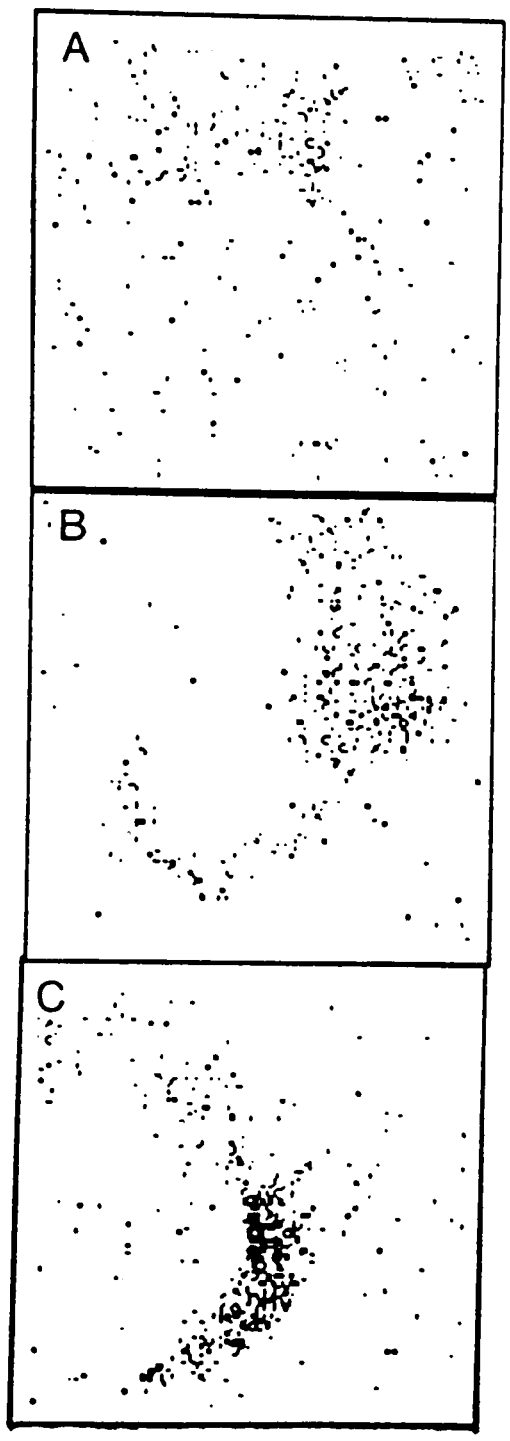

Figure 12

SPM Cu maps of lateral teeth at various stages of mineralisation along the limpet radula. Black represents the location of copper within each sample studied. No copper was observed in the sample taken from row 10 of the limpet radula.

(a) tooth from row 28

(b) tooth from row 35

(c) tooth from row 128

The pictures represent total areas as defined in figure 11.

levels higher at the superior side and decreasing further back to the base. Silicon was distributed preferentially in the anterior region of the cusp close to the junctional zone and its location could generally be mapped onto the regions of lowest iron concentration within the cusp. Thus there was less silicon at the posterior or anterior sides towards the tip of the cusp. Silicon levels in the base were much lower than in the cusp with a distinct boundary at the junctional zone. Levels in the base were highest towards the superior region. Calcium, phosphorus and sulphur remained localised in the base, with phosphorus being found towards the superior side and sulphur extending throughout the base. Very small traces of copper were found throughout the cusp and base with higher levels associated with the cusp, figure 12.

6.3.5 Solid state nuclear magnetic resonance of silica from limpet teeth

A sample of acid treated teeth was studied by magic angle spinning techniques. As insufficient material was available to pack the rotor, the sample was mixed with finely ground sucrose as previously described (6.2.5) and the resulting sample used to fill the rotor. A spectrum was easily obtained, figure 13. The spectrum shows the presence of $Si(\equiv OSi)_3(OH)$ and many $Si(\equiv OSi)_4$ groups. There were fewer silicon atoms with hydroxyl groups attached than for the plant sample of silica (chapter 3) but in all other respects the material was similar. A spectrum of untreated material was not obtained as the presence of iron in the Fe^{3+} state prevents analysis.

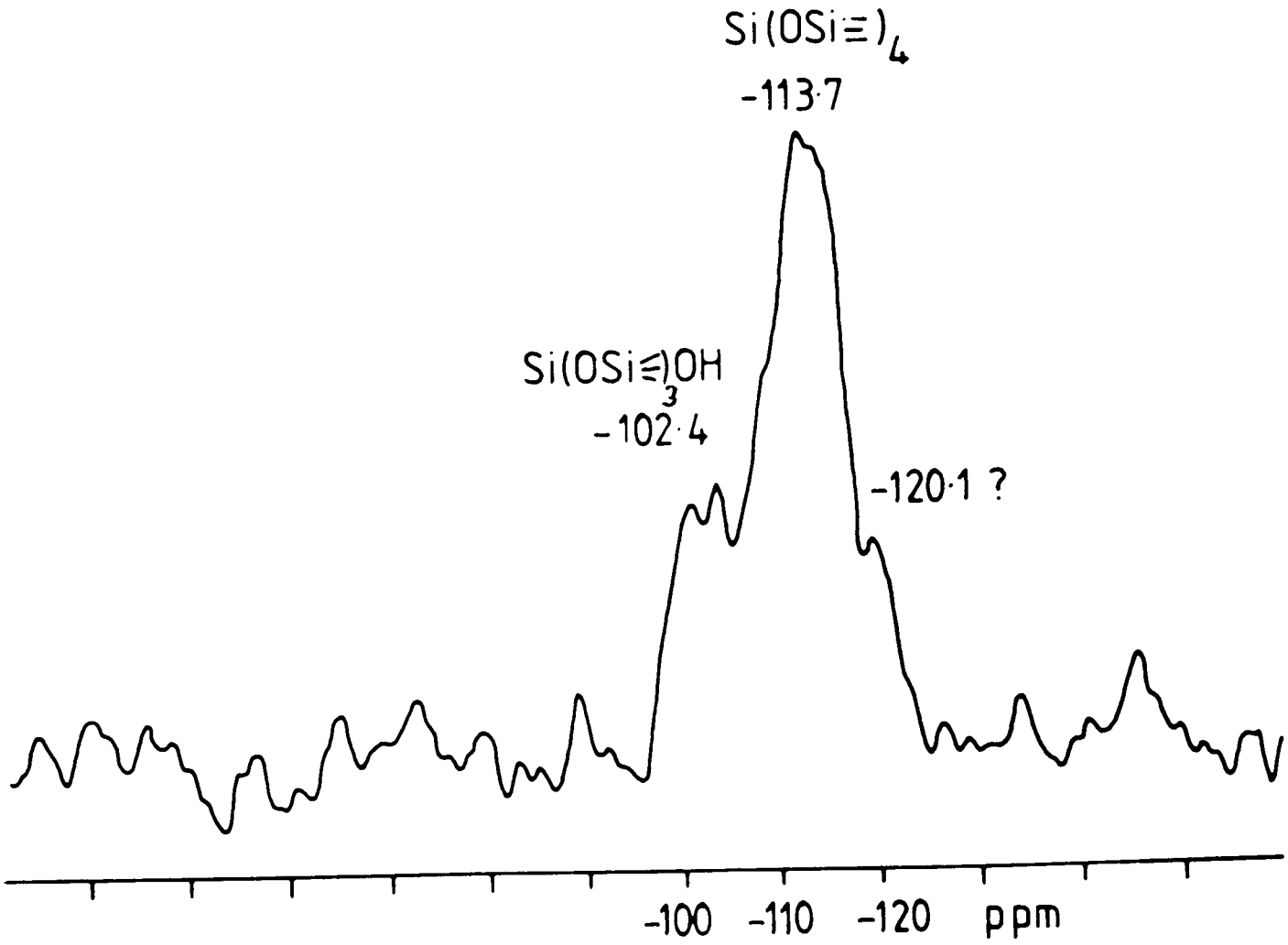

Figure 13

^{29}Si nmr of 'silica only' sample from limpet teeth. Peak assignments are as indicated.

6.4 Discussion

The mineralisation of the limpet radula is very complex and estimates of total mineral content give no indication of the complex distribution of the mineral phases within the teeth.

Following the pattern of chapters 3 and 4, a discussion of the chemical and structural nature of the silicified phase will be followed by a discussion of the analytical data obtained from the study of mineralising structures at the different stages of development.

The silicified phase is similar in nature to the silica found in plant macrohairs (see chapter 3). However, solid state ^{29}Si nmr has shown that there are fewer free hydroxyl groups within the silica and TEM studies have shown that the silica particles which form the ultrastructural morphologies are smaller than the particles found in macrohairs. The different ultrastructural arrangements observed are all formed from particles 5-15nm in diameter and for each structural type there is a large variation in the sizes of the structures ultimately formed. The globular particulate arrangement for the limpet teeth, as compared with that found in the plant macrohairs studied, is much smaller. The diameter of the particles is 30-50nm, as opposed to 40-120nm for the macrohairs. This difference in size suggests that silicification in limpet teeth may either occur more rapidly than in the macrohairs, or that the ionic environment associated with mineralisation is different. There may be a close interaction at the molecular level with the other phases present, but as yet there is little experimental evidence to support this.

The `silica only´ sample, when studied by SEM, contains many intact teeth, all areas of which analyse for silicon. If, however, radular teeth

are treated with aqueous hydrogen fluoride in order to remove the silica, no intact teeth remain and all that is observed is a fine powder of goethite crystals. It would appear, therefore, that the complete structure of the tooth is impregnated with silica, the iron merely acting as a filler which does not in any way determine the morphology of the tooth. On a microscopic scale, many hollow, silicified tubes of varying size were observed. Many of the goethite crystals were of similar dimensions (Mann, 1984) and it seems likely that these crystals are found within these hollow, silicified tubes. If we assume that the tubular, silicified structures are infilled with goethite crystals to form solid composite fibres, then the material of the tooth will be similar to many industrial composites where hard fibres are immersed in a softer matrix. This conclusion is contrary to that proposed by Runham (1969), who proposed that the fibres contained silicon and the matrix between the fibres iron. It may also be reasonable that some of the iron mineral is found between the tubes, but data presented here suggests the involvement of silicified, `tube-like´ structures with the mineralised tissues of this system.

The tubes appear to run along the axis of the tooth, except towards the tip, where the structures are bidirectional, figure 4.1 and figure 14 for a diagrammatic representation, and in the centre of the tooth where there are disordered regions of silicified material. The bidirectional nature of the material towards the tip appears to be related to the method of use of the teeth during feeding. In use, the tooth is dragged over or through a substrate, the hard posterior region of the tooth forming the leading edge. The plane of wear on the tooth is at 70° to the tooth axis, figure 14. The composite fibres in the hard posterior region

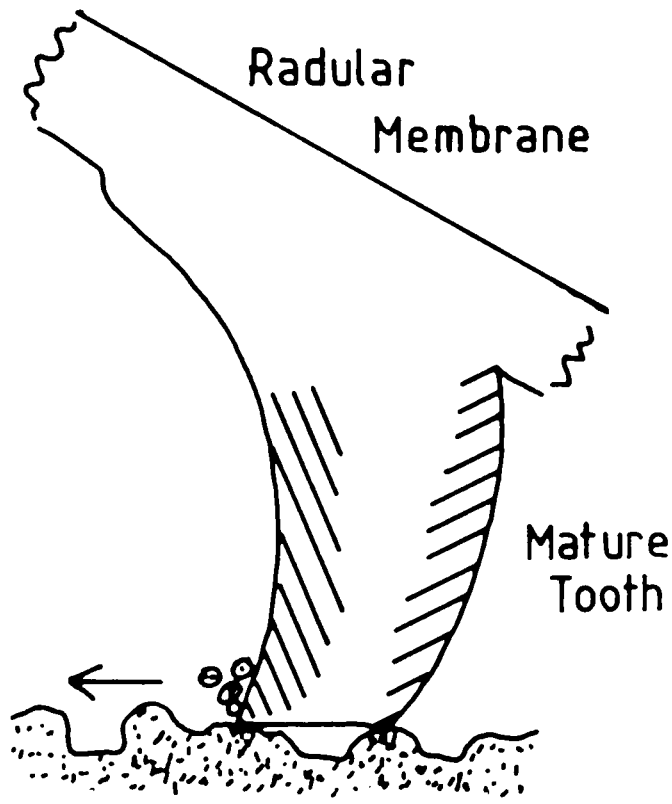

Figure 14

A diagram of the suggested mode of use during feeding of the radular teeth. The orientations of the fibres in the anterior and posterior regions of the cusp is indicated by the direction of hatching, and the direction of movement of the tooth during rasping is indicated by the arrow.

of the tooth cusp are normal to the plane of wear, while the composite fibres in the softer anterior region run parallel to it. This arrangement of composite fibres in the hard area gives rise to maximum strength (Lancaster, 1968) but, if cleavage does occur then a portion parallel to the axis of the tooth will be removed. This would result in structures such as figure 4.1. The composite fibres in the softer anterior region are approximately normal to the hard layer, which partly explains why there is a region of disordered material in the centre of the tooth where the changeover in orientation of the composite fibres occurs. This central area appears to have a large gap in it which does not contain silicified material. This will weaken the `silica only' sample, which may be the reason for finding fragments of teeth with the anterior side missing (figures 3.2 and 3.6).

No information on the spatial location of any other ultrastructural silica deposits within the teeth could be obtained.

Analytical studies on the biomineralisation processes occurring in the radular limpet teeth have shown that there are complex temporal and spatial variations in the inorganic composition in all regions of the teeth.

Data obtained by EDXA was similar to that of Runham (1969), except that sulphur was not detected at either the early or mature stages of development. A possible reason for this is that his samples were embedded in araldite which itself contains sulphur. We also did not observe such a large variation in structural composition for the posterior and anterior regions of the teeth cusps. Our data shows, in addition, that the junction zone between the cusp and the base has a complex chemical composition which may be significant to the mineralisation process. The technique was not able to determine, for the immature sample, a) whether

iron was first mineralised on the posterior or anterior side of the tooth cusp, b) whether other elements were involved with mineralisation at this stage, c) whether other trace elements were present, including their spatial location and d) the precise chemical compositional nature of the junction zone. For the mature sample it was not possible to determine a) the level of involvement of trace elements in the mineralised structures and b) the precise spatial characteristics of the mineralised deposits.

The utilisation of proton induced X-ray emission coupled to the scanning proton microprobe has provided answers to some of these problems.

The elemental maps presented in this work reveal the complex compositional changes that occur during the biomineralisation of limpet teeth. Previous studies have shown that iron was secreted into the teeth by cells in the superior epithelium from the thirteenth row of the radula (Runham, 1961), but it was thought that silicon was first present within the teeth at row 50 (Runham, 1969). The higher sensitivity available with the proton microprobe, compared with the electron microprobe, has shown the presence of both iron and silicon at earlier stages (row 10) in the development of the teeth, the pattern of involvement of these elements in development and the presence of several other elements in the tooth at all stages of development.

The presence of silicon in these early stages of radular development may indicate that silicon is a structural component of the preformed organic matrix. The function of the silicon presumably would be similar to the stabilizing role proposed for the maintenance of structural integrity in connective tissue such as collagen (Carlisle,1978). At this stage, it is likely that the only structural morphology which would

analyse for silicon in the electron microscope would be the thin outer edges of tube-like material such as is seen in figures 5.3, 5.5 and 5.6.

What follows is a possible explanation for the pattern of mineralisation which subsequently occurs within the radular teeth.

Iron mineralisation appears to involve both the cells of the superior epithelium and the junctional zone between the cusp and the base of the tooth. It is known that iron is secreted into the teeth by these cells, but the chemical nature of the iron is not known. At the early stages of mineralisation (row 28), however, the majority of detectable iron (SPM) is highly localised below the junctional zone in the presence of calcium and phosphorus. A plausible explanation of these facts involves soluble iron being transported through the tooth cusp via the tube-like structures, which are later more heavily silicified (Runham, 1984), to the junctional area where chemical transformation takes place, the resulting goethite crystals being pushed back into the tooth cusp. Previous workers (Runham, 1961) have shown that the junctional area between the cusp and the base exhibits different chemical properties from the surrounding tissue. Our results suggest that the induction of mineral formation may be chemically controlled within this region.

Iron mineralisation next occurs within the cusp, beginning above the junctional zone and extending towards the tip, whilst the base continues to be further impregnated. Thin sections of the unmineralised tooth (Luke, 1984) show the teeth to be well developed in both the cusp and base suggesting that the initiation of mineralisation in the cusp may correspond to changes in the surrounding cellular activity or to chemical modifications within the cusp environment.

There is no data relating to the mode of entry of silicon into the tooth, but mineralisation, as compared with iron, appears to be initiated in both the base and cusp of the lateral teeth and is not generally localised until relatively late in tooth development when the concentration in the cusp increases over that in the base and becomes greater in regions of the cusp close to the junctional region. Runham et al.(1969) have shown a distinct spatial differentiation of iron and silicon components in the mature lateral tooth. Our results show that, in the poorly mineralised cusps (row 28 and row 35), the two major mineralising phases, iron and silicon, are spatially differentiated but that at maturity (row 128) iron and silicon are found throughout the cusp. There are differences in the relative concentrations of the two elements, but we see no evidence (SPM or SEM) for the clear delineation of an iron rich posterior surface and a silicon rich anterior zone which Runham indicated (1969). Furthermore, the spatial distribution of the major minerals in the tooth base in our sample does not coincide with that of Runham. In the base, the highest concentrations of both iron and silicon are found on the superior side whereas Runham proposed that more silica was to be found on the anterior surface of the basal region, see figure 15.

However, the presence of other elements in the cusp and base (phosphorus, calcium, sulphur and copper) may be of significance in the regulation of mineralisation. Sulphur does not appear to be localised at any stage of development and therefore may be associated with organic components of the teeth. Both phosphorus and calcium are highly localised in the base with iron, in the early stages of mineralisation. The presence of copper in the base (immature teeth) and cusp (mature teeth)

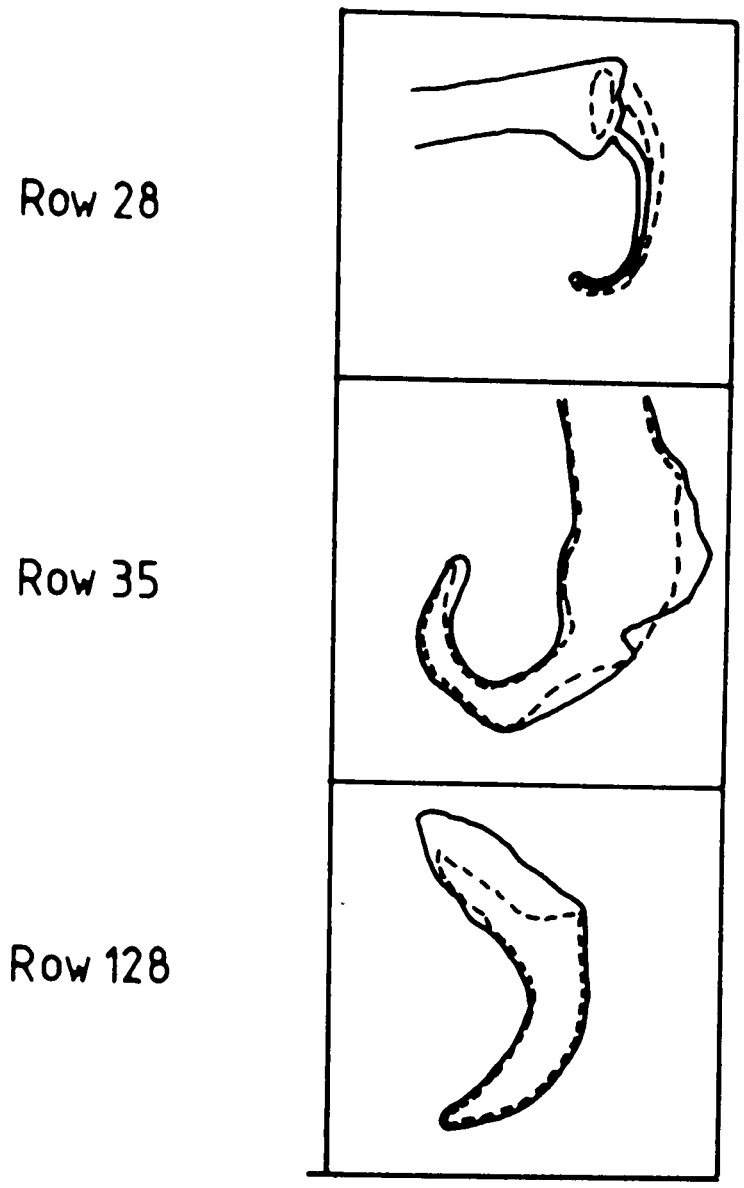

——— Iron boundary

------ Silicon boundary

Figure 15

A comparison of the spatial location of silicon and iron within lateral limpet teeth at different stages of development. The total area for each picture is as is given for the SPM analyses, figure 11.

may be related to an enzyme required for oxidation of the organic matter within the teeth, figure 12. It appears reasonable that mineralisation should be virtually complete before the enzyme becomes operative in the tooth cusp as this allows the crystalline goethite and amorphous silica to be deposited as a fairly flexible structure, which is only finally hardened when deposition is complete.

6.5 References

1. Carlisle, E.H. (1978) in Biochemistry of Silicon and Related Problems, ed. Bendz, G. & Lindqvist, I., Plenum Publ. pp.231-253.

2. Jones, E.I., McCance, R.A. & Shackleton, L.R.B. (1935) J. Exp. Biol. 12, 59-64

3. Lancaster, J.K. (1968) Brit. J. Appl. Phys. Ser. II, 1, 549-559.

4. Lowenstam, H.A. (1962) Science, 137, 279-280.

5. Luke, B. (1984) unpublished results.

6. Mann, S. (1984) personal communication.

7. Runham, N.W. (1961) Quart. J. Micros. Sci. 102, 371-380.

8. Runham, N.W., Thornton, P.R., Shaw, A.A. & Wayte, R.C. (1969) Z. Zellforsch., 99, 608-626.

9. Runham, N.W. & Thornton, P.R. (1967) J. Zool. (Lond) 153, 445-452.

10. Runham, N.W., (1984) personal communication.

11. Sollas, I.B.J. (1907) Quart. J. Microsc. Sci. 51, 115-136.

Chapter 7: General discussion and conclusions

In the previous chapters of this thesis, biomineralised structures have been discussed primarily in terms of structural morphology. In order to appreciate and attempt to understand the variations and control over the ultrastructures associated biochemical processes have been investigated. These include the spatial and temporal involvement of inorganic ions with the mineralisation process, and for the plant system, the changing chemical nature of the associated organic matrix. Some chemical compositional data for the organic matrix of the limpet teeth from Patella vulgata L. is already available (Runham, 1961). I will largely concentrate my discussions on the silicified material from the macrohairs of the grass Phalaris canariensis L.

In this chapter, the formation of fundamental silica particles will be considered initially and the effects of organic polymers and inorganic ions on formation will then be discussed. A discussion of the surface characteristics of the silica particles and the effect these have on aggregation follows. Aggregation of silica particles to give recognisable structural entities will then be considered in relation to both solution effects (the presence of inorganic ions and organic polymers in solution) and surface effects. The conditions necessary for the structural morphologies adopted in the system will be tentatively postulated. Finally, a comparison of the histochemical and spatial and temporal involvement of inorganic ions with mineralisation of the limpet radula will be discussed.

At the onset, it must be stated that nothing is known about the mode of entry of silicon into the system, or of its transport prior to mineralisation. The initial trigger for deposition appears to be related

to the emergence of the inflorescence, and hence to transpiration. However, it is interesting to note that all macrohairs on an individual caryopsis, are not simultaneously mineralised. The time point at which mineralisation commences appears to be related to the maturity of the cell wall in which deposition eventually occurs. The process of cell wall development is then interrelated with the deposition of silica. At emergence, the rate of wall synthesis is low (^{14}C studies). Once the primary cell wall has been completed, generally at emergence, secondary wall synthesis and mineralisation occur synchronously. It is apparent that there may be a close relationship between these two events, namely the commencement of secondary wall synthesis and silica deposition. It may be entirely coincidental that this point in the development of the cell wall coincides with the emergence of the inflorescence.

The formation of the primary silica particles involves polymerisation of silicic acid from solution. When the solubility product is exceeded at a concentration of 100-200ppm, spontaneous polymerisation by condensation occurs to form dimeric and higher molecular weight species of silicic acid. It is thought that the condensation polymerisation involves an ionic mechanism (Iler,1979). Above pH 2, the rate of polymerisation is proportional to the concentration of hydroxyl ions and is second order with respect to the disappearance of monomer. Below pH 2 the rate of polymerisation is proportional to the concentration of hydrogen ions and is third order with respect to the disappearance of monomer. Figure 1 shows the rate limiting steps for the two mechanisms of condensation. Polymerisation occurs maximising Si-O-Si bonds and minimising Si-OH groups. This leads to the formation of ring structures and internal condensation to the most compact state leaves Si-OH groups on the surface. These spherical units form nuclei which

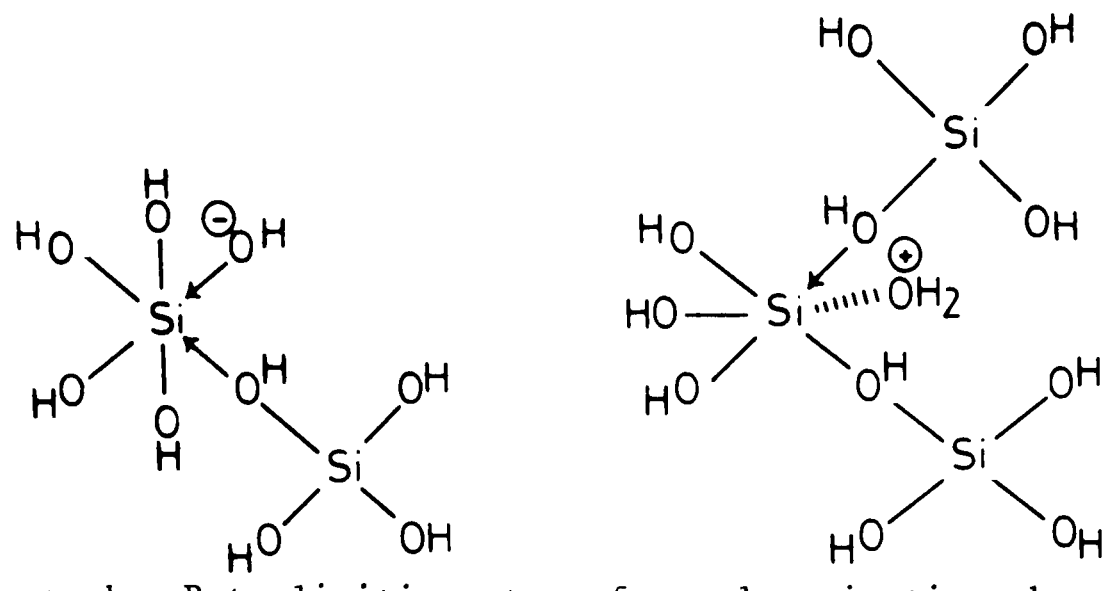

Figure 1 Rate limiting steps for polymerisation above and below pH 2.

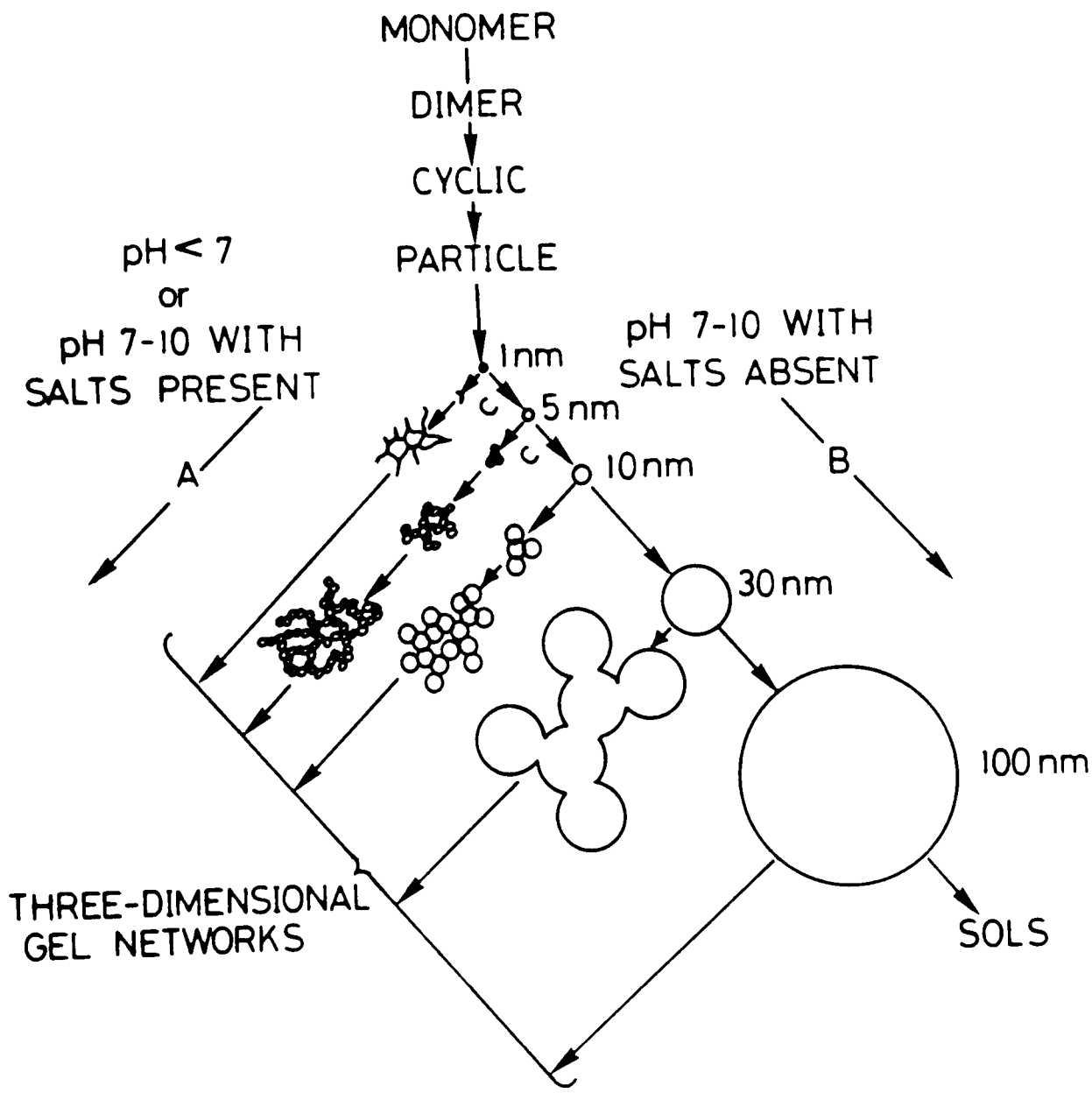

Figure 1a
Polymerisation behaviour of silica. In basic solution (B) particles grow in size with decrease in numbers; in acid solution or in the presence of flocculating salts (A), particles aggregate into 3-dimensional networks and form gels.

ultimately develop into much larger particles (Iler, 1979).

Two general pathways for silica polymerisation are known. They are graphically depicted in figure 1a. The two pathways to polmerisation depend upon the pH of the system and the presence or absence of salts or other flocculating agents. At high pH (7-10), and in the absence of salts, particles are negatively charged and repel one another. The rate of dissolution and deposition of silica is high and individual particles may grow in diameter up to 100nm at the expense of smaller particles by a process known as Ostwald ripening (Iler, 1979). This ultimately leads to sol formation.

If the pH of the system is less than 7, or between 7-10 and salts or flocculating agents are present then the negative charge at the surface of the silica particles may be reduced and aggregation of particles to give three dimensional gel networks occurs in preference to sol formation. Salt effects are greatest if polyvalent cations are present but monovalent cations such as sodium or potassium are effective if their concentration exceeds 0.2-0.3N. Flocculating agents such as alcohols, proteins, lipids and polysaccharides may also act on the surface of the particles, reducing surface charge and enabling condensation of the initially formed particles to occur. The gel network occupies the same volume of liquid as that prior to polymerisation and a precipitate is only formed if some of the water is removed.

The situation in the plant macrohair, however, does not only involve a liquid or solution phase. The region in which mineralisation occurs is surrounded by a cell wall. This surface possibly contributes to the mineralisation process.

The primary cell wall delineates the compartment in which

precipitation occurs. The primary cell wall therefore defines the boundaries for deposition and controls the overall shape and form of the inorganic deposit. It may be said that the primary cell wall provides a surface upon which nucleation of the precipitate can take place. The secondary cell wall, synthesised as mineralisation takes place, however, presents a very different level of involvement with precipitation. From the data presented in this thesis (particularly chapter 5 (on the organic fraction) and chapter 3 (nitrogen adsorption)) it seems most likely that the secondary cell wall is involved in matrix mediated mineralisation (Lowenstam,1981). Here, organic macromolecules do not merely induce nucleation of the mineral phase but act as a template for the selection of ultrastructural morphology, the resulting inorganic phase exhibiting defined microarchitectural structural features. This sophisticated mechanism of mineral formation ultimately leads to a structurally well defined mineral composite within which are embedded organic polymers. The organic material contributes to all the physical and chemical properties of the so-called mineral (Particularly infrared, electron microscopy and nitrogen adsorption).

The role of the heterogeneous organic matrix in silica deposition may be complex. It seems most likely that its function is more subtle than for crystalline materials where the mechanism for crystal formation most often proposed is that of epitaxial growth of the mineral phase upon an organic matrix template when matching atomic lattice parameters are observed (Weiner and Traub,1984). It is unlikely that the organic polymers in this system could be involved in such a process.

The function of the organic polymers may be to kinetically stabilise the formation of a given particle type at a particular point during wall development by its effect upon the surface characteristics of the silica

particle. The wall polymers could also interact with the preformed particles, ultimately leading to the structural arrangements observed.

It is reaonable to suppose, therefore, that the change in emphasis of polysaccharide synthesis during wall development must in some way be related to the size and ultrastructural arrangements of silica particles observed. One problem which is encountered is that wall synthesis occurs in advance of silica deposition (Hodson, 1984), and it is difficult, therefore, to correlate the data obtained from both the structural study and the study on the organic matrix. The following description is, however, feasible.

The sheet-like silicified material deposited at the early stages of secondary wall development is laid down within a matrix rich in a heavily substituted arabinoxylan and cellulose. The globular silicified material is then probably deposited within a matrix comprising cellulose, some(lower) arabinoxylan, some starch and some unidentified glucan(mixed link or callose). The fibrillar silicified material, deposited at the later stages of wall development is probably deposited in a cell wall rich in unidentified glucan, with some cellulose and a little arabinoxylan present. The differing proportions of the various polysaccharides at the time points selected for analysis must ultimately lead to slightly different chemical environments necessary to stabilise the various morphological ultrastructural variations observed in this system.

If we consider now the involvement of the inorganic ions with mineralisation, it will become apparent that two alternative, although not mutually exclusive roles exist. In the first instance, if we consider the heavy ionic localisation behind the initially formed silica deposit

(chapter 4, EDXA and SPM), it is feasible that in order to promote mineralisation, vast amounts of vacuolar fluid must be pumped through the system, the presence of a build up of ionic material occurring as a consequence of silicic acid being pumped into the system. This could occur if there was no preferential concentration of the silicic acid prior to mineralisation. If this was the case then at all stages of mineralisation one would expect to observe high levels of inorganic ions as even during the later stages of mineralisation, the rate of silica deposition does not decrease. This is not, however, observed. Although a certain (low) level of inorganic ions remain throughout mineralisation it is far more likely that the ions are involved in stabilising initially formed particles by alteration of their surface characteristics. This would ultimately lead to the incorporation of low levels of ions into the completed structures which is indeed the case. As yet there is no evidence to support either hypothesis but these two modes of involvement may both be important at the onset of mineralisation and as deposition continues.

It can be seen from the above discussion that the mineralisation process in specialised deposition cells such as in the macrohair cells from the lemma of the grass Phalaris canariensis is very complex. Although this study has yielded information relating to the involvement of both inorganic elements/ions and organic polymers with the deposition process, many questions remain to be answered before an indepth mechanistic knowledge of precipitation and spatial deposition in such biological materials can be reached.

The questions include:-

1) the organisation of SiO_4 tetrahedra within the different silicified particles, including the positions of any hydroxyl groups.

2) the precise location of the organic matrix in the solid state and its structural relationship with the inorganic mineral phase.

3) a detailed knowledge of the precise chemical nature of the organic phase and the involvement of silicon within the matrix.

4) a more detailed knowledge of temporal changes in the formation of the organic matrix, and

5) structural and mechanistic information on silica deposition in other biological systems.

Investigation of these problems could include the use of

1) neutron scattering (small angle) and general techniques used for the study of amorphous materials to determine the positions of hydroxyl groups and the degree of order within and between fundamental silica particles.

2) the application of high resolution electron energy loss spectroscopy to organic matrices in the solid state.

3) general chemical techniques involving chromatography, solution and solid-state nuclear magnetic resonance and mass spectrometry to study the organic phase.

4) a continuation of the in vivo radioactive labelling study to define more precisely the temporal nature of the matrix composition during mineralisation, and before general conclusions can be drawn regarding silica deposition;

5) parallel studies on other silicified biological systems need to be made which will utilise electron microscopy, EDXA and SPM analysis to follow the pathway and structural forms of deposition.

Mineralisation in limpet radular teeth may also be discussed in a similar manner to the plant system. There is no information available

relating to the temporal changes in morphology of the silicified deposits (if any) with mineralisation but information relating to changes in the inorganic and organic matrix composition are available. Runham's histochemical survey is presented in figure 2 (Runham,1961), and may be compared with the SPM data (chapter 6) which indicates changes in the mineral phase as mineralisation occurs. The stages at which SPM analyses were performed are indicated for comparative purposes in figure 2.

The radula is first secreted as a chitin-protein matrix. Very few changes subsequently occur in the radular membrane. Iron is not found in conjunction with the membrane at any stage of mineralisation.

Immediately prior to the onset of major mineralisation the teeth bases become impregnated with extra proteinaceous and polyphenolic/aminophenolic material. At this stage there is a localisation of P, Si and Fe in the front of the base of the tooth but Ca and S are found throughout the base and the radular mambrane. The increase in organic material present may be directly involved in chemical processes leading to the onset of mineralisation. An alternative role for the polyphenolic/aminophenolic material may be in quinone tanning (Runham, 1961) which would ultimately lead to a `hardening' of the total structure.

The tooth cusp does not appear to contain high levels of proteinaceous or polyphenolic/aminophenolic material at any stage of mineralisation. This may indicate that any chemical changes, necessary for mineralisation occur in the basal region and not in the tooth cusp. The cusp would then act largely as a store for the minerals produced.

The amount of chitin detected in both the cusp and base of teeth decreases prior to major mineralisation. It seems unlikely that any material would be removed from the system. What is more likely is that

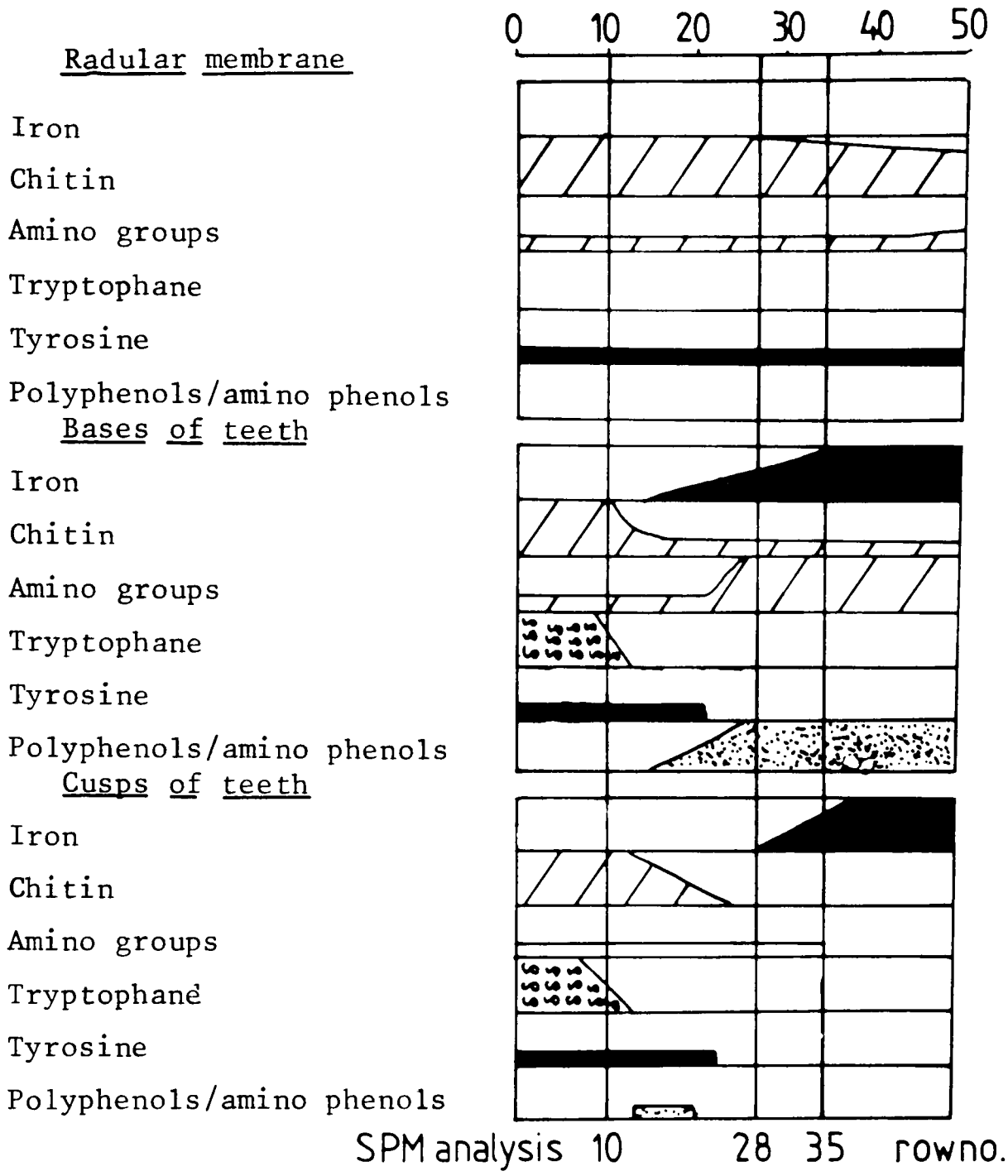

Figure 2

A summary of the histochemistry of the radula of Patella vulgata L. The numbers refer to the tooth row, numbering from the proximal end of the radula. The shading represents the intensity of the reaction. The rows at which SPM analysis was also performed are also indicated.

the hydroxyl and amino groups, necessary for identification of chitin by these procedures (Runham,1961) are chemically unavailable to the reagents employed. This would correspond to the possible early involvement of silicon in the initial strengthening of the organic matrix. The binding of silicon to the matrix, whether by covalent or hydrogen bonds would make the resulting material unreactive to reagents with specificity for hydroxyl or amino groups. (cf. chapter 5 where the presence of silica makes the polysaccharide matrix driselase resistant).

From the above discussion, it would appear that the spatial and temporal changes in localisation of the inorganic elements in the radular teeth from the common limpet Patella vulgata L. may be correlated with changes in the composition of the organic matrix.

The exact chemical and physical nature of the polymers which control mineralisation remain to be investigated.

7.1 References

1. Hodson, M.J., Sangster, A.G. & Parry, D.W. (1984) Proc. R. Soc. Lond. B 222, 413-425.

2. Iler, R.K. (1979) "The Chemistry of Silica", John Wiley & Sons, New York, Chapter 3.

3. Lowenstam, H.A. (1981) Science, 211, 1126-1131.

4. Runham, N.W. (1961) Quart. J. Micros. Sci. 102, 371-380.

5. Weiner, S. & Traub, W. (1984) Phil. Trans. R. Soc. Lond. B 304, 425-434.

Appendix 1

Examples of original EDXA analytical data (background subtracted)

Samples	Element Si	P	S	Cl	K	Cu
immediately prior to emergence.						
tip	0	14	39	12	0	22968
tip	0	56	0	0	37	9015
middle	5	34	0	69	6	13397
middle	0	27	21	16	24	9708
1½ days post emergence						
tip	3530	0	45	0	217	9490
0.02mm from tip	211	4	0	5	40	7462
0.03mm from tip	645	0	13	15	44	7545
0.056mm from tip	341	0	0	9	7	11681
tip	623	0	8	4	0	9764
0.07mm from tip	372	6	30	49	90	13050
0.133mm from tip	615	11	29	241	321	10169
tip	52	0	21	79	71	11575
0.056mm from tip	0	0	19	0	12	10794
0.15mm from tip	0	0	0	44	109	10329
5 days post emergence						
0.052mm from tip	3607	333	306	1665	4095	28766
0.057mm from tip	3579	499	451	1969	4787	63808
0.060mm from tip	3673	187	102	1310	3336	19301
0.061mm from tip	3872	432	255	1818	4495	20182
0.063mm from tip	3505	321	113	1528	4023	18307
0.067mm from tip	4123	544	179	1329	3628	25823
0.081mm from tip	4103	127	14	847	1792	32305
0.15mm from tip	3351	0	39	249	873	23339
0.21mm from tip	1438	0	56	78	114	8941
0.30mm from tip	326	23	32	29	0	12748
0.40mm from tip (base)	57	54	88	426	1089	17815
tip	10883	0	0	0	0	8052
0.006mm from tip	25059	0	41	38	524	12656
0.012mm from tip	22602	0	104	741	2176	13724
0.019mm from tip	13165	118	258	986	2916	8465
0.027mm from tip	11569	47	236	1789	4755	11442
0.049mm from tip	7888	14	93	296	964	10560
↓	8554	97	24	150	809	11972
towards	8094	231	275	615	2653	8900
middle of hair ↓	18563	17	0	0	554	20791

(day 5)

	Si	P	S	Cl	K	Cu
tip	12604	13	29	87	315	8701
0.003mm from tip	25656	7	135	192	408	11454
0.01mm from tip	14342	151	387	1065	2769	12071
0.015mm from tip	15888	108	244	637	1375	11558
0.02mm from tip	9267	0	139	239	813	10571
0.125mm from tip	10177	0	3	242	451	24538
0.15mm from tip	8496	16	171	136	460	10130
0.2mm from tip	11941	2	11	55	330	22316
base of broken piece						
0.052mm from tip	3607	333	306	1665	4095	28766
0.057mm from tip	3579	499	451	1969	4787	63808
0.060mm from tip	3673	187	102	1310	3336	19301
0.061mm from tip	3872	432	255	1818	4495	20182
0.063mm from tip	3505	321	113	1528	4023	18307
0.067mm from tip	4123	544	179	1329	3628	25823
0.081mm from tip	4103	127	14	847	1792	32305
0.15mm from tip	3351	0	39	249	873	23339
0.21mm from tip	1438	0	56	78	114	8941
0.3mm from tip	326	23	32	29	0	12748
0.4mm from tip	57	54	88	426	1089	17815
6 days post emergence						
tip	50032	0	18	1325	1409	42688
0.004mm from tip	80517	0	170	2510	1854	70376
0.008mm from tip	16349	97	103	1033	2139	26233
0.012mm from tip	6281	121	125	1139	4511	24371
0.016mm from tip	5331	179	183	1189	3701	24479
0.026mm from tip	4635	189	469	1608	5482	38684
0.086mm from tip	1260	26	61	482	1070	39279
0.096mm from tip	15728	0	105	467	1300	22157
0.113mm from tip	13573	26	7	254	1114	17145
0.159mm from tip (middle)	6345	83	29	288	821	52199
tip	58183	0	0	1634	1421	18418
0.004mm from tip	38035	105	172	2138	3537	17355
0.007mm from tip	35265	271	264	2551	4029	17884
0.009mm from tip	30156	517	359	4915	9772	21485
0.014mm from tip	24956	149	393	5791	11168	20137
0.032mm from tip	24455	704	736	5610	12065	25554
0.053mm from tip	11614	151	96	1363	3181	20423
0.116mm from tip	5524	81	61	365	936	22488
0.202mm from tip	3252	14	0	127	203	37572
0.225mm from tip (base)	1304	72	110	1189	3194	57811

9 days post emergence	Si	P	S	Cl	K	Cu
tip	19488	0	0	75	212	8812
0.045mm from tip	6713	149	188	159	980	15267
0.08mm from tip	12470	148	437	161	2222	11013
0.089mm from tip	10356	288	394	324	3362	10708
0.090mm from tip	12723	129	269	221	1747	10536
0.091mm from tip	20319	142	243	0	1680	14903
0.115mm from tip	21405	124	286	67	1476	13456
0.027mm from tip	9428	0	109	408	918	15561
0.044mm from tip	12012	0	27	454	1119	17216
0.057mm from tip	11016	14	279	446	1835	21908
0.077mm from tip	9662	0	60	461	642	17529
0.096mm from tip	7567	0	14	248	604	23582
0.153mm from tip	5718	270	86	145	587	19565
0.167mm from tip	10173	0	35	204	499	18038
0.183mm from tip	16998	0	262	536	887	26359
18 days post emergence						
0.006mm from tip	26049	0	0	0	138	19110
0.147mm from tip	22041	0	161	53	56	16677
0.162mm from tip	9675	0	73	9	0	11410
0.18mm from tip	42606	0	136	0	425	40358
0.266mm from tip	9963	0	56	58	278	42184
0.30mm from tip	10087	129	228	103	551	25215
tip	18440	0	0	0	0	88536
0.02mm from tip	10492	0	0	0	0	78409
0.1mm from tip	16742	0	0	78	217	14172
0.124mm from tip	16699	0	100	24	154	13553
0.142mm from tip (broken piece)	21668	0	62	89	215	16891

	Si	P	S	Cl	K	Cu
40 days post emergence						
tip	58595	0	262	92	666	58869
0.014mm from tip	70699	0	206	501	1211	216407
0.029mm from tip	109906	0	454	940	2038	161911
0.034mm from tip	24910	37	182	272	1070	118727
0.089mm from tip (broken piece)	18445	53	23	100	543	82367
0.0014mm from tip	43268	0	220	0	0	96249
0.007mm from tip	77903	0	275	0	427	36056
0.016mm from tip	89062	0	0	0	317	33085
0.027mm from tip	102240	0	26	108	225	33965
0.069mm from tip	94439	0	0	107	378	37394
0.166mm from tip	84687	0	58	0	300	206894
0.219mm from tip	49749	0	0	0	440	28475
0.269mm from tip	49098	0	125	229	489	24263
0.275mm from tip (base)	8695	0	0	6	172	18892
mature						
0.005mm from tip	13952	0	564	1848	741	116745
0.06mm from tip	69506	50	264	893	620	37598
0.07mm from tip	69924	60	217	626	752	31317
0.27mm from tip	94310	89	323	467	3030	57785
0.30mm from tip	111549	97	616	379	4503	95066
0.32mm from tip (towards base)	107681	0	397	544	5066	75802
0.008mm from tip	26708	32	154	230	244	112221
0.03mm from tip	116671	1	27	331	825	171201
0.055mm from tip	120560	12	274	242	687	87045
0.085mm from tip	115622	24	211	523	822	75129
0.132mm from tip	78033	0	413	346	793	182460
0.152mm from tip	49247	20	197	79	776	25890
0.160mm from tip (broken piece)	45289	40	242	136	800	21515
0.037mm from tip	29258	19	74	413	246	169413
0.063mm from tip	135691	128	292	634	1346	116592
0.11mm from tip	116858	115	314	747	1008	66849
0.113mm from tip	102594	0	248	481	749	62980
0.19mm from tip	116369	70	468	556	1276	104891
0.22mm from tip (broken piece)	97117	17	258	949	1784	121733